Defense Threat Reduction Agency
8725 John J. Kingman Road, MSC 6201
Fort Belvoir, VA 22060-6201

TECHNICAL REPORT

DTRA-TR-09-13

A Probabilistic Approach to Uncertainty Analysis in NTPR Radiation Dose Assessments

Approved for public release; distribution is unlimited

November 2009

HDTRA1-07-C-0015
Subcontract No. 06-792-SA

Weitz, Ronald L. et al.

Prepared by:
Science Applications International Corporation
8301 Greensboro Drive, Suite 500, M/S E-5-5
McLean, VA 22102

REPORT DOCUMENTATION PAGE

Form Approved
OMB No. 0704-0188

1. REPORT DATE *(DD-MM-YYYY)*	2. REPORT TYPE	3. DATES COVERED *(From - To)*
11-01-2009	Technical report	

4. TITLE AND SUBTITLE
A Probabilistic Approach to Uncertainty Analysis in NTPR Radiation Dose Assessments

5a. CONTRACT NUMBER
HDTRA1-07-C-0015

5b. GRANT NUMBER

5c. PROGRAM ELEMENT NUMBER
139D

6. AUTHOR(S)
Weitz, Ronald L; Case, David R; Chehata, Mondher; Egbert, Stephen D; Mason, Carol L; Singer, Harvey A; Martinez, Daniel G; McKenzie-Carter, Michael A; Shaw, Robert S; and Stiver, John S.

5d. PROJECT NUMBER
CS

5e. TASK NUMBER
AH

5f. WORK UNIT NUMBER

7. PERFORMING ORGANIZATION NAME(S) AND ADDRESS(ES)
Science Applications International Corporation
8301 Greensboro Drive, Suite 500, M/S E-5-5
McLean, VA 22102

8. PERFORMING ORGANIZATION REPORT NUMBER

9. SPONSORING/MONITORING AGENCY NAME(S) AND ADDRESS(ES)
Nuclear Technology Directorate
Defense Threat Reduction Agency
8725 John J. Kingman Road, Stop 6201
Fort Belvoir, VA 22060-6201

10. SPONSOR/MONITOR'S ACRONYM(S)
DTRA RD-NTSN

11. SPONSORING/MONITORING AGENCY REPORT NUMBER

12. DISTRIBUTION AVAILABILITY STATEMENT
Approved for public release; distribution is unlimited.

13. SUPPLEMENTARY NOTES

14. ABSTRACT
This report discusses the approach, technical basis, and special studies investigated in the process of developing probabilistically-based methods for performing radiation dose assessments for atmospheric nuclear weapons test participants of the Nuclear Test Personnel Review Program. Developed methods were applied to six case studies of exposed groups at three island locations in the Pacific Proving Ground (PPG), two ships in the PPG, and one US Marine Corps brigade at the Nevada Test site. Results of the case studies indicate that the methodologies successfully produced reliable estimates of doses from external sources and internally-deposited materials. Sample sensitivity analyses identified the relative contributions to uncertainty for input parameters and may serve as the basis for screening out less significant parameters for a given scenario of exposure.

15. SUBJECT TERMS
Nuclear Test Personnel Review, Veterans, Atmospheric Nuclear Weapons Test, Dose Reconstruction, Uncertainty, Probabilistic Methods, External Dose, Internal Dose

16. SECURITY CLASSIFICATION OF:			17. LIMITATION OF ABSTRACT	18. NUMBER OF PAGES	19a. NAME OF RESPONSIBLE PERSON
a. REPORT	b. ABSTRACT	c. THIS PAGE			Dr. Paul K. Blake
U	U	U	UU	268	19b. TELEPONE NUMBER (*Include area code):* ***703 767-3384***

Table of Contents

List of Figures

List of Tables

Acknowledgments

The authors thank Mr. Harold L. Beck, Mr. Paul G. Voillequé and Dr. Gary H. Zeman, members of the Subcommittee on Dose Reconstruction of the Veterans' Advisory Board on Dose Reconstruction (VBDR) for their critical review of this report and their valuable suggestions to improve its content. The authors also extend their gratitude and appreciation to Drs. David C. Kocher and F. Owen Hoffman of SENES Oak Ridge, Inc., who provided valuable discussions and advice in the early stages of the studies described in this report as well as a thorough review of the first draft of the report, which allowed substantial improvements in the project and final report.

EXECUTIVE SUMMARY

Summaries of the individual sections of this report are provided in this executive summary. Each heading within this summary is labeled with the section number of the narrative report for easy reference to additional details and discussion.

Introduction (1) and Background (2)

In October 2007, the Veterans' Advisory Board on Dose Reconstruction (VBDR) recommended that the Nuclear Test Personnel Review (NTPR) Program develop procedures to perform probabilistic uncertainty analyses for Radiation Dose Assessments (RDAs) (VBDR, 2007). Specifically, the NTPR standard operating procedures should specify whether uncertainty estimates from individual sources are independent or correlated and when and how uncertainties should be propagated. The Defense Threat Reduction Agency (DTRA) tasked Science Applications International Corporation (SAIC) to investigate methods that could be used for conducting analyses for NTPR RDAs (DTRA, 2007b). In response, SAIC identified the effort's main goal to develop and demonstrate a methodology and its enabling computational tools to perform probabilistic radiation dose assessments for NTPR atomic veterans. The objectives identified for the study are addressed in Section 1.

The NTPR Program's reconstructed radiation doses for atomic veterans have traditionally employed methods using high-sided estimates for parameters that are difficult to characterize, but were considered to overestimate actual doses and therefore provided reliable upper bounds.

In a 2003 review of DTRA's dose reconstruction program, a committee of the National Research Council of the National Academy of Sciences (NAS/NRC) concluded that although central estimates of reconstructed doses for external gamma exposures were valid in most cases, upper bounds could not always be shown to be at least as great as a 95 percent upper confidence limit (NRC, 2003). Therefore, the Committee recommended "… a comprehensive re-evaluation of the methods being used to estimate doses and their uncertainties to establish more credible upper-bound doses to atomic veterans." DTRA and the Department of Veterans Affairs (DVA) acknowledged these findings and committed to plans to improve models for dose reconstructions (DOD/DVA, 2004).

In addition, DOD and DVA jointly established the VBDR to oversee the dose reconstruction process. VBDR, Subcommittee 1 on dose reconstruction audited radiation dose assessments, reviewed methodologies, and developed conclusions and recommendations. In October 2007, the VBDR recommended to DTRA that it stop using default upper bound factors and develop procedures that make use of probabilistic uncertainty analyses in dose reconstructions (VBDR, 2007). DTRA endorsed efforts to pursue that VBDR recommendation, which forms the basis for the investigations documented in this report (DTRA, 2007c).

Radiation Dose Estimation and Uncertainty Modeling (3)

Types of Doses (3.1)

This report involves the calculation of "nominal," "probabilistic" and "deterministic" doses, which are described further in the following discussions. Nominal doses are based on observed data or best estimates; probabilistic doses are based on distributions of parameters using Monte

Carlo analyses; and deterministic doses are based on certain high-sided parameter estimates according to DTRA guidance. Doses fall into two main classes—whole body external dose, and internal dose.

Whole body external dose (3.2) results from exposure to radiation sources outside the body and involves initial nuclear radiation, and residual nuclear radiation. The most commonly encountered source of residual radiation is gamma rays emitted from fallout particles, but some test participants were also exposed to gamma rays emitted from neutron activation products in the soil.

Methods for estimating whole body external dose address external dose from **exposure to fallout (3.2.1)**, and external dose from **exposure to activated soil (3.2.2)**. Methods for external dose from fallout involve the **modeling of fallout intensity decay (3.2.1.1)**, and addressing the **effects of shielding (3.2.1.2)**. Doses from neutron-activated soil components arise from exposures to radionuclides produced in the soil by a detonation whose neutrons reached the surface, but whose fireball did not.

In addition to methods for calculating doses from intensity measurements, **film badge dosimetry (3.2.3)** provides an alternate method subject to biases and uncertainties that can be corrected.

Internal dose (3.3) involves dose in internal organs from exposures to radioactive sources inside the body. Participants in nuclear weapons tests could have accrued internal doses as a result of intakes of radionuclides by inhalation, ingestion, or absorption through the skin or open wounds. Intakes by inhalation are the most common pathway for the majority of participants; most exposure scenarios involve inhalation of descending fallout and/or fallout that had been deposited previously on the ground or other surfaces and subsequently resuspended into the air.

Calculation of internal organ doses requires the use of factors that convert intakes of radioactive material to the dose each organ would receive from that intake. The NTPR program develops composite *dose conversion factors* (*DCF*s) that apply to mixtures of radionuclides based on ICRP-recommended *dose coefficients*.

Internal doses derive from **inhalation intakes (3.3.1)**, and **ingestion intakes (3.3.2)**. Inhalation intakes address **inhalation of fallout resuspended from surfaces (3.3.1.1)**, **inhalation of descending fallout (3.3.1.2)**, and **inhalation of suspended soil activation products (3.3.1.3)**. All of these intakes require knowledge of the airborne radioactivity concentration and other factors—breathing rate, time of exposure as duration and clock time, and the *DCF*s.

Ingestion Intakes (3.3.2) arise from a chronic type of exposure that involves the daily intake of relatively small quantities of contaminated soil and dust containing a mixture of radionuclides that changes with time. Guidance (USEPA, 1996, 1997 and 2002; USACHPPM, 2003) provides soil/dust ingestion rates for use in calculations.

Uncertainty modeling (3.4) reviews the **statistical probability distributions (3.4.1)** available for use in describing the nature of assumed characteristics for the range and frequency distribution of parameters, data, and results. Five distributions considered in the study are **Uniform Distribution (Section 3.4.1.1)**, **Gaussian Distribution (Section 3.4.1.2)**, **Lognormal Distribution (Section 3.4.1.3)**, **Triangular Distribution (Section 3.4.1.4)**, and **Log-Triangular Distribution (Section 3.4.1.5)**. In addition, discussions address approaches to the **propagation of uncertainties (3.4.2)**, **the Monte Carlo Method (3.4.3)**, **quantifying uncertainty (3.4.4)**, and **the reporting of representative doses (3.4.5)**.

Technical Approach and Methodology (4)

This effort to investigate the use of probabilistic methods for dose reconstruction involved five major phases of the probabilistic uncertainty analysis studies for NTPR radiation dose reconstruction, which are:

- A pilot study and proof of concept designed to experiment and test the implementation of probabilistic methods using existing deterministic dose reconstruction and assessment models currently used in NTPR radiation dose assessments.
- Special studies to develop statistical models and uncertainty distributions of key input parameters used in whole body external gamma dose assessment.
- Application of prototype methods to three generic cohorts and comparison with dosimetry records. These allowed testing and verification that the selected computational tools and techniques were capable of producing the types of model results sought.
- Expansion of the methodology to include application to internal dose estimation where deterministic models were enhanced to incorporate improved estimation of input parameter central values and uncertainty distributions.
- Evaluation of the feasibility of the methods developed through six case studies that consisted of the three original and three additional cohorts. The selection of case study cohorts was based on criteria developed during the pilot study.

The **pilot study (4.1)** was carried out to select software tools, study groups, and develop and test the basic models using a probabilities approach to NTPR dose reconstructions and uncertainty analysis. **Software Selection (4.1.1)** resulted in choosing Mathcad® as the primary tool for Monte Carlo calculations and was supplemented with the Crystal Ball® adjunct to Microsoft Excel®, and Mathematica®. **Generation of parameter distributions (4.1.2)** discusses approaches to distributions that model variability and uncertainty of model parameters generated in Mathcad.

The special studies of model parameters, uncertainties, and distributions (4.2) describes detailed analyses to support the development of uncertainty models and input values for certain parameters, which include:

For External Dose Models:

- Intensity distribution from fallout on ship weather decks (4.2.1).
- Protection factors for land-based structures (4.2.2).
- Shielding factors for ships (4.2.3).
- Shot-specific radiological decay functions (4.2.4).
- Sources of uncertainty when estimating radiation intensity from measured intensities and iso-intensity maps (4.2.11).

For Internal Dose Models

- Gamma source modification factor (4.2.5).
- Resuspension factors (4.2.6).

- Breathing rate (4.2.7).
- Internal dose conversion factors (4.2.8).
- Characterization of descending fallout (4.2.9)
- Internal deposition fraction adjustment (4.2.10)
- Incidental ingestion of contaminated soil and dust (4.2.12).

Intensity distribution from fallout on ship weather decks (4.2.1) addresses the variability of intensity with topside location and its contribution to the uncertainty in the dose of an individual crewman and requires modeling this variability in topside intensity when calculating doses probabilistically. This study addressed variations in topside configuration, radiation transport through air, distributions pre- and post-decontamination, and application to various ship types. Models were benchmarked against available measurements for two ships involved in Operation CASTLE.

Protection factors for land-based structures (4.2.2) addresses the protection factor (*PF*) of a structure, defined as the quotient of the free-field radiation intensity outside and the free-field radiation intensity inside the structure. It is a measure of the radiation shielding provided by that structure. This study used building configurations on Enewetak Island contained in contractor reports to model *PF*s and test them for a 48-man barracks building and an 8-man tent. Mathcad software was used to calculate a distribution of *PF*s for locations inside a rectangular shelter with known length, width, height, and wall/roof thickness situated in a field of uniformly deposited fallout that extends infinitely in all directions. It was further assumed that the interior of the shelter was free of fallout, and walls of wood, aluminum, and iron were considered for buildings; wall thickness was set to 0 for tents. Fallout initially deposited on a pitched roof would run off and redeposit on the adjacent ground with a fraction of the fallout on the roof forming line sources alongside the structure.

Shielding factors for ships (4.2.3) addresses shielding factors (*SF*s), which are the ratio of intensity at some below-deck location to the average topside intensity. The shielding factor is dependent on the characteristics of the ship (e.g., beam or maximum width, length, number of decks, deck height, and decking thickness) and on one's position within the ship (deck and location on that deck). An approach similar to that for developing protection factors accounted for attenuation of radiation emitted by fallout deposited on the weather deck of a ship to various levels of interior spaces (decks).

Shot-specific radiological decay functions (4.2.4) obtained directly from the FIIDOS code were compiled in a database that provides relative intensities from 3 seconds to 5 years post-detonation for most shots and most operations. An empirical model of the uncertainty in the FIIDOS decay functions was developed for use in the case studies. The model presumed that the modeling error will generally increase with time from zero at the time of a known measurement to a later time with the amount of error drawn from a Gaussian distribution for each sample in the Monte Carlo analysis.

G**amma source modification factor (4.2.5) (***GSMF*) corrects for the fact that the contaminated surface was not infinite in spatial extent, as assumed in the FIIDOS calculations. A Monte Carlo approach is used in a Mathcad program to generate a distribution of *GSMF* values for a ship. The values in the distribution are averaged over all deck locations to produce an average

GSMF—designated <*GSMF*>. The uncertainty in <*GSMF*> is determined by considering factors that contribute to it for an aircraft carrier that include (1) shielding provided by aircraft that may have been located on the flight deck, (2) the impact of the superstructure, and (3) the deviations of the flight deck from the idealized rectangular configuration. Account is taken for these factors for aircraft carriers, and extended to other ship types considering similar factors to produce a collection of <*GSMF*> values for the common ship types involved in nuclear test operations.

Resuspension factors (4.2.6) relate air concentrations of radioactivity to ground contamination levels. Time-dependent models for deterministic and nominal point estimates for resuspension of fallout as used in the case studies for typical activities are given in that section. For the probabilistic analysis, the uncertainty associated with the nominal resuspension factor values (land and ship) is assumed to have a lognormal distribution with the median equal to the nominal value, and a 90-percent confidence interval between 0.1 and 10 times the median. Supplemental uncertainty models were developed to address special resuspension characteristics associated with the precursor and blast-wave regions that accompany nuclear detonations near the detonation point.

Breathing rate (4.2.7) is an important parameter for calculating intakes by inhalation and depends on the level of physical activity and other physiological parameters related to ventilation. It influences the volume and rate of air inhaled and the proportions entering through the nose and mouth, their penetration into the respiratory tract, and the quantities deposited. Summary data and guidance provided by the International Commission of Radiological Protection (ICRP, 1994), the National Council on Radiation Protection (NCRP, 1997) and the United States Environmental Protection Agency (USEPA, 1997) are used to construct probability distribution functions of breathing rates for various types of activity and to apportion time among such activities for atmospheric nuclear test participants.

Internal *dose conversion factors* (*DCF*s) (4.2.8) used in NTPR dose reconstructions are derived from published ICRP *dose coefficients* (ICRP, 1996; ICRP, 2002) and involve biases and uncertainties that must be addressed to perform best-estimate probabilistic analyses. Studies to address these included estimation of inhalation dose conversion factors using FIIDOS (4.2.8.1), uncertainty in inhalation and ingestion dose conversion factors (4.2.8.2), and maximum dose bias in inhalation *DCF*s (4.2.8.3).

Characterization of descending fallout (4.2.9)—Special studies were conducted (1) to calculate the fraction of the activity in descending fallout ("activity fraction") (4.2.9.1) that was carried by particles in each of three size classes and (2) to estimate the deposition velocities (4.2.9.2) in the breathing zone for particles in each size class.

Internal deposition fraction adjustments (4.2.10) are defined as the fractions of inhaled particles in a given size class that are respirable and non-respirable. The deterministic inhalation dose models assume that all of the fallout inhaled is in the size range between 1–10 μm. However, the use of this assumption for all scenarios is undoubtedly high-sided, especially for descending fallout. Probabilistic analyses require more realistic descriptions of the activity deposited by particles of various sizes. This section discusses an approach that characterizes the deposition in the respiratory tract of particles in the three inhalable size classes 1 (1–10 μm), 2 (10–20 μm) and 3 (20–100 μm).

Sources of uncertainty when estimating radiation intensity from measured intensities and iso-intensity maps (4.2.11) has a related uncertainty comprised of two components—the uncertainty due to errors introduced during the actual intensity measurement and when maps are created from a discrete and often sparse set of point observation measurements; and the additional uncertainty that arises when an estimate is made at any point on a map by interpolation (or in some cases by extrapolation) from an iso-intensity contour map.

Incidental ingestion of contaminated soil and dust (4.2.12) containing radioactivity is another route of entry for participants in atmospheric nuclear testing. As in analysis of exposure to internally-deposited materials, this depends on the intake amount of activity, which in turn depends on the ingestion rate of soil and soil density. A literature review identified guidelines compiled in USEPA (1997, 2001 and 2002) and the USACHPPM (2003), which served as the basis for preparing a skewed triangular distribution of soil ingestion rates. Soil density data for NTS and PPG locations were identified and used to develop a triangular distribution for input to Monte Carlo analyses.

Dependencies and correlations between model input parameters (4.3) for the distributions and sensitivity to model parameters of the reconstructed doses for the six case studies were estimated using probabilistically-based Monte Carlo simulation techniques. Model parameter values were randomly selected from each of their distributions. There are 54 explicit input parameters used in the six case studies, which have associated uncertainty distributions. Two types of correlations were considered: correlations among different parameters and those from shot to shot for the same parameter. The discussion focuses on the various aspect of parameter dependencies and correlations, and the basis for each correlation decision is presented in Table G-1 of Appendix G.

Case Study Results (5)

The methods and tools developed in this investigation were applied in six case studies to demonstrate their feasibility, and to check their validity through comparison to existing methods and to film badge data where available. Case studies were performed for the following cohorts:

- 7126th Army Unit (AU) Headquarters (HQ) Detachment, Enewetak Atoll, Operation REDWING (1956)
- Army Unit Administrative and Operations Detachments, Enewetak Atoll, Operation HARDTACK I (1958)
- 4th Marine Corps Provisional Atomic Exercise Brigade (MCPAEB) Maneuver at Shot HOOD, Operation PLUMBBOB (1957)
- USS ESTES (AGC 12), Operation REDWING (1956)
- USS BOXER (CVS 21), Operation HARDTACK I (1958)
- Army Personnel, Enewetak Atoll, Operation CASTLE (1954)

Sections 5.1 through 5.6 provide summaries of the scenarios, relevant film badge and other radiation data for the case, and detailed discussions of the results. Additional details about each unit's activities, assumptions about scenario parameters, and uncertainty distributions used in the probabilistic analysis are provided in Appendices A–F.

A summary of study results and discussions (Section 5.7) provide the ratios of deterministic (current NTPR high-sided) upper bound doses to the 95th percentile probabilistic doses—called upper bound dose ratios— for the six case studies investigated in this report, and shown in Table ES-1. These ratios illustrate the difference in upper bound doses estimated using deterministic and probabilistic methods at the current stage of development. The upper bound dose ratios for external doses exceed 1.0 in all cases considered, indicating that the upper bounds of the deterministic external doses are greater than the 95th percentiles of the corresponding probabilistically-calculated doses. The upper bound dose ratios for internal doses equal or exceed 1.0 for all case studies except for the scenario for the 4th MCPAEB maneuver at Shot HOOD, Operation PLUMBBOB (Case Study #3). Although these results support the reasonableness of DTRA's default uncertainty factors, general conclusions about these comparisons should not be made from these limited test cases.

Table ES-1. Ratios of Deterministic Upper Bound over 95th Percentile Probabilistic Doses

Case Study	Study Group	Upper Bound Dose Ratio External	Upper Bound Dose Ratio Internal α	Upper Bound Dose Ratio Internal β+γ		
			All Organs Evaluated	Thyroid	Lung	LLI wall
1	RW/Enewetak	1.6	1.4	1.5	3.7	1.3
2	HTI/Enewetak	1.5–1.6	2.5–2.6	1.8	4.6	1.8
3	PB	1.7	0.58-0.68	0.43	0.87	0.42
4	RW/USS ESTES	1.1	1.5	1.1	3.2	1.0
5	HTI/USS BOXER	1.3	4.0–4.2	2.0	6.2	2.0
6	CASTLE/Enewetak	1.5	2.5–2.6	2.2	5.6	2.2

Discussions of factors contributing to the results observed for internal doses are provided.

Sensitivity Analysis for the Dose Models of CASTLE Enewetak Case Study (6)

Sensitivity analyses were performed for the external and internal dose models applied to the Army personnel at Enewetak Atoll at Operation CASTLE (1954) (Case Study # 6) for a sample organ. These analyses were performed to evaluate to which input parameters the models are most sensitive, and to develop an approach on how to implement and use sensitivity analyses in NTPR dose reconstructions. It is not the intent of this analysis to develop generalized conclusions to be applied across many scenarios with a broad range of exposures and types of intakes, or across all target organs considered in NTPR dose assessments. Indeed, it is recognized that the parameters to which models are most sensitive would likely be different for different target organs.

Discussions of the **technical approach (6.1), external dose model sensitivity analysis (6.2), and internal dose model sensitivity analysis (6.3)** provide details of the sensitivity analyses. Results of sensitivity analyses for the sample scenario and target organ evaluated using 1000 Monte Carlo runs varying one parameter at a time indicate the following:

- The external dose model is most significantly sensitive to the variability and uncertainty in intensity measurement and data errors, fallout distribution and decay constants.
- The internal alpha and beta-plus-gamma dose models are most significantly sensitive to the uncertainties in the *DCF* for inhalation and the resuspension factor.

Conclusions and Recommendations (7)

The main goal of this study was to investigate and demonstrate a methodology and the enabling computational tools to perform probabilistic radiation dose assessments for NTPR atomic veterans. This goal was achieved through the use of Monte Carlo simulation techniques and available data and information. Probabilistic models for both external and internal dose calculations that account for uncertainty and variability of input parameters were developed, tested, and applied in six case studies. Extensive research of the relationship of fallout deposition times to particle size distributions constituted one of the most difficult aspects of model parameter characterization due to the limited availability of applicable data. Fallout deposition were developed and compared with the limited available data to provide reasonable estimates of the activity fractions in respirable and non-respirable particle-size classes. Despite this progress to date, further efforts are needed to enhance the characterization of particle size distributions in fallout that can be applied to a broader range of exposure situations.

A comparison of reconstructed external doses and film badge readings was carried out for units where reliable dosimetry data were available. For four groups, reconstructed probabilistic external doses matched well with the film badge doses, and the 95^{th} percentile of the probabilistic dose distribution exceeded the 95^{th} percentile of the film badge dose distribution. In addition, NTPR deterministic upper bound doses, determined by multiplying the external doses by a factor of 3 were higher than the probabilistic 95^{th} percentile external doses in all case studies.

For internally-deposited radioactive materials, the NTPR deterministic method resulted in internal upper bound doses, determined by multiplying the internal doses by a factor of 10, were higher than the probabilistic 95^{th} percentile internal doses, except in the case of the Marine unit at PLUMBBOB discussed in Section 5.7.

The case studies included in this investigation varied in type (land and two very different types of ships), number and time of occurrence of fallout events, radiation intensities and fallout deposition, time veterans spent at the PPG, etc. Therefore, implementation of the probabilistic methodologies can proceed but with the expectation that further refinements should take place and any adjustments will require revision of the standard methods as applicable.

A sensitivity analysis was performed to identify the possibility of screening out sources of uncertainty with small or limited impact on dose. A simple method that varied model parameters one-at-a-time was applied for both external and internal doses using the Army personnel at Enewetak during CASTLE and for one organ as an example. Successful application of this

methodology for sensitivity analysis provides a basis for use in future refinements of existing methods and extension to new exposure situations.

The results of this investigation are valid for the six case studies only and cannot be generalized to all exposure scenarios. Only the methodologies developed and presented in this report can be applied and expanded to other scenarios of exposure. The analyses conducted provide reasonable estimates of dose and associated uncertainties for the types of exposure scenarios studied and support implementation of the probabilistic approach to radiation dose assessments in the NTPR Program. The following recommendations are offered to achieve implementation of the approach:

- Conduct testing of probabilistic methods applied to other exposure scenarios, test series, and participant units to develop experience with preparing reasonable distributions of parameters to support implementation of these methods.
- Incorporate probabilistic approaches developed in this report to NTPR RDA procedures and methodologies.
- Implement the probabilistic analyses described herein when performing future radiation dose reconstructions and adapt model parameter distributions when case-specific scenarios are well documented.

1 INTRODUCTION

In October 2007, the Veterans' Advisory Board on Dose Reconstruction (VBDR) recommended that the Nuclear Test Personnel Review (NTPR) Program develop procedures to perform probabilistic uncertainty analyses for Radiation Dose Assessments (RDAs) (VBDR, 2007). Specifically, the NTPR standard operating procedures should specify whether uncertainty estimates from individual sources are independent or correlated and when and how uncertainties should be propagated. The Defense Threat Reduction Agency (DTRA) tasked Science Applications International Corporation (SAIC) to investigate methods that could be used for conducting analyses for NTPR RDAs (DTRA, 2007b). In response, SAIC identified the effort's main goal to develop and demonstrate a methodology and its enabling computational tools to perform probabilistic radiation dose assessments for NTPR atomic veterans. The specific objectives of this investigation are:

- Conduct technical studies and develop approaches for estimating uncertainties associated with model input parameters in the dose reconstruction process.
- Create a methodology for incorporating probabilistic uncertainty analysis into dose reconstructions related to exposures to external gamma rays and internally-deposited radioactive materials.
- Adapt dose models and create computational tools with improved capabilities in assessing uncertainty in reconstructed doses using accepted probabilistic methods for external gamma rays and internally-deposited radioactive materials.
- Demonstrate the feasibility of the developed methodologies and tools through application to case studies that are representative of large groups of participants.
- Compare the results of probabilistic dose reconstructions for the case studies with current methods that use high-sided estimates and upper bound factors mandated in interim policy.

The steps necessary to achieve the aforementioned objectives include the following:

- Identify key model parameter measurement- and activity-based uncertainty and variability and characterize corresponding probabilistic distributions.
- Select and develop appropriate software tools capable of performing Monte Carlo (MC) simulations for the purpose of estimating dose distributions for specific cohorts and exposure scenarios.
- Perform tests of the simulation models and assess the success of the methods for supplying reasonable dose estimates and associated uncertainties through application in the sample cohort case studies.

This report is organized into seven sections, a reference listing and seven appendices. Section 2 provides the background about the need for the study; Section 3 describes relevant dose calculation and statistical methods for radiation dose estimation and uncertainty modeling. Section 4 presents the technical approach and methodologies and concentrates on 11 parameters and dose reconstruction factors and associated uncertainty distributions. Section 5 reports the results of six case studies, Section 6 discusses the methods and results of a sensitivity analysis, and Section 7 discusses conclusions and provides recommendations. Appendices A through F provide detailed descriptions of the case studies for the selected participant units including

scenario of radiation exposures and environment, model input data, and results. Finally, Appendix G provides information and rationale used on the dependencies and correlations of model parameters.

2 BACKGROUND

The NTPR Program reconstructs radiation doses for atomic veterans when personnel dosimetry (film badge) results are not available according to the requirements specified in governing regulations (Title 32 Code of Federal Regulations Part 218) (DoD, 2009). The reconstructions combine information about personal activities, the radiation environment, and scientific and technical principles to estimate radiation doses and their uncertainties. Traditionally, the methods have used high-sided estimates for parameters and uncertainties that are difficult to characterize. These high-sided estimates were considered to overestimate actual doses and therefore provided reliable upper bounds.

In a 2003 review of DTRA's dose reconstruction program, a committee of the National Research Council of the National Academy of Sciences (NAS/NRC) concluded that although central estimates of reconstructed doses for external gamma exposures were valid in most cases, upper bounds could not always be shown to be at least as great as a 95 percent upper confidence limit (NRC, 2003). As a result, the Committee recommended "… a comprehensive re-evaluation of the methods being used to estimate doses and their uncertainties to establish more credible upper-bound doses to atomic veterans." In a 2004 report to Congress, DTRA and the Department of Veterans Affairs (DVA) acknowledged these findings and committed to plans to improve models for calculating the upper bound in the total reconstructed external gamma dose, and for estimating the inhalation dose to participants in Nevada tests (DOD/DVA, 2004).

In response to other NAS recommendations, DOD and DVA jointly established the VBDR with a memorandum prepared by the Undersecretary of Defense (USD, 2004) to oversee the dose reconstruction process. The VBDR established subcommittees to perform the majority of its work. Specifically, Subcommittee 1 on Dose Reconstruction audited radiation dose assessments, reviewed methodologies, and developed conclusions and recommendations. In October 2007, the VBDR recommended to DTRA to develop procedures that use probabilistic analyses in dose reconstructions, and to discontinue using default upper bound factors that were mandated in interim policy (VBDR, 2007). DTRA endorsed efforts to pursue thiss recommendation, which forms the basis for the investigations documented in this report (DTRA, 2007c).

In addition to the aforementioned activities toward implementation of the VBDR's recommendations, DTRA also tasked SENES Oak Ridge to investigate whether the DTRA policy of applying an upper bound factor of three to external reconstructed doses was adequate for providing an upper bound with at least 95 percent credibility. SENES approached the investigation by performing a review to verify whether upper bounds determined by applying the factor of three to doses supplied in previous unit dose reconstruction reports was adequate to contain at least 95 percent of the reported film badge readings for the same unit.

At about the same time, a committee of the National Council on Radiation Protection (NCRP) published a report that addressed uncertainties in external dose reconstruction (NCRP, 2007). This report provides important information for the approach and methods employed in this study. A complementary study addressing uncertainties in internal radiation dose reconstruction is underway by another committee of the NCRP and will be reviewed for relevance to this study after it is published.

3 RADIATION DOSE ESTIMATION AND UNCERTAINTY MODELING

This Section contains general discussions of the dose reconstruction methodologies and uncertainty distributions relevant to the case studies of this report. Section 3.1 defines the three types of doses that are calculated. Methodologies used for external dose reconstruction are described in Section 3.2, and those for internal dose reconstruction in Section 3.3. The fundamentals of uncertainty modeling are discussed in Section 3.4.

3.1 Definitions of Types of Parameters and Doses

This report involves the calculation of "nominal," "probabilistic" and "deterministic" doses, which are described further in the following discussions.

3.1.1 Nominal Doses

To build model input parameter distributions for the probabilistic analyses conducted in this study, realistic central estimates (or best estimates) are useful, many of which were recorded from measurements and documented in operational and technical reports. In other cases where data are not available or not well documented, surrogate data are used. Analysts with extensive knowledge of NTPR-related historical information used their collective and subjective judgments within a collaborative process to make best estimates of input parameters and related uncertainty distributions. The best estimates for central values of model parameters are termed "nominal values."

As nominal values are usually based on documented observed data or best estimates, they are used in building the statistical distributions of each uncertain parameter. Other nominal values are extracted from numerically generated distributions which are based on physical and mathematical models that characterize input parameters and their uncertainty and variability. Nominal dose calculations provide point estimates using a dose reconstruction model with nominal values for all of its input parameters.

In addition, nominal values are used as input parameters for model sensitivity analyses. In this case, model parameters or groups of related parameters are varied one at a time. While one single input parameter is allowed to vary within its range of values based on its own distribution, all other parameters in the model are held to their nominal values. The outcome of such analyses allows evaluating the sensitivity of a dose model to its input parameters, thus showing which parameter uncertainties would have the most influential effect on the dose distribution.

3.1.2 Probabilistic Doses

The probabilistic models use nominal values as central estimates to define the probability distributions for each input parameter. Depending on the type of distribution employed, the central estimate can be the arithmetic mean (hereafter called mean), geometric mean, median or mode (peak). A full probabilistic analysis, where all uncertain input parameters are assigned distributions, results in a dose distribution that reflects both uncertainty and variability of the reconstructed dose. The upper bound dose for a probabilistic analysis is defined for the purpose of this report as the 95^{th} percentile value of the dose distribution. The uncertainty factor is

defined as the ratio of the 95th percentile value to the central value of the dose distribution. Note that "uncertainty analysis" is sometimes used in this report in place of "probabilistic analysis."

3.1.3 Deterministic "NTPR" Doses

The NTPR program has historically relied on dose reconstruction models that utilize conservative "high-sided" input parameters and processes to generate what are termed in this report "deterministic" doses. Such doses are not the same as nominal doses and should, in principle, be equal to or higher than nominal doses.

The "deterministic upper bound" dose is defined as the deterministic dose multiplied by a fixed factor. The fixed factors are currently equal to three (×3) for external reconstructed doses and 10 (×10) for internal reconstructed doses, as defined by an interim action referenced in the NTPR Policy and Guidance Manual (DTRA, 2007a). These factors are believed to result in upper bound doses equal to or greater than the 95th percentile of a probabilistically-based distribution prepared using credible distributions of the important parameters that contribute to uncertainty. The deterministic upper bound dose is expected to equal or to be higher than the 95th percentile value of the dose distribution resulting from a credible probabilistic analysis.

3.2 Whole Body External Dose

Whole body external dose results from exposure to radiation sources outside the body whose emissions are sufficiently penetrating so as to deposit energy throughout the body. The radiation sources relevant to NTPR include:

- Initial nuclear radiation: Neutrons and gamma rays emitted from the fireball and the cloud column during the first minute after a nuclear explosion.
- Residual nuclear radiation: Nuclear radiation emitted from fission products, soil activation products, and other radioactive debris at times greater than 1 minute after a nuclear detonation.

In the case studies described in this report, none of the participants were exposed to initial nuclear radiation. The most commonly encountered source of residual radiation is gamma rays emitted from fallout particles, but some test participants were also exposed to gamma rays emitted from neutron activation products in the soil. Methodologies useful in reconstructing doses from exposures to these two source types are discussed in Sections 3.2.1 and 3.2.2, respectively. The whole body external doses from gamma radiation were frequently measured by individual film badges affixed to the external clothing of the participants; film badge dosimetry for nuclear test participants is addressed briefly in Section 3.2.3.

3.2.1 External Dose from Exposure to Fallout

Fallout was the prevalent source of exposure for most nuclear test participants. The geographical pattern of the fallout field was determined primarily by the direction and magnitude of the prevailing winds above the test site. At the Nevada Test Site (NTS), test participants operated in the vicinity of both freshly deposited fallout and fallout that had been deposited days or weeks prior to exposure while in the test area, and occasionally resided in camps that received light fallout. Personnel who participated in the oceanic tests also were exposed to both freshly

deposited and older fallout on residential and recreational land areas and on ships supporting the operation. The fallout fields are characterized by radiation intensity measurements taken at specific times and locations after the detonation. The intensities at later times can be readily estimated from these data because fallout intensity decays in a reasonably predictable manner.

For NTS tests, monitors conducted radiological surveys shortly after virtually all of the shots, documenting exposure rates (typically referred to in this report as "intensities") at specified times and locations (Hawthorne, 1979). Thus, the radiation intensities in the vicinities of these shots are relatively well known and can be estimated for later times using time scaling techniques discussed below. A test participant marching through or operating in such a fallout field experienced radiation intensities that varied in time due to (1) his movement through the non-uniform field and (2) radiological decay. Let $I(t,\vec{r}(t))$ denote the free field intensity at a participant's time-varying location $\vec{r}(t)$ at time t. $I(t,\vec{r}(t))$ is often expressed in units of roentgen per hour (R hr^{-1}). The dose D (rem) from operating in that fallout field is then given by:

$$D = 0.7\int_{t_1}^{t_2} I(t,\vec{r}(t))dt \qquad (3\text{-}1)$$

where the interval $t_1 \rightarrow t_2$ encompasses the time he spent in the fallout field. The coefficient 0.7, often called the "film badge conversion factor," converts from roentgen (as measured by a survey instrument) to rem (as would be assigned from a film badge reading) by taking into account the shielding of the film badge to gamma radiation by the human body for a person standing upright in a large planar fallout field. It is acknowledged that the film badge conversion factor has associated uncertainties; however quantification of the uncertainties is deferred for future studies. The integration in Equation 3-1 must often be performed numerically, since $I(t,\vec{r}(t))$ generally cannot be reduced to a tractable functional form.

In many scenarios of interest, a test participant remained for significant periods of time in an essentially uniform fallout field or in a possibly non-uniform field for which only an average intensity is known. This occurred for NTS and oceanic participants whose residential, working or recreational areas were contaminated by fallout, and for oceanic participants who resided on ships that received topside fallout, or were exposed to shine or contaminated surfaces. In these cases, the intensity takes the simplified functional form $I(t)$, indicating that a participant's dose (Equation 3-1) does not depend on the details of his movement within the field. In the latter scenario involving a non-uniform field, $I(t)$ is interpreted as the intensity averaged over a confined area of contamination such as an island or ship's weather deck.

The following section discusses various representations of the time dependence of intensity.

3.2.1.1 Modeling of Fallout Intensity Decay

The change in fallout intensity with time is dependent on radiological decay as well as environmental processes such as weathering and human influences such as decontamination. In general, only radiological decay is explicitly accounted for in NTPR analyses, except when specific actions such as decontamination are known to have occurred. However, in cases where a decay function is based on measured intensities, all processes that affect the intensities are

implicit in the measured values, and hence the intensity function, over the period of time the measurements were taken.

The functional dependence of fallout intensity on time can be specified in various ways. For the time interval during which fallout was descending, time-intensity data pairs are often available. A generic example of such data is shown in Table 1.

These early-time intensity data are modeled by applying a curve fitting algorithm to produce an "early time intensity function," named $I_{early}(t)$ in this example. Mathcad®, the principal computational platform used for NTPR dose reconstruction, offers a number of options for functional fitting of data sets. Linear interpolation in logarithmic space is often used for the early-time intensity function. In Mathcad syntax, this takes the form

$$Iearly(t) = 10^{linterp[T,\ log(EarlyI),\ t]} \tag{3-2}$$

The right side of this equation is simply 10 raised to the power of the base-10 logarithm of the intensity at time t, as linearly interpolated ("*linterp*") from the time-intensity data of Table 1, where T is the time vector (t_0, t_1, t_2) and *EarlyI* is the intensity vector (I_0, I_1, I_2). Linear interpolation in linear space and cubic spline fitting ("cspline") have also been used for this purpose.

Table 1. Generic Example of Early Time Intensity Data

Time after Detonation (*t*, in hours)	**Measured Intensity (*EarlyI*, in R hr^{-1})**
$t < t_0$	0
t_0	I_0
t_1	I_1
t_2	I_2
t_3	I_3
t_4	I_4

It is well documented (e.g., Glasstone and Dolan, 1977, p. 451) that, following the end of deposition, the time variation of the radiation intensity of the fallout can be approximated as $t^{-\lambda}$, where t is the time after detonation and λ is constant over specified periods of time. The most frequently used values of λ are 1.2 for the first 6 months (4380 hours) after detonation and 2.2 thereafter. However, the decay of fallout material from specific shots is sometimes better characterized by other values of λ. Decay rate uncertainties have been addressed in the probabilistic analysis, as discussed in Section 4.2.4. As an example of shot-specific decay, the contaminants produced by Shot BAKER of Operation CROSSROADS were observed to decay as $t^{-1.3}$, so a value of $\lambda = 1.3$ is generally used in that case (Weitz et al., 1982). Occasionally multiple values of λ, each applicable for a specified period of time, are used to better quantify the time variation of the post-deposition fallout intensity for specific shots. A generic example is given in Table 2. In this example, time t_3, found in Table 1 and Table 2, corresponds to the time of peak intensity, and t_4, found in Table 1, corresponds to the last early time intensity. Time t_5, found in Table 2, corresponds to the end of the operational period; this time is often used to

define a period for use of a unique decay constant (λ_2), so determined such that when used, legacy tabulations of intensity measurements can be matched.

Table 2. Generic Example of Multiple Decay Exponents

Time Interval (hours)	Decay exponents λ_i
t_3 to t_5	λ_1
t_5 to 4380	λ_2
$t > 4380$	2.2

The pre- and post-deposition intensity parameterizations can be integrated into a single "intensity calculator function," $ICF(t)$, which is applicable for all times. The intensity calculator function for the generic parameters in Table 1 and Table 2 can be expressed as

$$
\begin{aligned}
&ICF(t) = 0 && \text{if } t < t_0 \\
&ICF(t) = I_{early}(t) && \text{if } t_0 \le t < t_3 \\
&ICF(t) = I_3 \, (t_3/t)^{\lambda_1} && \text{if } t_3 \le t < t_5 \\
&ICF(t) = I_3 \, (t_3/t_5)^{\lambda_1} \, (t_5/t)^{\lambda_2} && \text{if } t_5 \le t < 4380 \\
&ICF(t) = I_3 \, (t_3/t_5)^{\lambda_1} \, (t_5/4380)^{\lambda_2} \, (4380/t)^{2.2} && \text{if } t \ge 4380
\end{aligned}
\qquad (3\text{-}3)
$$

A plot of $ICF(t)$ (solid black curve) overlaid on early-time measured intensity data (squares) is shown in Figure 1 for the following time/intensity pairs, which specify the intensity on Parry Island, Enewetak Atoll, caused by fallout from Operation GREENHOUSE Shot EASY:

- $t_0 = 17$ hr, $I_0 = 0.0001$ R hr^{-1}
- $t_1 = 20$ hr, $I_1 = 0.00035$ R hr^{-1}
- $t_2 = 22$ hr, $I_2 = 0.00065$ R hr^{-1}
- $t_3 = 24$ hr, $I_3 = 0.001$ R hr^{-1}
- $t_4 = 30$ hr, $I_4 = 0.00085$ R hr^{-1}

The $ICF(t)$ curve in Figure 1 was decayed using $\lambda_1 = 1.1$ for the interval t_3 to t_5 (=978 hrs), $\lambda_2 = 1.2$ for the interval t_5 to 4380, and $\lambda = 2.2$ thereafter. Note that in this example, the last early time/pair (t_4, I_4) is not used to define $ICF(t)$ because it occurs after the peak time (t_3, I_3) and falls on the decay curve.

The computer code FIIDOS (Fallout Inhalation and Ingestion Dose to Organs, Version 4) was developed in the NTPR Program as a primary tool for internal dose reconstruction (Raine et al., 2007). Starting with a shot-specific initial inventory of radionuclides (taken, for example, from Hicks, 1984), the code calculates the subsequent production and decay of fission products, activation products, and actinides. (It is generally assumed in these calculations that no

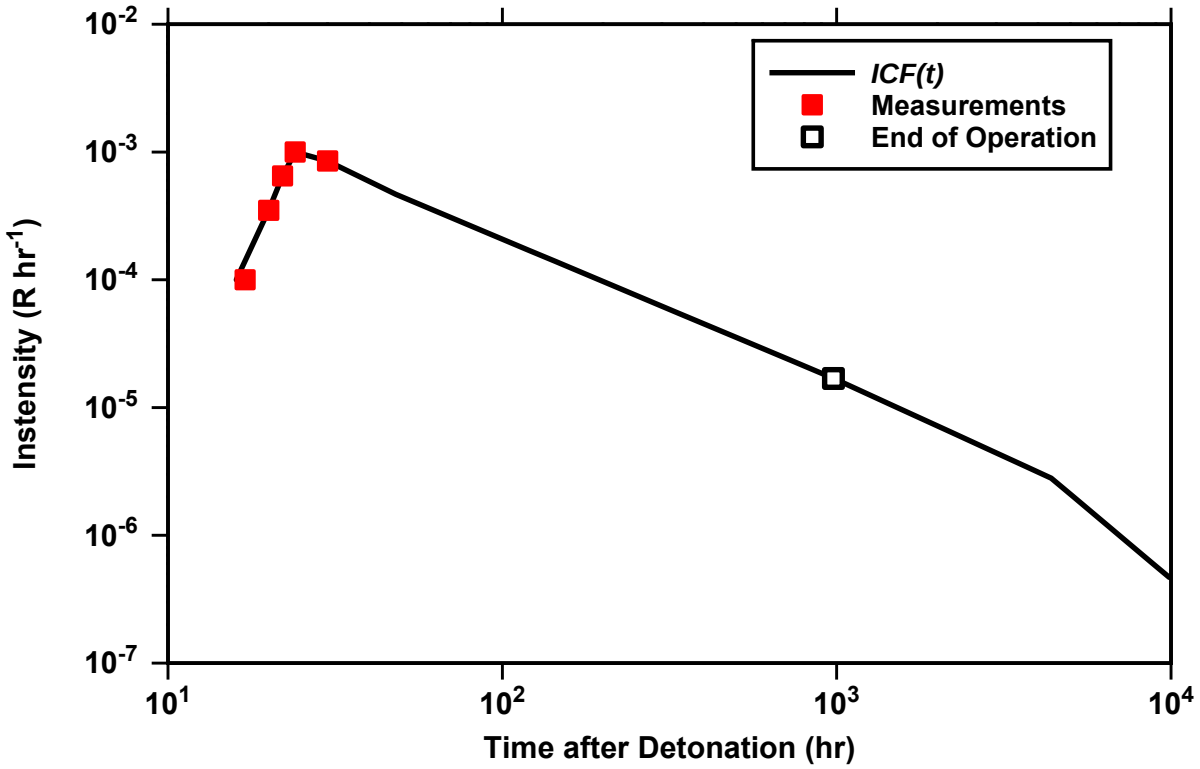

Figure 1. Graph of *ICF*(*t*) and Early Time Intensity Data

fractionation occurred except for the removal of noble gases. However, additional fractionation and other processes such as weathering may be included in the future as refinements to the FIIDOS inventories.) The code tallies (among other things) the collective gamma emissions and intensities at 42 times ranging from 3 seconds to 5 years after the detonation. This output can be utilized directly to define $I(t)$ for virtually any shot of interest. Intensities as functions of time for selected shots, normalized to $I = 1$ R hr^{-1} at $t = 1$ hour, are plotted in Figure 2.

In the above (FIIDOS) representations of fallout intensity decay, weathering has been neglected. Weathering generally causes the intensity to diminish at a faster rate due to runoff, leaching and migration of the contaminants into the soil. As a result, the use of these formulations may result in somewhat high-sided dose estimates for exposures that took place a few weeks or more after deposition.

3.2.1.2 Effects of Shielding

The radiation intensity inside a structure surrounded by fallout was less than that which existed outside the structure due to (1) attenuation of the radiation by the walls, roof, and other intervening materials and (2) the displacement of the radiation source from interior locations. The shielding afforded participants while inside structures for land-based scenarios is quantified in terms of a "protection factor," defined as the average free-field intensity outside the structure

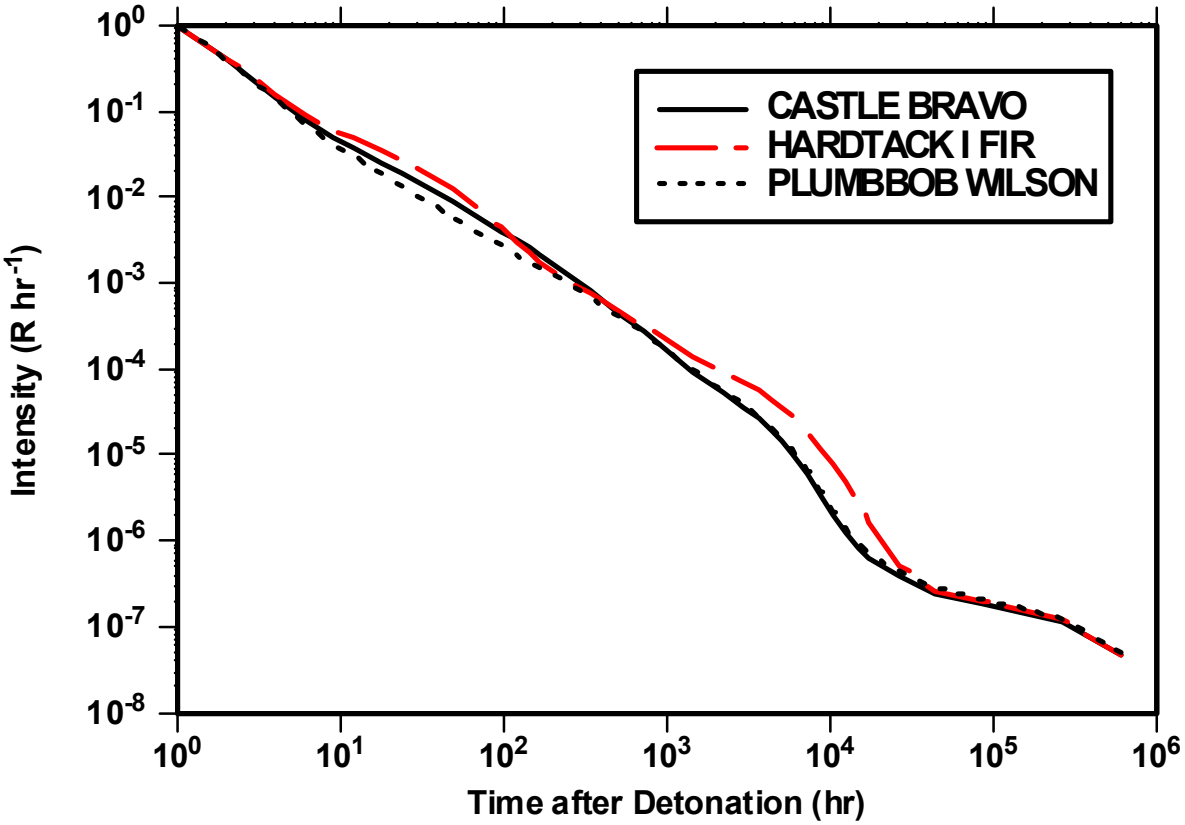

Figure 2. FIIDOS-Derived Intensity Functions for Selected Shots

divided by the free-field intensity inside the structure. Thus, the dose accrued during a given time interval spent inside a structure with protection factor *PF* is equal to the dose that would have been accrued during the same time interval outside the structure divided by *PF*. Specific values of *PF* that have frequently been used in deterministic dose reconstructions are 2.0 for permanent and semi-permanent structures such as barracks, office buildings, and Quonset huts, and 1.5 for tents (Goetz et al., 1987). Because the intensity inside a structure varies with location, *PF* can be expressed as a probability distribution, as described in Section 4.2.2.

In an analogous manner, the shielding afforded crewmen while below deck on a ship that had received topside fallout is frequently expressed as a shielding factor, defined as the free-field intensity below deck divided by the free-field intensity topside. (Note that this is the reciprocal of the protection factor.) Thus, the dose accrued during a given time interval spent below deck, where the shielding factor was *SF*, equals the dose that would have been accrued during the same time interval topside multiplied by *SF*. A value of $SF = 0.1$ is frequently used for below deck areas (Rinnert, 1957) in deterministic dose reconstructions. As with the protection factor, the shielding factor can be represented by a probability distribution, reflecting the range and frequency of values of *SF* at the various below deck locations. It is recognized that during early times post detonation the specific times of shielding, as opposed to the fraction of time shielded, are important because of the rapidly decaying exposure rate. Additional consideration of this effect is a matter for future refinements.

3.2.2 External Dose from Exposure to Activated Soil

For shots at NTS that were detonated at altitudes such that the neutrons reached the surface but the fireball did not, the residual radiation intensity near ground zero (GZ) was dominated by neutron-activated radionuclides in the soil. In these cases, nearly circular radiation intensity contours were formed around GZ due to the neutron activation of the soil. These contours were measured by radiation monitors shortly after the detonations and are documented in Hawthorne (1979). Doses to personnel who traversed the activated area can be reconstructed by evaluating Equation 3-1, but the temporal dependencies discussed above for fallout no longer apply. An accurate determination of the intensity of an activation field as a function of time requires knowledge of the elemental constituents of the soil in the vicinity of the burst, the neutron absorption cross sections of the constituents, the decay properties of the reaction products, and the attenuation of the emitted radiation by the intervening soil. This analysis can be performed in a spreadsheet, supplemented by a limited number of radiation transport calculations. In this manner, it is found that sodium-24 (^{24}Na, half-life = 15 hours) was the dominant radioisotope the first two days after a detonation over typical NTS soil. Other activation products relevant for NTS exposures include manganese-56 (^{56}Mn, half-life = 2.6 hours) and potassium-42 (^{42}K, half-life = 12.4 hours). Although the uncertainties in this analysis are not currently included here, future refinements could include uncertainties in variables such as concentrations of elemental constituents in the soil, and attenuation by soil.

3.2.3 Film Badge Dosimetry

During the period of U.S. atmospheric nuclear weapon testing, the exposure of military and civilian personnel to external radiation was monitored primarily with film badge dosimeters. Specific details regarding film badge dosimetry practices employed for the atmospheric nuclear testing operations are found in NRC (1989). That detailed information can be summarized as follows: prior to Operation CASTLE in 1954, film badges were typically issued only to individuals involved in activities with anticipated potential for radiation exposure (e.g., cloud samplers and associated ground crews, sample recovery teams, decontamination crews, radiation safety personnel). At CASTLE, cohort badging was introduced as a means of monitoring the radiation exposures of all individuals, regardless of their anticipated potential for exposure. At Operation REDWING in 1956, film badge dosimetry practices were further expanded. Permanent film badges, which were to be worn at all times, were issued to all individuals who entered the test area. In addition, individuals involved in activities with potential for radiation exposure were issued mission badges for those activities. Mission badges were to be worn with the individual's permanent film badges. For test series subsequent to Operation REDWING, most individuals were issued one or more film badges for the duration of their participation.

NRC (1989) identifies three principal types of error that affected film badge dosimetry results for atmospheric nuclear test participants: radiological, laboratory, and environmental. Based on an evaluation of the impact of these errors on the film badges used at each test series, this reference provides, by series, an overall "exposure" bias factor B and an uncertainty factor K. The interpretation of B and K and their application to quantifying the uncertainty in a film badge reading are addressed in Section 3.4.1.3. It is noted here that, for the purpose of comparing film badge readings with reconstructed doses, the bias should first be removed from those readings by dividing them by B (or incorporated into the reconstructed doses by multiplying them by B). The

overall topic of cohort badges is to be the subject of a separate report and is thus outside the scope of this report.

3.3 Internal Dose

Internal organ doses result from exposures to radioactive sources inside the body. Participants in nuclear weapons tests could have accrued internal doses as a result of intakes of radionuclides by inhalation, ingestion, or absorption through the skin or open wounds. Intakes by inhalation are the most common pathway for the majority of participants; most exposure scenarios involve inhalation of descending fallout and/or fallout that had been deposited previously on the ground or other surfaces and subsequently resuspended into the air. Additional pathways of internal exposure involve the consumption of food and/or water that has been contaminated by fallout and the incidental ingestion of contaminated soil. Absorption of radionuclides through the skin or an open wound is uncommon in exposures of atomic veterans and is not considered in the case studies.

Internal dose cannot be measured directly but must be estimated based on other available data. Because no relevant air monitoring data and very little bioassay data are available for atmospheric nuclear test participants, indirect methods must be used. The methods are based on available data, such as gamma intensity measurements, used in conjunction with models and various assumptions. (Barrett et al., 1986)

Calculation of internal organ doses requires the use of factors that convert intakes of radioactive material to the dose each organ would receive from that intake. Organ doses resulting from intake of a single radionuclide, such as a soil activation product, are calculated using ICRP-recommended *dose coefficients*. These dose coefficients relate organ-specific equivalent doses to intake of a single radionuclide, and are generally tabulated in units of sievert per becquerel (Sv Bq^{-1}). Because most internal exposure scenarios associated with nuclear testing involve intakes of mixtures of radionuclides, the dose to an organ or tissue of concern is the sum of the doses from intakes of all of the radionuclides. Thus, composite *dose conversion factors* (*DCF*s) that apply to mixtures of radionuclides have been calculated with the FIIDOS code using ICRP *dose coefficients* and are used in most assessments. As used in this report, the term *dose coefficient* recommended by the ICRP pertains to the equivalent dose from a unit intake of a single radionuclide, and the term *dose conversion factor* pertains to a similar dose quantity for mixtures of radionuclides, such as in fallout, and is reported in units of rem per curie (rem Ci^{-1}). The radionuclide composition of any mixture is based on shot-specific radiochemistry data. The concentration and composition of radionuclides on the ground and in air, and the associated composite *DCF*s, are time-dependent due to radioactive decay and in-growth.

3.3.1 Inhalation Intakes

Any estimate of inhalation dose is based on the following simplified equation:

$$\Delta D = AA \cdot BR \cdot \Delta T \cdot DF \tag{3-4}$$

where:

ΔD = 50-year committed equivalent dose (CED) (rem) to the organ or tissue of interest over an incremental time period

AA = airborne activity concentration (Ci m^{-3}) of radioactive material

BR = breathing rate (m^3 hr^{-1})

ΔT = incremental time period of exposure (hr), with established start and stop times

DF = CED inhalation dose factor for the organ or tissue of interest (rem Ci^{-1}) (DF can be an inhalation dose coefficient or an inhalation dose conversion factor)

There are four basic pathways for the inhalation of radioactive material by nuclear test participants: (1) inhalation of fallout particles deposited on the ground or other surfaces and resuspended by mechanical or natural disturbances, or, in limited cases, by thermal effects of a shot; (2) inhalation of radioactive material contained in descending fallout; (3) inhalation of neutron-induced radioactivity in the soil (or other material) lofted into the air by mechanical or natural disturbances; and (4) inhalation of radioactive material in an atmospheric cloud. (Barrett et al., 1986)

The following sections describe methods that have been used to estimate inhalation doses to atomic veterans for the first three pathways identified above. Inhalation of radioactive material in an atmospheric cloud is not a common exposure pathway, is not relevant to the case studies addressed in this report and is thus excluded from this report.

3.3.1.1 Inhalation of Fallout Resuspended From Surfaces

Because measured air concentrations of radionuclides are not generally available for contaminated areas occupied or visited by nuclear test participants, air concentrations resulting from resuspension of radioactive material from surfaces must be estimated. For this pathway, the inhalation intake is assumed to occur concurrently with the accrual of external dose from the deposited material. An airborne concentration of radioactive material is estimated through the use of a factor that relates the surface activity (SA) in curies per square meter (Ci m^{-2}) to the corresponding gamma radiation intensity, I (R hr^{-1}), measured at a given distance (nominally 1 meter) above the surface. Time-dependent surface activity-to-intensity factors ($SA/I(t)$ denoted $FR(t)$) for each shot have been calculated for specific times post-detonation using the FIIDOS code. Thus, by using the measured radiation intensity and a pre-calculated surface activity-to-intensity factor, a time-dependent surface activity is effectively estimated. By multiplying by a resuspension factor K (m^{-1}), which is the ratio of air activity concentration in Ci m^{-3} to surface activity density in Ci m^{-2}, an air concentration is estimated. (Barrett et al., 1986, p. 5)

A generalized expression for the calculation of organ doses as 50-year CEDs from the inhalation of resuspended fallout is

$$D_{inh}(t) = GSMF \cdot \int_{T_{Start}}^{T_{End}} I(t) \cdot FR(t) \cdot K(t') \cdot BR \cdot DCF_{inh}(t) \cdot dt \qquad (3\text{-}5)$$

where:

$D_{inh}(t)$ = 50-year CED to the organ (rem)

$GSMF$ = gamma source modification factor

T_{Start}	=	start of exposure, generally when fallout was deposited (hr)
T_{End}	=	end of exposure, generally when individual left the contaminated area (hr)
$I(t)$	=	gamma radiation intensity (R hr^{-1})
$FR(t)$	=	time-dependent and shot-specific ratio of surface activity density to radiation intensity (Ci m^{-2} per R hr^{-1})
$K(t')$	=	resuspension factor (Ci m^{-3} per Ci m^{-2}, or m^{-1})
BR	=	breathing rate (m^3 hr^{-1})
$DCF_{inh}(t)$	=	time-dependent and shot-specific inhalation dose conversion factors (rem CED per curie of intake) for a specific organ
t	=	time after detonation of exposure (hr)
t'	=	time after deposition of fallout (hr)

In this formulation, *GSMF* adjusts the activity density for finite sources relative to infinite plane sources to achieve a given intensity measurement. This is necessary because the $FR(t)$ ratios were calculated with FIIDOS assuming an infinite plane source. This applies primarily to shipboard exposures, where a typical value of *GSMF* is 2.

The resuspension factor $K(t')$ adopted for use in deterministic land-based calculations as discussed in Section 3.1.3 is given by the time-dependent expression:

$$K(t') = 10^{-5} \cdot e^{-0.01\frac{t'}{24}} + 10^{-9} \tag{3-6}$$

where t' is in hours after deposition and $K(t')$ is in m^{-1}. This formulation, reported in Till and Meyer (1983), is similar to functions proposed by other studies.

The resuspension factor $K(t')$ adopted for use in nominal land-based calculations is given by the time-dependent expression:

$$K(t') = 10^{-5} \cdot e^{-0.07\frac{t'}{24}} + 6 \cdot 10^{-9} \cdot e^{-0.003\frac{t'}{24}} + 10^{-9} \tag{3-7}$$

where t' is in hours after deposition and $K(t')$ is in m^{-1}. This formulation, reported in Anspaugh et al. (2002), is based on an extensive review of all resuspension measurement data. Because the formulation is intended to describe the observed results over the entire span of an expanded dataset, it is currently used for both NTS and PPG scenarios. For shipboard applications, a resuspension factor of 10^{-5} m^{-1} for the first 4 days after deposition and zero thereafter is utilized. The use of a value of zero after 4 days is based on the fact that naval ships were routinely washed or scrubbed regardless of the presence of any contamination. Therefore, any fallout remaining on a ship after several days would be strongly bound to the surface and would not be susceptible to resuspension.

Inhalation of fallout that was resuspended by the thermal pulse or blast (shock) wave produced by a detonation is also a potential source of exposure at the NTS. This pathway is limited in its

applicability, and NTPR addresses it using an evaluation of potential inhalation doses resulting from this resuspension conducted by Kocher et al. (2006)[1]. That report provides central estimates and associated uncertainty for "effective" resuspension factors as well as other resuspension factors that are useful for the nominal and probabilistic resuspension analyses in this report. Kocher et al. use the term "effective" to indicate that these resuspension factors do not necessarily correspond to actual values that may have applied to radionuclides that could have been inhaled at the time of exposure, but rather they are to be used to ensure that credible upper bounds of inhalation doses are obtained in deterministic NTPR dose analyses for scenarios involving resuspension by detonations. Resuspension factors for two regions around ground zero are available: the precursor region, where resuspension was caused by the initial thermal pulse from a detonation, and the more distant blast-wave region, where resuspension was caused by blast effects (high winds). The other relevant resuspension factors available in Kocher et al. (2006) that were used in the nominal and probabilistic analyses described in this report are those that account for respirable and for inhalable but non-respirable forms of resuspended fallout. The factors considered in developing these resuspension factors are discussed in detail in Kocher et al. (2006), and the values from that report that are used in the PLUMBBOB case study are given in Section 4.2.6.

A deterministic breathing rate of 1.2 m^3 hr^{-1} has generally been used in the NTPR Program. This breathing rate applies to an adult male during light activity, comparable to walking at a rate of 3 miles per hour on a flat firm surface (Barrett et al., 1986, p. 13; NCRP, 1997, p. 31). For more or less strenuous activity, different breathing rates can be applied as appropriate. Additional breathing rates and probability distribution functions for breathing rate for different levels of activity for NTPR participants are discussed in detail in Section 4.2.7.

3.3.1.2 Inhalation of Descending Fallout

The inhalation of descending fallout (Barrett et al., 1986, p. 24–26) can be considered the ground-based analog of the inhalation of cloud debris. Except for the onset of fallout or for very fine particles, the radiation intensity at the breathing zone (nominally the 1.6 meter of air immediately above the Earth's surface) is dominated by fallout already deposited. This follows from the deposition velocities of fallout particles, the range of gamma radiation, and the duration of fallout deposition at a given position.

A generalized expression for the calculation of organ dose from inhalation of descending fallout is given in Weitz (2009a) as

[1] This draft report was recently published with several changes in terminology, resuspension values, and values for uncertainty factors for several parameters. See Kocher, D. C., Trabalka, J.R., and Apostoaei, A.J., 2009. Derivation of Effective Resuspension Factors in Scenarios for Inhalation Exposure Involving Resuspension of Previously Deposited Fallout by Nuclear Detonations at Nevada Test Site. DTRA-TR-09-15, *SENES, Oak Ridge, Inc.*, Oak Ridge, TN and Defense Threat Reduction Agency, Fort Belvior, VA.

$$D_{inh} = GSMF \cdot I(t_p) \cdot \left[\begin{array}{l} FBCF \cdot H_0 \cdot \frac{BR}{BR_0} \cdot \left(\sum_{i=1}^{n} \frac{AF_i}{V_i} \cdot \frac{R_i}{R_1} \right) \cdot DCF'_{inh}(t_p) \\ \quad + BR \cdot \left(\sum_{i=1}^{n} \frac{AF_i}{V_i} \cdot \left[NR_i - NR_1 \cdot \frac{R_i}{R_1} \right] \right) \cdot FR(t_p) \cdot DCF_{ing}(t_p) \end{array} \right] \quad (3\text{-}8)$$

where:

D_{inh} = 50-year CED to the organ (rem) from inhalation

$GSMF$ = gamma source modification factor

$FBCF$ = film badge conversion factor (0.7 rem R^{-1} from Raine et al. (2007))

H_0 = nominal height of stabilized cloud, 10^4 m

BR = breathing rate (m^3 hr^{-1})

BR_0 = deterministic breathing rate of 1.2 m^3 hr^{-1}

i = index of particle-size class bins

n = number of particle size bins employed (typically 3)

AF_i = activity fraction—the fraction of all activity deposited in a fallout event by particles in the i^{th} particle size class

R_i = fraction of i^{th} size class particles deposited in the thoracic airways of the respiratory tract (bronchial, bronchiolar, and alveolar-interstitial regions)

R_1 = fraction of particles in the 1-10 μm (i = 1) size class deposited in the thoracic airways of the respiratory tract

NR_i = fraction of i^{th} size class particles initially deposited in the posterior extra-thoracic (ET_2) region of the respiratory tract and subsequently cleared to the gastro-intestinal (GI) tract

NR_1 = fraction of particles in the 1-10 μm (i = 1) size class initially deposited in the ET_2 region and subsequently cleared to the GI tract

V_i = deposition velocity (m hr^{-1}), or average velocity of descent for i^{th} sized particles

t_p = time after detonation (hr) of maximum radiation intensity from fallout deposited on the ground or other surface, such as the weather deck of a ship

$I(t_p)$ = gamma radiation intensity (R hr^{-1}) at t_p

$FR(t_p)$ = FIIDOS-generated time- and shot-dependent ratio of surface activity density to intensity (Ci m^{-2} per R hr^{-1}) referred to as the "FIIDOS ratio"

$DCF'_{inh}(t_p)$ = shot-specific inhalation dose conversion factors at t_p with unit rem CED rem^{-1}; i.e. CED in rem to organ per dose to the whole body (rem) from a film badge reading

$DCF_{ing}(t_p)$ = shot-specific dose conversion factors at time t_p for CED from ingestion (rem Ci^{-1}) for the organ of interest (applies to those particles initially deposited in the ET_2 region and subsequently cleared to the GI tract)

In this formulation, *GSMF* and *BR* are as discussed for inhalation of resuspended fallout. The film badge conversion factor (*FBCF*) adjusts free-in-air exposure above a fallout field to exposures in the same fallout field reported for a film badge placed on a human body, which is generally at chest height. The factors related to particle size class including activity fractions AF_i, fractions of particles depositing in the thoracic airways R_i and the posterior extra-thoracic (ET_2) region NR_i, , and settling velocity V_i are discussed in detail in Weitz (2009a). Particle size classes designated Class 1, Class 2 and Class 3 are associated with particles with aerodynamic diameters of 1–10 μm, 10–20 μm, and 20–100 μm, respectively (Weitz, 2009a).

This formulation assumes the duration of fallout deposition at the site of interest was much smaller than the time after detonation at which it occurred (Weitz, 2009a). Two additional assumptions reduce Equation 3-8 to the more approximate form of the dose equation used in deterministic assessments.

- All fallout particles have aerodynamic diameters in the range of 1–10 μm, corresponding to the $i = 1$ size bin. This implies that $AF_1 = 1$, and $AF_i = 0$ for $i > 1$.
- Deposition velocity $V_1 = H_0/t_p$, the nominal height of the stabilized cloud divided by the time (after detonation) of the peak intensity at the site of interest.

The resulting deterministic form (Weitz 2009a) is

$$D_{inh} = GSMF \cdot FBCF \cdot \frac{BR}{BR_o} \cdot t_p \cdot I(t_p) \cdot DCF'_{inh}(t_p). \tag{3-9}$$

For the internal dose evaluation from descending fallout to be valid, the measured intensities must correspond to the deposited fallout and personnel exposure must correspond to the full period of deposition.

3.3.1.3 Inhalation of Suspended Soil Activation Products

The method for estimating airborne concentrations of radionuclides due to suspension of radioactive material produced by neutron activation in soil is similar to the method used in Section 3.3.1.1 involving resuspension of deposited fallout.

Relative activities of neutron-induced radioisotopes in soil are estimated on the basis of field intensity measurements, known elemental compositions of soil, neutron transport in air and soil, neutron capture in nuclei of stable elements in soil, and known decay characteristics of the product radioisotopes. Activities of radionuclides per unit volume of surface soil (Ci m^{-3}) are then determined by scaling the estimated relative activities to a calculated photon exposure in air above ground or exposure rate at a particular time that matches available measurements with film badges or field instruments, taking radioactive decay into account. Radionuclide activities per unit volume of surface soil are converted to equivalent surface concentrations (Ci m^{-2}) by assuming the top 1 cm of soil can be suspended in the air. Finally, an appropriate resuspension factor is applied to the calculated concentrations of radionuclides in surface soil to obtain an

estimate of the concentrations in air. As with resuspension of deposited fallout, an important condition in using this method is that the film badge or instrument readings must be due primarily to activation products in soil (Barrett et al., 1986, pp. 20–22; NRC, 2003, p. 97).

3.3.2 Ingestion Intakes

A pathway considered in the case studies of land-based units is incidental ingestion, which is a chronic type of exposure that involves the daily intake of relatively small quantities of contaminated soil and dust containing a mixture of radionuclides that changes with time. The sources of the ingested contamination include direct contact with airborne soil and dust due to walking, vehicular traffic, and wind-driven lofting of contaminated particles in areas where military personnel were temporarily stationed. Routine daily activities by test participants may also have involved the inadvertent ingestion of small quantities of soil and dust particles that adhered to food, beverages, cigarettes, or their hands. Technical guidance on incidental ingestion rates is available in publications from the U.S. Environmental Protection Agency (USEPA) and the U.S. Army Center for Health Promotion and Preventive Medicine (USACHPPM) (USEPA, 1996, 1997 and 2002; USACHPPM, 2003).

For this incidental intake of soil and dust scenario, the ingestion dose is calculated as follows:

$$D_{ing} = \int_{T_{Start}}^{T_{End}} I(t) \cdot \frac{SA}{I}(t) \cdot \frac{q_{ing}}{Thick_{soil} \cdot \rho_{soil}} \cdot DCF_{ing}(t) \cdot dt \qquad (3\text{-}10)$$

D_{ing} = 50-year committed equivalent dose (rem, CED) to an organ due to ingestion of contaminated material with either alpha or beta-plus-gamma emitting radioactive materials

ρ_{soil} = bulk density of soil (g m^{-3})

q_{ing} = average incidental ingestion rate (g hr^{-1})

$DCF_{ing}(t)$ = time-dependent and shot-specific ingestion dose conversion factors (rem CED per curie of intake) for a specific organ

$Thick_{soil}$ = thickness of soil layer available for intake, generally assumed to be 1 centimeter (0.01 meter)

After due consideration of the cited references, a soil/dust ingestion rate of 500 mg day^{-1} was selected for the deterministic soil ingestion model in all case studies as an upper bound value for the entire period of residence for military personnel who were stationed at NTS facilities, where dusty conditions were prevalent. This ingestion model is also applicable to personnel located on shore at the Pacific Proving Ground (PPG); the incidental ingestion rate for shipboard personnel is assumed to have been zero because ship decks were routinely washed or scrubbed. Because 500 mg day^{-1} rate is consistent with the highest value recommended in USEPA screening level guidance and USACHPPM exposure guidance for deployed military personnel, the resultant doses are credible estimates of upper bound doses. Parameter distributions for the probabilistic and nominal soil ingestion model are discussed in Section 4.

In addition, an upper-bound pathway considered in deterministic dose reconstructions is the ingestion of fallout material deposited on food. For each episode of descending fallout that could

reasonably have occurred during mealtimes, the test participant is assumed to have ingested an amount of fallout equivalent to a 15-minute deposition on a 9-inch diameter plate at the average rate of deposition. The ingestion dose conversion factors cited in Equation 3-10 are also employed in evaluating this internal dose component.

3.4 Uncertainty Modeling

3.4.1 Overview of Probability Distributions

Generally, probability distributions are mathematical expressions for calculating probability. The probability distributions used in this uncertainty analysis study are briefly described in this section. They include the uniform, Gaussian, lognormal, triangular, and log-triangular distributions. These are all continuous probability distributions, because the random variable of interest can take any real value within a defined continuous range (domain). When a distribution is normalized so that it sums (or integrates) to unity, it is referred to as a probability density function (pdf).

In a graph of a pdf, the vertical scale does not represent the actual probability of the corresponding x-axis value; the probability of a single x value is zero. Instead, it represents the probability (per x-axis unit) of generating a value within a very small range around the x-axis value. Specifically, the probability of finding a continuous random variable X between two values x_1 and x_2 is equal to the area under the pdf curve from x_1 to x_2. The probability that X will take a value not exceeding x_1 is the area under the pdf curve from its lower bound to x_1; this is often referred to as a cumulative probability function (cpf). The area under the entire pdf and the upper limit of the cpf are both one.

The references for Section 3.4.1 in its entirety are Bulmer (1979), Doane and Seward (2009), Hahn and Shapiro (1967), Kirchner (2008), NCRP (2007), NIST (2009), and Vose (2008).

3.4.1.1 Uniform Distribution

The uniform (or rectangular) distribution applies if all values of random variable X between a minimum value a and a maximum value b have an equal probability of being sampled. More precisely, X has the uniform distribution if the probability that X can take values within any segment of a fixed width in the range from a to b is the same for all segments of the same width. Alternatively, a random variable is uniformly distributed whenever the probability is inversely proportional to the interval's length. The uniform distribution is shown in Figure 3.

The uniform distribution is a cumulative distribution in the sense that probabilities for specified ranges of X are associated with areas under the bounding rectangle for the distribution. For any value x^*, $a \le x^* \le b$ ($a < b$), the probability that X will be at most x^* (cpf) is

$$Prob(X \le x^*) = \frac{x^* - a}{b - a} \tag{3-11}$$

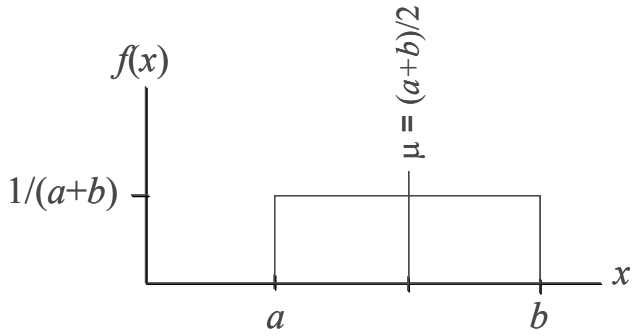

Figure 3. Probability Density Function of a Uniform Distribution

The probability that X will take any value between c and d, $a \le c \le d \le b$ ($a < b$), is

$$Prob(c \le x \le d) = \frac{c-d}{b-a} \tag{3-12}$$

The mean and standard deviation of an uniform distribution are, respectively,

$$\mu = \frac{a+b}{2} \qquad \sigma = \frac{b-a}{\sqrt{12}} \tag{3-13}$$

The median (the 50th percentile) of the uniform distribution is μ. However, the uniform distribution has no mode (that is, all values are equally probable).

The uniform distribution is used as a very approximate model when there is little or no available data. It is often used to assess whether it is appropriate to assign uncertainty to a parameter. In this use, a parameter is assigned a uniform distribution with reasonably wide bounds and a sensitivity analysis is performed to determine whether or not the parameter produces any influence on the output uncertainty; if it does not, it may as well be left as a single-valued parameter. Rarely, a parameter may truly be uniformly distributed, as the angular resting position of a camshaft after spinning.

3.4.1.2 Gaussian Distribution

Also known as the normal distribution, the Gaussian distribution is defined by two parameters, the mean μ and the standard deviation σ. The Gaussian distribution has the following properties:

- The curve of the Gaussian distribution (referred to hereafter as the Gaussian curve) is "bell-shaped" with one central peak.
- The width of the bell is measured by the standard deviation σ.
- The peak occurs at the mean μ.
- The Gaussian curve is symmetrical about its mean μ.

- The mean divides the curve (and the range of the random variable) in half.

- All measures of central tendency are equal to each other.
  - The mean, median (the 50th percentile), and mode (the most probable value) are equal.
- The random variable X has an infinite range: $-\infty < X < \infty$.
- The Gaussian curve asymptotes to (i.e., approaches but never touches) the horizontal axis.
- There is an infinite family of normal curves, each defined by its own unique pair of μ and σ.

Although the Gaussian has an infinite range, as a practical matter the interval $\mu - 3\sigma < X < \mu + 3\sigma$ contains almost all (99.73 percent) of the possible values of X.

The Gaussian distribution is a cumulative distribution in the sense that probabilities for specified ranges of X are associated with areas under the Gaussian curve. The pdf of the Gaussian distribution has the equation

$$f(x) = \frac{1}{\sigma\sqrt{2\pi}} e^{-\left[(x-\mu)^2/2\sigma^2\right]} \tag{3-14}$$

The probability that X will take any value less than some given specific value x^* is

$$\begin{aligned} Prob(X \le x^*) &= \int_{-\infty}^{x^*} f(x)\,dx \\ &= \frac{1}{\sigma\sqrt{2\pi}} \int_{-\infty}^{x^*} e^{-\left[(x-\mu)^2/2\sigma^2\right]}\,dx \end{aligned} \tag{3-15}$$

Note that the entire Gaussian curve encloses unit area. The Gaussian distribution is shown in Figure 4.

The probability that X may take any value in the range between the values c and d ($c < d$) is the area under the normal curve between the range limits c and d, that is,

$$\begin{aligned} \text{Prob}(c \le X \le d) &= \int_{c}^{d} f(x)\,dx \\ &= \frac{1}{\sigma\sqrt{2\pi}} \int_{c}^{d} e^{-\left[(x-\mu)^2/2\sigma^2\right]}\,dx \end{aligned} \tag{3-16}$$

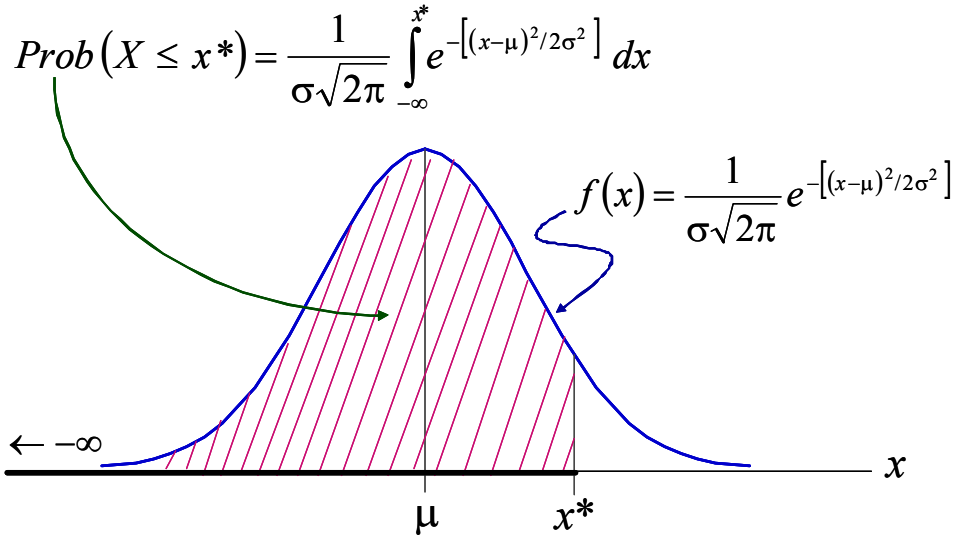

Figure 4. Probability Density Function of a Gaussian Distribution

Every normally distributed random variable X has its own unique pair of μ and σ and therefore its own unique Gaussian distribution. Because there are an infinite number of possible X's, this will entail an infinite number of Gaussian distributions. For this reason, the original random variable X is transformed by subtracting the mean μ and dividing the result by the standard deviation σ to obtain the standardized variable Z. If X is Gaussian, then Z has the standard Gaussian distribution with mean 0, standard deviation 1, and density

$$f(z) = \frac{1}{\sqrt{2\pi}} e^{-z^2/2} \quad \text{where} \quad z = \frac{x-\mu}{\sigma} \tag{3-17}$$

The standard Gaussian has been tabulated. The important point is that there is only one standard Gaussian distribution, which has been tabulated. In practice, the task is to make any Gaussian look like the standard Gaussian, so that the single standard Gaussian can be applied in all cases.

There are many reasons for the prominence of the Gaussian distribution. For one, the Gaussian describes the distributions observed in many natural processes and phenomena (e.g., most biometrical data). It is also the basis for population modeling (population proportions and tolerance intervals), statistical inference (sampling distributions, confidence intervals, and hypothesis testing) and linear regression (for the distribution of errors). Moreover, the Gaussian is used to approximate both the binomial and Poisson distributions, which model nuclear decay processes. Perhaps most importantly, it is a good approximation for the distribution of an estimated parameter. This follows from the central limit theorem, which states that the sum of a number of independent random variables, all of which have the same distribution, will asymptotically approach a Gaussian, regardless of distribution of the individual variables.

Caution should be used when applying a Gaussian distribution to model the uncertainty of a random variable that inherently has zero or positive values (e.g., dose), because the lower tail of the distribution may produce values that are less than zero, which are not possible. A truncation rule that eliminates negative values or the use of a properly chosen lognormal or triangular

distribution that adequately replicates the Gaussian distribution in the region of positive values will avoid this problem.

3.4.1.3 Lognormal Distribution

If the distribution of the logarithms of the random variable is Gaussian, then the random variable itself is lognormally distributed. That is, the random variable X is lognormally distributed if $Y = ln(X)$ is normally distributed. Also, if Y is a random variable with a normal distribution, then $X = e^Y$ has a lognormal distribution. (The base of the logarithmic function does not matter: if $log_a(Y)$ is normally distributed, then so is $log_b(Y)$, for any two positive numbers a, $b \neq 1$.)

The rationale of the lognormal distribution lies in the central limit theorem, which states that the sum of a many independent random variables will be nearly Gaussian regardless of their individual distributions. The theorem only applies if the variables are independent and additive. If the variables are multiplicative, so that the effect produced at any stage is proportional to its current magnitude, then their logarithms will be additive. The resulting distribution of the sum of the logarithms of the independent variables is normally distributed.

The density function of the lognormal is:

$$f(x) = \frac{1}{x\sigma\sqrt{2\pi}} e^{-\left[\left[ln(x)-\mu\right]^2/2\sigma^2\right]} \tag{3-18}$$

for $x > 0$, where μ and σ are the mean and standard deviation of the variable's natural logarithm, that is, of $X = ln(Y)$ (and X is normally distributed). The lognormal is right (positively) skewed.

If X is lognormally distributed, then its mean or expected value $E(X)$, variance Var, standard deviation SD, *mode* (the most probable value), geometric mean GM or *median* (the 50th percentile), and geometric standard deviation GSD are given by the following equations.

$$E(X) = e^{\mu+\sigma^2/2} \qquad Var(X) = \left(e^{\sigma^2}-1\right)e^{2\mu+\sigma^2} \qquad SD(X) = e^{\mu+\sigma^2/2}\sqrt{e^{\sigma^2}-1}$$

$$mode(X) = e^{\mu-\sigma^2} \qquad median(X) = GM = e^{\mu} \qquad GSD(X) = e^{\sigma} \tag{3-19}$$

Lognormal pdf's for six values of σ, where $\mu = 0$, are presented in Figure 5.

As already noted, the lognormal is used to describe the distribution of the product of random variables. Lognormal distributions often provide a good representation for a physical quantity that is positive definite, that is, it extends indefinitely over only the positive values.

Lognormal distributions are important in human and ecological risk assessment because many physical, chemical, biological, toxicological, and statistical processes tend to create random variables that follow lognormal distributions. For example, the physical dilution of one material (say, a miscible or soluble contaminant) into another material (say, surface water in a bay) tends to create non-equilibrium concentrations which are lognormal in character.

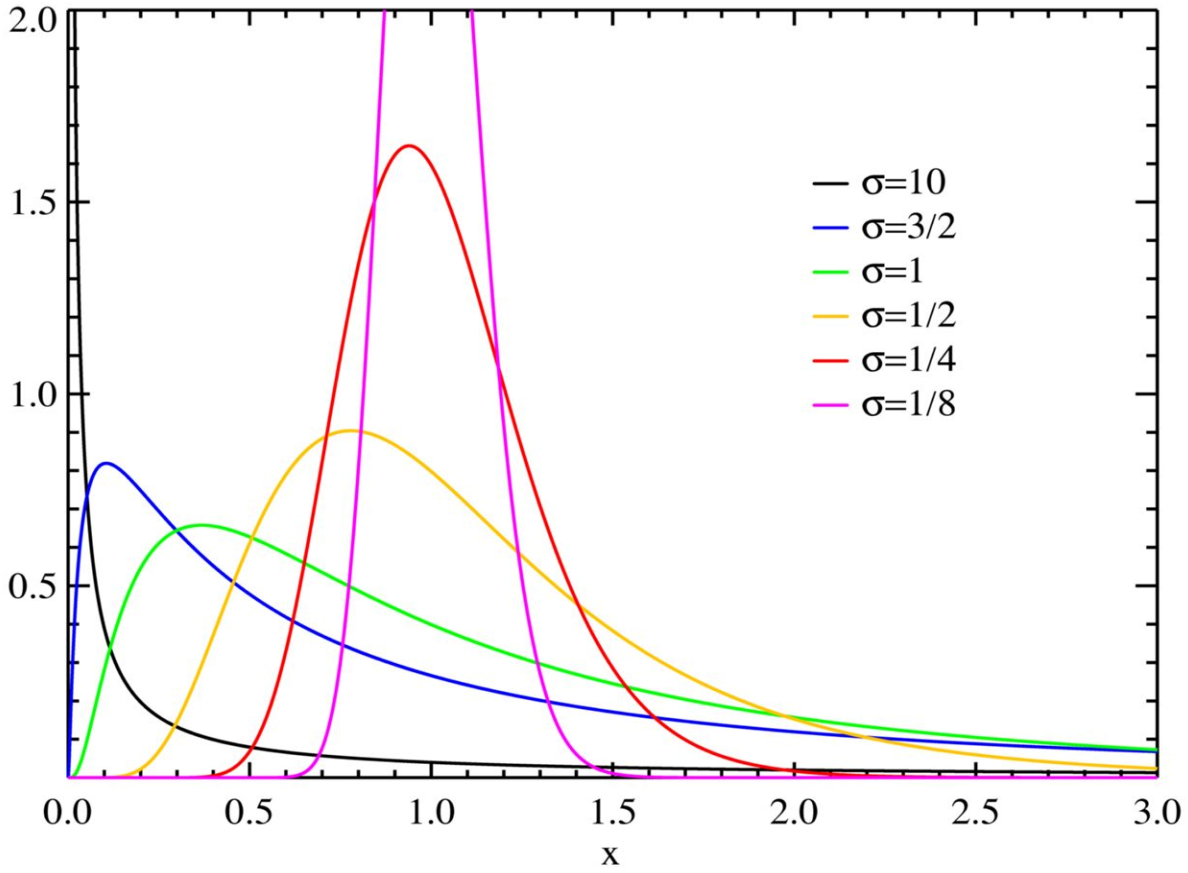

Figure 5. Probability Density Functions of the Lognormal Distribution for Various Values of σ

The uncertainty in film badge exposure readings is also modeled by a lognormal distribution (NRC, 1989, pp. 61–74). It is useful to define two quantities when assessing film badge uncertainty: the measurement bias B and the 95th percentile uncertainty factor K. As the name implies, B is the estimated systematic error or bias introduced into the measurement process by, for example, an error in film calibration, pre-issue exposure of the film to radiation, or fogging of the film due to heat and/or humidity. K is a measure of the random error characterized by the lognormal distribution, and is related to the geometric standard deviation by

$$K = GSD^{1.645} \tag{3-20}$$

The usefulness of this parameterization lies in the fact that there is only a 5-percent probability that the true exposure associated with a film badge-measured exposure E is greater than $K \cdot E/B$. Estimates of B and K, by nuclear test series, are provided in NRC (1989).

3.4.1.4 Triangular Distribution

The triangular distribution is a simple distribution whose continuous random variable X can take on any value in the finite, fixed range from a to c such that $a < X <$ c) with mode (or peak value) at b ($a \le b \le c$). Triangular distributions are shown in Figure 6.

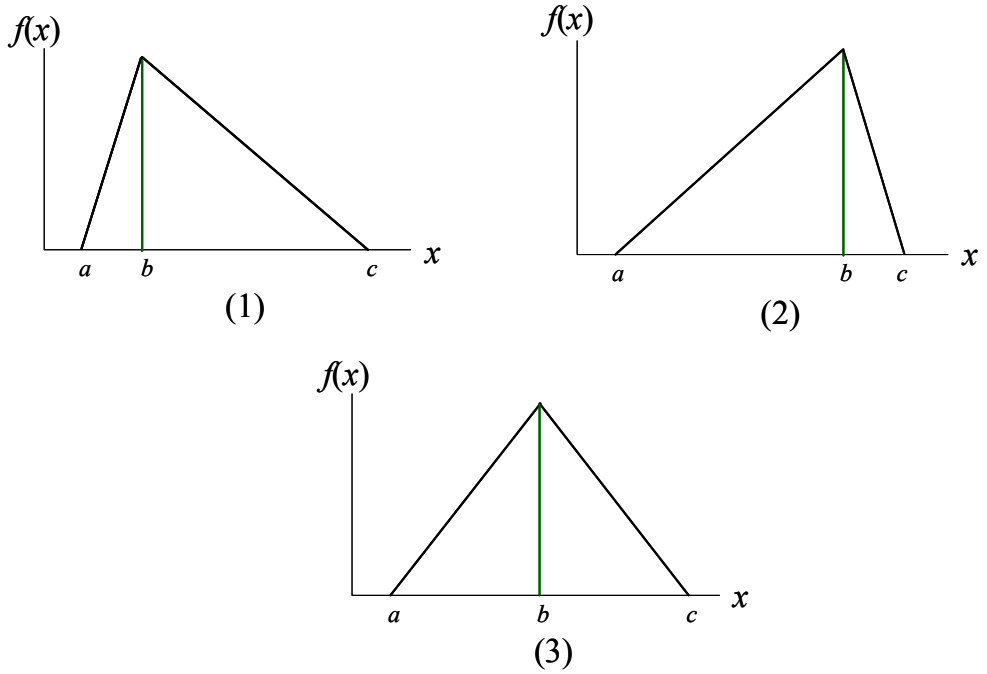

Figure 6. Probability Density Functions of a Triangular Distribution (1) Skewed Right, (2) Skewed Left, and (3) Symmetric

The pdf of the triangular distribution is given by:

$$f(x) = \begin{cases} \dfrac{2(x-a)}{(b-a)(c-a)} & for \;\; a \le x \le b \\ \dfrac{2(c-x)}{(c-a)(c-b)} & for \;\; b \le x \le c \end{cases} \tag{3-21}$$

The triangular distribution is a cumulative distribution in the sense that probabilities for specified ranges of X are associated with areas under its pdf curve. The probability that X will take any value less than some given specific value x^* is:

$$Prob(X \le x^*) = \begin{cases} \dfrac{(x^* - a)^2}{(b-a)(c-a)} & for \;\; a \le x^* \le b \\ \dfrac{(c - x^*)^2}{(c-a)(c-b)} & for \;\; b \le x^* \le c \end{cases} \tag{3-22}$$

It is important to note that a is the absolute minimum below which values of X are prohibited; the minimum a has zero probability of occurrence. Likewise, c is the absolute maximum above which values of X are prohibited; the probability of occurrence of the maximum c is zero.

The mean μ and standard deviation σ of X are:

$$\mu = \frac{a+b+c}{3} \qquad \sigma = \sqrt{\frac{a^2 + b^2 + c^2 - ab - ac - bc}{18}} \tag{3-23}$$

An interesting special case is a symmetric triangular distribution centered at 0, with range $-d \le X \le d$ (i.e., whose lower limit is identical to its upper limit except for sign). This distribution has mean 0 and standard deviation $d/\sqrt{6}$. The median (the 50th percentile) and mode (the most probable value) are both 0. Setting $d = 2.45$, the symmetric triangular distribution closely resembles a standard normal distribution, as shown in Figure 7. Random samples from this symmetric triangular distribution are very similar to samples drawn from the standard normal distribution.

The triangular distribution is the sum of two random variables that each have uniform distributions. In particular, a symmetric triangular is the sum of two identically distributed uniform variates.

Although it has no theoretical basis, the appeal of the triangular is its great flexibility. The triangular distribution is most often used when the true distribution is unknown but the extremes and the mean or mode of the distribution can be estimated. That is, if the range (a and c) and most likely value (b) can be estimated, then probabilities can be calculated from a fitted triangular. Unlike the Gaussian, the triangular can be symmetric or skewed in either direction. If symmetric, the triangular has a single central peak, like the Gaussian. On a practical level, the finite range of the triangular is often preferred over the infinite range of the Gaussian; this is especially so when the random variable of interest is inherently positive.

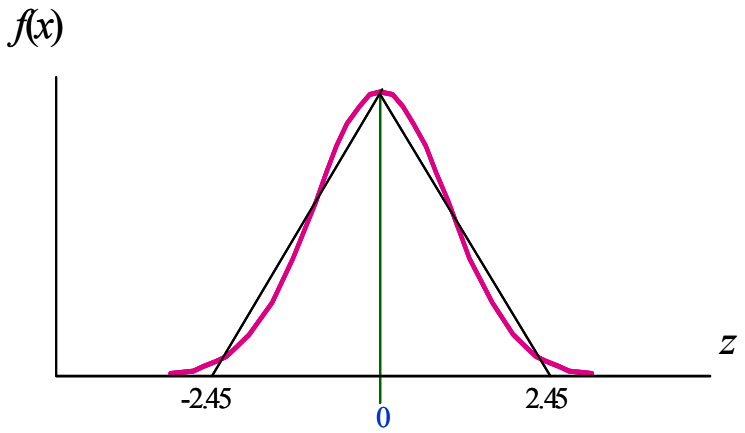

Figure 7. Symmetric Triangular Approximation to the Gaussian Distribution

3.4.1.5 Log-Triangular Distribution

The log-triangular distribution is obtained when the distribution of the logarithms of the random variable is triangular. Like the triangular distribution, the log-triangular distribution is not easily associated with natural phenomena. On the other hand, a triangular distribution of the values in log space may reflect that underlying exponential processes are driving the random variable. Also like the triangular distribution, it can be used to model a process in the absence or scarcity of data to represent uncertainty. The log-triangular distribution is most useful when the range of the possible values covers several orders of magnitude (a property shared with the lognormal distribution) and when uncertainties are large. A severely right-skewed log-triangular distribution is shown in Figure 8, in which values extend over nine orders of magnitude.

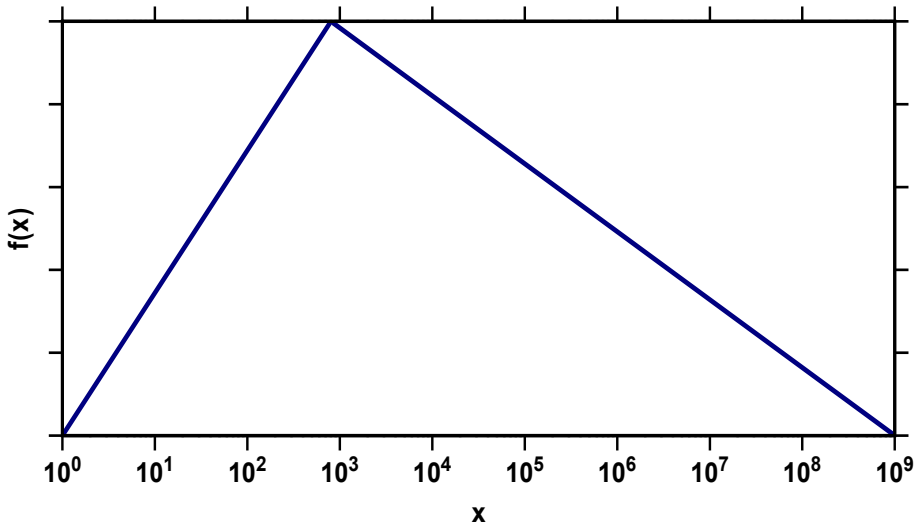

Figure 8. A Right-Skewed Log-Triangular Distribution

There is no theoretical basis for the log-triangular model. The appeal of the log-triangular distribution is its great flexibility. It is typically used to represent subjective uncertainties when the range of possible values extends over several orders of magnitude. It is often used as a rough model in the absence of data when the random variable is known to be asymmetric and bounded, that is, when the values toward the middle of a range of possible values in log space are more likely to occur than values near either extreme.

3.4.2 Propagation of Uncertainties

The methods to propagate through a model the uncertainties in the parameters used may be classical analytical or numerical uncertainty propagation methods (Hoffman and Gardner, 1983; Morgan and Henrion, 1990; NCRP, 1996). The analytical methods are outlined below.

Let X and Y be two random variables with means μ_x and μ_y and standard deviations σ_x and σ_y, respectively. The standard deviations are taken as representations of the uncertainties in the random variables. If W is defined as the random variable $X + Y$, then the mean of W is $\mu_w = \mu_x + \mu_y$. If X and Y are independent, the selection of a value x from the distribution of X does not influence the selection of a value y from the distribution of Y, and vice versa. In such cases, the uncertainties in X and Y are uncorrelated and the uncertainty in W can be expressed as:

$$\sigma_w = \sqrt{\sigma_x^2 + \sigma_y^2} \tag{3-24}$$

The term "uncorrelated" is used in the sense that there is no association or relationship between X and Y. When the uncertainties propagate in this manner, they are said to be combined in quadrature. Conversely, if X and Y are strongly dependent such that the value of x has a large influence on the value of y, then the uncertainties in X and Y are highly correlated and propagate as:

$$\sigma_w \approx \sigma_x + \sigma_y \tag{3-25}$$

The degree of correlation between two random variables is given by the correlation coefficient ρ, which measures the strength of the linear association between the variables on a scale from -1 to +1; the stronger the relationship, the closer the absolute value of ρ is to 1. In general, the uncertainty in W can be expressed as:

$$\sigma_w = \sqrt{\sigma_x^2 + 2\rho\sigma_x\sigma_y + \sigma_y^2} \tag{3-26}$$

If X and Y are totally uncorrelated so that $\rho = 0$, then Equation 3-24 is obtained. If X and Y are perfectly correlated so that $|\rho| = 1$, then Equation 3-25 is obtained.

As an example, consider X and Y to be two reconstructed doses. If these are doses received years apart by a test participant at different test series where different film badge types and/or radiation measurement equipment were used, they can reasonably be considered independent and Equation 3-24 expresses the uncertainty in his total dose. If, however, doses X and Y were received on successive days at the same location in the same fallout field, it is likely their errors are correlated since any error in characterizing the local radiation environment would affect both

doses in a similar way (i.e., both reconstructed doses are likely to be high or both low). In this case, Equation 3-25 applies. Often X and Y are partially correlated ($-1 < \rho < 1$, where $\rho \neq 0$). If ρ is known, the error can be calculated from Equation 3-26. If ρ is not known, judgment is required in the selection of the most appropriate method of uncertainty propagation.

This discussion of uncertainty propagation has used the simple function $W = X + Y$ as an illustrative example. Other simple functions such as $W = X \times Y$, $W = X \div Y$, as well as other functions such as exponential functions, are used in this uncertainty analysis. However, the simple function $W = X + Y$ was included only as an illustration, and a more thorough discussion of propagation of uncertainties, including additional functional types, is beyond the scope of this report. The reader is referred to other more in-depth discussions such as those included in NCRP Report No. 158 (NCRP, 2007). However, the aforementioned approaches are tedious and difficult to implement. For that reason, an alternative approach is to conduct the Monte Carlo simulation that is discussed in the next section.

3.4.3 Monte Carlo Method

The Monte Carlo method was developed at Los Alamos by scientists working on the Manhattan Project and later on thermonuclear weapon design. Their approach to solving complex physics problems was to consider all key parameters to be random variables with associated probability density functions. By running many trials (commonly called "histories"), and on each history selecting random values from each of the pdf's, they were able to conduct "numerical experiments" and derive critical data efficiently and accurately. These methods and attributes are applicable to a wide range of problems, including probabilistic dose reconstruction of the type addressed in this report.

3.4.3.1 Method Overview

In a Monte Carlo simulation, a random sample of scenarios is selected to represent all possible scenarios. Each scenario is generated by randomly selecting a value for an input parameter, regarded as a random variable, according to its assigned probability distribution. In so doing, a distribution is built for the output variable, which is representative of all possible output values. (Morgan and Henrion, 1990; Hahn and Shapiro, 1967; Vose, 2008)

Operationally, for a model described by k stochastic parameters, each parameter is sampled at random from its respective distribution. Altogether, this set of k random parameter values defines a scenario, also referred to as a history, and is used as input to the model; a scenario is a complete model run. A new set of randomly sampled k parameter values is used as input for each and every one of the m scenarios performed, resulting in m sets of calculated values. These m output values are arranged into a probability distribution, which is characterized by standard statistical methods. (Morgan and Henrion, 1990; Hahn and Shapiro, 1967; Vose, 2008)

The resulting distribution for the output using this approach is an approximation to the exact distribution. The accuracy of a Monte Carlo scheme, that is, to the degree to which the output distribution approximates the exact distribution, can be increased simply by increasing the sample size of scenarios. As a result, very large numbers of Monte Carlo runs are performed; typically, m may be of the order of up to tens of thousands, with the result that execution time may become a significant issue. Moreover, the accuracy can be estimated with standard

statistical techniques. An important point is that, for a given output distribution, its accuracy depends on the number *m* of scenarios and not on the number *k* of inputs.

For large, complex models, Monte Carlo methods are computationally intensive—both *k* and *m* contribute to the computational burden and long execution times of the Monte Carlo dose simulations performed in the case studies. The effort to run the model for each scenario is generally proportional to *k*. Even so, the amount of effort expended in a Monte Carlo simulation is less than other methods, particularly full enumeration of all possible scenarios. (Morgan and Henrion, 1990; Hahn and Shapiro, 1967; Vose, 2008)

There are a variety of measures of uncertainty propagation through a Monte Carlo simulation. One approach is to attribute output uncertainty to the individual inputs. This is the approach adopted for the sensitivity analysis in Section 6. An overall measure of uncertainty propagation through a Monte Carlo simulation is taken to be the variance of the output distribution. This is the measure adopted throughout this uncertainty analysis (Morgan and Henrion, 1990)

In the present analyses of nuclear test-related exposures, a multitude of key parameters such as radiation intensities, stay times, and structure protection factors are considered random variables. The uncertainties of these random variables are expressed as distributions of the type discussed in Section 3.4.1 or derived via the Monte Carlo technique from the uncertainties of more fundamental parameters. A typical dose reconstruction production run for each of the case studies presented in this report consists of 10,000 histories, each involving the random sampling of up to 40 distributions. The specific *k* parameters used, their assigned distributions, and their nominal values are listed in the parameter tables for external and internal doses in the individual case studies. The results of this effort are distributions of external and internal doses. These distributions well characterize the uncertainties of these doses in terms of their means, standard deviations, percentile uncertainty factors, etc.

As alluded to in the previous section, potential correlations among uncertainties of key parameters must be considered in formulating the Monte Carlo sampling. Two uncertainty distributions that are uncorrelated are each sampled independently by drawing separate random numbers during each history, while two highly correlated distributions are jointly sampled with the same random number. Assumptions regarding correlations of uncertainties are addressed elsewhere in Appendix G.

3.4.3.2 Characterizing Resulting Distributions

A random variable that follows a lognormal distribution will appear as a straight line on a log-probability plot, in which the logarithm of the random variable is graphed on the vertical axis and cumulative probability is graphed on the horizontal axis. This appears to be generally true for the external gamma, internal alpha, and internal beta-plus-gamma dose distributions derived in the case studies. The linearity of the internal dose log-probability plots (for all example organs considered) is particularly strong. The downturn of the lines at lower doses is a result of the assignment of zeros to negative values that occasionally occur when the uncertainties of positive-definite parameters are modeled with Gaussian distributions.

It is reasonable that the case study doses are distributed lognormally. As discussed in Section 3.4.1.3 the lognormal distribution arises naturally from the product of all the contributing

independent random variables, regardless of their individual distributions. The important issue is the independence of the contributing variables, not their individual pdf's.

The probabilistic doses reported herein are calculated as the product of their contributing parameters. Many of these parameters are independent (uncorrelated) of each other; others are mutually dependent upon each other. For the latter, the correlations may be weak or strong. Even so, most of the plotted points fall close to a straight line. This implies that any departures from strict independence only lead to slight departures from a straight line. Even weak to moderate dependencies do not cause severe departures from linearity in log-probability plots.

As a result, and without presupposing any distribution for dose (only for its constituent parameters), a lognormal distribution is obtained in all case studies. On this basis, it may be concluded that the lognormal distribution is the logical and appropriate choice to model the probabilistic doses derived in the case studies.

3.4.4 Quantifying Uncertainty

As used herein, uncertainty is the lack of sureness or confidence in predictions of models or results of measurements. Uncertainty may be due either to random variation (e.g., gambling) or to a lack of knowledge (level of ignorance) resulting from an incomplete specification, understanding, or measurement of the quantity of interest (e.g., chance of rain in numerical weather prediction). This is as opposed to variability, which is the natural heterogeneity, diversity, or range of variation that is inherent in a measured value or parameter (e.g., differences in height and weight in a population) or in a response (e.g., differences in sensitivity to a hazardous agent in a population). Further study cannot reduce variability but may reduce uncertainty by providing greater confidence in quantitative characterizations of variability. Note that there is a cause-effect relationship: variability may lead to or cause uncertainty. (NCRP, 2007)

A parameter will in general be variable from one history to another. As a result, the parameter is regarded as a random variable; the chance that the parameter will take any specific value for a particular history is described by a probability distribution with its mean as the expected value. The uncertainty in the parameter is often quantified by the variance or standard deviation or some other measure of variation of the parameter about the mean. The approach taken herein to quantify the uncertainty of a parameter is to select a probability distribution that best models the parameter behavior and then select best values for the mean and standard deviation of that parameter. That distribution and its chosen parameterization are held fixed for the Monte Carlo simulation described in Section 3.4.3, with the result that the same parameter distribution is repeatedly sampled for each and every one of the Monte Carlo histories.

3.4.4.1 Quantification Methods

There are various numerical methods for quantifying uncertainty. Alternatively, the quantification of uncertainty may simply reflect the state of knowledge or the quality of the data. Usually, quantification of uncertainties requires analysis and interpretation of incomplete data and other complementary information; it may also use professional judgment, which is inherently subjective in nature. Thus, different analysts may produce different statements quantifying the uncertainty in a parameter.

Often, quantifying the uncertainty of a parameter is based on expert opinion and judgment. The quantification itself is expressed using mathematical probability (Morgan and Henrion, 1990). The assignment of probability distribution functions to model parameters can rely on analysis of data (i.e., fitting probability distribution curves through existing data). More often, it relies on expert judgment about how available data may be used to represent the uncertainty in that model parameter. This often comes down to applying common sense rules.

Consider the probability distributions summarized in Section 3.4.1. If a parameter can be thought to vary with equal probability between a minimum and maximum value, then a uniform probability distribution may be assigned to describe the parameter. If one value of the parameter is more probable than others, and the possible values range between known (or presumed) minimum and the maximum values, then a triangular distribution may be assumed for the parameter. When minimum and/or maximum values cannot be set, unbounded distributions (e.g., Gaussian or normal, lognormal) are used to ensure that a small probability is assigned to any outlying parameter value. On the other hand, bounded or truncated distributions must be used when the parameter has physical limits (e.g., a parameter representing a proportion is always greater than zero and is expected to be less than one). If parameter values are expected to vary over more than one order of magnitude, giving rise to a highly right skewed distribution modeled by a lognormal, then the selected distribution should be logarithmic, e.g., log-uniform or lognormal (see Sections 3.4.1.3 and 3.4.5 for the latter). Some of these distributions may be used in combination over portions of the parameter range, for example, using piecewise uniform distributions in different possible ranges as suggested by expert opinion.

The selection of a probability function is often based on the degree of belief that the possible values of the parameter are within a certain range (with some subjectively assigned probability), rather than describing the statistical frequency of measured values. Additional information about the mechanics of assigning probability distributions to model parameters can be found in Morgan and Henrion (1990) and NCRP (1996).

3.4.4.2 Stating Parameter Uncertainties

Uncertainties in parameters are stated in terms appropriate to the probability distribution used to describe that parameter. For example, if a Gaussian distribution is assigned to a parameter, then its uncertainty is quantified by its standard deviation about its mean; if a lognormal distribution is assigned, then the uncertainty is quantified by its geometric standard deviation about the geometric mean. In general, the uncertainty in a parameter is expressed by at least two numbers (e.g., a lower and an upper bound of an uncertainty range, or a mean and a standard deviation), complemented by a probability for the confidence that the actual value is contained within the reported range.

There are several ways to state the uncertainty in a parameter. One way is to specify an interval which should contain some representative value of the parameter (e.g., its mean, median, etc.) with some degree of confidence (e.g., the actual dose is expected to be between 0.05 and 0.5 rem, with 90 percent confidence). These intervals are called “confidence intervals” in classical statistics and “credibility intervals” in Bayesian statistics; sometimes the more generic term “uncertainty ranges” is used.

Another way to state the uncertainty in a parameter is as a “factor of x”, where x represents the ratio of the upper and lower bounds of the parameter or of the upper bound and the central value

of the parameter (e.g., the actual dose is expected to be within a factor of 3 above or below 0.05 rem, with 90 % confidence). Finally, uncertainties can be expressed as a "± x", where x may be one standard deviation (e.g., the actual dose is expected to be 0.05 ± 0.01 rem) or a margin of error, with a confidence probability (e.g., the actual dose is expected to be 0.05 ± 0.01 rem at 90% confidence).

There are methods to propagate through a model the uncertainties in the parameters used. The methods may be classical analytical or numerical uncertainty propagation methods (Hoffman and Gardner, 1983; Morgan and Henrion, 1990; NCRP, 1996). The result is a statement quantifying the uncertainty about the output parameter. Suppose a Monte Carlo (MC) simulation is built through which parameter uncertainties are propagated; the MC simulation is exercised to produce m realizations. The resulting m-sized output can be used to obtain a complete description of the uncertainty in the parameter in terms of its mean or median value, standard deviation, and desired confidence intervals. Moreover, parameter uncertainties can be combined (or aggregated) into a summary statement of uncertainty. See Section 3.4.2 for combining uncertainties.

3.4.5 Reporting of Representative Doses

The (arithmetic) mean μ, is the appropriate measure of central tendency and the best point representation for randomly sampled data that is at most only slightly or moderately skewed and for random variables that follow many probability distribution functions, particularly the Gaussian (Section 3.4.1.2). The objective and rational measure of variability about μ is the standard deviation σ. However, the arithmetic mean is strongly affected by extreme values, in which case it may be misrepresentative and misleading. This is a particularly severe problem for random variables whose range of variability may extend over several orders of magnitude, as occurs for many of the parameters in radiation dose reconstruction. In this case, the geometric mean is more appropriate. (Doane and Seward, 2009; Hahn and Shapiro, 1967; Vose, 2008; NCRP, 2007)

The geometric mean GM of a set of n positive numbers is the multiplicative average calculated as the n^{th} root of their product. GM is the antilogarithm of the mean of the logarithms of all the values. In this way, GM mitigates the influence of high extremes which will strongly skew the arithmetic mean. GM is the appropriate measure of central tendency for highly skewed data that is all positive valued and for random variables that follow the lognormal distribution (see Section 3.4.1.3). The appropriate measure of the variability about the GM is the geometric standard deviation GSD, which is the antilogarithm of the standard deviation of the logarithms of all the values. (Doane and Seward, 2009; Hahn and Shapiro, 1967; Vose, 2008; NCRP, 2007)

The normal distribution, characterized by μ and σ, is appropriate to model events that are randomly affected by very many random variables that all contribute *additively*; see Section 3.4.1.2. In particular, the size or magnitude of a quantity that follows the normal distribution is a function of the *sum* of all contributing random variables. The lognormal distribution, characterized by GM and GSD, is best to model events which are randomly affected by very many random variables that all contribute *multiplicatively*; see Section 3.4.1.3. In particular, the size or magnitude of a quantity that follows the lognormal distribution is a function of the *product* of all the contributing random variables. (Doane and Seward, 2009; Hahn and Shapiro, 1967; Vose, 2008; NCRP, 2007)

4 TECHNICAL APPROACH AND METHODOLOGY

The probabilistic uncertainty analysis studies for NTPR radiation dose reconstruction were carried out in five major phases consisting of the following:

- A pilot study and proof of concept designed to experiment and test the implementation of probabilistic methods using existing deterministic dose reconstruction and assessment models currently used in NTPR radiation dose assessments.
- Special studies to develop statistical models and uncertainty distributions of key input parameters used in whole body external gamma dose assessment.
- Application of prototype methods to three generic cohorts and comparison with dosimetry records. These allowed testing and verification that the selected computational tools and techniques were capable of producing the types of model results sought.
- Expansion of the methodology to include application to internal dose estimation where deterministic models were enhanced to incorporate improved estimation of input parameter central values and uncertainty distributions.
- Testing and implementation of the methods developed through six case studies that consisted of the three original and three additional cohorts. The selection of case study cohorts was based on criteria developed during the pilot study.

The five phases were designed and implemented with the primary objective that the investigation of probabilistic uncertainty would ultimately help improve current NTPR radiation dose assessment procedures and methods and develop better ways to estimate realistic uncertainties. Work under the various phases was performed to develop a standard dose reconstruction uncertainty model framework. From simple computational tools to sophisticated science-based physical models, the best available information relevant to NTPR case studies was accessed, reviewed and used in the development of the methods and techniques provided in this report.

The steps listed above were implemented in the first stages of the investigation. Additional consultation with experts and multiple meetings provided the technical bases for making adjustments to early selections and further refinements of both the approach and methodology. This section first describes the pilot study proof of concept that demonstrated the feasibility of the probabilistic approach and the application of Monte Carlo techniques for NTPR dose reconstruction. It then presents key model input parameters, their formulation and the sub-models used to develop their central estimates and probability distribution functions. This section describes the first four phases of the investigation, whereas the case study results are summarized in Section 5 and details of the analyses are provided in Appendices A–F.

4.1 Pilot Study

A pilot study was carried out to select software tools, study groups, and develop and test the basic models using a probabilities approach to NTPR dose reconstructions and uncertainty analysis. This proof-of-concept approach was employed to investigate best methods of incorporating probabilistic techniques in NTPR dose assessment procedures. The specific objectives of the pilot study were to develop an uncertainty model applicable to three representative cohorts of atmospheric nuclear test participants, generate distributions of

reconstructed external gamma doses for those cohorts, and compare the results to deterministic reconstructed doses and dose distributions from film badge dosimetry records. Once the uncertainty model was verified and tested, it was to be applied to three more groups of nuclear test participants and further expanded for the analysis of uncertainties in internal doses.

The pilot study involved the following steps:

- Investigate and select appropriate software tools based on study requirements to include statistical analysis and Monte Carlo simulation capabilities.
- Select representative study groups based on the following criteria:
  - Reliable individual film badge dosimetry.
  - Adequate number of participants within the group for statistical analysis of dosimetry records and comparison to corresponding probabilistic analysis of reconstructed doses.
  - Cohesive participants' activities performed in the radiation environment within each group.
  - Well-characterized radiation environment with adequately-documented data or surrogate information that can be used to make best estimates of input parameters to the dose models.
- Characterize the pdf of input parameters that are significant in the dose reconstruction of the selected study groups through review of the literature and the expert judgment of experienced radiation analysts. These pdfs were updated and improved through an iterative review process and only the distributions used in the case studies described in Section 5 are presented later in this Section and in Appendices A–F.
- Construct a working model for whole body external gamma dose estimation that incorporates Monte Carlo simulation capabilities and estimate dose distributions.
- Compare external gamma dose distributions resulting from the probabilistic uncertainty analysis to those from film badge dosimetry.

4.1.1 Software Selection

Three commercially available software packages were considered for Monte Carlo model development, all of which have the required functionalities. The three packages were Mathcad, the Crystal Ball® adjunct to Microsoft Excel®, and Mathematica®. Mathcad was the favored platform for model development because it is the primary calculation tool for NTPR dose assessments, and template worksheets have already been prepared for most units and test series. Preliminary investigation revealed that modifying existing Mathcad deterministic dose calculation worksheets to include Monte Carlo simulations is fairly straightforward. Thus, Mathcad was selected as the principal software tool for this project. Because Crystal Ball is widely accepted in the scientific community and has been extensively validated and verified, it was selected to generate some distribution types for comparison to those generated in Mathcad. Mathematica was also used for one study group during the pilot and initial implementations as a supplemental tool to probabilistically model the spatial movement of a participant within a radiation environment.

4.1.2 Generation of Parameter Distributions

Monte Carlo simulation capability was added to existing dose reconstruction models coded in Mathcad calculation worksheets during the pilot study and subsequently to case studies involving six atmospheric test groups. Dose reconstruction simulations using distributions that model variability and uncertainty of model parameters generated in Mathcad from simple random sampling were compared to simulations using distributions generated in Crystal Ball with Latin hypercube (McKay et al., 1979) random sampling. No discernible difference was seen when the number of simulations exceeded 500. Because the six case study analyses were to employ 10,000 simulations and the NTPR reports 95th percentile upper bounds, potentially under-represented sampling from quantiles greater than two standard deviations above the mean did not present an issue.

4.2 Special Studies: Model Parameters, Uncertainties, and Distributions

Some of the dose reconstruction model input parameters and their associated variability and uncertainty are sufficiently complex to warrant special studies with detailed analyses. Distributions of several such parameters were estimated in separate auxiliary models and input numerically as cumulative distribution functions to the case study models.

The dose reconstruction models were continually refined and improved based on the results of ongoing analyses and feedback from several analysts and subject matter experts. Specific input parameters were analyzed and refined through special studies or thorough review of existing investigations and guidelines. The dose input parameters listed below were addressed in special studies.

For External Dose Models:

- Intensity distribution from fallout on ship weather decks.
- Protection factors for land-based structures.
- Shielding factors for ships.
- Shot-specific radiological decay functions.
- Sources of uncertainty when estimating radiation intensity from measured intensities and iso-intensity maps.

For Internal Dose Models

- Gamma source modification factor.
- Resuspension factors.
- Breathing rate.
- Internal dose conversion factors.
- Characterization of descending fallout
- Internal deposition fraction adjustment.
- Incidental ingestion of contaminated soil and dust.

Details of the resulting methodologies are presented in the following sections along with the mathematical and physical models on which they are based. Discussions of the results and decisions on model input parameter distributions are also included.

Conversely, a few parameters were assigned fixed values in this study although some uncertainty or variability may exist regarding those values. A brief listing of parameters falling into this category follows.

- Fallout event times – times associated with specific intensity readings during a fallout event.
- Film badge conversion factor (*FBCF*) – the ratio of dose recorded on a properly worn film badge to free-in-air integrated intensity. This factor, which accounts for body shielding of the film badge to gamma radiation, was assigned the deterministic value of 0.7 in this study.
- Bias factors (*Biasα* and *Biasβγ*) – parameters to remove high-sided bias in inhalation dose conversion factors (discussed in Section 4.2.8). These factors are aggregated for three organ groups (Table 14) and are assumed to be constant in time.
- Surface activity density-to-Intensity (*SA/I*) ratios – parameters used to infer activity densities from concurrent intensity readings.
- Distribution of exertion levels (*BRfrac*) – fraction of time at rest, or in light, moderate, or heavy activity, assumed constant in the present breathing rate formulation (Section 4.2.7).
- Indoor/outdoor scenario during fallout event – treated in a time-averaged manner in present study instead of randomly selecting specific indoor/outdoor scenarios for periods of potentially significant exposure.

Parameters such as fallout event times and *FBCF* have well-established central values and small uncertainties, and therefore were treated as constants in this analysis. The *SA/I* ratios utilized in the study were derived with FIIDOS assuming no fractionation. Because of the complexity of the fractionation process, formal treatment of the uncertainty of *I/SA*, along with an assessment of its impact on other fractionation-sensitive parameters such as internal dose conversion factors, have been deferred until time and resources are available to thoroughly research this subject. The significance of uncertainty in the bias factors, the exertion level distribution, and the indoor/outdoor scenario for descending fallout remain to be evaluated.

4.2.1 Intensity Distribution from Fallout on Ship Weather Decks

For ships that received fallout from a nuclear test, the *average* topside intensity was frequently documented in deck logs or operational reports, or an *average* intensity can reasonably be inferred from intensity readings reported on nearby ships or land masses. While this area-averaged intensity is useful for calculating a deterministic "best estimate" dose for generic crewmen, the variability of intensity with topside location contributes to the uncertainty in the dose of an individual crewman, who may have manned a topside workstation where the intensity differed significantly from the average. It is therefore necessary to model this variability in topside intensity when calculating doses probabilistically. This special study investigates the distribution of gamma intensities on the weather decks of fallout-contaminated ships.

4.2.1.1 Technical Approach and Methodology

In the idealized scenario of uniform fallout deposition on a flat weather deck of a ship, a theoretical distribution of topside intensities can be constructed using a point-kernel method (Stevens and Trubey, 1972, pp. 46–53) to calculate relative intensity for random topside locations. The point kernel used here is given by

$$PK(x,y,X,Y) = \frac{\mathrm{Prop}\left[\sqrt{(x-X)^2+(y-Y)^2+H^2}\right]}{(x-X)^2+(y-Y)^2+H^2} \tag{4-1}$$

where x and y are the Cartesian coordinates of a point source, X and Y the coordinates of an observer's topside location, and H the height above the deck (taken as 1 meter). The propagation function $Prop(R)$ used in this assessment was derived from two-dimensional transport results obtained with the ITS CYLTRAN code (Halbleib et al., 1992) for propagation of gamma rays through air over an iron substrate. Fission gamma spectra given in Finn et al. (1979) were used in these CYLTRAN calculations to characterize the source radiation. A fit to these data resulted in the Mathcad functional expression shown below, where the independent variable R is the slant distance from the source in meters.

$$\begin{aligned} Prop(R) &= exp(0.4547 \cdot R^{-0.5796} - 0.5) && \text{if } R < 17.35 \\ &= exp(0.5404) \cdot R^{-0.3344} && \text{if } 17.35 \le R < 31.65 \\ &= exp(5.18 \cdot 10^{-8} \cdot R^3 - 2.966 \cdot 10^{-5} \cdot R^2 + \\ &\qquad 1.2016 \cdot 10^{-4} \cdot R - 0.5906) && \text{if } 31.65 \le R < 316.2 \\ &= 0.6971 \cdot exp(-0.004787 \cdot R) && \text{if } R \ge 316.2 \end{aligned} \tag{4-2}$$

The intensity at a particular topside location (X_i, Y_i) is obtained by integrating the point kernel over that part of the topside area A that is within the field of view of an observer at (X_i, Y_i). Designating the latter area A_i, the intensity can then be expressed as

$$I(X_i, Y_i) = \iint_{A_i} PK(x,y,X_i,Y_i)\,dx\,dy \tag{4-3}$$

It is assumed in performing this integration that (1) the weather deck on an aircraft carrier is rectangular with no obstructions (so A_i = length × width), and (2) the weather decks for all other ships are elliptical with centrally located superstructures that are opaque to radiation (so $A_i < A$). The dimensions of the rectangle/ellipse and superstructure are selected to best characterize the ship of interest. Details of this integration for the various ship types are provided in Weitz (2009b). The observation point (X_i, Y_i) is sampled randomly ($i = 1,\ldots,n$ for a sample size of n) over the area A_i to generate a distribution of intensities. An example of a distribution thus derived with n = 10,000 for a Liberty ship (YAG) is shown in Figure 9. This distribution has been normalized to a mean of 1 R hr^{-1}. The highest intensities pertain to locations in the relatively open areas in front and back of the superstructure, where shielding is minimal. As

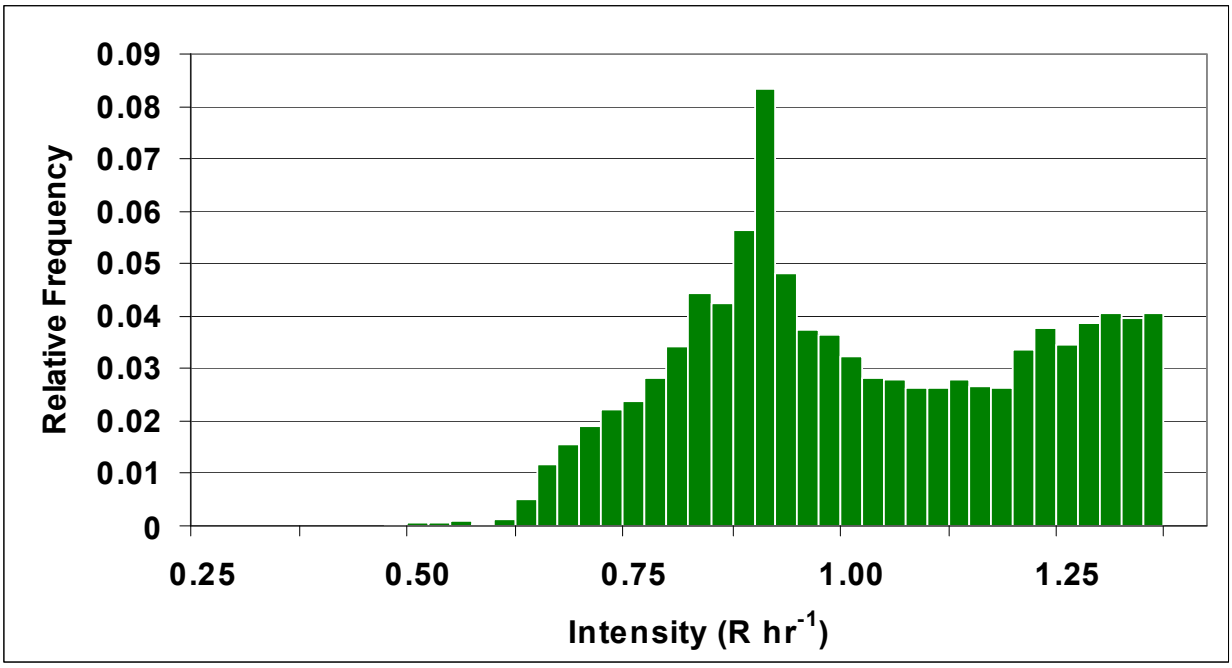

Figure 9. Distribution of Intensities for Fallout Deposited Uniformly on Weather Deck of YAG (normalized to a mean of 1 R hr^{-1})

there are many such locations, the probability of randomly occupying one of them is substantial. The modal peak is associated with the numerous locations available alongside the superstructure, while the low intensity tail results from locations very near the superstructure where shielding is maximized.

It is shown in Molumphy and Bigger (1957), however, that the fallout deposition on ships is *not* uniform. These deposition data, graphically represented as beta surface activity contours, were collected aboard the test ships YAG-39 and YAG-40 after both had been intentionally subjected to fallout during Operation CASTLE (1954). The significant non-uniformity of deposition indicated in those contour plots introduces an element of uncertainty in the intensity $I(X_i, Y_i)$ of Equation 4-3. This uncertainty is modeled by multiplying each value of $I(X_i, Y_i)$ by a number $g_i(\mu, \sigma)$ drawn randomly from a Gaussian distribution with mean $\mu = 1$ and standard deviation σ. This Gaussian "spreading function" further spreads the intensity distribution in Figure 9.

A companion set of gamma intensity data for the YAG test ships, also provided in Molumphy and Bigger (1957), was utilized to determine σ, the standard deviation of the spreading function. This database includes three contour plots constructed from measurements taken on YAG-40 after that ship had received fresh fallout following Shots ROMEO, UNION, and YANKEE, but before any decontamination was attempted (the "pre-decon" data set). In addition, it contains two contour plots based on measurements made after partial decontamination of YAG-40 following ROMEO and on YAG-39 following YANKEE (the "post-decon" data set). Because YAG-39 employed an automatic wash down system during periods of fallout deposition, there are no pre-decon data for that ship.

The first step in establishing reasonable values for σ (one each for the pre- and post-decon environments) was to convert the contour plots into intensity probability distributions. To accomplish this, the contours for a given ship and fallout event were digitized and the enclosed areas integrated using the DIGITIZE-PRO (Danon, 2008) and DPLOT (HydeSoft Computing, 2008) software packages. It is straightforward to then recast these areal distributions into the intensity probability distributions (i.e., the relative frequency plots) in Figure 10 and Figure 11 for the pre- and post-decon environments, respectively. Both the individual ship/fallout event distributions and the composite (averaged) distributions are displayed in these figures. In all cases, the distributions have been normalized such that the average intensity is 1 R hr^{-1}. The pre-decon plots in Figure 10 are fairly symmetrical, aside from secondary peaks in the very low intensity region, while Figure 11 indicates that partial decontamination results in a skewed distribution. This is not unexpected because wash down will remove the more loosely bound contaminant fraction, but some areas of high concentration are more resistant to removal due to difficulty of access (e.g., scuppers) or the presence of grease or porous surfaces (e.g., wood decking).

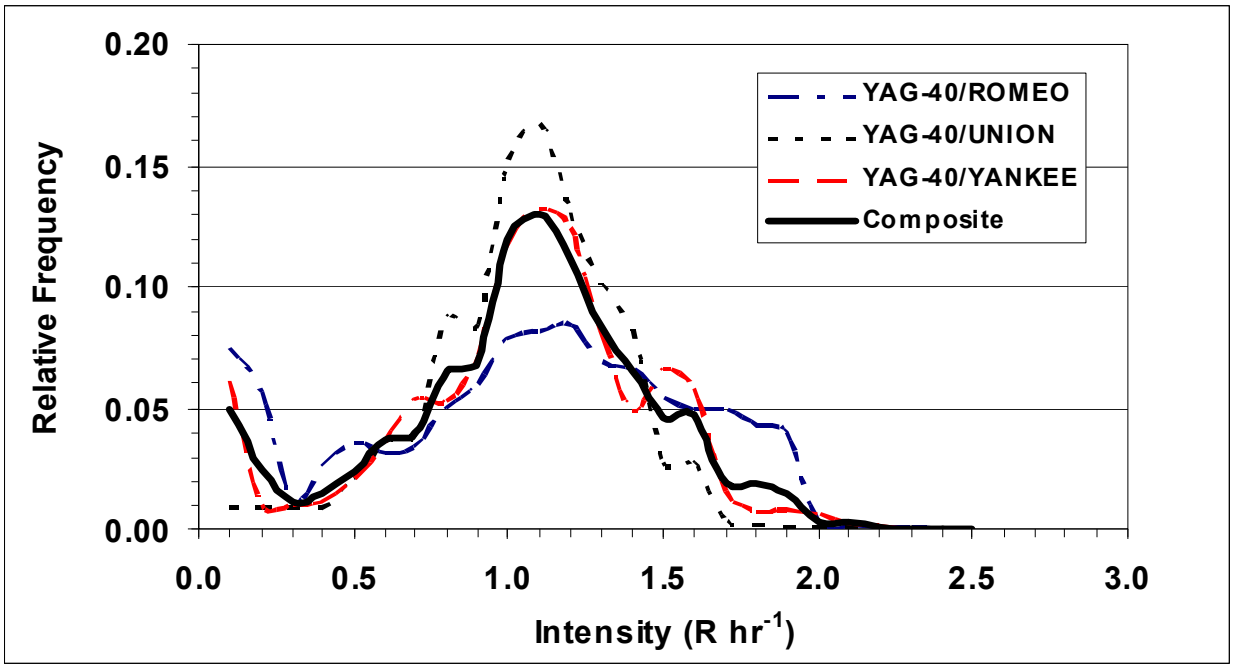

Figure 10. Topside Intensity Distributions on YAG Prior to Decontamination (normalized to a mean of 1 R hr^{-1})

The next step was to generate distributions of $g_i(\mu, \sigma)\cdot I(X_i, Y_i)$ to determine the value of σ that gives the best fit to the composite YAG pre-decon distribution (black curve in Figure 10). For convenience, the secondary peak near zero intensity that appears in Figure 9 was neglected in this fitting. The best fit to the pre-decon distribution, shown in Figure 12, occurs for $\sigma = 0.23$. A similar procedure was applied to the YAG post-decon distribution by using the black curve in Figure 11 as the standard to be matched by varying σ. This produced the best fit with $\sigma = 0.50$, as shown in Figure 13.

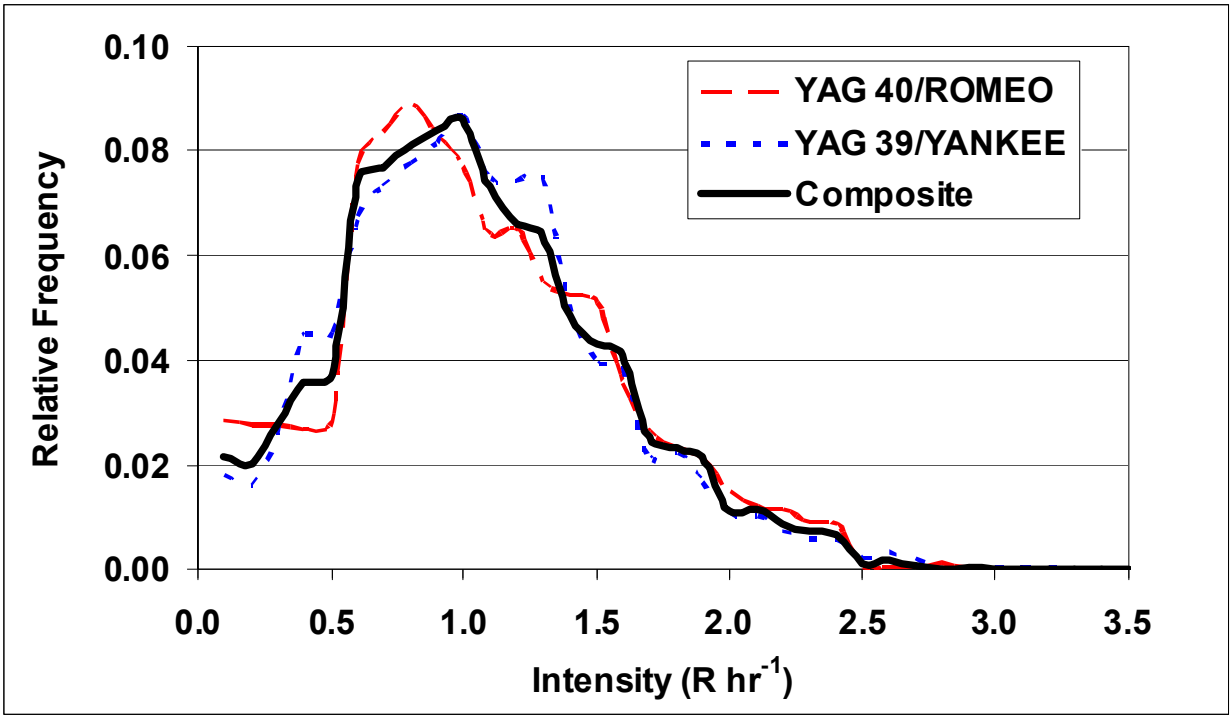

Figure 11. Topside Intensity Distribution on YAG after Partial Decontamination (normalized to a mean of 1 R hr^{-1})

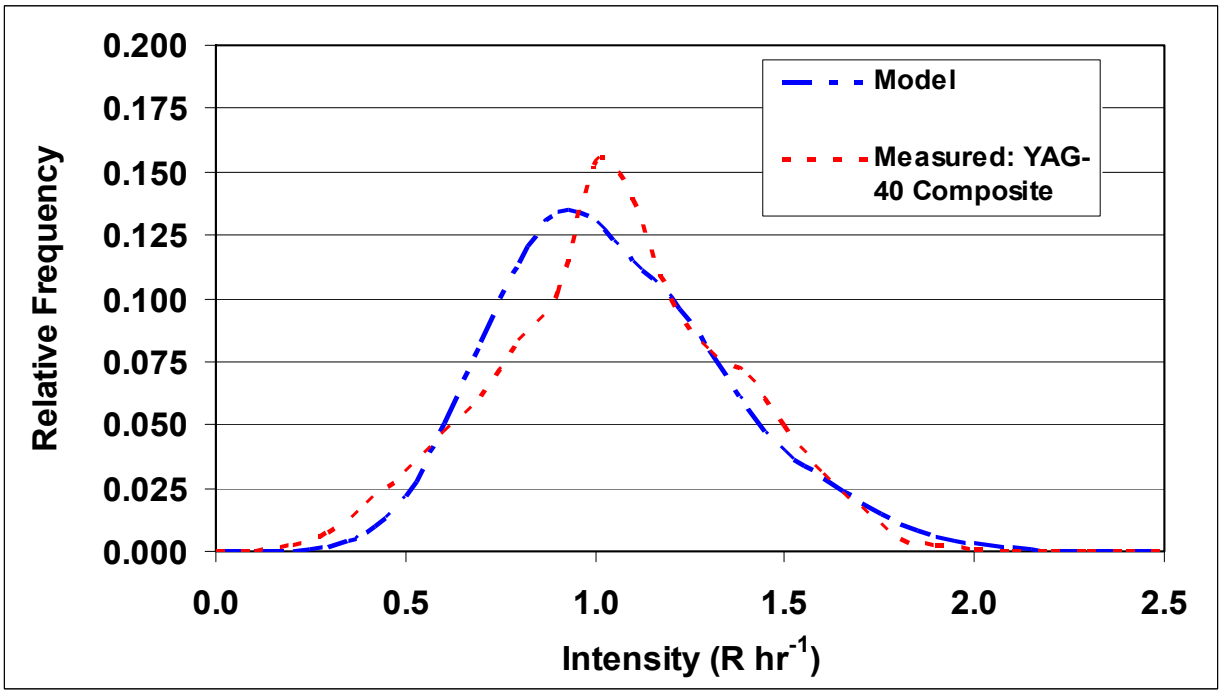

Figure 12. Best Fit to YAG Pre-Decon Intensity Distribution (normalized to a mean of 1 R hr^{-1})

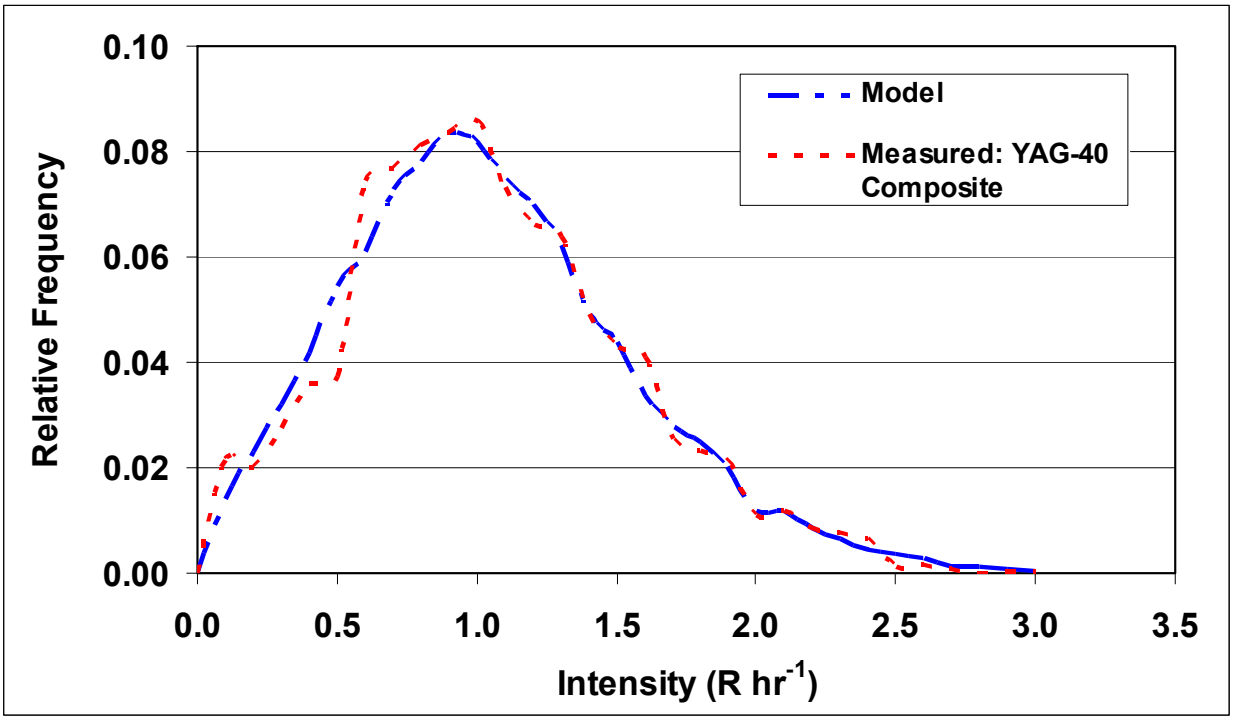

Figure 13. Best Fit to YAG Post-Decon Intensity Distribution (normalized to a mean of 1 R hr^{-1})

These pre- and post-decon values for σ were derived on the basis of intensity data taken on a single ship type, the YAG. An additional uncertainty is therefore encountered when applying them to ships that are not YAGs. Based on subjective judgment, these values of σ were each doubled, to 0.46 and 1.0 respectively, when used for other ship types. This was done so that the uncertainty associated with the application of this model to ship types other than that on which the data were taken is adequately reflected in the analysis, thereby ensuring that a 95th-percentile upper bounds of doses calculated on the basis of this model are not underrepresented.

4.2.1.2 Results and Discussion

The model described above was applied to the amphibious force flagship USS ESTES and the aircraft carrier USS BOXER. The resulting intensity distributions (probability density functions) for these ships are shown in Figure 14 and Figure 15, respectively. The pre- and post-decon distributions derived by this algorithm are ship-specific because they are obtained by "spreading" a ship-specific uniform-deposition distribution in a prescribed manner.

These results, recast in the form of cumulative probability distributions, were utilized in the USS ESTES and USS BOXER case studies to model the distribution of topside intensities in the *EDM* (external dose multiplier) parameter (defined in Section 4.2.3). The arithmetic mean of the intensity distributions displayed in Figure 14 and Figure 15 is 1 R hr^{-1} so they will not introduce a bias in probabilistic dose reconstructions. However, they will cause significant dispersion of the topside-accrued doses. The 95th percentile upper bounds of the pre- and post-decon distributions for USS ESTES are 2.0 and 2.3 R hr^{-1}, respectively; those for BOXER are 1.8 and

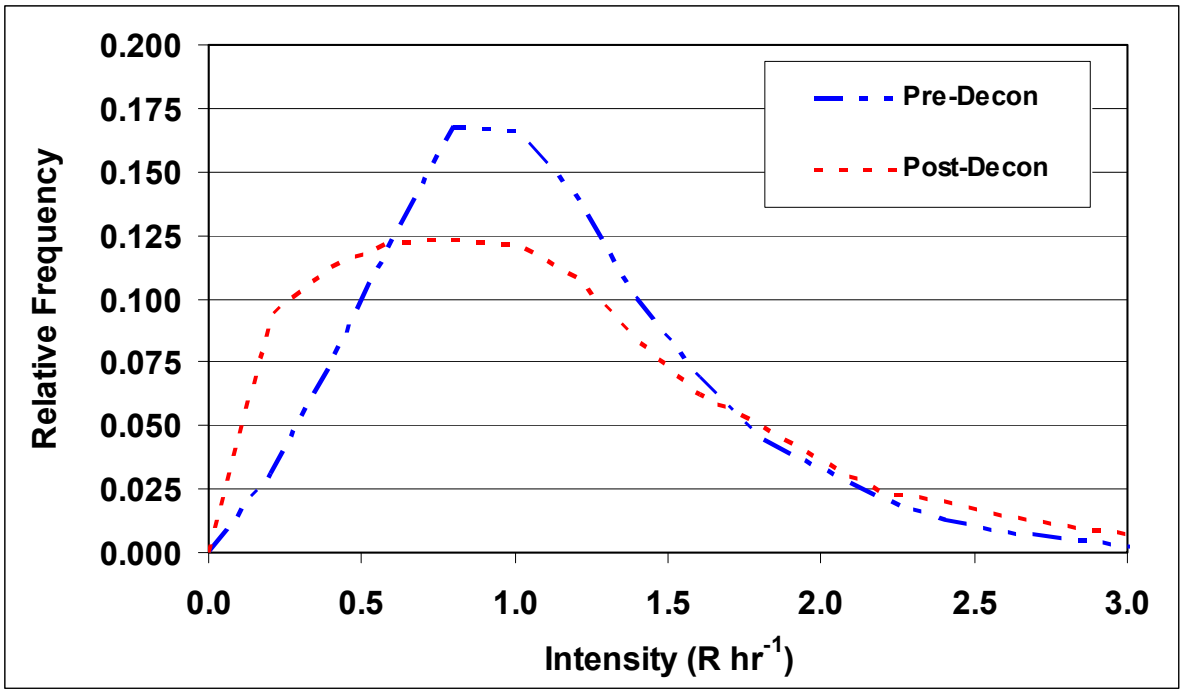

Figure 14. Pre- and Post-Decon Topside Intensity Distributions for USS ESTES (normalized to a mean of 1 R hr^{-1})

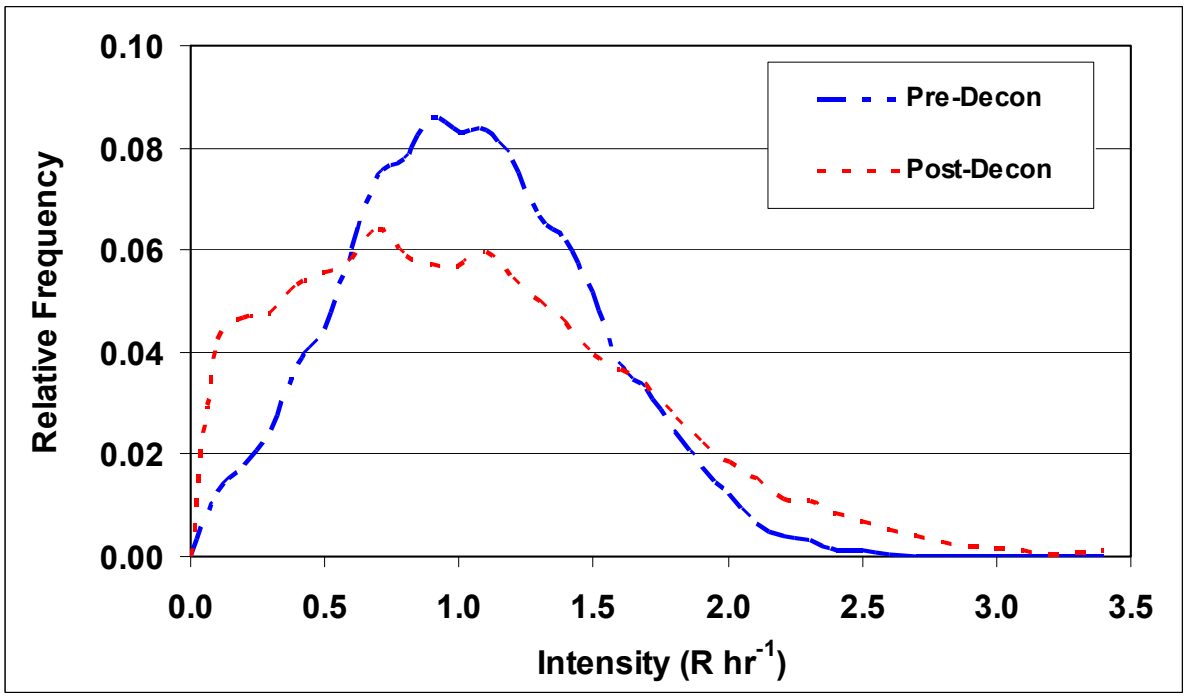

Figure 15. Pre- and Post-Decon Topside Intensity Distributions for USS BOXER (normalized to a mean of 1 R hr^{-1})

2.2 R hr^{-1}, respectively. (Because both distributions in Figure 14 and Figure 15 are normalized to 1 R hr^{-1}, the fact that the post-decon upper bound values are greater than the pre-decon upper bounds merely indicates that the post-decon distribution is broader than the pre-decon distribution.)

4.2.2 Protection Factors for Land-Based Structures

The protection factor (*PF*) of a structure, defined as the quotient of the free-field radiation intensity outside and the free-field radiation intensity inside the structure, is a measure of the radiation shielding provided by that structure. In deterministic dose reconstructions, point-value protection factors of 2 for buildings and 1.5 for tents have generally been used. When performing probabilistic dose reconstructions for land-based personnel, however, the uncertainty in *PF* must also be characterized. The *PF* in a structure depends both on the physical properties of the structure (e.g., width, length, type of construction material) and on the location within the structure. The modeling of *PF* uncertainty is addressed in this section.

4.2.2.1 Technical Approach and Methodology

The Operation REDWING contractor completion report (Holmes & Narver, 1956) provides illustrations of the types and numbers of tents and buildings occupied by Army personnel at Enewetak during nuclear testing. Based on this report, the dimensions of the various structures can be estimated with confidence. It is assumed that the basic building configuration from REDWING adequately describes those properties for Operations CASTLE and HARDTACK I.

Mathcad software was used to calculate a distribution of *PF*s for locations inside a rectangular shelter of length L, width W, height V, and wall/roof thickness t_{wall} situated in a field of uniformly deposited fallout that extends infinitely in all directions. It was assumed that the interior of the shelter was free of fallout. For buildings, walls of wood, aluminum, and iron are considered. The wall thickness t_{wall} was set to 0 for tents. Because the roofs of these buildings were generally pitched, fallout initially deposited on a roof would, over time, run off and redeposit on the adjacent ground. This was also modeled, allowing a fraction f of the fallout on the roof to form line sources alongside the structure. Because f is unknown, its value was selected from a uniform distribution between 0 and 1.

The point-kernel method (Stevens and Trubey, 1972, pp. 46–53) was utilized in this analysis. The propagation of gamma radiation over a distance R through air was modeled by a point kernel $Prop(R)/R^2$, where $Prop(R)$ accounts for all the propagation effects (e.g., absorption, scattering, build-up, air-ground interface) except for $1/R^2$ dispersion. The function $Prop(R)$ was derived with the two-dimensional transport code CYLTRAN (Halbleib et al., 1992) for propagation of gamma radiation through air over soil. Spectra provided in Finn et al. (1979) were used to characterize the gamma radiation emitted by the fallout field. The resultant data were then fit piecewise in Excel to obtain the Mathcad equation shown below, where R is in meters.

$$
\begin{aligned}
Prop(R) &= exp(-0.0356) \cdot R^{-0.0932} && \text{if } R < 17.35 \\
&= exp(0.5762) \cdot R^{-0.3063} && \text{if } 17.35 \le R < 31.65 \\
&= exp(4.423 \cdot 10^{-8} \cdot R^3 - 2.7241 \cdot 10^{-5} R^2 + \\
&\qquad 2.3763 \cdot 10^{-4} \cdot R - 0.46368) && \text{if } 31.65 \le R < 316.2 \\
&= 0.8088 \cdot exp(-0.0047213 \cdot R) && \text{if } 316.2 \le R
\end{aligned}
\qquad (4\text{-}4)
$$

The attenuation of gamma radiation through wall materials was modeled in Mathcad by means of similar functional fits to results obtained with the one-dimensional transport code CEPXS (Lorence et al., 1989).

The distribution of *PF*s for a specific structure was calculated by randomly sampling horizontal locations in that structure and, for each location, integrating the point kernel over the external gamma source to obtain the intensity at a height of 1 meter above the floor. At each step in the integration, the gamma radiation was attenuated through the proper slant thickness of the designated wall material. This algorithm was tested by comparing predicted values of *PF* with those derived from intensity measurements taken on Enewetak Island of Rongerik Atoll following fallout deposition from Operation CASTLE Shot BRAVO and reported in Scoville (1954). It was found that the *PF*s deduced from Scoville's measurements could be reproduced only by accounting for the additional shielding effects of incidental materials in the structures, such as wall studs, wall coverings, desks, bedding, footlockers, and filing cabinets. Because of the unknown and unpredictable positioning of many such objects, this incidental material is not localized in the model, but instead is treated as a heavy dust suspended in the air. The Scoville data allows an estimation of the range of densities for incidental dust. Assuming the incidental materials had the shielding characteristics of wood, a triangular distribution of the incidental dust density thus derived has a minimum of 0.01 gram per cubic centimeter (g cm^{-3}), mode of 0.033 g cm^{-3}, and maximum of 0.06 g cm^{-3}. An incidental dust density randomly drawn from this distribution was applied in calculating the attenuation of radiation coming through the sides of the structure. It was not applied to the radiation emitted from fallout deposited on the roof since most of the incidental material (and conceptually the dust) would have been located in the lower portion of the structure. A more detailed discussion of the *PF* uncertainty algorithm is available in Weitz (2009c).

4.2.2.2 Results and Discussion

Examples of distributions derived with this algorithm are presented as histograms in Figure 16 and Figure 17 for two structures representative of the types used at PPG:

- A 48-man barracks building (L = 38.6 m, W = 8.6 m, V = 4 m, t_{wall} = 1.27 cm (½") wood)
- An 8-man tent (L = 8.6 m, W = 4.3 m, V = 3.5 m, t_{wall} = 0)

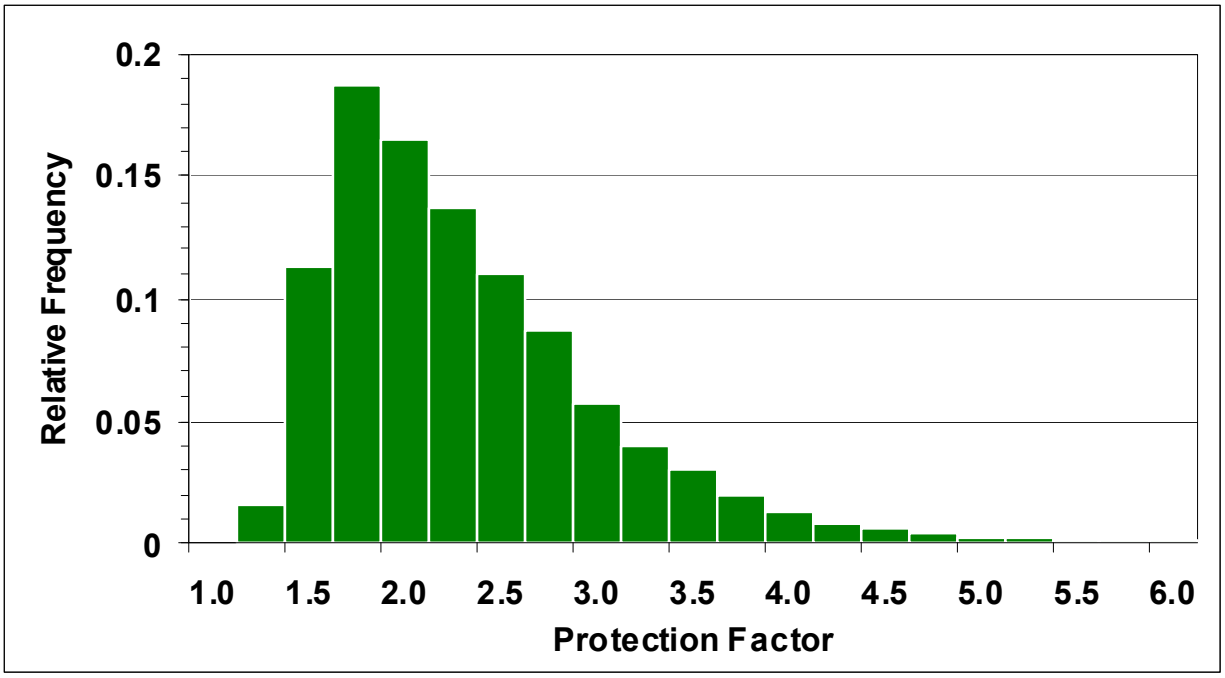

Figure 16. Calculated Protection Factor Distribution for 48-man Barracks

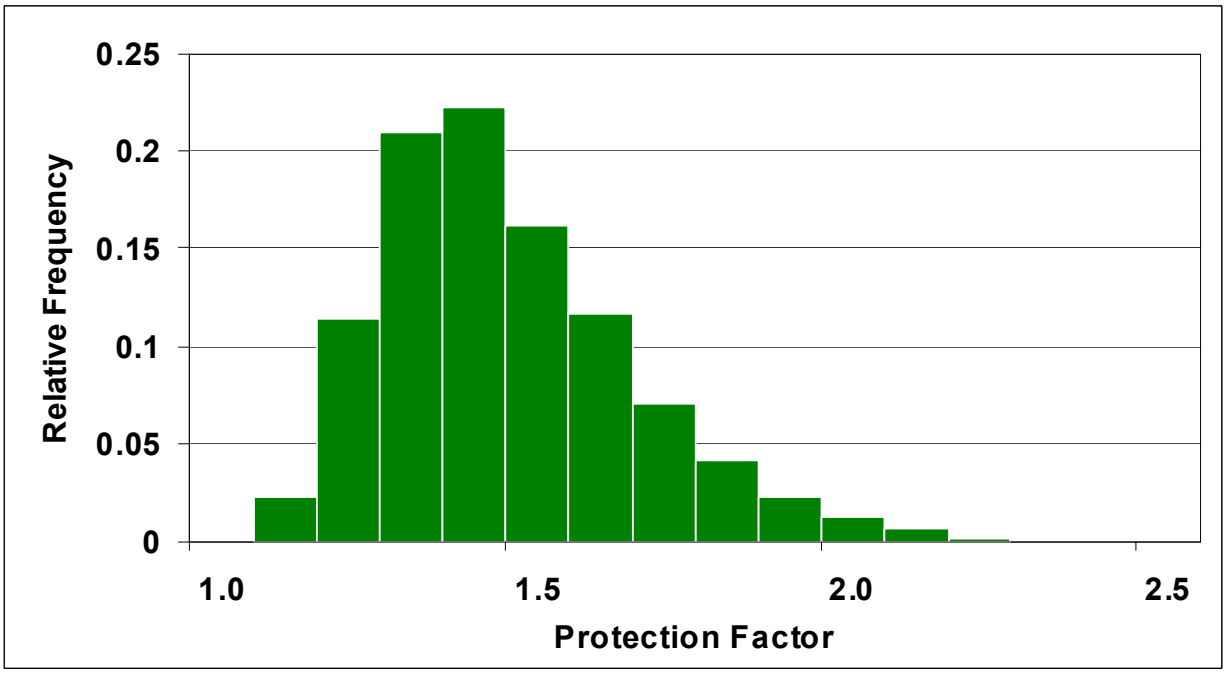

Figure 17. Calculated Protection Factor Distribution for 8-man Tent

It was assumed that the values of L, W, and V are known without error, based on the quality of the information provided in the Holmes & Narver completion report and on the insensitivity of the computed values of PF to small changes in these parameters. The uncertainties in t_{wall} and

wall material composition are subsumed in the uncertainty model of the incidental material. The mean *PF* and 95th percentile upper bound for the barracks building are 2.2 and 3.6, respectively. Corresponding values for the tent are 1.4 and 1.8.

It is generally straightforward to calculate the film-badge equivalent dose *D** a hypothetical participant would have received by remaining outside and thereby continuously exposed to the average outdoor intensity. The dose *D* for a real participant who spent only part of his time outside will vary from *D** because (1) he spent the remaining part of his time inside one or more structures where the intensity was reduced by a factor 1/*PF* due to displacement and shielding, and (2) his time outside was spent at a location that had an intensity different from the average. An external dose multiplier (*EDM*), defined as the ratio *D/D**, can be calculated to facilitate the determination of *D*.

The distribution of *EDM* is computed based on the following assumptions regarding the locations of a participant and relevant radiation intensities:

- A participant was outside a fraction F_{os} of his time at a location where the relative outside intensity was I_1. *Relative outside intensity* is defined as the ratio of the local outside intensity to the average outside intensity.
- He spent a fraction F_t of his indoor time billeted or working in a tent with a protection factor PF_t where the relative outside intensity was I_2.
- He spent the remainder of his time in a building with protection factor PF_b and relative outside intensity I_3.

The equation for *EDM* for this scenario is given by:

$$EDM = F_{os} \cdot I_1 + (1 - F_{os}) \cdot \left[\frac{F_t}{PF_t} \cdot I_2 + \frac{(1 - F_t)}{PF_b} \cdot I_3 \right] \tag{4-5}$$

The relative outside intensities I_1, I_2, and I_3 are drawn from a distribution that characterizes the variation in outside intensity. In the present study, the values of the relative outside intensities, assumed to be uncorrelated, were drawn separately from a lognormal distribution with a geometric standard deviation of 1.5. If a person remained at essentially the same location most of the time, the relative outside intensities could be considered equal ($I_1 = I_2 = I_3$) or proportional ($I_1 \propto I_2 \propto I_3$). In these special cases, the intensities at the three locations are fully correlated and a single draw from the distribution would suffice. This would produce a slightly broader distribution for *EDM*. (Note that I_1, I_2, and I_3 do not include measurement error since this error is treated as a fully-correlated multiplicative bias in this study and cancels when forming the local-to-average intensity ratios.) The protection factors PF_b and PF_t are sampled from the distributions shown in Figure 16 and Figure 17. An example of a distribution of *EDM* values derived for personnel at Enewetak during Operation HARDTACK I is presented in Figure 18; the distributions of F_{os} and F_t are specified in Table 3.

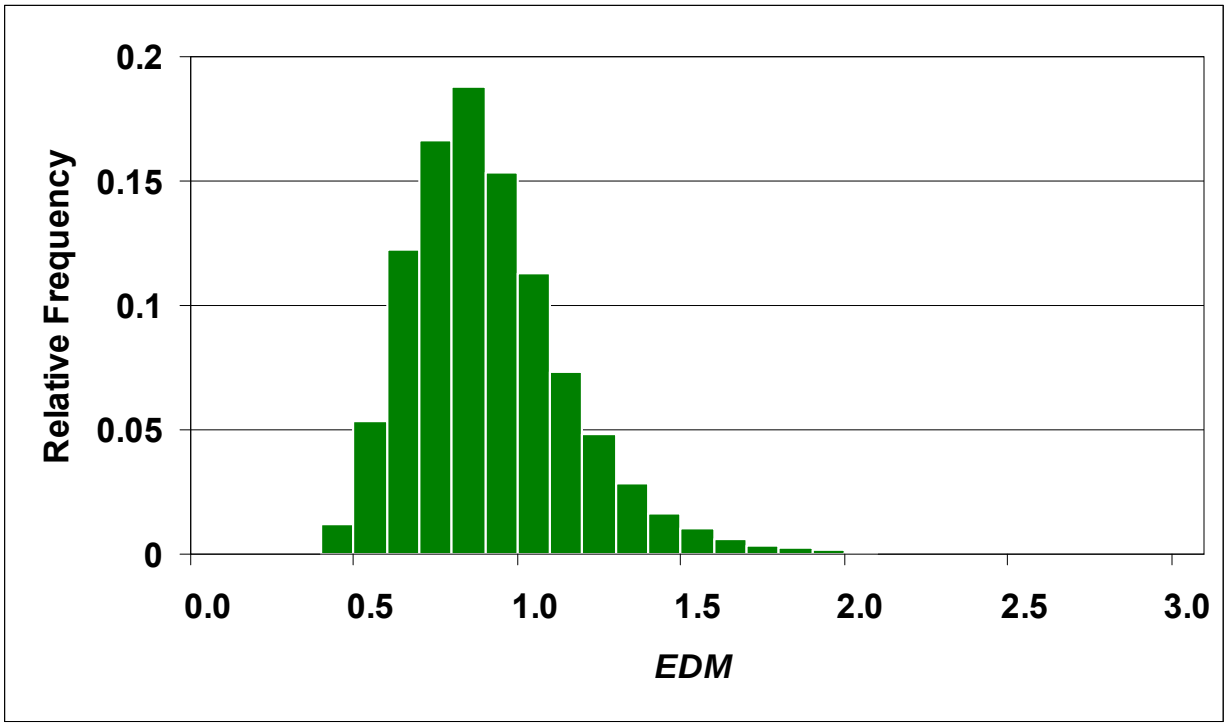

Figure 18. Estimated *EDM* Distribution for Land-based Personnel

Table 3. Distribution Specifics for F_{os} and F_t for Land-Based Personnel on Enewetak during Operation HARDTACK I

Parameter	Definition	Distribution for Probabilistic Analysis (*)	Nominal Value for Central Estimation	Deterministic(*)
F_{os}	Fraction of time spent outside	Triangular min = 2/24 mode = 8/24 max = 16/24	0.34 (or 8/24)	0.6 (or 14.4/24)
F_t	Fraction of inside time spent in tent	Triangular min = 0 mode = 0.5 max = 1	0.5	0

(*) High-sided per guidance in NTPR Policy and Guidance Manual (DTRA, 2007).

4.2.3 Shielding Factors for Ships

A shielding factor (*SF*) is defined as the ratio of intensity at some below-deck location to the average topside intensity. An investigation of shielding factors in interior spaces of ships from contaminants deposited on weather deck surfaces is conducted in this special study. The

shielding factor is dependent on the characteristics of the ship (e.g., beam or maximum width, length, number of decks, deck height, and decking thickness) and on one's position within the ship (deck and location on that deck). A Mathcad program was developed to calculate ship- and deck-specific distributions of *SF*, assuming uniform topside deposition of fallout.

4.2.3.1 Technical Approach and Methodology

A methodology analogous to that employed in the calculation of protection factors was used here: the propagation of gamma radiation over a distance *R* through air was modeled with a point kernel $AirAttn(R)/R^2$, where $AirAttn(R)$ accounts for all propagation effects (e.g., absorption, scattering, build-up, air-ground interface) except $1/R^2$ dispersion. The function $AirAttn(R)$ was derived with the two-dimensional transport code CYLTRAN for propagation of Finn-spectra gamma radiation through air over iron. The resultant data were then fit piecewise in Excel to obtain the equation shown below, where *R* is in meters.

$$
\begin{aligned}
AirAttn(R) &= exp(0.4547 \cdot R^{-0.5796} - 0.5) && \text{if } R < 17.35 \\
&= exp(0.5404) \cdot R^{-0.3344} && \text{if } 17.35 \le R < 31.65 \\
&= exp(5.18 \cdot 10^{-8} \cdot R^3 - 2.966 \cdot 10^{-5} \cdot R^2 + \\
&\qquad 1.2016 \cdot 10^{-4} \cdot R - 0.5906) && \text{if } 31.65 \le R < 316.2 \\
&= 0.6971 \cdot exp(-0.004787 \cdot R) && \text{if } R \ge 316.2
\end{aligned}
\tag{4-6}
$$

The attenuation of gamma rays passing through deck materials was modeled by first using the CEPXS transport code to calculate ratios of doses for normally-incident Finn-spectra gamma radiation before and after passing through various thicknesses of shielding materials. The results were then fit in Excel to obtain the equations displayed below for steel and wood. The deck thickness *t* is in centimeters in these expressions.

$$
\begin{aligned}
SteelAttn(t) &= exp(-0.000307 \cdot t^4 + 0.006608 \cdot t^3 - 0.05135 \cdot t^2 \\
&\qquad - 0.16737 \cdot t) && \text{if } t < 10 \\
&= exp(-0.4179 \cdot t + 0.9044) && \text{otherwise}
\end{aligned}
\tag{4-7}
$$

$$
\begin{aligned}
WoodAttn(t) &= exp(-1.0695 \cdot 10^7 \cdot t^4 + 2.3021 \cdot 10^{-5} \cdot t^3 \\
&\qquad - 0.0017024 \cdot t^2 - 0.16737 \cdot t) && \text{if } t < 100 \\
&= exp(-0.0847 \cdot t + 2.1541) && \text{otherwise}
\end{aligned}
$$

In this Mathcad algorithm, the weather deck surface is assumed to be either rectangular (for aircraft carriers) or elliptical (for all other ships). The distribution of *SF* for a given deck on a specific ship was calculated by randomly sampling horizontal locations on that deck. Then, for

each location, the point kernel $AirAttn(R)/R^2$ was integrated over the gamma source, which is assumed to have been uniformly distributed over the weather deck of the ship, to obtain the intensity at a height of 1 meter above the decking. At each step in the integration, the gamma radiation was attenuated via $SteelAttn(t)$ for steel decks or $WoodAttn(t)$ for wooden decks. In these expressions, "t" is the line-of-sight thickness of all decking material between the source point and the location of interest, multiplied by a factor f_w ("Waldorf factor") to account for miscellaneous materials such as pipes, bulkheads, etc. Measurements made in the late 1950s on the test ship USS COWPENS (a light aircraft carrier originally designated CVL 25, but relegated to the reserve fleet and re-designated AVT 1 by the time of the experiment) and reported in Waldorf (1959) indicate that the best estimate of f_w is 2.35 ± 0.27. In the present formulation, the distribution of f_w is assumed to be Gaussian with a mean of 2.35 and a standard deviation of 0.27 for all ship types. This estimate should be fairly representative for aircraft carriers, but its applicability to other ship types is less certain. The question of applicability manifests itself as an increase in uncertainty which could be incorporated by increasing the standard deviation of the distribution.

A more detailed discussion of the *SF* uncertainty algorithm is available in Weitz (2009d).

4.2.3.2 Results and Discussion

Distributions of below-deck shielding factors for various ship types were generated using the algorithm discussed above. Examples of these distributions are presented in Figure 19 for five decks of the aircraft carrier USS BOXER and in Figure 20 for the three decks of USS ESTES. In this analysis, the uncertainty in deck height was modeled as a triangular distribution with minimum of 2.2 m, mode of 2.44 m, and maximum of 3 m. The uncertainty in decking thickness was modeled as triangular distribution with deck-specific minima, peaks, and maxima derived from thicknesses reported for USS COWPENS (Tomoeda et al., 1959). The mean *SF*s for the five decks of USS BOXER, in descending order below the flight deck, are 0.16, 0.074, 0.038, 0.013, and 0.005, and for the three decks of USS ESTES are 0.20, 0.035, and 0.017.

An approach utilizing the *EDM* concept, similar to that discussed in the preceding section for land-based personnel, was also applied here. It is straightforward to calculate the film-badge equivalent dose D^* that a hypothetical crewman would have received by remaining topside and being continuously exposed to the average topside intensity. The dose D for a real crewman who spent only part of his time topside will vary from D^* because (1) he spent the remaining portion of his time below deck where the intensity is reduced by a factor *SF* due to displacement and shielding, and (2) his time topside was most likely spent at a location that had an intensity different from the average. As before, *EDM* is defined as the ratio D/D^* and is used to determine D.

In this case, *EDM* is calculated based on the following assumptions regarding the locations of a generic crewman and relevant radiation intensities:

- A crewman was topside a fraction F_{ts} of his time at a location where the relative topside intensity was I_1. *Relative topside intensity* is defined here as the ratio of the local topside intensity to the average topside intensity.

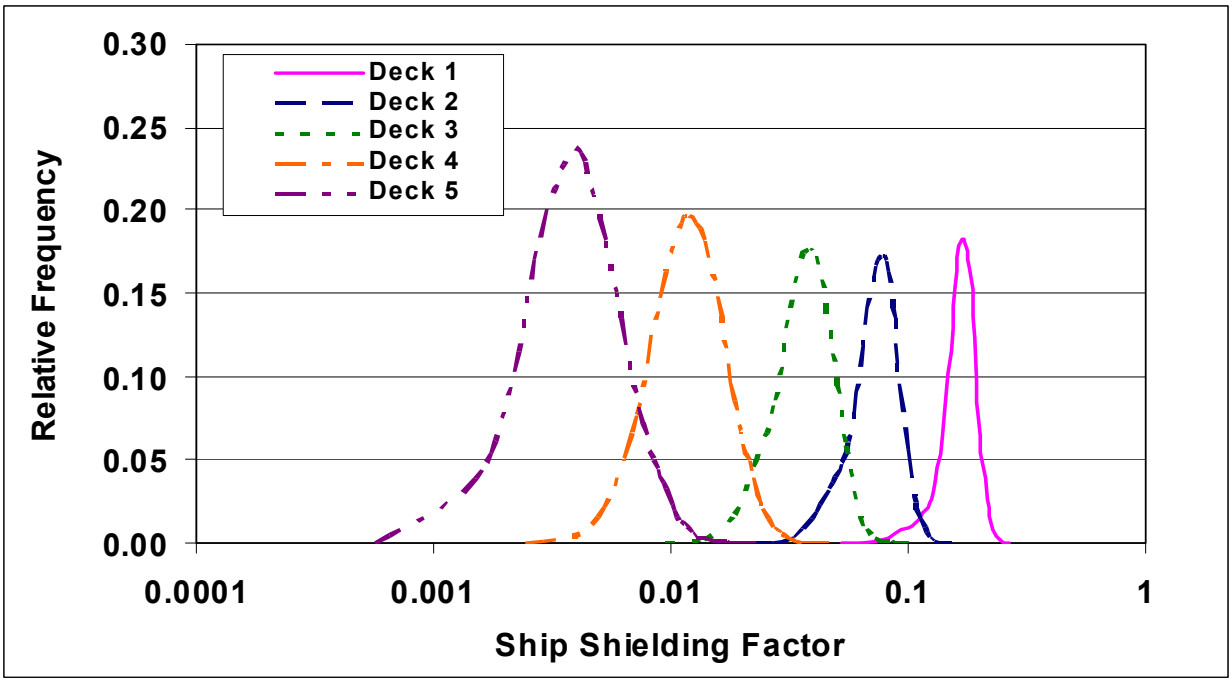

Figure 19. Distribution of Below-Deck Shielding Factors for USS BOXER

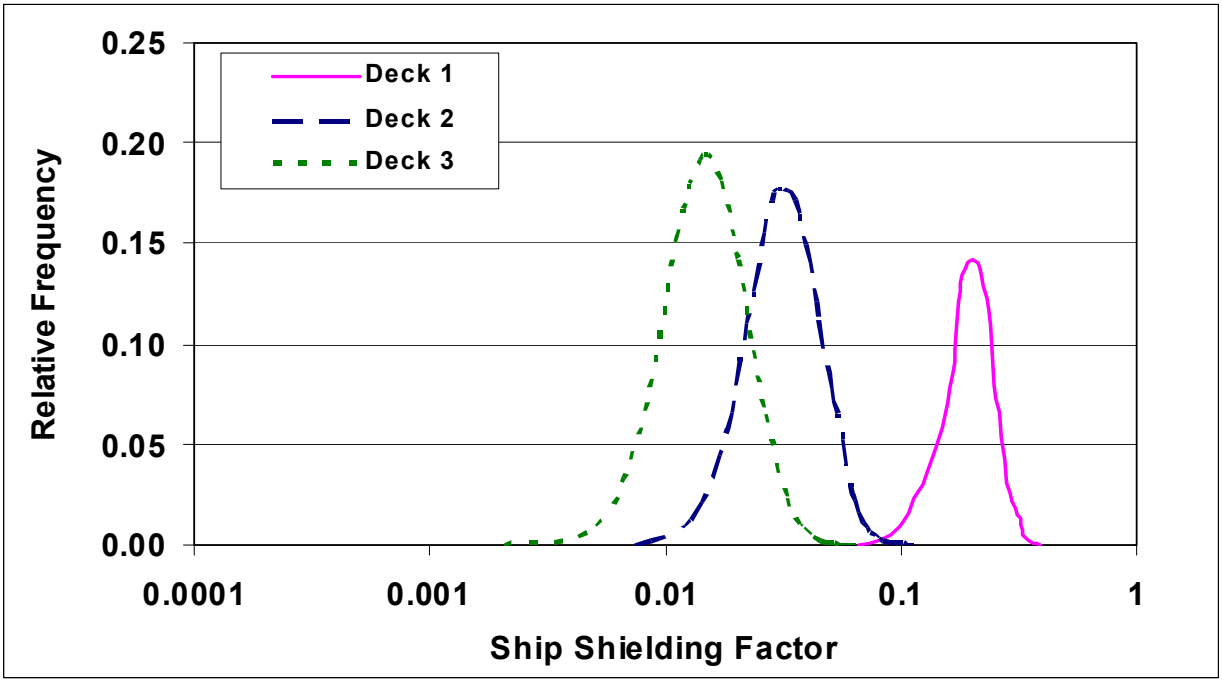

Figure 20. Distribution of Below-Deck Shielding Factors for USS ESTES

- He split his below-deck time evenly between his worksite, where the shielding factor was SF_w and the relative topside intensity was I_2, and his billet location characterized by analogous parameters SF_b and I_3. (The distribution of time between worksite and billet location could appropriately be treated as a random variable and drawn from yet another distribution). For a below-deck location, the relative topside intensity is the intensity at the topside location vertically above the below-deck location divided by the average topside intensity.

EDM for this scenario is then given by:

$$EDM = F_{ts} \cdot I_1 + \left(\frac{1 - F_{ts}}{2}\right) \cdot \left[SF_w \cdot I_2 + SF_b \cdot I_3\right] \tag{4-8}$$

The relative topside intensities I_1, I_2, and I_3 may be drawn from a distribution that characterizes the variation in topside intensity, such as those shown in Figure 14 and Figure 15. Similarly, SF_w and SF_b, which are treated as fully correlated test to test, can be sampled from distributions such as those shown in Figure 19 and Figure 20. Examples of *EDM* distributions thus derived are displayed in Figure 21 for personnel on the aircraft carrier USS BOXER and in Figure 22 for personnel on the USS ESTES.

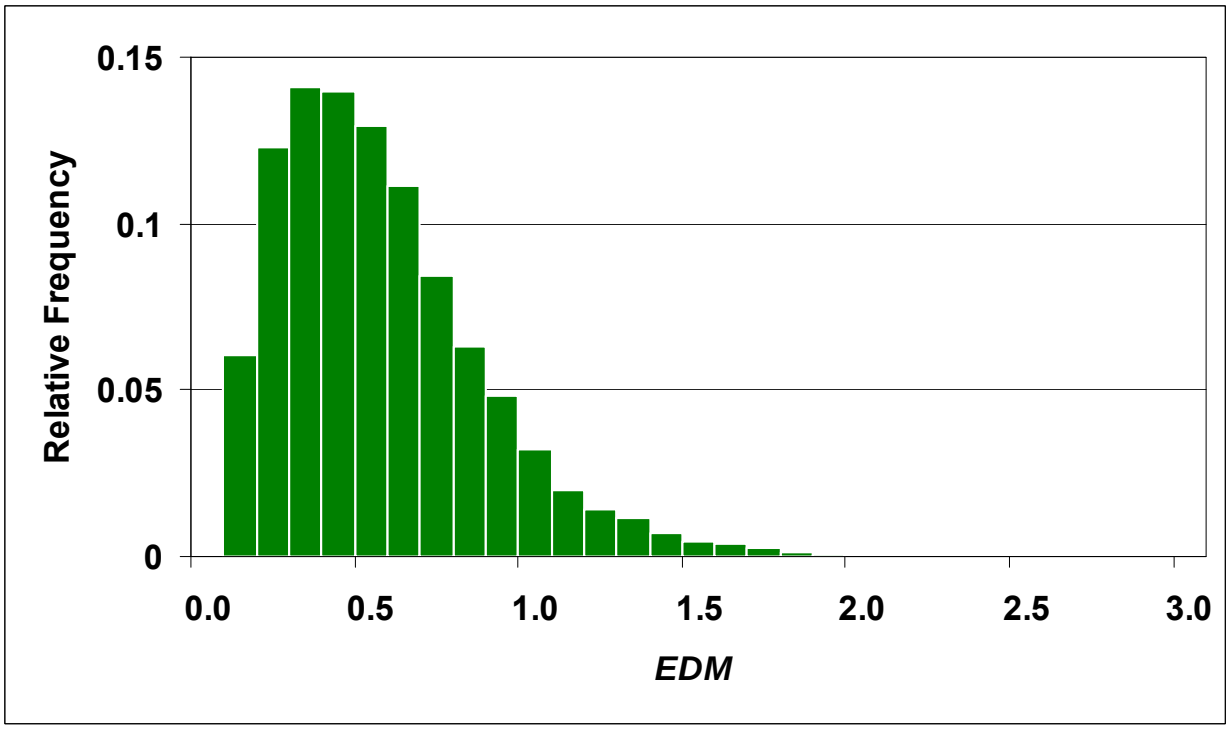

Figure 21. *EDM* Distribution for Personnel on USS BOXER

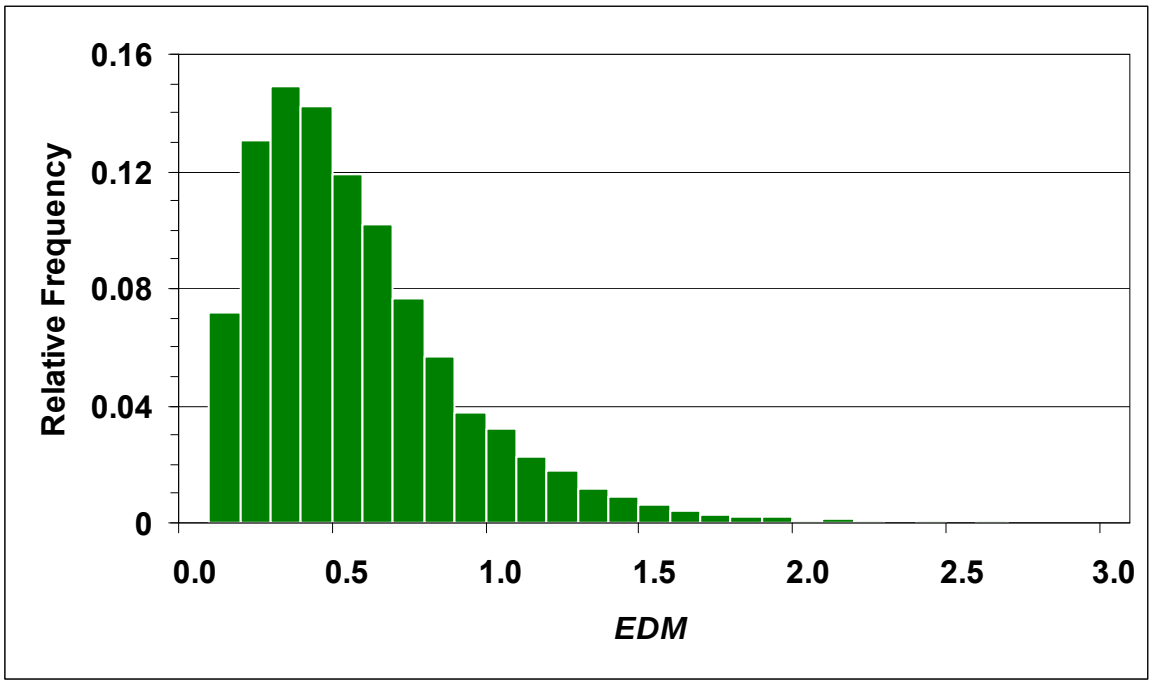

Figure 22. *EDM* Distribution for Personnel on USS ESTES

A value of 0.1 for the shielding factor of below-deck spaces has been used in deterministic dose reconstructions. Because the shielding factors developed in this study depend on deck level, the appropriate average shielding factor for a particular case depends on the fraction of time the subject spent on each deck. For example, if the worksite of a representative crewman aboard BOXER is equally likely to have been on either of the first two decks below the flight deck, and his billet area equally likely to have been on either of the two decks below that, as assumed in Case Study 5, his composite average shielding factor is 0.072.

4.2.4 Shot-Specific Radiological Decay Functions

As discussed in Section 3.2, shot-specific, time-dependent decay functions can be obtained directly from the FIIDOS code. A database compiled from FIIDOS output provides relative intensities from 3 seconds to 5 years post-detonation for most shots and most operations. This database was utilized in the present case studies to characterize the time dependence of fallout intensity.

The key uncertainty in the FIIDOS-derived decay functions is most likely the degree to which radiochemistry data based on cloud samples are representative of the radionuclide mix that was deposited and remained on the ground at any given location, that is, how much fractionation took place during the deposition process and thereafter due to weathering. Inherent in the FIIDOS database is the assumption that no fractionation, other than removal of noble gases, occurred during and after deposition. A rigorous study of fractionation is beyond the scope of the present effort, but constitutes an area for future research and model refinement. In the meantime, an empirical model of the uncertainty in the FIIDOS decay functions was developed for use in the case studies.

4.2.4.1 Technical Approach and Methodology

Most fallout events are characterized by a set of early-time intensity-time pairs (as illustrated in Table 1 of Section 3), the last pair of which is typically used as the baseline or starting point for extrapolating the intensity forward in time. In the case studies, the extrapolation in time for any Shot X was accomplished with the FIIDOS-generated, shot-specific decay function $I_X(t)$. Let I_b be the baseline intensity for Shot X and t_b be the time (after detonation) at which I_b occurred, such that $I_X(t_b) = I_b$. The model intensity $I_X(t)$ and the actual intensity $I'_X(t)$ agree at t_b but will generally deviate thereafter. The difference between $I_X(t)$ and $I'_X(t)$ is the modeling error at time t. The premise is that the modeling error will generally increase with time from zero at t_b. (Any uncertainty in I_b is attributable to measurement (and/or possibly other) error, but not to the decay model.) The following equation represents a family of possible decay paths that satisfy this premise.

$$I'_{Xi}(t) = \left(\frac{t}{t_b}\right)^{a_i} \cdot I_X(t) \tag{4-9}$$

In a Monte Carlo simulation, a different decay path is followed each time the exponent a_i is drawn. In this implementation, a_i is drawn for each history from a Gaussian distribution with mean $\mu_a = 0$ and standard deviation $\sigma_a = 0.15$; the basis for this value of σ_a is discussed below.

4.2.4.2 Results and Discussion

The criterion for determining σ_a is that about two-thirds of the population of real intensity decay functions fall within the bounds $I_X(t) \cdot K$ and $I_X(t)/K$, where

$$K = \left(\frac{t}{t_b}\right)^{\sigma_a} \tag{4-10}$$

Shot-specific decay data extending to 6 months or more after the detonation are sparse. Decay functions for the following three shots were deduced from experimental measurements and are used here to quantify σ_a.

- Operation GREENHOUSE Shot EASY, using decay data from the example following Table 2 in Section 3.2.
- Operation CASTLE Shot BRAVO, a power law decay function $t^{-\lambda}$ with six values of λ for specific time intervals (Thomas et al., 1984).
- Operation PLUMBBOB Shot SHASTA, with a power law decay function defined on page 94 of Goetz et al. (1979).

For the decay function uncertainty model described above to be judged adequate on the basis of this admittedly small data set, two of these measurement-based decay functions should fall essentially between the bounds established by Equation 4-10, and the third should spend significant time outside these bounds. Results for the aforementioned three shots are displayed

in Figure 23–Figure 25. In each of these figures, the dashed line is the FIIDOS-derived decay function $I_X(t)$, the two dotted lines are the bounds about $I_X(t)$ given by Equation 4-10 for σ_a = 0.15, and the solid line is the measured decay function. It is seen that, for the most part, the measurement-based decay functions are appropriately bounded by the uncertainty model. Therefore, the model passes the two-thirds criterion, although the sample of measurement-based decay functions is quite small.

4.2.5 Gamma Source Modification Factor

Ratios of surface activity density to intensity [Ci m^{-2} per R hr^{-1}], generated with the FIIDOS code (Raine et al., 2007) for infinite plane sources, are used in internal dose calculations to estimate airborne activity concentrations based on intensity measurements. The Gamma Source Modification Factor (*GSMF*) corrects for the fact that the contaminated surface was not infinite in spatial extent, as assumed in the FIIDOS calculations. For land-based applications, the area of fallout deposition was generally large enough that the correction is insignificant. Thus, for exposures to fallout on land, *GSMF* is set equal to 1. However, for shipboard exposure scenarios, the contaminated area was limited to the weather deck of the ship and the correction is necessary. A deterministic value of 2 has typically been used for *GSMF* in internal dose assessments of shipboard personnel performed in the NTPR Program. This section discusses the formulation of *GSMF* for probabilistic assessments of shipboard exposures.

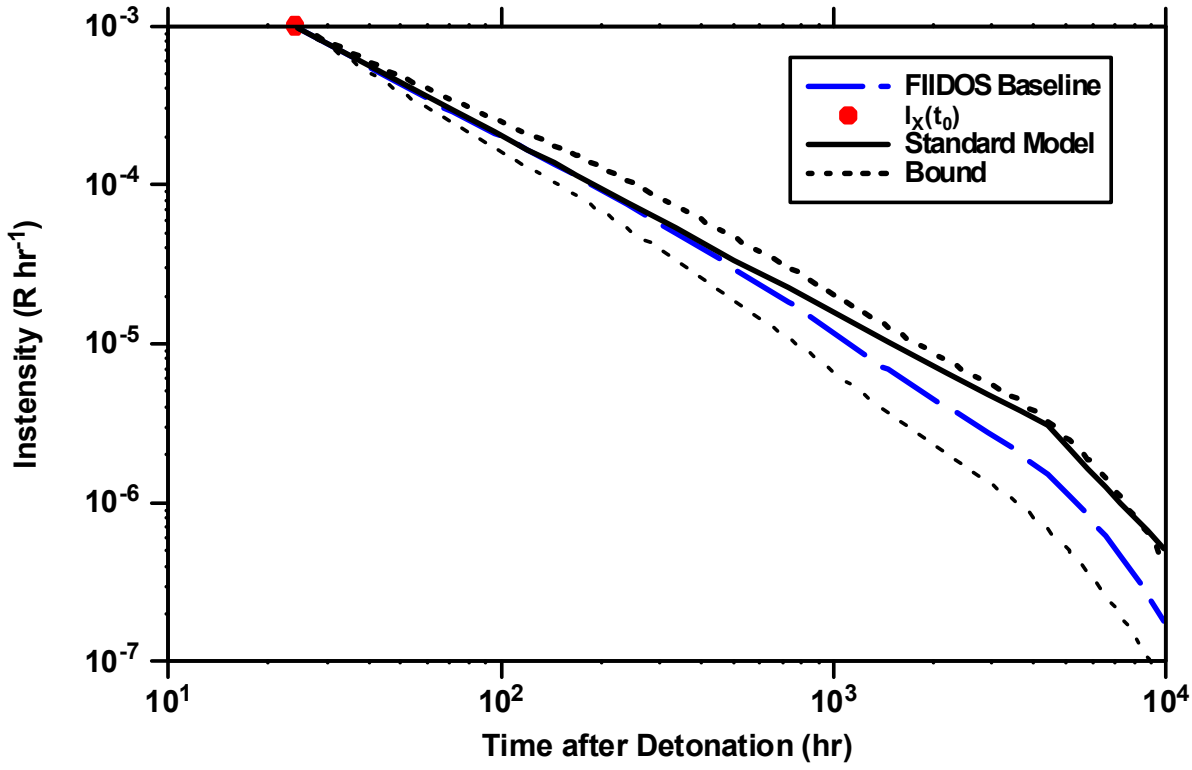

Figure 23. Uncertainty Model Comparison for Operation GREENHOUSE Shot EASY

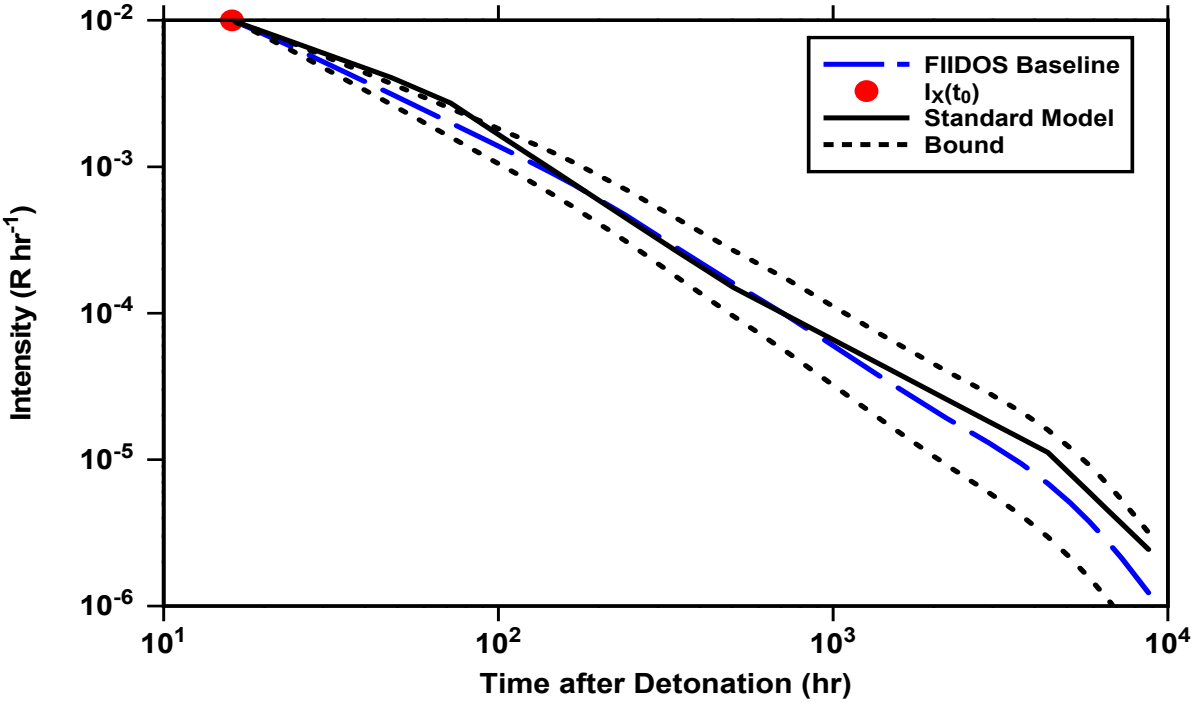

Figure 24. Uncertainty Model Comparison for Operation CASTLE Shot BRAVO

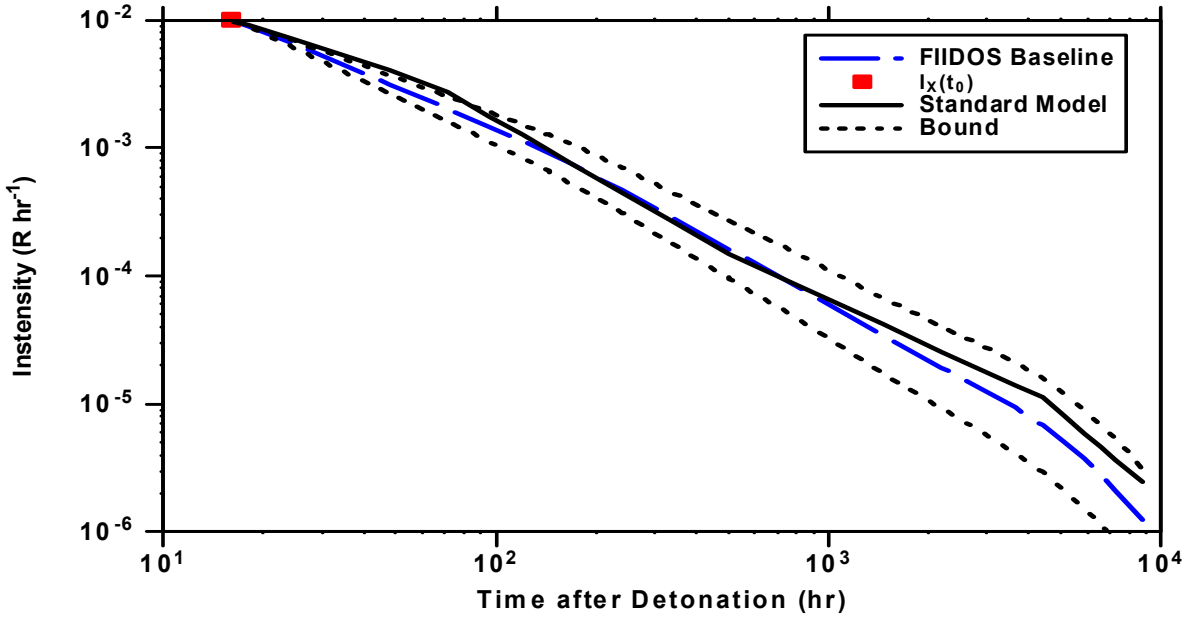

Figure 25. Uncertainty Model Comparison for Operation PLUMBBOB Shot SHASTA

4.2.5.1 Technical Approach and Methodology

In the present formulation, it is assumed that homogeneous fallout material was deposited uniformly over the weather deck of a ship. The dose rate at a height of 1 meter above the deck from an increment of gamma-emitting fallout on the deck at a horizontal distance R is modeled by a point-kernel function $Prop(R)/R^2$, as in the analysis of intensity distribution from fallout on ships discussed in Section 4.2.1. The function $Prop(R)$ is given by Equation 4-2.

GSMF Distribution for Aircraft Carrier

An aircraft carrier presents the simplest case for calculating *GSMF*: its flight deck is nearly rectangular, and the superstructure is isolated on the starboard side of the ship so that, as a first approximation, it can be ignored. The value of *GSMF* for a topside location specified by the Cartesian coordinates (X,Y) on an aircraft carrier whose flight deck has width W and length L is calculated by the following Mathcad expression:

(4-11)

$$GSMF(X,Y) = \frac{\int_{-\infty}^{\infty}\int_{-\infty}^{\infty} \frac{Prop\left(\sqrt{x^2+y^2+H^2}\right)}{x^2+y^2+H^2}\,dy\,dx}{\int_{-\frac{L}{2}}^{\frac{L}{2}}\int_{-\frac{W}{2}}^{\frac{W}{2}} \frac{Prop\left[\sqrt{(x-X)^2+(y-Y)^2+H^2}\right]}{(x-X)^2+(y-Y)^2+H^2}\,dx\,dy}$$

In this equation, H is the height above the topside surface, taken as 1 meter in this analysis.

A Monte Carlo approach is used in a Mathcad program to generate a distribution of *GSMF* values for this ship. Specifically, n sets of coordinates (X_i, Y_i), each representing a possible observer location, are selected randomly such that $\{-½W \le X_i \le ½W\}$ and $\{-½L \le Y_i \le ½L\}$ for $i = 1,\ldots,n$. These coordinates are than used in Equation 4-11 to generate values of *GSMF* corresponding to the random topside locations. One such distribution, generated for the aircraft carrier USS BOXER (L = 271 m, W = 45 m) with a sample size of n = 10,000, is shown in Figure 26. The probability, expressed as relative frequency, is strongly peaked at the lower values of *GSMF* because much of the topside area of a uniformly contaminated aircraft carrier has a relatively uniform intensity profile. Near the boundaries of the topside area (i.e., near the edges of the flight deck), the intensity decreases because the radiation, on average, must travel farther to reach these locations and, hence, is subject to increased dispersion and attenuation. This causes the denominator of Equation 4-11 to decrease and *GSMF* to increase, resulting in the "tail" of higher *GSMF* values evident in Figure 26.

The details of this distribution are not particularly relevant here—the important feature is its value when averaged over all topside locations, designated <*GSMF*>. Based on the dynamics of fallout deposition, it is likely that the airborne activity concentration, $C_a(t)$, at any time t during a

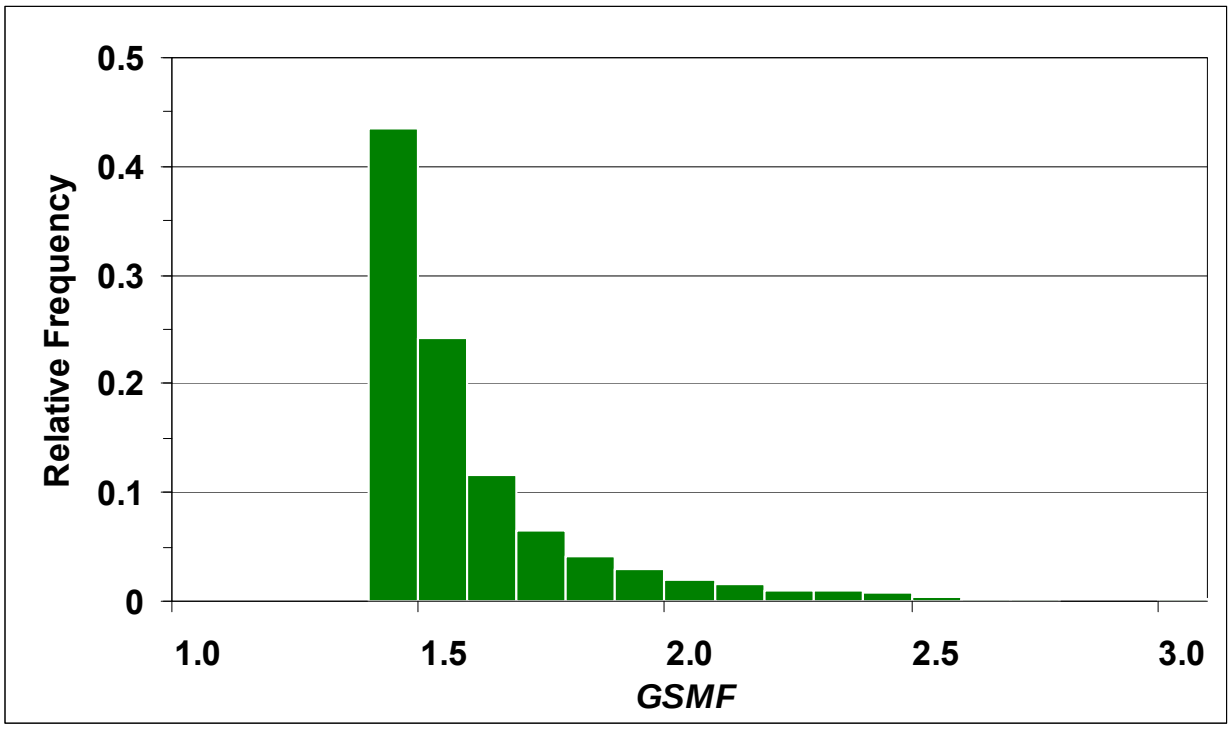

Figure 26. *GSMF* Probability Distribution for USS BOXER

fallout event was nearly uniform over the extent of a ship. Therefore, it can be assumed that all personnel who were topside during such an event were exposed to the same $C_a(t)$, regardless of their specific locations. The general approach employed in the NTPR Program to quantify $C_a(t)$ is to use the aforementioned FIIDOS surface activity density-to-intensity ratios in conjunction with average topside intensities that were recorded in deck logs and/or in operational reports, or that were reconstructed on the basis of average intensity data reported on nearby ships or islands. Thus, it is appropriate to also use the topside-averaged value of *GSMF* when correcting $C_a(t)$ for the finite extent of the source.

The task now is to estimate the uncertainty in $\langle GSMF \rangle$. Factors that contribute to this uncertainty for an aircraft carrier include (1) shielding provided by aircraft that may have been located on the flight deck, (2) the impact of the superstructure, and (3) the deviations of the flight deck from the idealized rectangular configuration.

Photographs of carriers, including USS BOXER, taken during operations circa 1950's (available http://www.navsource.org/archives/) indicate that aircraft were frequently parked in tight formation on the aft of the ship, typically spanning the width W of the flight deck and occupying an area of roughly $W \times W$ to $2W \times W$. To the extent that these parked aircraft attenuated the gamma radiation emitted by fallout deposited around and behind them, the length L of the flight deck was effectively reduced by an increment δ. In the limit of total attenuation, δ ranges from 0 (when no aircraft were parked on the flight deck) to $2W$ (when parked aircraft occupied an area of $2W \times W$), with the most likely reduction perhaps being W. While the parked aircraft could not have provided such effective shielding, use of this seemingly high-sided assumption allows for

the shielding effects of various other aircraft and equipment that may have been located in other areas of the flight deck. On this basis, δ is treated here as a random variable drawn from a triangular distribution with minimum = 0, mode = W, and maximum = $2W$. The "effective" length of the flight deck is then $L_{eff} = L - \delta$.

In an analogous manner, deviations from the idealized rectangular configuration of the fallout field due to the presence of the superstructure and variations in the topside width can be crudely modeled as a reduction in the overall width of the flight deck. Photographs of various carriers indicate that the superstructure and associated "clutter" occupy roughly 5–10 percent of the topside area. Another 5–10 percent of the idealized rectangular fallout field is "lost" due to a narrowing of the flight deck in the forward section of the carrier. This relatively minor perturbation would most affect those working in that area. To incorporate these features into the uncertainty model, the nominal width W of the flight deck is reduced by a fraction f to determine an "effective" width $W_{eff} = (1-f)\times W$. The random variable f is assigned a triangular probability distribution with minimum = 0, mode = 0.1, and maximum = 0.2.

The distribution of <*GSMF*> for fallout deposition on an aircraft carrier is derived by a Monte Carlo algorithm employing two loops: an outer loop in which randomly selected values of δ and f are used to define L_{eff} and W_{eff}, and an inner loop where, given these dimensions, the locations (X,Y) on the flight deck are randomly sampled and *GSMF* computed for each. Each inner loop provides a *GSMF* distribution similar to that shown in Figure 26, and from that, one value of <*GSMF*>. The probability distribution of <*GSMF*> shown in Figure 27 was thus obtained with a composite sample size of 90,000 (300 outer loops x 300 inner loops) for USS BOXER. The average value of <*GSMF*> in this example is 1.56. It is seen that the distribution of <*GSMF*> is narrow, indicating that this uncertainty does not have significant impact.

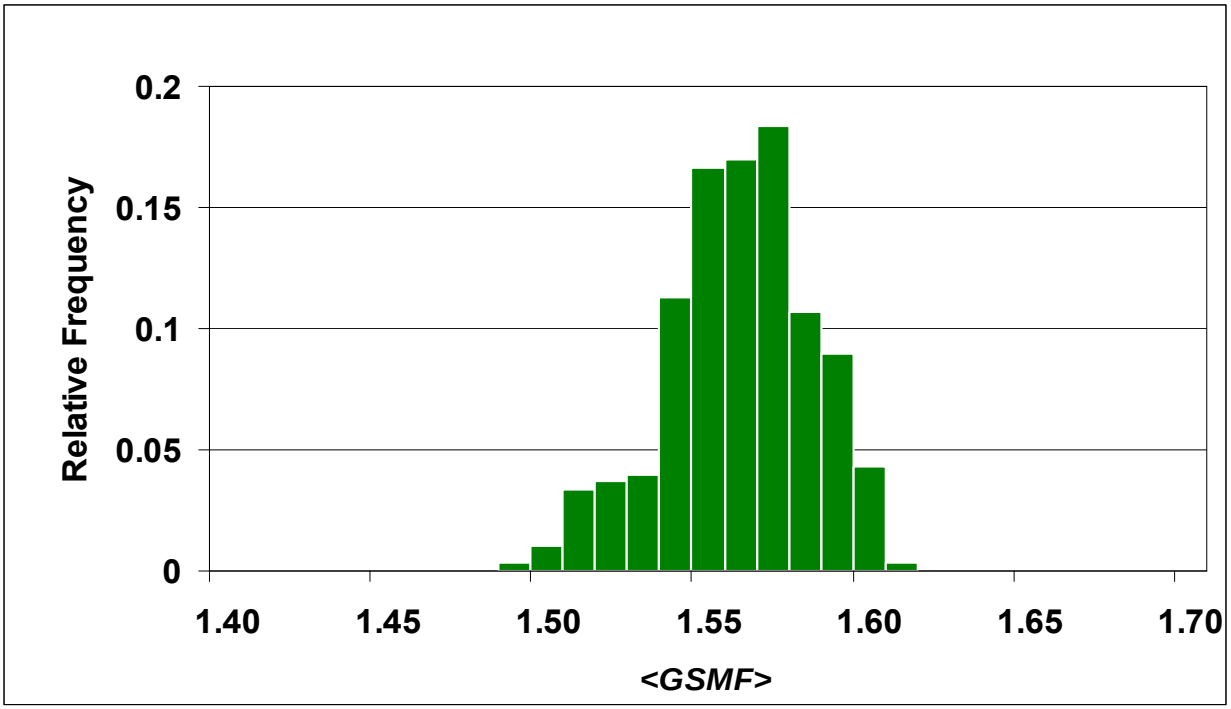

Figure 27. Probability Distribution of Average *GSMF* for USS BOXER

***GSMF* Distributions for Other Ship Types**

All ship types other than aircraft carriers are modeled as having an elliptical topside configuration with major axis equal to the length L of the ship and minor axis equal to the ship's maximum width (beam) W. If the ship did not have a superstructure, *GSMF* could be calculated by simply integrating over the elliptical surface, as indicated in the denominator of Equation 4-12.

$$GSMF(X,Y) = \frac{\int_{-\infty}^{\infty}\int_{-\infty}^{\infty} \frac{Prop\left(\sqrt{x^2+y^2+H^2}\right)}{x^2+y^2+H^2}\,dy\,dx}{\int_{-\frac{L}{2}}^{\frac{L}{2}}\int_{-W\cdot\left[\frac{1}{4}-\left(\frac{y}{L}\right)^2\right]^{\frac{1}{2}}}^{W\cdot\left[\frac{1}{4}-\left(\frac{y}{L}\right)^2\right]^{\frac{1}{2}}} \frac{Prop\left[\sqrt{(x-X)^2+(y-Y)^2+H^2}\right]}{(x-X)^2+(y-Y)^2+H^2}\,dx\,dy} \qquad (4\text{-}12)$$

On most ship types, however, the superstructure significantly impacts the topside topology. The configuration of the superstructure is generally quite complex and difficult to treat analytically. To simplify the analysis, the superstructure is modeled as an ellipse with a reduced length $\sqrt{S}\times L$ and a reduced width $\sqrt{S}\times W$ (with $0 < S < 1$), concentric and co-oriented with the ellipse that defines the ship's topside boundary. The parameter S is the fraction of the ship's total topside area that is occupied by the superstructure. The values of S are chosen to best characterize the superstructure's "footprint" for each type of ship. For example, S is approximately 0.25 for a liberty ship (YAG), 0.3 for a tank landing ship (LST), and 0.5 for an attack transport (APA), amphibious cargo ship (AKA), and destroyer (DD). For given values of W, L, and S, the outer and inner ellipses are defined in Cartesian (x,y) coordinates by Equations 4-13 and 4-14, respectively.

$$\left(\frac{x}{½W}\right)^2+\left(\frac{y}{½L}\right)^2=1 \qquad (4\text{-}13)$$

$$\left(\frac{x}{½W}\right)^2+\left(\frac{y}{½L}\right)^2=S \qquad (4\text{-}14)$$

This ellipse-in-ellipse configuration is shown in Figure 28.

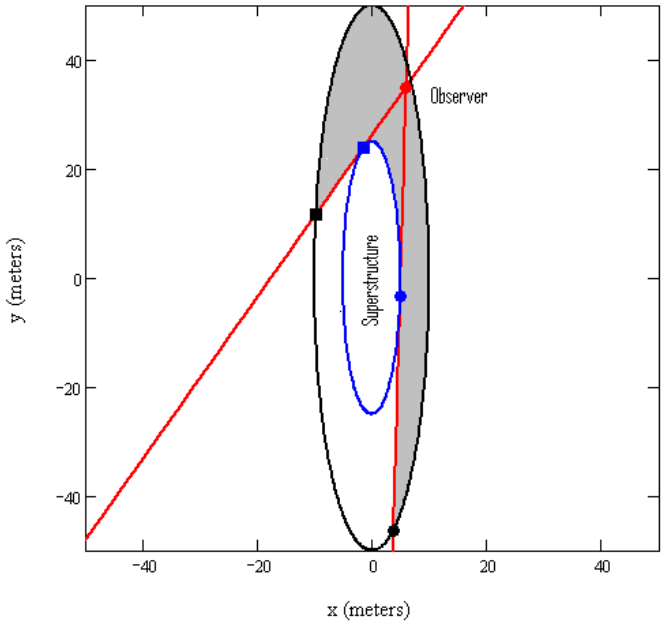

Figure 28. Superstructure Model

The superstructure is assumed to be opaque to radiation, and therefore provides complete shielding to a topside observer from radiation emitted by fallout that is not within his direct field of view. Thus, in the denominator of Equation 4-12, the limits of integration must be adjusted so that only the topside area within the field of view of the observer is included. For an observer at the topside location indicated by the red dot in Figure 28, his field of view of the fallout field is bounded by the two red lines drawn through his location to the points of tangency on the inner ellipse (superstructure). The area of integration is the shaded region indicated in the figure. The geometric formulae that are relevant to establishing the limits of integration are provided in Weitz (2009e).

The top of the superstructure of a ship consists primarily of horizontal surfaces 8 feet or more above the main deck. Most of the contaminants deposited on the exterior of these surfaces were therefore not in the field of view of an observer standing on the main (topside) deck, and radiation emitted by these contaminants is strongly attenuated by the superstructure material before reaching that person. For this reason, radiation from contaminants deposited directly on the superstructure is neglected as a first approximation.

Monte Carlo sampling is used in the Mathcad program to calculate the distribution of *GMSF* over the topside surface of an elliptically-shaped ship. Sets of coordinates (X_i, Y_i), each representing a possible observer location, are selected randomly such that $\{-½W \le X_i \le ½W\}$ and $\{-½L \le Y_i \le ½L\}$. The coordinate pair (X_i, Y_i) is accepted only if $S \le \left(\frac{X_i}{½\mathrm{W}}\right)^2 + \left(\frac{Y_i}{½\mathrm{L}}\right)^2 \le 1$, thus ensuring that the observer is on or within the boundary defined by Equation 4-13 and on or outside the boundary defined by Equation 4-14 (i.e., between the two ellipses shown in Figure 28). A value of *GSMF* is then calculated for each acceptable set of coordinates with an

expression similar to Equation 4-12, but with the integration in the denominator limited to the line-of-sight regions of the topside area, exclusive of the superstructure. The probability density function of *GSMF* obtained in this manner for USS ESTES, an amphibious force flagship with parameters L = 140 m, W = 19 m, and S = 0.40, is displayed in Figure 29.

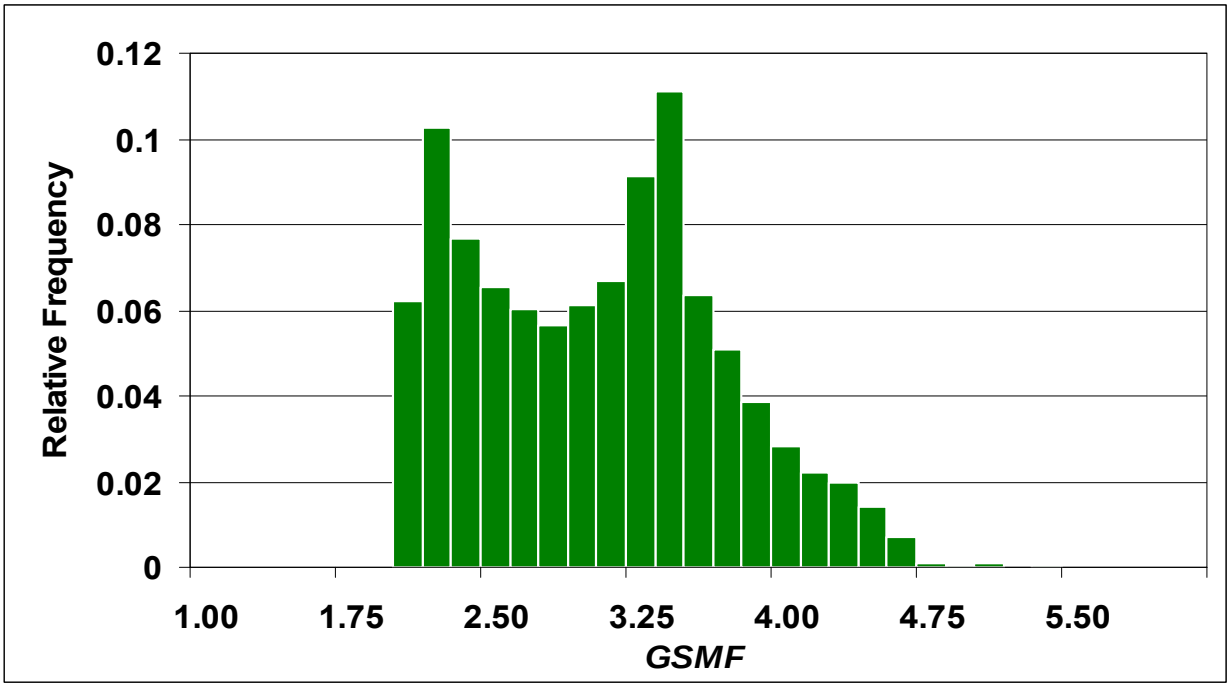

Figure 29. *GSMF* Probability Distribution for USS ESTES

As with the aircraft carrier, the details of the distribution in Figure 29 are not particularly important for the present purpose, where only the mean value <*GSMF*> is needed. The mean of this distribution (2.95), along with those obtained by varying *S,* are plotted in Figure 30 as a function of *S*.

To estimate the uncertainty in average *GSMF* (<*GSMF*>), *S* is treated as a random variable with a triangular distribution having a minimum value of 0 (no superstructure effect, conceivably because the "shine" from fallout that adhered to the superstructure exactly compensated the shielding it provided); a mode of S_{nom}, the nominal value of *S* for the ship of interest (corresponding to a "black" superstructure—one that totally absorbs incident radiation and has no shine); and a maximum given by $S_{nom} + ½(1 - S_{nom})$ (black superstructure plus shielding from topside "clutter" taken as equivalent to expanding the superstructure to encompass half of the area outside the superstructure footprint). The distribution of <*GSMF*> for USS ESTES is shown in Figure 31; it has a mean of 2.95.

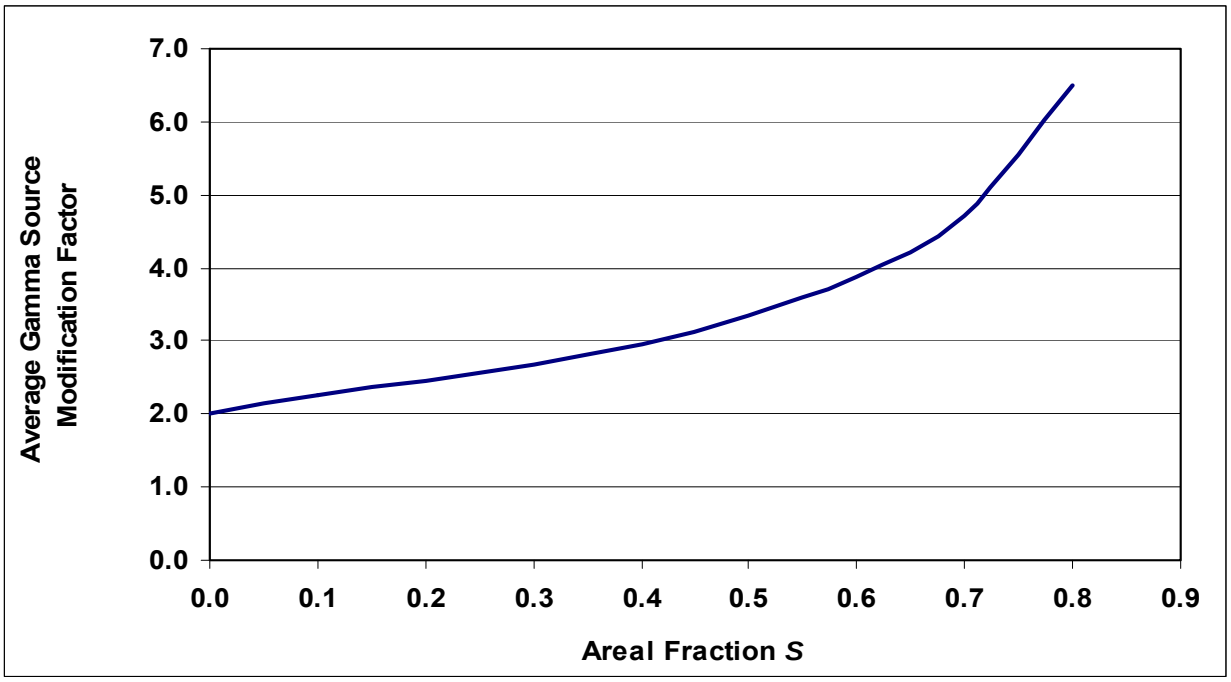

Figure 30. Dependency of Average *GSMF* on Areal Fraction *S* for USS ESTES

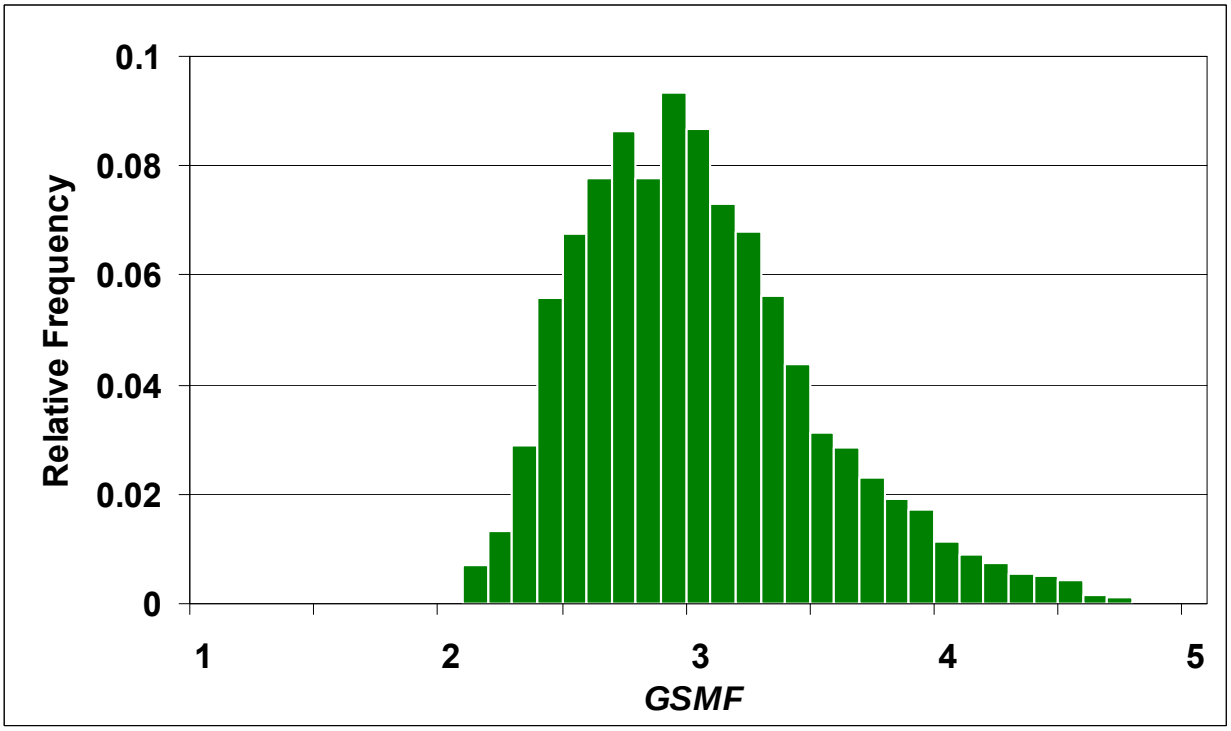

Figure 31. Probability Distribution of Average *GSMF* for USS ESTES

4.2.5.2 Results and Discussion

The average values of *GMSF* for various ship types, obtained with Mathcad implementations of the models described in this Section, are provided in the rightmost column of Table 4, together with the characteristic values of length *L*, width *W*, and nominal superstructure areal fraction S_{nom} used in these analyses. These results are based on Monte Carlo runs of 10,000 histories each. The average values of *GSMF* obtained for similar vessels without allowance for superstructure are included for comparison ("Average *GSMF* w/o SS" column). It is apparent from Table 4 that the presence of the superstructure can significantly impact the value of the *GSMF* for ship types other than an aircraft carrier. While the deterministic value of 2 is representative of the average *GSMF* obtained when the superstructure is neglected, it significantly under-represents the average value of <*GSMF*> obtained for ships (other than aircraft carriers) when accounting for the superstructure.

The distributions of <*GSMF*> used in the case studies of USS BOXER and USS ESTES are shown in Figure 27 and Figure 31.

Table 4. Average *GSMF* for Various Ship Types

Ship Type	Designation	*L* (m)	*W* (m)	S_{nom} (fraction)	Average *GSMF* w/o SS	Average *GSMF* w/SS
Aircraft Carrier	CVS	271	45	0*	1.56	1.56
Amphibious Force Flagship	AGC	140	19	0.40	1.99	2.95
Attack Transport	APA	139	19	0.50	1.99	3.33
Destroyer	DD	115	12	0.50	2.35	4.32
Dock Landing Ship	LSD	140	22	0.40	1.90	2.78
Fleet Tug	ATF	62	12	0.35	2.42	3.66
Salvage Ship	ARS	65	12	0.50	2.42	4.47
Store Ship	AF	103	15	0.30	2.17	3.02
Tank Landing Ship	LST	100	15	0.30	2.18	3.03

* As a first approximation, the superstructure of an aircraft carrier was neglected in this assessment because it is located on the extreme starboard side of the flight deck and therefore provides little shielding to those crewmembers who worked on the flight deck.

4.2.6 Resuspension Factors

Resuspension factors are defined in Section 3, and time-dependent models for deterministic and nominal point estimates for resuspension of fallout as used in the case studies for typical

activities are given in that section. For the probabilistic analysis, the uncertainty associated with the nominal resuspension factor values (land and ship) is assumed to have a lognormal distribution with the median equal to the nominal value, and a 90-percent confidence interval between 0.1 and 10 times the median. This is based on the results of a study reported in conjunction with the basic formulation of the nominal resuspension factor (Anspaugh et al., 2002).

The remainder of this section discusses resuspension factors used for the special case of resuspension of fallout in the vicinity of detonations at NTS.

4.2.6.1 Technical Approach and Methodology

The characterization of the resuspension factors for resuspended fallout in the vicinity of detonations at the NTS is based on a study conducted by Kocher et al. (2006). Of the case studies documented in this report, this type of resuspension is applicable only to the Marine unit at Operation PLUMBBOB. Two general regions of enhanced resuspension in the vicinity of a detonation have been identified. The area closest to ground zero (GZ) is referred to as the precursor region[1], where the peak overpressure associated with a blast wave was 6 pounds per square inch (psi) or greater and resuspension was due to the thermal pulse produced by the detonation. The second region is referred to as the blast-wave region, where the peak overpressure associated with the blast wave was between 6 and 2 psi and resuspension was due to high winds associated with the blast wave of the detonation. The extent of each of these regions is shot-specific, and each is a function of yield and height of burst of the detonation (Glasstone and Dolan, 1977). In the study (Kocher et al., 2006) the contributions of several factors to the overall uncertainty of inhalation doses due to resuspension of previously-deposited fallout in both regions were studied. Those several factors include the following:

- ground surface concentrations of radionuclides
- effects of the detonation on resuspension of deposited fallout
- inhalability and respirability of the resuspended radionuclides
- breathing rates
- inhalation dose coefficients

One conclusion of that report forms the basis for the deterministic model resuspension factors (see Section 3.3.1.1) that were used in the PLUMBBOB case study, i.e., estimation of "effective" resuspension factors for each region that should ensure that deterministic inhalation doses for these scenarios result in credible upper bound doses when used with point estimates of all other parameters normally used in NTPR dose reconstructions. In addition to deterministic values, probability distributions of resuspension factors were available that were used for the

[1] The term "precursor" was changed to "thermal pulse" in a revision to Kocher et al. (2006) recently published as Kocher, D. C., Trabalka, J.R., and Apostoaei, A.J., 2009. Derivation of Effective Resuspension Factors in Scenarios for Inhalation Exposure Involving Resuspension of Previously Deposited Fallout by Nuclear Detonations at Nevada Test Site. DTRA-TR-09-15, *SENES, Oak Ridge, Inc.*, Oak Ridge, TN and Defense Threat Reduction Agency, Fort Belvior, VA. However, the definition of the region did not change, and the term "precursor region" is retained in this report.

probabilistic analysis. Several of the key factors listed above, the uncertainties of which are lumped in the Kocher et al. (2006) analysis into the effective resuspension factor used in the deterministic model, are included separately from the resuspension factor in the inhalation dose probabilistic analysis of the PLUMBBOB case study. In particular, the factors explicitly addressed include uncertainties in breathing rates and inhalation dose coefficients. Therefore, the resuspension factors from the Kocher et al. (2006) report judged to be appropriate for use in the current probabilistic analysis of the PLUMBBOB case are those that account only for uncertainties in the resuspension factors and in the respirable and non-respirable portions of resuspended fallout.

4.2.6.2 Results and Discussion

Values obtained from Kocher et al. (2006) and used in the PLUMBBOB case study are shown in Table 5 for respirable and for inhalable but non-respirable forms of fallout resuspended by nuclear detonations. Based on descriptions in the Kocher et al. (2006) report, and specifically for the purposes of estimating the doses from this pathway, "respirable" is taken to mean particles with activity median aerodynamic diameters (AMAD) less than 10 μm, and "non-respirable" means particles with AMAD between 10 μm and 100 μm (see Section 4.2.10 for an alternate definition of these terms for use in the descending fallout analysis). Accordingly, and consistent with the modeling of descending fallout in this probabilistic study, unbiased inhalation *DCF*s were applied to the respirable portion of this resuspended fallout, and ingestion *DCF*s were applied to the non-respirable portion. ET_2 deposition (i.e., ingestion) of the non-respirable portion of this pathway is currently taken to be 1.0, but this will be the subject of a future modification. Unbiased inhalation *DCF*s are discussed later in this section.

The deterministic resuspension factors shown in Table 5 are significantly larger than the median values used in the probabilistic analysis, also shown in Table 5. This large difference is explained by considering the basis of each of the values. The deterministic values are not intended to represent central estimates, but are instead intended to result in credible upper bound doses by this pathway. In addition, the deterministic values are applied to all particles, not just inhalable or respirable. So, for example in the precursor region, the two 95th percentile probabilistic values (for respirable and non-respirable) can be combined as approximately 2.5×10^{-4} m^{-1}, and this value would be applicable to an upper bound value for particles with an AMAD of less than 100 μm. This value can then be compared to the deterministic value of 1×10^{-3} (also applicable to an upper bound dose), yielding a ratio of 2.5 rather than the ratios of greater than 100 when comparing the deterministic value for each region to the medians for that region.

Table 5. Resuspension Factors (m^{-1}) for Fallout Resuspended by Nuclear Detonations at the NTS

	Median or point estimate(*)	5th percentile	95th percentile
Precursor region			
Deterministic – for all resuspended radionuclides	1×10^{-3}	n/a	n/a
Probabilistic – Respirable form(†)	1×10^{-6} (GSD = 10.8)	4×10^{-8}	5×10^{-5}
Probabilistic – Non-respirable form(†)	8×10^{-6} (GSD = 7.08)	3×10^{-7}	2×10^{-4}
Blast-wave region			
Deterministic – for all resuspended radionuclides	1×10^{-4}	n/a	n/a
Probabilistic – Respirable form(†, ‡)	1×10^{-7} (GSD = 10.8)	4×10^{-9}	5×10^{-6}
Probabilistic – Non-respirable form(†, ‡)	8×10^{-7} (GSD = 7.08)	3×10^{-8}	2×10^{-5}

(*) Median values (and GSDs) are given for probabilistic analysis values and point estimates for the deterministic analysis values.

(†) Modeled distributions for these resuspension factors are lognormal, with distributions characterized by the listed median, 5th and 95th percentile values for each category.

(‡) The distributions for the blast-wave region resuspension factors were recently revised in an update to Kocher et al. (2006)[3] that was published after the analyses described in this report were conducted. The revised distributions are characterized by median (and GSD) values of 1×10^{-8} (GSD ≈ 26) for respirable particles, and 8×10^{-8} (GSD ≈ 22) for non-respirable particles.

4.2.7 Breathing Rate

Physiological parameters related to ventilation influence the volume and rate of air inhaled and the proportions entering through the nose and mouth, thus affecting the amount of radioactive particles and gases inhaled, their penetration into the respiratory tract, and the quantities deposited. Such parameters directly impact radiation doses to tissues of the respiratory tract, but also influence doses to other organs and tissues of the body from the inhalation pathway.

Breathing characteristics and respiratory parameters vary among individuals because they are largely a function of age and body size, level of physical activity, state of health of the respiratory tract, and if the individual is a smoker. The population of atmospheric nuclear test participants was more homogeneous than the population at large with regard to breathing characteristics, having been comprised mainly of Caucasian males in their late teens to early 30s.

[3] Kocher, D. C., Trabalka, J.R., and Apostoaei, A.J., 2009. Derivation of Effective Resuspension Factors in Scenarios for Inhalation Exposure Involving Resuspension of Previously Deposited Fallout by Nuclear Detonations at Nevada Test Site. DTRA-TR-09-15, *SENES, Oak Ridge, Inc.*, Oak Ridge, TN and Defense Threat Reduction Agency, Fort Belvior, VA.

Variability and uncertainties in breathing rates of test participants result principally from differences in duties and activity levels and to a lesser extent, individual physiological variation.

A large amount of data is available on the variability of breathing rates in human populations based on age, gender, race, health conditions, smoking status, and other factors. For this report, summary data and guidance provided in ICRP (1994), NCRP (1997) and USEPA (1997) are used to construct probability distribution functions (pdf) of breathing rates for various types of activity and to apportion time among such activities for atmospheric nuclear test participants. Each of these source documents contains extensive descriptions of data that form the basis for the parameter values used in the analyses described in this report.

4.2.7.1 ICRP 66, Human Respiratory Tract Model (HRTM) for Radiological Protection

The ICRP Committee obtained respiratory physiological data for representative ethnic groups of both sexes, different ages, and for different levels of activity. From these data, reference values representing working Caucasian males and females (17 years and older) were selected for use in the dosimetric respiratory tract model for workers. A second set of values, representing non-working Caucasian males and females of all ages was selected for use in the dosimetric model for the general population.

Because the physiological attributes and activity levels of Caucasian workers are most representative for nuclear test participants, only the reference values for adult males are utilized in the analyses performed for this report. These data are provided in Table 6 (ICRP, 1994, Annex B).

Table 6. ICRP Reference Breathing Rates for Workers

Activity Level	Percent of Maximum Workload [a]	Breathing Rate (m^3 hr^{-1})
Sleep	8	0.45
Rest, sitting	12	0.54
Light exercise	32	1.5
Heavy exercise	64	3.0

[a] Maximum workload = 250 Watts (ICRP, 1994, Annex B)

The recommended daily time fractions associated with each activity are provided in Table 7 (ICRP, 1994).

Table 7. ICRP Daily Time Apportionment for Workers

Activity	Duration (hr day^{-1})
Sleep	8
Occupational	
(5.5 hr light exercise and 2.5 hr rest, sitting)	8
(7 hr light exercise and 1 hr heavy exercise)	8
Non-occupational	
(4 hr rest or sitting, 3 hr light exercise and 1 hr heavy exercise)	8

4.2.7.2 NCRP Report 125: Deposition, Retention and Dosimetry of Inhaled Radioactive Substances

NCRP (1997) cites the reference breathing rates shown in Table 8 for adults (18 years old). The reported values are adapted from Phalen et al. (1985). While an in-depth review of the bases for these values is not provided in the source document, they are similar to the ICRP values.

4.2.7.3 USEPA Exposure Factors Handbook, Volume 1, General Factors

USEPA (1997) provides a comprehensive discussion of respiratory parameters for human populations categorized by age, gender, and activity. Values relevant to nuclear test participants are those for adults from 19 to over 65 years old and outdoor workers for short-term exposures. Breathing rates and corresponding activity patterns are provided in Table 9.

Table 8. NCRP Reference Breathing Rates for Workers

Activity Level	Breathing Rate (m^3 hr^{-1})
Rest [a]	0.6
Light Exertion [b]	1.2
Heavy Exertion [c]	3.6

[a] About 30 percent above basal with respect to minute volume
[b] Matched to minute volume of a reference man (ICRP, 1977)
[c] About 50 percent of maximum level that can be sustained for a few minutes)

Table 9. USEPA Reference Breathing Rates for Adults and Outdoor Workers for Short-Term Exposures

Adults		Outdoor Worker	
Activity Level	**Breathing Rate (m^3 hr^{-1})**	**Activity Level**	**Breathing Rate (m^3 hr^{-1})**
Rest	0.4		N/A
Sedentary activities	0.5		N/A
Light activities	1.0	Slow activities	1.1
Moderate activities	1.6	Moderate activities	1.5
Heavy activities	3.2	Heavy activities	2.5

Activity levels for the average adult male are defined by USEPA as:

- Rest: lying down.
- Sedentary: sitting and standing.
- Light: walking on a level firm surface at 3 miles per hour (mph).
- Moderate: fast walking or slow running (3.3 to 4 mph), climbing stairs, digging with a spade.
- Heavy: fast running (4.5 to 6 mph), cross-country skiing.

The outdoor worker cohort consisted of 15 men and 5 women between the ages of 15 and 50, who worked outdoors at least 10 hours per week. Activity (exertion) levels, self-reported by the test subjects as slow, moderate, and fast, are nominally equivalent to normal walking, moderate walking, and running, respectively. Table 10 presents summary data for adult males that list breathing rate ranges by age and activity level (USEPA, 1997, Table 5A-7).

Table 10. USEPA Summary of Breathing Rates for Adult Males

Breathing Rate (m^3 hr^{-1})				
Activity Level	**Sample Size (n)**	**Low**	**Mean**	**High**
Rest	454	0.14	0.73	1.13
Light	102	0.14	0.83	1.66
Moderate	102	0.86	2.45	4.68
Heavy	267	2.08	4.8	11.00

The low and high values in Table 10 above are from reported ranges in Table 5A-7 in USEPA (1997) and therefore represent the minima and maxima of the data sets.

4.2.7.4 Results and Discussion

A comparison of the USEPA summary data in Table 10 with values reported in ICRP (1994) and NCRP (1997) (Table 6 and Table 8, respectively) reveals a disparity for light and heavy exercise levels. The USEPA mean value of 0.83 m^3 hr^{-1} for light exercise is only about 62 percent of the average of the ICRP and NCRP values (1.35 m^3 hr^{-1}) and that the USEPA mean value of 4.8 m^3 hr^{-1} for heavy exercise is about 1.46 times the average of the ICRP and NCRP values (3.3 m^3 hr^{-1}).

Deterministic NTPR dose assessments for the inhalation of airborne contaminants have traditionally been based on a breathing rate of 1.2 m^3 hr^{-1}, which is the NCRP value that corresponds to light physical exertion. For this analysis we selected mean breathing rates of 1.35 and 3.3 m^3 hr^{-1} for light and heavy exercise, respectively, which correspond to the average of the ICRP and NCRP mean values. Reference breathing rates for rest and moderate exercise are taken directly from the USEPA data having values of 0.73 and 2.45 m^3 hr^{-1}, respectively.

The breathing rate is correlated with the exertion level, as discussed above. Consistent with standard NTPR assumptions, it is assumed that the inhalation of contaminants only occurred while participants were outside. It is further assumed that, while outside, a participant spent 25 percent of his time sitting/resting, 60 percent in light activity, 8 percent in moderate activity, and 7 percent in heavy activity. Although some variability in these values is likely, they are taken as constants in this report in order to simplify the analysis. The triangular pdf was selected to characterize the variability of breathing rates for each activity level. This choice was based on several factors, including the somewhat subjective definition of exertion levels, that the underlying data distributions are not well defined, and uncertainty as to the degree that the data is representative of breathing rates of nuclear test participants. The breathing rates at the various activity levels are assumed to be fully correlated; that is, someone who has an above-average breathing rate while at rest will have above-average breathing rates during light, moderate, and heavy activities as well. Given these assumptions, the mean and lower and upper limits of the breathing rate distributions by activity level are presented in Table 11.

Table 11. Breathing Rate Distributions by Activity Level–NTPR Test Participants

Activity Level	Low	Mean	High
Rest	0.1	0.7	1.1
Light	0.2	1.4	2.7
Moderate	0.9	2.5	4.7
Heavy	1.4	3.3	7.6

For the probabilistic modeling, triangular distributions were defined for breathing rates for each activity level, with low, mean, and high values used as minimum, mode, and maximum values, respectively, of each distribution. Samples from the distributions were then multiplied by the activity fractions defined above; e.g., 0.25 × (sample from triangular distribution for "Rest"). The products were then summed for each simulation. Table 12 provides sample statistics from a run of 10,000 Monte Carlo simulations of the breathing rate formulation based on the forgoing parameters, with results also shown in Figure 32. Note that these results are sample statistics, and because the distribution is generated for each dose calculation, actual statistics in any particular dose calculation may be slightly different. All breathing rates are in units of $m^3\ hr^{-1}$.

Table 12. Breathing Rate Distribution Parameters: 10,000 Monte Carlo Histories

Parameter	Breathing Rate ($m^3\ hr^{-1}$)
Mean (peak)	1.53
Minimum	0.33
Maximum	2.79
95th percentile	2.40
Standard deviation	0.51
95th percentile/mean ratio	1.57

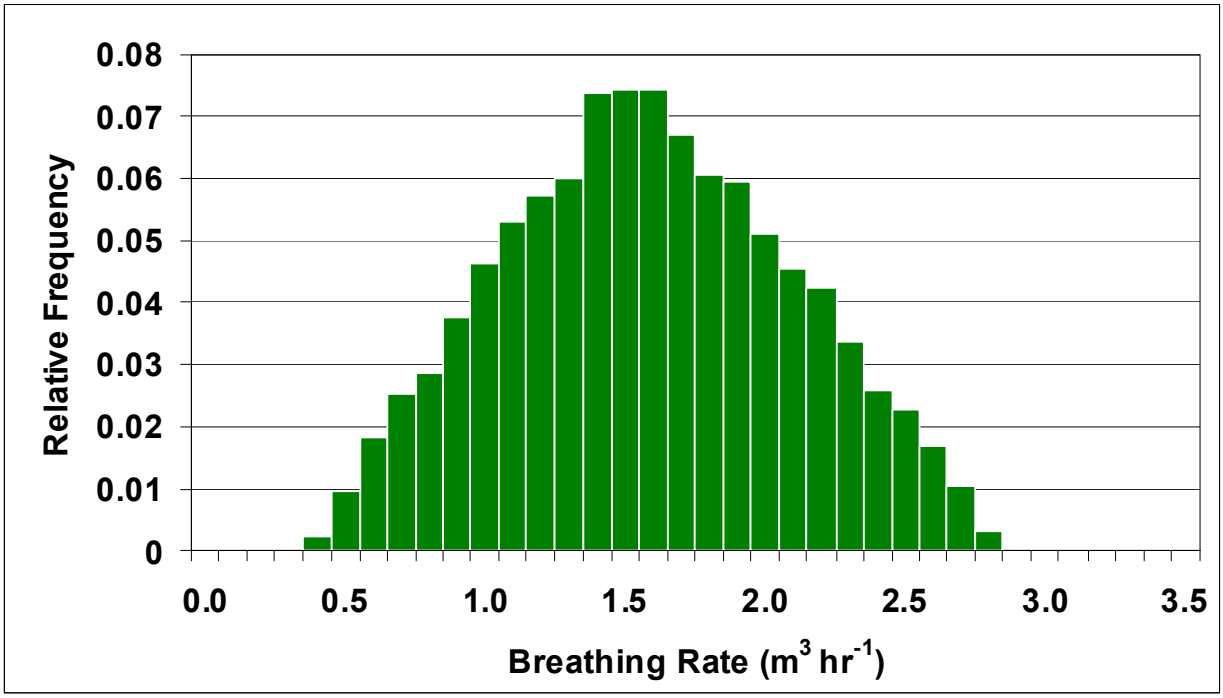

Figure 32. Sample Breathing Rate Distribution for Atmospheric Nuclear Test Participants

4.2.8 Internal Dose Conversion Factors

This section discusses biases and uncertainties in the internal dose conversion factors (*DCF*), which are derived from published ICRP dose coefficients (ICRP, 1996; ICRP, 2002). *DCF*s are used in NTPR dose reconstructions for the assessment of doses accrued from internally-deposited radionuclides by the inhalation and ingestion routes of entry.

4.2.8.1 Estimation of Inhalation Dose Conversion Factors Using FIIDOS

NTPR uses the computer program FIIDOS to calculate the 50-year committed equivalent doses (CEDs) to various body organs and tissues that would result from the ingestion or inhalation of radioactive material produced by a nuclear detonation. These organ dose calculations are based on the amount of radioactive material ingested or inhaled, the radionuclide composition of the material, and organ *DCF*s for each radionuclide. A library of published ICRP dose coefficients (listed in units of rem μCi^{-1}) is used in FIIDOS, which are tabulated for individual organs and effective dose for up to 148 fission products, 17 activation products, and 18 actinides. These dose coefficients have been used with shot-specific radiochemistry data to produce lookup tables of shot-specific, time-dependent composite *DCF*s for the assessment of tissue or organ dose commitments from the ingestion and inhalation routes of entry. Composite *DCF*s are reported either in units of rem CED Ci^{-1} intake or rem CED per rem film badge equivalent (FBE) dose for the calculation of internal doses based on a radiation intensity or external dose measurement. All routine inhalation dose calculations (i.e., inhalation of descending or resuspended fallout), are typically evaluated using composite *DCF*s in the unit rem CED per rem FBE. Equations for evaluating ingestion doses are normally formulated using composite ingestion *DCF*s in the unit rem CED Ci^{-1}.

As described in the FIIDOS manual (Raine et al., 2007), dose reconstructions performed before 2006 used radionuclide-specific *DCF*s as input to FIIDOS that were based in large part on internal dosimetry models recommended in ICRP Publication 30 (ICRP, 1979). Current NTPR dose reconstructions use *DCF*s that are based on radionuclide-specific dose coefficients from current ICRP recommendations for adult members of the public (ICRP, 1996; ICRP, 2002). Table 13 lists the 23 organs and tissues, and the quantity—effective dose—for which ICRP-72 dose coefficients were available as input to FIIDOS.

For NTPR, a subset of ICRP-72 inhalation dose coefficients was selected and assembled for input to FIIDOS, to address concerns about particle size distribution. Developed for use in the deterministic dose calculations, this set uses the dose coefficient for the particle size distribution that produces the highest dose to the organ of interest from among 1-, 3-, 5-, and 10-micrometer (μm) activity median aerodynamic diameter (AMAD) particle size distributions for the absorption type applicable to the oxide form of each constituent radionuclide. This set of "maximum dose" inhalation dose coefficients supplants all previous sets for NTPR internal dose assessments. The composite *DCF*s derived from these dose coefficients are inherently biased (high-sided), and their use with the entire inventory of descending or resuspended fallout results in high-sided doses for many inhalation scenarios. This is especially the case for scenarios involving descending fallout, for which the particle size distributions may include particles much larger than respirable sizes. To obtain the deterministic upper bound internal doses, an uncertainty factor of 10 is then applied to the deterministic internal dose estimates (DTRA, 2003). The uncertainty factor is thus the ratio of the upper bound dose to the

Table 13. FIIDOS Target Organs

Organ Name	Organ Name
Adrenals	Muscle
Bone Surfaces	Ovaries
Brain	Pancreas
Breast	Red Marrow
Stomach Wall	Skin
Small Intestine Wall	Spleen
Upper Large Intestine Wall	Testes
Lower Large Intestine Wall	Thymus
Kidneys	Thyroid
Liver	Uterus
Extra-Thoracic Region	Urinary Bladder Wall
Lung	Effective Dose

deterministic point estimate. Use of the uncertainty factor of 10 with the deterministic point estimate is believed to result in an upper bound dose that is not an underestimate of the true 95th percentile dose.

The regulation governing the NTPR RDA process (32 CFR 218 [DoD, 2009]), specifies that only published conversion factors are to be used to estimate internal doses. Furthermore, The NTPR Policy and Guidance Manual (DTRA, 2007a) requires the use of dose coefficients currently recommended by the ICRP. Because some diseases and conditions for which claims are filed do not have well-defined sites of origin or published *DCF*s, "surrogate" organs and their *DCF*s are sometimes used. Surrogate organs are assigned based on target organs and tissues that are judged to be most similar to the organ or tissue of concern with regard to biokinetic modeling. It is recognized that these *DCF*s are inherently more uncertain with regard to dosimetry and biokinetics when applied to other organs or tissues. However, addressing this source of uncertainty is beyond the scope of the current study.

While the high-sided approach currently used for NTPR deterministic analyses is in the spirit of providing test participants with the maximum benefit of the doubt, as articulated by DTRA, use of high-sided *DCF*s as central estimates is not appropriate in an uncertainty analysis.

Accordingly, a credible application of inhalation *DCF*s for uncertainty analysis, particularly with regard to inhalation of descending fallout scenarios, requires use of nominal *DCF*s and explicit treatment of uncertainties. The following sections discuss sources of bias and uncertainty in the deterministic *DCF*s, and how these were addressed in the uncertainty analysis. The adjustments in the following sections addressing uncertainty in dose conversion factors and maximum dose bias were applied to all special study cases; the adjustments addressing deposition fraction and activity fraction in the two subsequent sections were used with the PPG special study cases because only those cases involved inhalation of descending fallout.

4.2.8.2 Uncertainty in Inhalation and Ingestion Dose Conversion Factors

The primary sources of uncertainty in dose conversion factors used by NTPR stem from uncertainties in the dosimetric and biokinetic models used by the ICRP to estimate dose coefficients that form the basis for NTPR *DCF*s. These uncertainties vary depending on factors such as target organ, radionuclide, type of radiation, and chemical form of the radionuclide. In addition to inherent model uncertainties, a complicating factor is that biokinetic models used by ICRP may be based on studies of chemical and physical forms of radionuclides that differ substantially from chemical and physical forms in fallout. A comprehensive review of published studies on uncertainties in dose coefficients was undertaken by SENES Oak Ridge, Inc., in support of a study on inhalation doses from high resuspension scenarios for NTPR program participants (Kocher et al., 2006)[4]. The SENES analysis, in conjunction with subsequent discussions with the primary author, provides the basis for the selection of uncertainty factors and probability distribution function (pdf) parameters used in this report.

Because of the impracticality of developing and implementing estimates of DCF uncertainties for all combinations of organs and radionuclides, a rigorous analysis of uncertainty in dose coefficients for inhalation or ingestion of radionuclides in fallout was not attempted in this study. Such an undertaking would have required consideration of uncertainties in dose coefficients for essentially all organs or tissues, including organs or tissues that are not major sites of deposition but often are of concern in dose reconstructions, and for hundreds of radionuclides. Furthermore, uncertainties appear to be well characterized for only a few combinations of radionuclide and organ or tissue, and those organs or tissues usually are not of concern in NTPR dose reconstructions because they are considered presumptive for the purposes of adjudicating claims for service-connected disability for atomic veterans. (DVA, 2002; Kocher et al., 2006).

In Kocher et al. (2006), uncertainties in dose coefficients for inhalation of fission and activation products were evaluated separately from uncertainties in dose coefficients for plutonium. This separation was based on the potential for greater uncertainties in dosimetric models for alpha-emitting radionuclides than for beta/gamma emitters. The SENES report also notes that, unless there are strong correlations among dose coefficients for important radionuclides, the uncertainty in a dose coefficient for mixtures of radionuclides should be no larger than the largest uncertainty that applies to any radionuclide in a mixture when exposures generally should involve some radionuclides for which the uncertainty is relatively small. On the other hand, some correlation among dose coefficients for different radionuclides is likely and, therefore, adding doses from different radionuclides may increase the overall uncertainty more than would otherwise be expected. The impact of correlations among dose coefficients of different radionuclides requires further study. For this current study, to maximize the uncertainties in composite *DCF*s, the dose coefficients for all alpha emitters are assumed to be fully correlated with each other, and those for the beta-gamma emitters are also assumed to be fully correlated with each other.

[4] The studies on uncertainties in dose coefficients were updated in Kocher, D. C., Trabalka, J.R., and Apostoaei, A.J., 2009. Derivation of Effective Resuspension Factors in Scenarios for Inhalation Exposure Involving Resuspension of Previously Deposited Fallout by Nuclear Detonations at Nevada Test Site. DTRA-TR-09-15, *SENES, Oak Ridge, Inc.*, Oak Ridge, TN and Defense Threat Reduction Agency, Fort Belvior, VA. and will be considered during further testing and refinement of internal dose methods.

The NTPR approach to accounting for uncertainty in *DCF*s for inhalation and ingestion is to develop estimates of such uncertainty that are applicable to all exposure situations of concern. This approach should result in uncertainty estimates that do not underestimate the upper bound doses for any combination of radionuclides and organ or tissue of concern. Under current procedures, a single uncertainty factor of 10 is applied to the deterministic internal doses to most organs and tissues from the inhalation or ingestion of any mixture of fission products, activation products, and actinide elements (DTRA, 2003).

For this probabilistic study, NTPR has incorporated *DCF* uncertainty distributions defined by distinct uncertainty factors associated with alpha *DCF*s and beta-plus-gamma *DCF*s. An uncertainty factor of 10 is used for beta-plus-gamma *DCF*s for all organs and tissues, which is recommended by SENES as the upper bound factor that produces a reasonable estimate of uncertainty in the dose coefficients for mixtures of fission and activation products currently published by ICRP (Kocher et al., 2006; ICRP, 2002). An uncertainty factor of 15 is used for alpha *DCF*s, based on discussions and recommendations in the 2006 SENES report[5]. In particular, uncertainties in *DCF*s for inhalation or ingestion of plutonium, due to uncertainties in dosimetric and biokinetic models, should be substantially larger than uncertainties in dose coefficients for mixtures of beta/gamma-emitting fission and activation products. This conclusion is based mainly on two considerations: (1) the greater importance of uncertainties in dosimetric models for alpha-emitting radionuclides in some organs or tissues (e.g., the skeleton and gastro-intestinal (GI) tract) compared with beta-gamma emitters and (2) the larger uncertainty in absorption of plutonium in the GI tract compared with uncertainties in GI-tract absorption for many other fission and activation products (Eckerman et al., 1999; Harrison et al., 2001). Kocher et al. (2006) also note that estimated uncertainties in dose or risk coefficients for plutonium are among the highest for any radionuclide. Finally, two additional considerations from the SENES report support an uncertainty factor of 15 for alpha *DCF*s: (1) an estimated uncertainty factor greater than 10 in the risk coefficient for plutonium ingestion in USEPA's Federal Guidance (USEPA, 1997), and (2) an assumption that uncertainties in deposition of plutonium at minor sites should be significant, given the low concentrations of plutonium in soft tissues other than the liver and the apparent variability in those concentrations among different soft tissues (Kocher et al., 2006).

The uncertainties in inhalation and ingestion *DCF*s are incorporated into the NTPR modeling by multiplying the unbiased *DCF*s (see below for a discussion of bias adjustments) by values randomly drawn from lognormal distributions with geometric means equal to 1, and geometric standard deviations such that the ratios of 95th percentile to the geometric means are 15 for alpha *DCF*s and 10 for beta-plus-gamma *DCF*s. As noted earlier, the recommended alpha *DCF* uncertainty factor was changed from 15 to 30 after completion of the case study analyses described in this report. If NTPR adopts the revised uncertainty factor, the probabilistic internal organ alpha doses and uncertainties will be impacted. The impacts will vary somewhat depending on organ, scenario, and correlations between doses, but some generalizations about these impacts can be predicted as described below.

[5] The alpha DCF uncertainty factor was changed from 15 to 30 in an update to Kocher et al. (2006) that was published after the completion of the analyses described in this report as Kocher, D. C., Trabalka, J.R., and Apostoaei, A.J., 2009. Derivation of Effective Resuspension Factors in Scenarios for Inhalation Exposure Involving Resuspension of Previously Deposited Fallout by Nuclear Detonations at Nevada Test Site. DTRA-TR-09-15, *SENES, Oak Ridge, Inc.*, Oak Ridge, TN and Defense Threat Reduction Agency, Fort Belvior, VA.

- The geometric means of the individual exposure pathways and the total alpha doses will not change.
- The arithmetic means and the 95th percentiles of the individual exposure pathways and total alpha doses will increase by factors of roughly 2×; increases in total alpha doses will be driven by the dominant exposure pathway.
- Because of the increase in 95th percentile doses, the spreads of the distributions of doses will increase by roughly two times. As a measure of the spread, the uncertainty factors (ratios of 95th percentiles to geometric means) will increase accordingly with increases in 95th percentiles.
- Because of the increase in 95th percentile doses, the ratios of deterministic upper bound to the 95th percentile doses will decrease accordingly with increases in 95th percentiles.

Specific details about these impacts and their implications for implementing a probabilistic approach to NTPR radiation dose assessments will need to be assessed in future technical efforts.

4.2.8.3 Maximum Dose Bias in Inhalation *DCF*s

As discussed in Section 4.2.8.1, a "maximum dose" strategy was employed in developing inhalation *DCF*s for use in NTPR deterministic internal dose calculations. This strategy was implemented through the selection of the *DCF*, for the absorption type applicable to the oxide form of each radionuclide, from among those for 1, 3, 5, and 10- μm AMAD particle size distributions that provide the highest dose to the organ of interest. The composite *DCF*s derived in this manner are inherently high-sided. In order to produce inhalation *DCF*s for use in the uncertainty analysis, the bias introduced by this procedure must be removed. The amount of bias and method of removal were investigated (McKenzie-Carter, 2009). This research focused on two representative shots: BADGER, a 23-kiloton shot detonated atop a 300-foot tower at Operation UPSHOT-KNOTHOLE (1953) at the Nevada Test Site (NTS), and TEWA, a 5-megaton shot detonated on a barge at Bikini Atoll during Operation REDWING (1956). For each shot and organ, the differences between the maximum dose *DCF* (DCF_{max}) and the average of the *DCF*s for the four particle size classes (DCF_{avg}) were computed separately for alpha and beta-plus-gamma radiations for all times post-detonation and were used to construct bias factors *BF*, defined as

$$BF = \frac{DCF_{Max}}{DCF_{avg}}. \tag{4-15}$$

Similar patterns of bias for both alpha and beta-plus-gamma *DCF*s are observed for Shots BADGER and TEWA. For all organs except the ET region, alpha bias factors were closely grouped at values between 1.25 to 1.30. For the ET region, the alpha bias factors were slightly lower, with consistent values at about 1.15 for all post-detonation times. For beta-plus-gamma *DCF*s, bias factors for lung, breast, thymus, adrenals, spleen, liver, and pancreas peak at about 1.35 to 1.45 at about 4 months post-detonation, while bias factors for all other organs were clustered around 1.20 at all times.

Based on the results described above, bias adjustment factors shown in Table 14 were selected for use in removing bias from the *DCF* values (McKenzie-Carter, 2009).

Table 14. Organ-Specific Bias Adjustment Factors

Organ(s)	Alpha Radiation	Beta-Plus-Gamma Radiation
lung, breast, thymus, adrenals, spleen, liver, and pancreas	1.30	1.35
extra-thoracic region	1.15	1.20
all FIIDOS organs not listed elsewhere in table	1.30	1.20

Incorporation of these bias factors into the stochastic dose modeling was accomplished according to the following equation:

$$DCF_{adj} = \frac{DCF}{BF} \tag{4-16}$$

where DCF_{adj} is the adjusted (unbiased) shot-specific, time-dependent inhalation *DCF* (rem CED rem^{-1} film badge dose)

The adjusted shot-specific, time-dependent inhalation *DCF*s produced by removal of the "maximum dose" bias effect are effectively inhalation *DCF*s that are the average values over the 1-, 3-, 5-, and 10-μm sizes.

4.2.8.4 Summary of Results

The parameters and uncertainty distributions relevant to the stochastic modeling of DCFs are summarized in Table 15. Also indicated are the values used in nominal and deterministic analyses.

4.2.9 Characterization of Descending Fallout

Special studies were conducted (1) to calculate the fraction of the activity in descending fallout ("activity fraction") that was carried by particles in each of three size classes and (2) to estimate the settling velocities in the breathing zone for particles in each size class. These parameters are inputs to Equation 3-8 in the calculation of internal dose from inhalation of descending fallout. The results of these studies are summarized in this section; details of the analyses leading to these results are contained in Weitz (2009f).

Table 15. Model Parameters for Dose Conversion Factor Distributions

Parameter	Definition	Distribution for Uncertainty Analysis	Nominal Value for Central Estimation	Deterministic Analysis
DCFInhα *DCFIngα*	Inhalation and ingestion dose conversion factors for fallout α radiation	*DCF*s calculated with FIIDOS multiplied by Lognormal (GM=1.0, GSD=5.19)	*DCF*s calculated with FIIDOS	*DCF*s calculated with FIIDOS
DCFInhβγ *DCFIngβγ*	Inhalation and ingestion dose conversion factors for fallout β+γ radiation	*DCF*s calculated with FIIDOS multiplied by Lognormal (GM=1.0, GSD=4.05)	*DCF*s calculated with FIIDOS	*DCF*s calculated with FIIDOS
Biasα *Biasβγ*	Bias factors to adjust high-sided inhalation *DCF* values	Assumed to be Constant (see Table 14)	See Table 14	1.0 1.0

4.2.9.1 Activity Fractions

As discussed above, the inhalation *DCF*s have been applied previously to all of the activity (intensity) associated with descending or resuspended fallout, under the high-sided assumption that all radioactive particles have aerodynamic diameters in the range 1–10 μm. ("Aerodynamic diameter" is the diameter of a sphere of density 1 g cm^{-3} that exhibits the same settling velocity as the particle in question.) However, descending fallout generally included particles of non-respirable and even non-inhalable sizes that may have contained a significant fraction of the total fallout radioactivity. A compounding factor is that the activity was distributed non-uniformly with particle size (Glasstone and Dolan, 1977; Kellogg et al., 1957). The objectives of this special study were (1) to develop a method to estimate activity fractions for specific descending fallout exposure scenarios, and (2) to formulate uncertainty distributions for these fractions. The particle size classes utilized in this study are defined by the following ranges of aerodynamic diameters: 1–10 μm (designated Class 1), 10–20 μm (Class 2), and 20–100 μm (Class 3).

Particles with aerodynamic diameters larger than 100 μm are generally non-inhalable and thus contribute little to internal dose through the inhalation route of entry. The class-specific activity fractions, AF_i, i = 1, 2, and 3, that appear in the internal dose Equation 3-8 are related to the total activity fraction AF_{100} for sub-100 μm particles by:

$$AF_{100} = AF_1 + AF_2 + AF_3. \quad (4\text{-}17)$$

A paucity of data exists on particle size distributions and activity fractions for most fallout deposition times relevant to the PPG case studies. Although extensive fallout measurements were made at Operation REDWING (Triffet and LaRiviere, 1982), collection stations were usually located within 10 to 20 nautical miles from surface zero so that most particle size and activity distribution data were collected during the first few hours post-detonation. In contrast, almost all fallout events relevant to the case studies took place more than 10 hours after detonation. It was therefore decided to develop a physics-based, probabilistic fallout deposition model that could be benchmarked with the available particle size-activity data at early times and then used to characterize the fallout at the later times of interest. The deposition model provides estimates of activity fractions for fallout that descended on specific locations (i.e., on residence islands and on certain ships) during defined periods of time. Since the locations are fixed, only

the vertical motion of the fallout particulates is of interest and a one-dimensional equation of motion suffices. The formulation of the algorithm, its implementation in Mathcad, sample results, and comparison with REDWING measurements are discussed in Weitz (2009f).

4.2.9.2 Deposition Velocity of Fallout Particles

"Deposition velocity" is defined here to be the velocity at which fallout particles descend to the ground in the breathing zone, which nominally extends from the surface to 1.6 meters above the surface. An average deposition velocity is calculated by dividing the initial debris height H by the time T it takes a particle to reach the ground. This average is a valid estimate for the larger particles whose descent is governed predominantly by gravity and atmospheric drag. However, some of the smaller particles become entrained in vertical air currents and carried downward at rates determined by the vertical wind velocities, which may be much different than the average descent rate of H/T. The vertical component of the air current must vanish near the ground because the Earth serves as a boundary in that direction. Therefore, the velocity of small particles entrained in the air can slow significantly as they approach and enter the breathing zone. A formulation based on the Stokes equation was utilized to estimate these small-particle deposition velocities, as discussed in Weitz (2009f).

4.2.9.3 Results and Discussion

In the present approach, the activity fractions AF_i in particle size classes 1, 2, and 3 are derived as follows. First, the total activity fraction AF_{100} for the combined class consisting of all particles with aerodynamic diameters less than 100 μm is determined by randomly drawing from the relevant event-specific triangular distribution defined Table 16 in terms of its minimum, mode, and maximum values. Derivation of this table is discussed in Weitz (2009f). Second, the fractions of AF_{100} attributable to the three size classes, denoted as $frac_1$, $frac_2$, and $frac_3$, are determined by drawing $frac_1$ and $frac_2$ from the respective triangular distributions defined in Table 17 and then using the relation

$$frac_3 = 1 - frac_1 - frac_2 \tag{4-18}$$

Finally, the activity fraction for the i^{th} size class is calculated from

$$AF_i = frac_i \cdot AF_{100} \tag{4-19}$$

(Within the Mathcad program, the activity fractions are referred to as "activity adjustment factors" and denoted by RNA.)

Table 16. Triangular Distributions of Total Activity Fraction (AF_{100}) for PPG Case Study Units

Operation Unit	Event	Deposition Interval (H+hr)	Tp (H+hr)	Minimum	Peak	Maximum
CASTLE						
Enewetak Island	BRAVO	H+9–H+16	16	0.071	0.391	0.770
	ROMEO 1	H+10.5–H+14.5	14.5	0.132	0.462	0.812
	ROMEO2	H+39–H+77.5	77.5	1.000	1.000	1.000
	NECTAR	H+12–H+14.7	14.7	0.543	0.781	0.971
REDWING						
Enewetak Island	ZUNI	H+8–H+18	11	0.094	0.280	0.565
	MOHAWK	H+2–H+3	3	0.013	0.070	0.140
	APACHE	H+18–H+22	21	0.939	0.973	1.000
	TEWA	H+10–H+26	25	0.403	0.572	0.732
USS ESTES	ZUNI	H+27–H+40	37	1.000	1.000	1.000
	FLATHEAD	H+30–H+44	44	1.000	1.000	1.000
	NAVAJO	H+18–H+22	22	1.000	1.000	1.000
	TEWA	H+18	18	0.396	0.587	0.801
HARDTACK I						
Enewetak Island	FIR/KOA	H+45–H+58	58	1.000	1.000	1.000
	REDWOOD	H+10.5–H+13.5	12	0.609	0.787	0.971
	OAK	H+14	14	0.469	0.732	0.975
USS BOXER	FIR/KOA	H+45–H+58	58	1.000	1.000	1.000
	REDWOOD	H+10.5–H+16.5	16.5	0.624	0.816	0.986
	OAK	H+12.25–H+14	14	0.469	0.732	0.975

The following class-specific average settling velocities were obtained using the methodology described in Weitz (2009f): 13 cm s^{-1} (V_3) for Class 3 particles (20-100 μm), 0.83 cm s^{-1} (V_2) for Class 2 particles (10-20 μm), and 0.22 cm s^{-1} (V_1) for Class 1 particles (1-10 μm). The uncertainty of the settling velocity for each size class is modeled with a log-triangular distribution, that is, a distribution in which the natural logarithm of velocity is assumed to obey a triangular distribution. The parameters defining these distributions are provided in Table 17, which summarizes the uncertainty distributions relevant to the probabilistic characterization of descending fallout. Also indicated are the values used in nominal and deterministic analyses.

Table 17. Model Parameters for Activity Fraction and Settling Velocity

Parameter	Definition	Distribution for Uncertainty Analysis	Nominal Value for Central Estimation	Deterministic Analysis
AF_{100}	Fraction of all activity carried to surface on particles with aerodynamic diameter <100 μm	Triangular min, mode, max (see Table 16)	Mode of distributions (see Table 16)	1.0
	Fraction of AF_{100} carried	Triangular min, mode, max	Mode of distributions	
$frac_1$	by Class 1 particles	0, 0.00136, 0.01	0.00136†	1.0
$frac_2$	by Class 2 particles	0, 0.025, 0.1	0.025†	0.0
	Particle settling velocities	Log-triangular min, mode, max (cm s^{-1})	Mode of distributions	
V_1	Class 1 particles	0.22/2, 0.22, 27.8	0.22 cm s^{-1}	10^6(cm) / T(sec)
V_2	Class 2 particles	0.83/2, 0.83, 27.8	0.83 cm s^{-1}	
V_3	Class 3 particles	13.0/2, 13.0, 27.8	13.0 cm s^{-1}	

†For Shots FLATHEAD and NAVAJO at Operation REDWING on the USS ESTES $frac_1$ and $frac_2$ are set to 0.0.

4.2.10 Internal Deposition Fraction Adjustment

Calculation of internal dose is based on the patterns of internal deposition fractions—designated R_i in Equation 3-8. These are defined as the fractions of inhaled particles in a given size class that deposit in the thoracic airway and in the posterior extra-thoracic airway. An inherent assumption of the NTPR deterministic inhalation dose models is that all of the fallout is in the size range 1–10 μm. However, the use of this assumption for all scenarios is undoubtedly high-sided, especially for descending fallout, which likely contains larger particles that are less likely to deposit in the thoracic airway. All activity associated with particles of size 1–10 μm is considered to apply for inhalation dose conversion factors. However, adjustments to the descending inhalation dose conversion factors were developed to provide a more credible accounting of deposition in the respiratory tract for larger particles in the size classes 2 (10–20 μm) and 3 (20–100 μm).

4.2.10.1 Estimation of Internal Deposition Fractions

Based on the ICRP 66 human respiratory tract model (HRTM) (ICRP, 1994), for particles 20 μm or larger, about half of the available inhaled activity is deposited in the ET region and about half of that is subsequently ingested. Thus, one approach to adjusting internal dose calculations for large particle exposures would be to use ingestion *DCF*s and adjust them by a factor of about 0.25. However, such an approach would produce averaged results with their own associated

uncertainty and would involve reworking all of the NTPR internal dose calculations to be based on activity intake instead of being based on film badge equivalent dose. Because of resource constraints, that approach was judged to be impractical.

The approach used for the NTPR uncertainty study is based on data from Bolch et al. (2001), which describes a systematic review of the deposition component within the ICRP 66 HRTM in which probability density functions were assigned to all input parameters. These distributions were subsequently incorporated within a computer code LUDUC (*LU*ng *D*ose *U*ncertainty *C*ode) in which Latin hypercube sampling techniques were used to generate multiple trials for all of the model parameters needed to assess particle deposition within the ET (anterior and posterior), bronchial, bronchiolar, and alveolar-interstitial regions of the ICRP 66 HRTM. Particle deposition values for the various trial simulations were shown to be well described by lognormal probability distributions.

Using the data in Table 7 of Bolch et al. (2001), a Mathcad model was constructed to generate deposition fraction distributions for each of the lung regions based on those data. The distributions were then combined to estimate total respiratory tract deposition for a given particle size class. Effective filtration in each region is included (inhalation and exhalation are not modeled separately) and the model limits total deposition to unity. Region ET_1 is considered for filtration but not for total deposition because material deposited in that region is cleared quickly externally (e.g., nose blowing). A second Mathcad model was used to calculate geometric mean deposition fractions and associated geometric standard deviation for selected ranges of particle size classes in respirable and non-respirable regions of the respiratory tract. For the purposes of this uncertainty study, particle size classes of 10–20 μm and 20–100 μm were explicitly considered, in addition to the 1–10 μm size class. Using results reported in Bolch, the "respirable" fraction, defined as the fraction of each size class depositing in the thoracic airways (bronchial (BB), bronchiolar (bb), and the alveolar-interstitial (AI) regions, and the "non-respirable" fraction, defined as the fraction of each size class depositing in the posterior extra-thoracic region (ET_2), were determined. The non-respirable (ET_2) fraction is essentially cleared entirely to the digestive tract in a short time (the mean retention time in ET_2 prior to swallowing is about 15 minutes) (ICRP, 1994; McKenzie-Carter and Stiver, 2009). Because the nonrespirable fraction is defined here as the fraction depositing in ET_2, ingestion *DCF*s can be applied to the entire non-respirable fraction, as numerically defined in the following section.

4.2.10.2 Results and Discussion

Lognormal distributions of respirable and non-respirable internal deposition fractions, derived on the basis of the Bolch et al. (2001) results in McKenzie-Carter and Stiver (2009), are listed in Table 18. These distributions corresponding to the terms R_i and NR_i of Equation 3-8 are designated by their Mathcad representations RND_{Res1}, RND_{Res2} and RND_{Res3} for the respirable portions of size classes 1, 2 and 3, and by $RND_{NonRes1}$, $RND_{NonRes2}$ and $RND_{NonRes3}$ for the respective non-respirable portions. These multiplicative parameters are used only in descending fallout scenarios of probabilistic and nominal value assessments; they are not used in deterministic analyses because of the assumption that all radioactive particles have aerodynamic diameters in the range of 1–10 μm.

RND_{Res1} and $RND_{NonRes1}$ depend on the age of the individual, level of activity, whether breathing from the nose, the mouth, or both, and ventilation rate (Bolch et al. 2001). Assuming RND_{Res1} is

set to 1.0 and $RND_{NonRes1}$ is set equal to 0.0 simplifies Equation 3-8 to the form used in the six case studies discussed in Section 5. Limited tests with both RND_{Res1} set to 1.0 and $RND_{NonRes1}$ set to 0.0 show that these assumed values estimate total internal doses that are less than 4 percent smaller than the doses for the organs (LLI wall, lungs, and thyroid) assessed in Case Study #6 for the unit at Enewetak Atoll during Operation CASTLE discussed in Section 5. Because values for RND_{Res1} and $RND_{NonRes1}$ were not evaluated for this study, the simplified formulation was used in all case studies discussed in Section 5. However, better estimates for these parameters should be developed for future case studies or radiation dose assessments.

Table 18. Model Parameters for Internal Deposition Fractions

Parameter	Definition	Distribution for Uncertainty Analysis	Nominal Value for Central Estimation	Deterministic Analysis
	Respirable deposition fractions	Lognormal GM, GSD	Geometric Mean	
RND_{Res1}	Class 1 particles	1.0 (assumed constant)	1.0 (assumed constant)	n/a
RND_{Res2}	Class 2 particles	0.0056, 1.744	0.0056	
RND_{Res3}	Class 3 particles	0.001, 1.65	0.001	
	Non-Respirable deposition fractions	Lognormal GM, GSD	Geometric Mean	
$RND_{NonRes1}$	Class 1 particles	0.0 (assumed constant)	0.0 (assumed constant)	n/a
$RND_{NonRes2}$	Class 2 particles	0.363, 1.106	0.363	
$RND_{NonRes3}$	Class 3 particles	0.285, 1.185	0.285	

4.2.11 Sources of Uncertainty When Estimating Radiation Intensity from Measured Intensities and Iso-Intensity Maps

When using measurements or iso-intensity maps to estimate point values in time and space (location), the related uncertainty is comprised of two components. The first component is the uncertainty due to errors introduced during the actual intensity measurement and when maps are created from a discrete and often sparse set of point observation measurements. The second component is the additional uncertainty that arises when an estimate is made at any point on a map by interpolation (or in some cases by extrapolation) from an iso-intensity contour map. In addition, when assessing the radiation environment for atmospheric nuclear test participants, information on the reliability of data collection and processing is often lacking.

4.2.11.1 Uncertainty in Recorded Intensity Data

In the case of iso-intensity maps used in dose assessment for atmospheric nuclear test participants, some uncertainties are hard to quantify because the original survey measurements and even processed data are unavailable. When assessing uncertainty, an analyst uses all available information to estimate and bound its distribution. In doing so, it is important to consider essential factors that have the potential to affect the reliability and confidence in the recorded or estimated data. These factors include:

- Documentation of data collection plans and procedures.
- Conditions of data collection.

- Accuracy and calibration of measuring instruments.
- Experience and training of field monitors.
- Availability of raw measurements versus processed or graphed data.
- Processing of raw measurements.
- Methods used to process and transform raw measurements.
- Quality assurance and control in the collection, recording and reporting of raw and processed data.

In many cases, uncertainties have to be estimated through subjective judgment based on an analyst's confidence in the documentation, understanding of the impact of the sources of errors listed above, and the levels of related uncertainties.

4.2.11.2 Uncertainties Due to Creating Iso-Intensity Maps from Survey Data

The main sources of error that affect the accuracy of iso-intensity maps, which are due to data collection and plotting of such maps, mainly involve (Stearns, 1968): 1) measurements and data processing, 2) simultaneity of measurements, and 3) data interpolation. Interpolation here refers to the determination and positioning of iso-intensity values to create iso-intensity contour lines based on the measured values at the observation points. Point value interpolation is discussed in the following subsection.

Measurement and Data Processing

Iso-intensity maps are produced from the measurement of three types of variables:

- Quantity being observed (i.e., radiation intensity).
- Time of the observation.
- Position of the observation, which involves the measurement of one or more geographic coordinates.

Measurement of each of the above types of variables is impacted by one or more of the following sources of errors:

- Instrument precision and calibration.
- Operator manipulation during observation and data recording, including verbal and radio-transmitted communication of data in some cases.
- Reduction, correction, scaling and other pre-processing of data before being documented in data logs or reports.

Simultaneity of Measurements

The lack of simultaneity of observations of a quantity that varies in time results in uncertainties that impact iso-intensity maps. These uncertainties may be reduced through accurate estimation

of the time dependency of the measured variable and processing the observed data to a reference time map. In the case of radiation intensity maps used in NTPR, knowledge of the time decay functions was generally used to create iso-intensity maps for the reference time of one hour after a detonation (H+1). Simultaneity uncertainties are also called synopticity uncertainties.

Interpolation (when producing Contour Lines from Observation Data)

Many interpolation schemes have been used to create iso-line maps from scattered data points. These can range in sophistication from manual linear interpolation between pairs of observation points to geostatistical techniques that allow estimation of interpolation uncertainties under certain assumptions about the quantity being mapped (Chilès and Delfiner, 1999). Although automated mapping techniques have been developed and used widely, human judgment remains critical in specifying such assumptions and making decisions concerning the types and parameters of the interpolating functions employed, as well as the determination of discontinuities and boundary conditions. The interpolation scheme that NTPR used to create iso-intensity contour maps for most NTS shots is described in (Goetz et al., 1980). Many of the initial and follow-up survey maps appear to have been drawn by hand.

Most mapping interpolations rely on sets of data points with an irregular layout also termed scatter points. In such instances, most automated contour mapping is conducted in three steps. First, pre-processed observation data is used to interpolate values at closely-spaced points (or cells) on a regular grid. This step is appropriately called gridding. Second, the discrete location of iso-values is estimated along the grid lines using the regularly-spaced interpolation points and their corresponding interpolated values. Last, smooth contouring functions are used to connect iso-values.

Each of the aforementioned three steps requires input parameters that an operator supplies to guide the automated mapping. The discrete point data (either original or gridded) do not in and of themselves lead to a unique set of mapped contours (Chilès and Delfiner, 1999). A trial and error iterative process is usually followed to create the "best estimate" of a contour map through knowledge of the physical characteristics of the mapped variable, the distribution of collected data, and other related conditions.

4.2.11.3 Uncertainties from Estimating Point Values of a Variable Using an Iso-intensity Map

Estimating point values from a digital map can be rendered highly precise, given the sophistication of modern computer-aided interpolation. This is not the case when using hardcopy iso-intensity contour maps. Manually estimating discrete point values from a hardcopy iso-intensity contour map introduces several types of potential errors in the estimated value at any particular location. Additional uncertainty in the final point estimate may result from one or more of the following sources of error:

- Scale of map and distance between contour lines.
- Thickness of contour iso-lines.
- Point positioning and measurement of distance on a map.

- Distortion from duplication and printing.
- Interpolation method (linear, logarithmic, other) and relevance to underlying variable gradients.
- Eye-balling estimates versus calculated interpolation.
- Extrapolation outside of contours, especially where high gradients are observed.

Each of these sources of uncertainty is in addition to those inherent in making the map and adds to the uncertainty in the final estimate at the location of interest. Some uncertainties, such as those from positioning or measuring distances on the map, can be minimized through use of proper procedures. Others, such as those due to distortion and thickness of contour lines, are inherent to the map used and cannot be reduced.

4.2.11.4 Guidelines for Selecting Uncertainty Factors for Point Estimates Derived from Iso-Intensity Data and Contour Maps

Each source of error related to the use of iso-intensity data and maps in determining point estimates in space and time discussed above contributes to the overall uncertainty of the final mapped contour lines or iso-lines and in the subsequent estimation of point values. The relative importance of each source of uncertainty should be assessed and accounted for in creating a basis for the overall uncertainty distributions of the mapped variable and point estimates.

The guidelines in Table 19 provide ranges of uncertainty factors that are based on the various sources of uncertainties and their cumulative effects (Chehata, 2009). The ranges were developed based on the collective experience and expertise of radiation analysts who regularly used NTPR iso-intensity maps, NCRP Report 158 (NCRP, 2007), and experience using geostatistics in other fields of science (Chehata et al., 2007). The selection of an uncertainty factor within the suggested ranges should be based on knowledge of the reliability of the documentation and the methods used to produce the supporting iso-intensity map. As discussed elsewhere in this report, the uncertainty factor is defined as the ratio of the 95^{th} percentile to the central estimate of the variable distribution, generally the mean, the geometric mean, the median or the mode. As defined, the uncertainty factor is a dimensionless quantity to be used as a multiplier on the estimated central value of radiation intensity.

Table 19. Proposed Ranges of Uncertainty Factors for Estimating Point Values Using Measured Intensities and Iso-intensity Contour Maps

Source of Uncertainty	Uncertainty Factor (*)	Distribution	Note
Instrument precision, calibration and operator error (this is applicable when no interpolation is carried out, i.e., where a measurement was recorded at the location of interest)	1.5–2	Normal	Location and time known
With additional uncertainty due to contouring scatter point data	2–3 (†)	Lognormal/ triangular	Lognormal most adequate for intensity distributions around and not far away from GZ
With additional uncertainty due to using contour maps to determine point estimates by interpolation (factor is higher when location and time of measurements are unknown or inaccurate)	3–5 (†)	Lognormal/ triangular	Lognormal most adequate for intensity distributions around and not far away from GZ
Additional uncertainty due to using contour maps to determine point estimates by extrapolation	5–10 (†)	Lognormal/ triangular	Lognormal most adequate for intensity distributions around and not far away from GZ
Extrapolation with high uncertainty from all other sources and surrogate data are used	10–15 (‡)	Lognormal/ triangular	Lognormal most adequate for intensity distributions around and not far away from GZ

(*) The 95-percent uncertainty factor (UF) is the ratio of the 95th percentile to the central estimate of the distribution, which in most cases is the median, mean, or geometric mean (e.g., lognormal distributions).

(†) Combined uncertainty factors which include instrument and operator error and all antecedent uncertainty sources.

(‡) When surrogate data are used, estimates are presumed to be made by extrapolation, e.g., as when using processed intensity data from a neighboring ship or island.

4.2.12 Incidental Ingestion of Contaminated Soil and Dust

4.2.12.1 Soil Ingestion Rate

A literature review was conducted to determine rates of incidental ingestion of potentially contaminated soil and dust that can be used in internal dose assessment for atmospheric nuclear test participants. The review examined guidelines mainly from the USEPA and the USACHPPM, which are agencies with major roles in environmental health protection programs for the general public and the military.

Information compiled in USEPA (1997, 2001 and 2002) and the USACHPPM (2003), and studies cited therein, provide the basis for estimating rates of incidental ingestion of soil and dust for atmospheric nuclear test participants. The estimated maximum incidental ingestion rate is 500 mg day^{-1} (Chehata and Stiver, 2009). Mean ingestion rates for long-term exposures are in the range of 50 to 100 mg day^{-1}. Proposed rates for children are not applicable for NTPR personnel, as children ingest higher quantities of soil when mouthing objects and hands while playing outside and eating dirt.

Based on this investigation, the rate of incidental soil ingestion for NTPR personnel assumed to have been outdoors part of the day and inside tents or temporary buildings the rest of the day, varies between 10 and 500 mg day^{-1}, with a central estimate of about 50 to 100 mg day^{-1}. In the current study, a nominal value of 100 mg day^{-1} was selected. For uncertainty analyses, the distribution of incidental ingestion rates is assumed to be best described by a skewed triangular distribution with a peak value of 100 mg day^{-1} and bounds of 10 and 500 mg day^{-1}. A more precise distribution is not warranted due to a lack of data. Given the low doses obtained when the highest rates were used in actual internal dose estimates (Chehata and Stiver, 2009), it became clear that the dose contribution to internal organs and tissues from the incidental ingestion pathway are expected to be relatively small.

4.2.12.2 Soil Density

The estimation of internal doses using measurements of activity on the ground requires knowledge of the bulk density of soil. At NTS, surface soils are characterized by being moderately to poorly sorted sand to silty loam. These soils have a bulk density that ranges from 1.3 to 1.6 g cm^{-3} with an average of 1.45 g cm^{-3} (Hillel, 1980). Soil density at the PPG residence islands would be slightly higher but within a similar range. A symmetrical triangular or a uniform probability distribution can be used unless site-specific data supports another type of distribution. In this study, a symmetric triangular distribution was used in all land-based scenario case studies.

4.3 Dependencies and Correlations between Model Input Parameters

The distributions and sensitivity to model parameters of the reconstructed doses for the six case studies were estimated using probabilistically-based Monte Carlo simulation techniques. Model parameter values were randomly selected from each of their distributions. There are 54 explicit input parameters used in the six case studies, which have associated uncertainty distributions. To better understand and interpret the results of the uncertainty analyses, known or potential

correlations among input parameters were qualitatively examined and are summarized in this section. Two types of correlations were considered: correlations among different parameters and those from shot to shot for the same parameter.

Five of the explicit input parameters were not varied for any case study group because they were known to a high enough degree of certainty not to have an impact on the overall uncertainty of the calculated total doses. The remaining 49 input parameters are impacted by both uncertainty and variability, and were assigned uncertainty distributions based on experimental, theoretical, or reasoned estimates. A thorough discussion among radiation analysts and peers led to choosing these 49, which with three exceptions, were only weakly or not correlated to each other. Therefore, it was assumed that parameter-to-parameter correlations were zero for the 46 model parameters. The three exceptions are the fallout intensity distribution pairs for both island and ship case studies. These are fully correlated because the same fallout intensity is used for both the external and internal dose models in a single Monte Carlo history. The other exception is the breathing rate, which combines weighted distributions from two sub-input parameters, the activity level and metabolic rate as described earlier in this section.

Of the 46 independent parameters, not all were used in each case study. For example, for the case study groups that participated on Enewetak Island, typically 9 and 17 independent input parameters were varied to estimate external and internal doses, respectively. For case study units that were aboard a ship, typically 10 and 16 independent parameters were varied for the calculation of external and internal doses, respectively.

External dose inputs for land-based personnel are the fraction of time outside, fraction of inside time in a tent, protection factors for tent and building, intensity distribution outside, near a tent and near a building, decay rate, and errors resulting from measured intensity data. Ship-based external dose inputs are the fraction of time topside, protection factors for work and sleeping areas, intensity distribution of fallout, which affects topside, work and sleeping areas, decay rate, and errors resulting from measured intensity data.

Internal dose input parameters are dose conversion factors for α and $\beta + \gamma$ radiation, breathing rate, a number of respirable and non-respirable deposition fractions, multiple activity adjustment factors and particle settling velocity. Additionally, land-based dose models include the time-dependent resuspension factor and ship-based models comprise the gamma source modification factor and ship resuspension factors, which are treated differently from those for land.

For some case studies, additional parameters were varied to simulate an uncertainty on arrival and departure time, end of film badge exposure dates, and proportion of debris cloud mixing. For the NTS-based case study additional sources of variation and uncertainty include the use of iso-intensity contour map for point estimate of exposure rates, troop maneuver start time, march rate, linger time when not maneuvering, and adjusted resuspension factors in the precursor[6] and blast-wave regions.

[6] The term "precursor" was changed to "thermal pulse" in a revision to Kocher et al. recently published as Kocher, D. C., Trabalka, J.R., and Apostoaei, A.J., 2009. Derivation of Effective Resuspension Factors in Scenarios for Inhalation Exposure Involving Resuspension of Previously Deposited Fallout by Nuclear Detonations at Nevada Test Site. DTRA-TR-09-15, *SENES, Oak Ridge, Inc.*, Oak Ridge, TN and Defense Threat Reduction Agency, Fort Belvior, VA., however it is retained in this report.

Most case study exposures extended over a long period, some the entire length of an operation. For these, fallout was deposited from several shots or from several deposition events from a single shot. So the question was for a single Monte Carlo history, does an input parameter value remain the same for exposure to all fallout throughout the period of presence or does it randomly vary within its distribution for each day or each shot? After a thorough evaluation, a matrix was compiled to examine each input parameter and to state why it might change or stay the same for each Monte Carlo history. While dose input parameters have varying degrees of autocorrelation from shot-to-shot, it was decided to assume either full correlation or weak to no correlation.

A complete matrix showing model input parameters, correlation state, and basis for each correlation decision is presented in Table G-1 of Appendix G. The parameter in each row is uncorrelated to the parameter in any other row, but for the three exceptions mentioned earlier. Parameters shown together in the same row, such as DCF_{inh} and DCF_{ing}, are selected from a single random number draw and are fully correlated to each other. Their absolute distributions differ, but the values picked for a given history are at the same cumulative probability. For each case study, model input parameters and distributions with their nominal and NTPR high-sided deterministic values are given in the respective appendices.

When different components of dose depend on a common input parameter, they will be correlated to some extent with each other. An example would be the breathing rate, which is an input parameter for both descending and resuspended internal dose, and deviates from the nominal breathing rate the same for the entire operation for a given Monte Carlo history. A lower than nominal breathing rate would tend to result in a lower internal dose for all shots for all inhalation pathways. However, because each internal pathway and shot depends on other input parameters, which may be independent from each other, there is only partial correlation between inhalation dose components.

The list of parameters in Appendix G does not include dependent variables, such as the fraction of time inside shielding, which is one minus the fraction of time outside. Because this parameter is derived within the Monte Carlo simulation, it does have a negative correlation to the time outside. These derived parameter distributions and their correlations are not listed in the tables.

An example is provided here to illustrate the evaluation of shot-to-shot correlation for a single parameter. Consider the parameter F_{os} defining the fraction of time each day that an individual spent outdoors on an island, i.e., not in a tent or a building. The uncertainty distribution for F_{os} is such that a given participant could have spent a minimum of 2, a maximum of 16, with most likely 8 hours outdoors each day. A triangular distribution was employed to describe this parameter mathematically. Because most personnel on islands participated in essentially the same activities from day-to-day and from shot-to-shot, it is reasoned that the value of F_{os} for a particular participant is likely the same throughout the operation for a single Monte Carlo history. Therefore, an individual's daily time outside after one shot is fully correlated with his daily time outside after another shot. For each Monte Carlo history, the amount of time outdoors is drawn once and utilized for all days following all events from all shots. For each succeeding history a new fraction of time outdoors is randomly selected.

5 CASE STUDY RESULTS

Six case studies to test methods discussed in Sections 3 and 4 were conducted successfully and provide relevant results that identify limitations of the methods, identify areas of further study and confirm important approaches to conducting radiation dose assessments that include full uncertainty analyses. The studies were conducted for representative units selected on the basis of their ability to satisfy some or all of the following criteria that were identified in a pilot study.

- Adequate number of participants within the group for statistical analysis of dosimetry and comparison to corresponding probabilistic analysis of reconstructed doses.
- Cohesive group participants' activities that were performed in the radiation environment.
- Well-characterized radiation environment with adequately documented data or surrogate information that can be used to make best estimates of input parameters to the dose models.
- Reliable individual film badge dosimetry.

The six units comprise five from the PPG and one from the NTS and are:

- 7126th Army Unit (AU) Headquarters (HQ) Detachment, Enewetak Atoll, Operation REDWING (1956)
- Army Unit Administrative and Operations Detachments, Enewetak Atoll, Operation HARDTACK I (1958)
- 4th Marine Corps Provisional Atomic Exercise Brigade (MCPAEB) Maneuver at Shot HOOD, Operation PLUMBBOB (1957)
- USS ESTES (AGC 12), Operation REDWING (1956)
- USS BOXER (CVS 21), Operation HARDTACK I (1958)
- Army Personnel, Enewetak Atoll, Operation CASTLE (1954)

Based on input from external review boards and DTRA, probabilistic uncertainty analysis methods include internal dose assessments in addition to the external dose methods developed during in the initial pilot phase, which were further refined in this study. Probability distribution functions were generated for the uncertainty parameters as discussed in Section 4. These were incorporated into Monte Carlo simulation models for each of the six study groups. Mean and upper bound internal doses were calculated for thyroid, lung, and lower large intestine to provide example analyses for several organs.

Sections 5.1 through 5.6 provide summaries of the scenarios, relevant film badge and other radiation data for each case, and detailed discussions of the results. Additional details about each unit's activities, assumptions about scenario parameters, and uncertainty distributions used in the probabilistic analysis are provided in Appendices A–F.

For each study unit, a summary of external dose is provided as follows:

- Film badge doses (if available): unbiased mean and 95th percentile of the distribution of readings.
- Monte Carlo doses: arithmetic mean, standard deviation, and the 95th percentile dose.

- Deterministic doses: dose and upper bound based on the upper bound multiplier of 3.
- The ratio of the deterministic upper bound dose to the 95th percentile dose.

The CEDs from internally-deposited radionuclides are reported separately for alpha and beta-plus-gamma emitters. For CEDs from Monte Carlo simulations, all of which were lognormally distributed, geometric mean, geometric standard deviation and 95th percentile dose are reported for each of the three organs mentioned above. Finally, the geometric mean and 95th percentile CEDs from Monte Carlo simulations are compared to the deterministic CEDs and upper bounds, respectively.

5.1 Case Study #1: Operation REDWING (1956), 7126th Army Unit Headquarters (HQ) Detachment, Enewetak Atoll

5.1.1 Case Description and Cohort Participation Scenario

The 7126th AU provided most of the personnel for the Army Task Group (TG), designated TG 7.2. It was the permanent garrison force at Enewetak Island between Operations CASTLE and REDWING. Except for its military police detachment and several mail clerks on Eneu and Parry Islands, the 7126th AU was stationed on Enewetak Island. TG 7.2 was, in effect, a housekeeping unit, providing garrison and support elements for the joint task force in the PPG (Bruce-Henderson et al., 1982). To accommodate the buildup to Operation REDWING's operational phase, the 7126th AU was reorganized into the following four detachments: Headquarters (HQ), Service, Transportation, and Military Police. The HQ Detachment, consisting of 39 officers and 348 enlisted personnel, was stationed on Enewetak Island during Operation REDWING. (Bruce-Henderson et al., 1982).

Assigned personnel arrived at Enewetak Island prior to the first nuclear detonation of the series. By the nature of their duties, it is likely that most HQ Detachment personnel remained on the island continuously, or nearly so, throughout the operation. Further details of this analysis are included in Appendix A.

5.1.2 Available Dosimetry

Complete records of film badge results are available for the HQ Detachment. Most personnel in the unit were issued three consecutive permanent film badge dosimeters during their stay in the test area, which covered a total period extending from mid-April to early August 1956. However, most film badges issued for periods of 4 weeks or more at Operation REDWING were damaged by the high heat and humidity in the test area (NRC, 1989), which resulted in overstated readings. Thus, most of the badges for the unit were not suitable as a benchmark for comparison with reconstructed doses. It was, therefore, necessary to identify a set of badges worn for a shorter period and for which previous analysis had demonstrated the integrity of the readings. Based on previous experience in identifying damaged dosimeter films and a review of the Operation REDWING dosimetry database, a group of film badge doses for this unit was analyzed for a period extending from July 11 to August 3, 1956. As a result, a set of 323 badges was selected. Bias was removed from the film badge readings based on guidance on film badge dosimetry (NRC, 1989). The average unbiased film badge reading for the distribution is 2.9 rem,

with a standard deviation of 0.61 rem. Figure A-1 of Appendix A displays the distribution of film badge readings (adjusted for bias) for the HQ Detachment.

5.1.3 External Dose

External gamma dose reconstruction for personnel stationed on Enewetak Island during Operation REDWING was accomplished by incorporating uncertainty distributions for various parameters into the model discussed in Section 3. This model incorporates the fallout-induced radiation environments discussed in detail in Appendix A, and the fallout intensity decay model and effects of shielding as discussed in Section 3.

5.1.3.1 Exposure Pathways

The only sources of potential external radiation exposure for personnel stationed at Enewetak Atoll during Operation REDWING were residual gamma radiation from fallout due to Shots ZUNI, MOHAWK, APACHE, and TEWA. See Appendix A for additional details.

5.1.3.2 Assumptions and Parameter Uncertainty

The following specific uncertainty distributions, discussed in Section 4, were used in the uncertainty analysis for external gamma dose calculations:

- Amount of time spent outdoors each day.
- Fraction of time spent indoors that was spent in a tent-type structure or in a building.
- Protection factors for tents and buildings.
- Distributions of fallout intensity at locations on the island where a veteran most likely spent time, i.e., during time spent outdoors, location of the tent for the time spent indoors in a tent, and location of a building for the time spent indoors in a building.
- Measurement error associated with intensity measurements on the island.
- Uncertainty in shot-specific radiological decay functions.

The types of distributions, means, and confidence intervals for each of these distributions are shown in Table A-4 of Appendix A. The values used in the deterministic analysis that generated the deterministic doses reported for the film badge period of July 11 to August 3, 1956, are also summarized in Table A-4 of Appendix A.

5.1.3.3 Results and Discussion

The results of the external gamma dose deterministic analysis and the probabilistic analysis are shown in Table 20. These results indicate that the probabilistic analysis yields mean doses that are similar to the deterministic dose, and that the 95th percentile dose from the probabilistic analysis is lower than the upper-bound deterministic dose. In addition, the probabilistic mean dose is approximately 25 percent higher than the mean film badge dose, just inside the standard deviation of the film badge doses for this study group. Figure 33 provides a comparison of the probabilistic dose distribution with the distribution of film badge readings. Note the much

broader distribution for the probabilistic analysis, which is likely attributed to the many uncertain parameters involved with the calculation of reconstructed doses.

Table 20. Summary of External Dose for the 7126th Army Unit Stationed at Enewetak Atoll during Operation REDWING

Mean Dose (rem)			Upper Bound Dose (rem)			
Film Badge	**Probabilistic***	**Deterministic (NTPR)**	**Film Badge (95th Percentile)**	**Probabilistic (95th Percentile)**	**Deterministic (NTPR)**	**Ratio (Deterministic/ Probabilistic)**
2.9	3.4 (1.5)	3.4	4.0	6.2	10	1.6

* The arithmetic mean (and standard deviation) are shown. The geometric mean external dose is 3.1 rem.

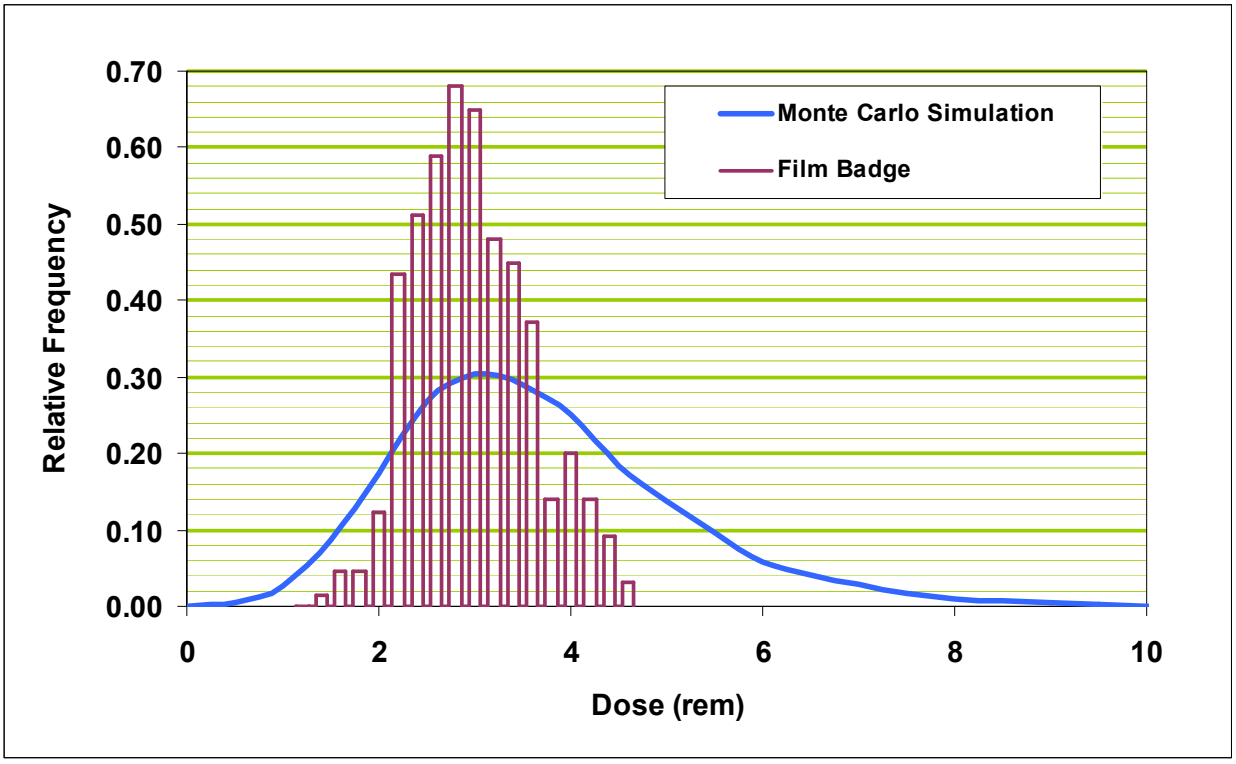

Figure 33. Comparison of the Dose Distribution from Probabilistic Analysis with Unbiased Film Badge Readings for the 7126th AU at Enewetak Atoll during Operation REDWING

5.1.4 Internal Dose

Internal dose reconstruction for army units stationed on Enewetak Island during Operation REDWING was accomplished by incorporating uncertainty distributions for various parameters into the models discussed in Section 3. These models incorporate the fallout-induced radiation environments discussed in detail in Appendix A, and the fallout intensity decay model and various other parameters discussed in Sections 3 and 4.

5.1.4.1 Exposure Pathways

Internal dose pathways included in the probabilistic analysis are inhalation of descending fallout, inhalation of resuspended fallout, and incidental ingestion of soil and dust based on the models discussed in Section 3.

5.1.4.2 Assumptions and Parameter Uncertainty

The following specific uncertainty distributions, discussed in Section 4, were used in the uncertainty analysis for internal dose calculations:

- Amount of time spent outdoors each day.
- Time-dependent resuspension factor $K(t)$.
- Breathing rate distribution correlated with activity levels.
- Time-dependent shot-specific dose conversion factors (*DCF*s).
- Bias factors for inhalation *DCF*.
- Deposition fractions for particle size classes deposited in the thoracic airways of the respiratory tract.
- Deposition fractions for particle size classes deposited in ET_2 and cleared to digestive tract.
- Activity fractions for inhalation of descending fallout for three particle size classes; activity fractions vary for Shots ZUNI, MOHAWK, APACHE, and TEWA.
- Ingestion rate and soil bulk density for incidental ingestion of soil and dust.

The types of distributions, means, and confidence intervals for each of these distributions are shown in Table A-6 of Appendix A. The values used in the deterministic analysis that generated the doses for the film badge period of July 11 to August 3, 1956 are also summarized in Table A-6.

5.1.4.3 Results and Discussion

Fifty-year committed equivalent dose (CED) distributions to three organs, thyroid, lung, and lower large intestine (LLI) wall, were derived using the probabilistic model for a sample size of 10,000 (i.e., 10,000 Monte Carlo histories). The geometric mean and 95th percentile CEDs of the distribution for each organ are given in Table 21. The ratio of the deterministic upper bound CED to the probabilistic 95th percentile CED, provided in the rightmost column, is a factor of 1.3 or greater for alpha doses and for beta-plus-gamma doses. These results indicate that the probabilistic analysis yields lower central doses than the doses calculated using deterministic

models based on methodologies discussed in Section 3 with nominal or mean values of various parameters as shown in Table A-6 of Appendix A. This result is primarily due to the partitioning of the descending inhalation dose based on estimates of the fraction deposited in the respiratory tract and inhaled versus the fraction deposited in ET_2 and ingested. It is also concluded that the probabilistic analysis 95th percentile doses are lower than the upper-bound deterministic internal doses, indicating that the upper bound factor of 10 used in the deterministic analysis results in a conservative estimate of the upper-bound internal dose for this specific set of exposures.

Table 21. Summary of Estimated Internal Doses for the 7126th Army Unit Stationed at Enewetak Atoll during Operation REDWING

Organ	Mean Dose (rem)		Upper Bound Dose (rem)		
	Probabilistic*	Deterministic (NTPR)	Probabilistic (95th Percentile)	Deterministic (NTPR)	Ratio (Deterministic ÷ Probabilistic)
Alpha Dose					
Thyroid	0.000024 (8.6)	0.00011	0.00083	0.0011	1.4
Lung	0.00029 (8.7)	0.0014	0.010	0.014	1.4
LLI wall	0.000024 (8.5)	0.00011	0.00085	0.0011	1.4
Beta plus Gamma Dose					
Thyroid	0.72 (4.8)	1.5	9.7	14	1.5
Lung	0.16 (6.6)	1.4	3.8	14	3.7
LLI wall	0.54 (4.8)	1.0	7.2	9.6	1.3

* Geometric means and (geometric standard deviations) from the probabilistic analysis are shown.

The relative frequency distribution and the probability plot of estimated doses to the LLI Wall from alpha radiation are shown in Figure 34 and Figure 35, respectively, and for the doses from beta plus gamma radiation are shown in Figure 36 and Figure 37, respectively. These figures demonstrate that the distributions are well represented by lognormal distributions, and are formally similar to the plots of the same results for the other two organs studied.

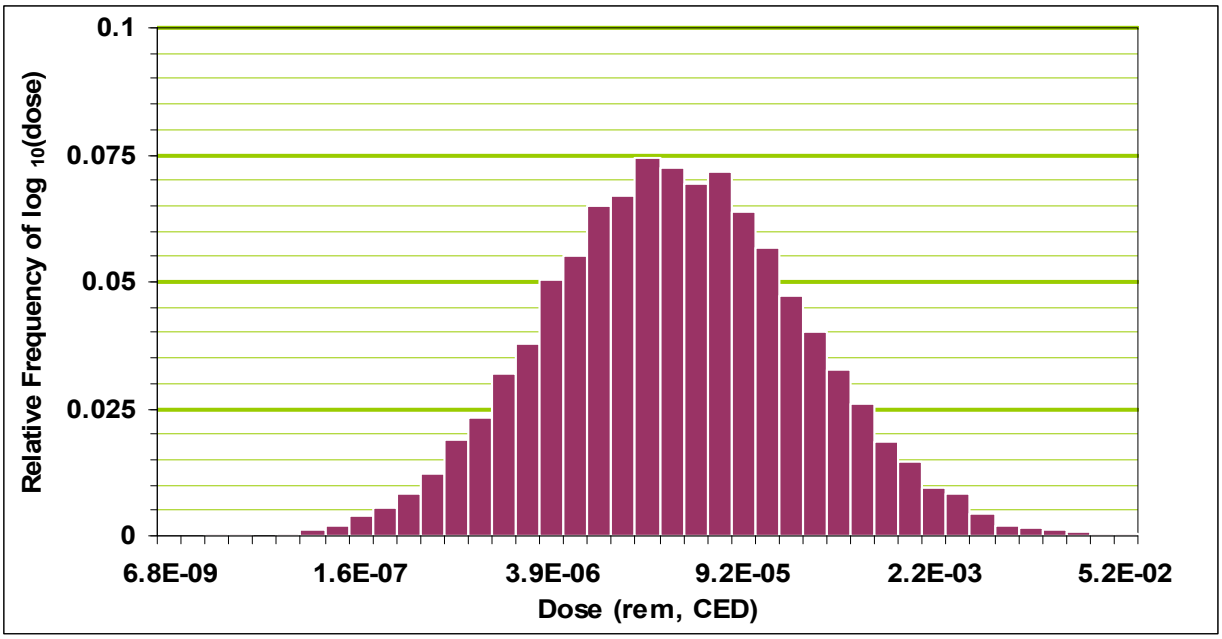

Figure 34. Distribution of Estimated LLI Wall Doses from Alpha Radiation for the 7126th Army Unit Stationed at Enewetak Atoll during Operation REDWING

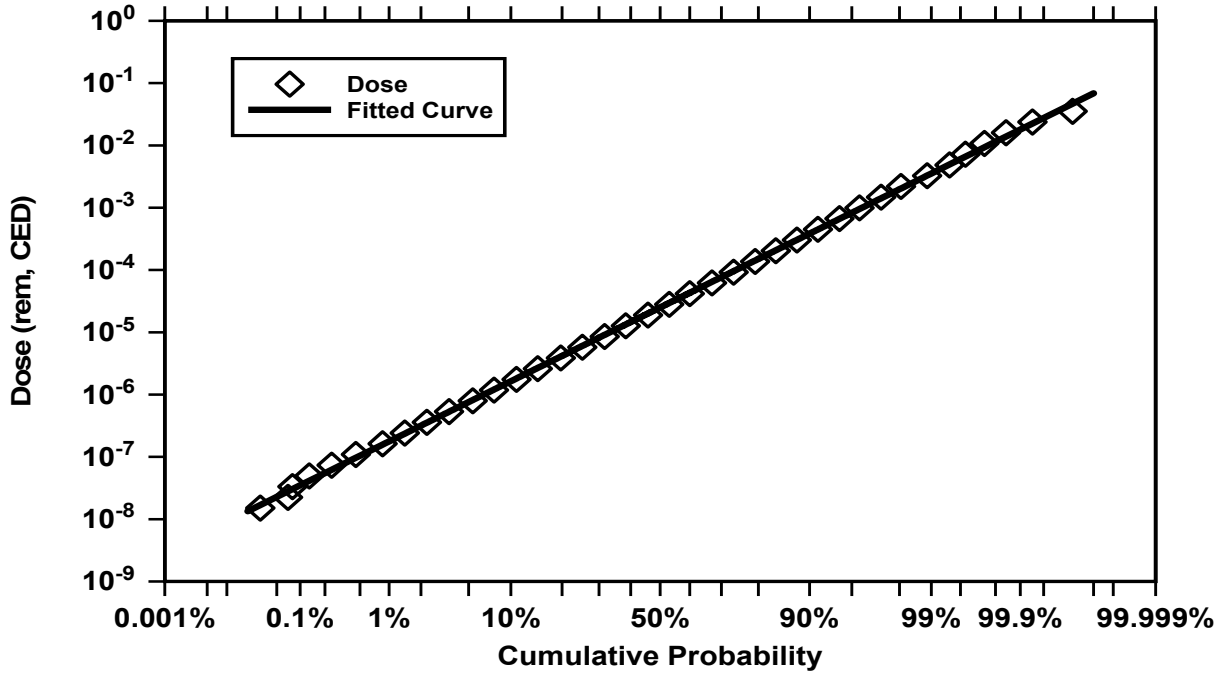

Figure 35. Probability Plot of Estimated LLI Wall Doses from Alpha Radiation for the 7126th Army Unit Stationed at Enewetak Atoll during Operation REDWING

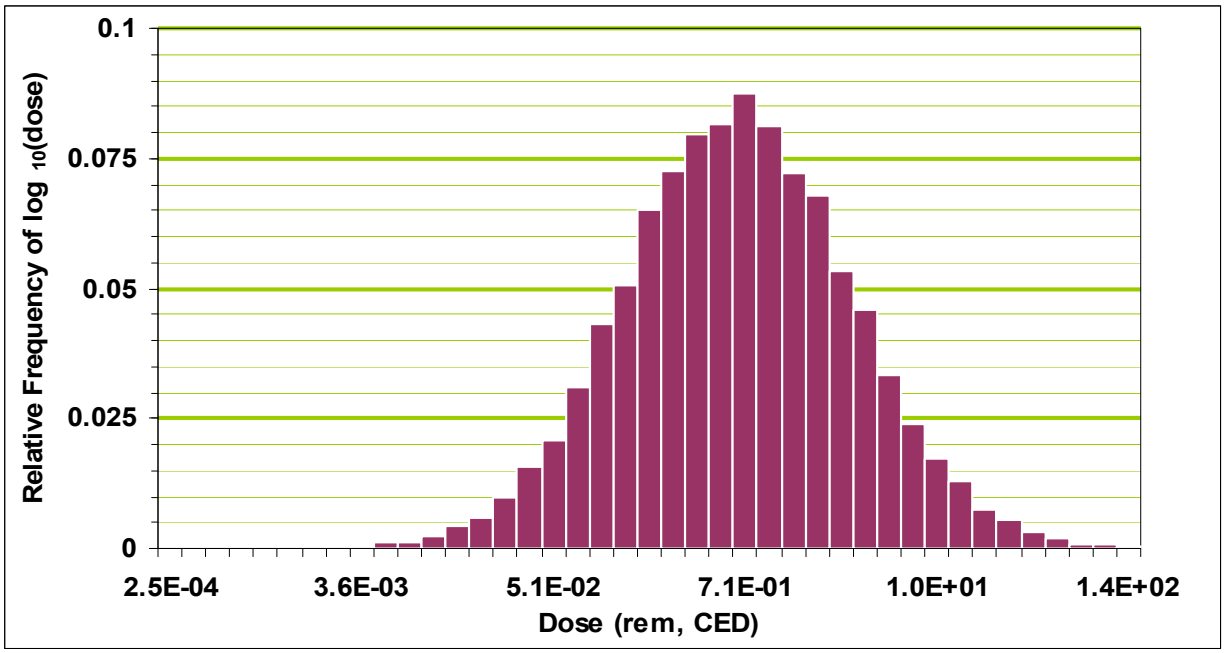

Figure 36. Distribution of Estimated LLI Wall Doses from Beta plus Gamma Radiation for the 7126th Army Unit Stationed at Enewetak Atoll during Operation REDWING

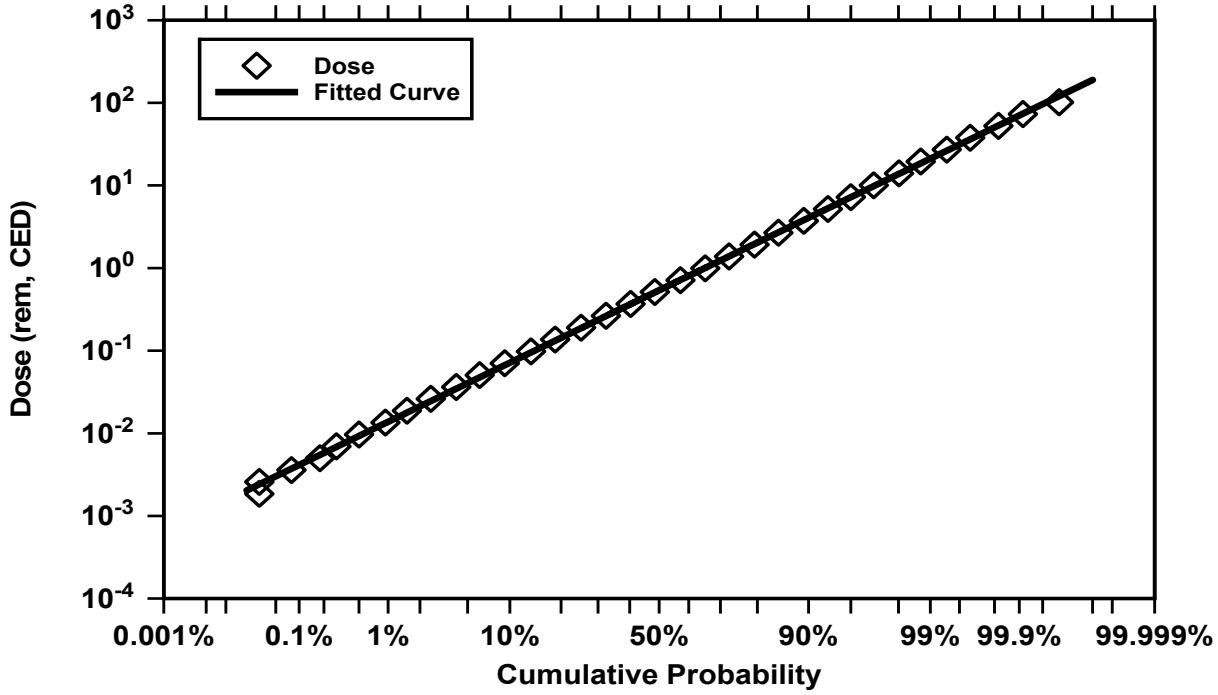

Figure 37. Probability Plot of Estimated LLI Wall Doses from Beta plus Gamma Radiation for the 7126th Army Unit Stationed at Enewetak Atoll during Operation REDWING

5.2 Case Study #2: Operation HARDTACK I (1958), Army Unit Administrative and Operations Detachments, Enewetak Atoll

5.2.1 Case Description and Cohort Participation Scenario

Permanent base camps were established on three islands to support the operations at Enewetak Atoll during Operation HARDTACK 1. The largest of the three, Enewetak Island (or Site Fred), was manned continuously during the operation with a maximum population of approximately 3200 people. Among the units assigned to Enewetak Island were two Army detachments, the Army Administrative Detachment and the Army Operations Detachment. The compositions and duties of these detachments are as follows (Gladeck et al., 1982):

- Administrative Detachment (AD): Personnel of this detachment supported the Chaplain, the Provost Marshal, and the Finance, Information, and Postal Sections. Its scheduled strength was 50 officers and 482 enlisted men during the operational period.
- Operations Detachment (OD): Duties of this detachment were administrative and logistic support for assigned personnel, including laundry, medical, dental, commissary, engineering, depot, gear loft, truck motor pool, and maintenance support. Its scheduled strength was 25 officers and 379 enlisted men.

A complete record of film badge data was obtained for these units. By the nature of their duties, it is likely that most personnel remained on the island continuously, or nearly so, throughout the operation. Further details of this analysis are included in Appendix B.

5.2.2 Available Dosimetry

About 18,000 test participants received film badge dosimetry during Operation HARDTACK I to measure exposure to external gamma radiation, and approximately 62,000 individual film badges were issued and processed. Most participants had such dosimetry throughout their period of service at Enewetak Proving Ground (EPG). A study of the HARDTACK I film badge design and the calibration, issue, exchange, and processing procedures utilized during the operation concluded that the dosimetry, while generally reliable, over-reported exposures by about 20 percent due to environmental effects in the hot, humid Pacific test area. (NRC, 1989)

Complete files of film badge data were obtained for these units. The databases were then processed to (1) correct for apparent inconsistencies in the recorded return dates of some badges and (2) distill the records to a subset of readings that most likely represent the exposure conditions of those personnel continuously resident on Enewetak Island throughout the operation. The statistics derived for these film badges are summarized in Table B-1 of Appendix B.

5.2.3 External Dose

External gamma dose reconstruction for army units stationed on Enewetak Island during Operation HARDTACK I was accomplished by incorporating uncertainty distributions for various parameters into the model discussed in Section 3. This model incorporates the fallout-

induced radiation environments discussed in detail in Appendix B, the fallout intensity decay model and effects of shielding as discussed in Section 3.

5.2.3.1 Exposure Pathways

The only sources of potential external radiation exposure for army units stationed at Enewetak Atoll during Operation HARDTACK I were residual gamma radiation from fallout due to Shots FIR/KOA, REDWOOD, and OAK. See Appendix B for additional details.

5.2.3.2 Assumptions and Parameter Uncertainty

The following specific uncertainty distributions, discussed in Section 4, were used in the uncertainty analysis for external gamma dose calculations:

- Amount of time spent outdoors each day.
- Fraction of time spent indoors that was spent in a tent-type structure or in a building.
- Protection factors for tents and buildings.
- Distributions of fallout intensity at locations on the island where a veteran most likely spent time, i.e., during time spent outdoors, location of the tent for the time spent indoors in a tent, and location of a building for the time spent indoors in a building.
- Measurement error associated with intensity measurements on the island.
- Uncertainty in fallout proportion from combined debris clouds for Shots FIR and KOA.
- Uncertainty in shot-specific radiological decay functions.

The types of distributions, means, and confidence intervals for each of these distributions are shown in Table B-2 of Appendix B. The values used in the deterministic analysis that generated the deterministic doses reported in Table 22 for the various film badge periods are also summarized in Table B-2.

5.2.3.3 Results and Discussion

The Monte Carlo-derived (arithmetic) mean and 95th percentile doses for each subunit are listed in Table 22. Also provided for comparison are similar statistics based on the distribution of film badge doses and on deterministic doses with the "times 3" upper bound convention. The last column displays the ratio of the deterministic upper bound dose to the probabilistic 95th percentile dose. It is seen that both the probabilistic and deterministic approaches compute mean doses that are generally consistent with the average film badge doses of the various subunits. The deterministic upper bound doses exceed the probabilistic 95th percentile doses by a nearly constant factor of 1.5–1.6; the latter doses exceed the 95th percentile film badge doses for all subunits. Figure 38 illustrates the relative comparisons of these quantities for the Administrative Detachment and the Operations Detachment.

Table 22. Summary of External Dose for Army Units Stationed at Enewetak Island during Operation HARDTACK I

Parent Unit	FB Turn-in Date (1958)	Dose (rem)			Upper Bound (NTPR) or 95th Percentile Doses (rem)			
		Mean FB	Mean MC	NTPR Det.	FB	MC	NTPR UB	Ratio NTPR UB/ MC
AD	May 31	0.54	0.889	0.85	0.74	1.65	2.6	1.6
OD	May 31	0.57	0.889	0.85	0.76	1.65	2.6	1.6
OD	Jun 4	0.89	0.939	0.90	1.15	1.75	2.7	1.5
AD	Jun 5	0.76	0.950	0.91	1.04	1.77	2.7	1.5
OD	Jun 5	0.89	0.950	0.91	1.26	1.77	2.7	1.5
AD	Jun 7	1.09	0.970	0.93	1.38	1.82	2.8	1.5
AD	Jun 10	0.98	0.997	0.95	1.18	1.87	2.9	1.5
OD	Jun 10	1.06	0.997	0.95	1.38	1.87	2.9	1.5
OD	Jun 11	1.39	1.01	0.96	1.85	1.88	2.9	1.5
OD	Jun 12	0.72	1.01	0.97	0.97	1.90	2.9	1.5
OD	Jun 13	1.31	1.02	0.98	1.84	1.91	2.9	1.5
AD	Jun 17	1.11	1.05	1.00	1.28	1.97	3.0	1.5
AD	Jun 27	1.00	1.10	1.05	1.28	2.09	3.1	1.5
AD	Jun 28	1.09	1.11	1.05	1.40	2.10	3.2	1.5
AD	Jun 29	1.00	1.12	1.06	1.25	2.11	3.2	1.5
AD	Jul 7	1.01	1.17	1.10	1.49	2.20	3.3	1.5

FB: film badge dose
MC: dose from the probabilistic model (Monte Carlo simulation)
Det.: dose from the deterministic model (NTPR)

5.2.4 Internal Dose

Internal dose reconstruction for army units stationed on Enewetak Island during Operation HARDTACK I was accomplished by incorporating uncertainty distributions for various parameters into the models discussed in Section 3. These models incorporate the fallout-induced radiation environments discussed in detail in Appendix B, and the fallout intensity decay model and various other parameters discussed in Sections 3 and 4.

5.2.4.1 Exposure Pathways

Internal dose pathways included in the probabilistic analysis are inhalation of descending fallout, inhalation of resuspended fallout, and incidental ingestion of soil and dust based on the models discussed in Section 3.

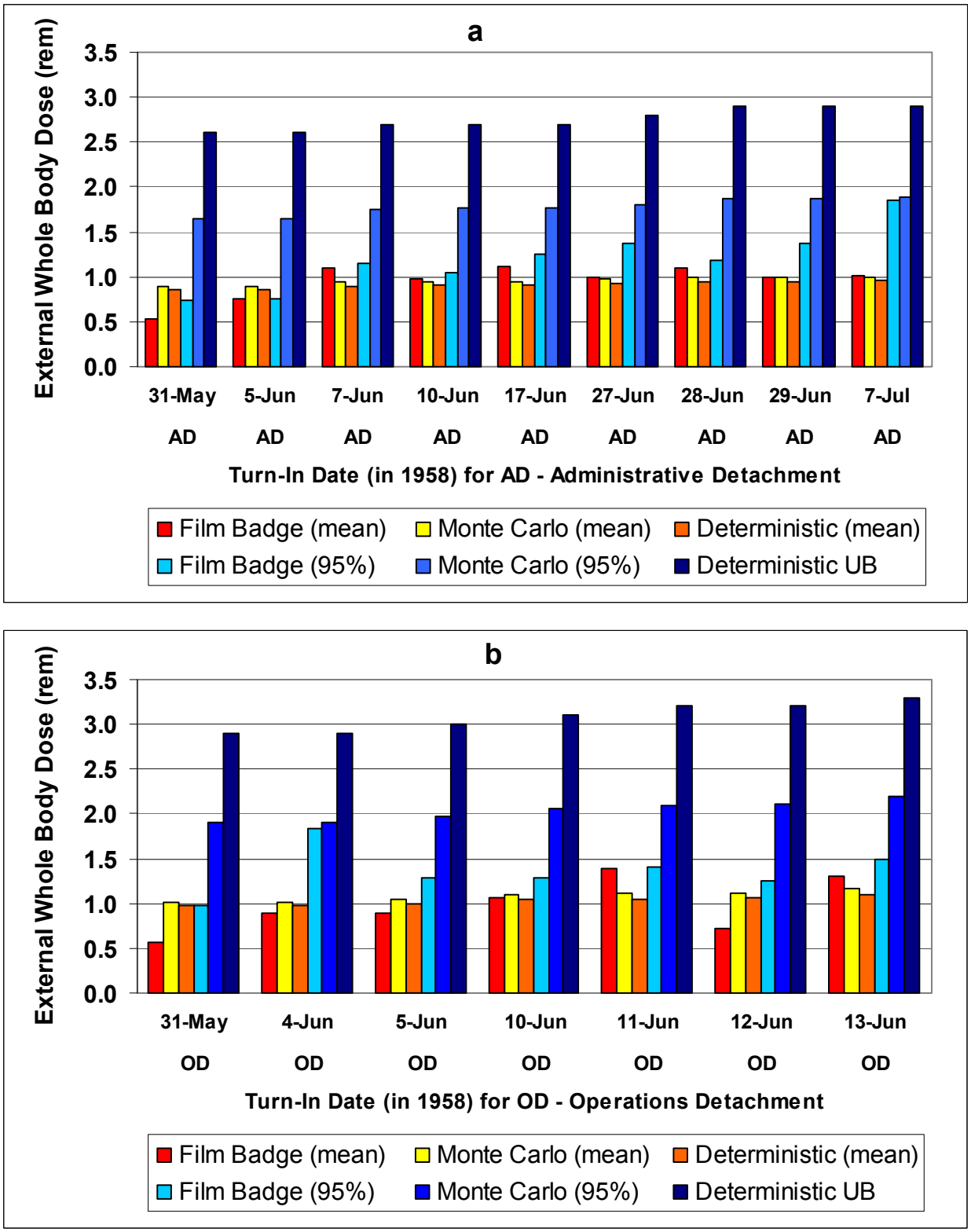

Figure 38. Comparison of Film Badge, Monte Carlo, and Deterministic Results for the Administrative Detachment (a) and the Operations Detachment (b) at Operation HARDTACK I

5.2.4.2 Assumptions and Parameter Uncertainty

The following specific uncertainty distributions, discussed in Section 4, were used in the uncertainty analysis for internal dose calculations:

- Amount of time spent outdoors each day.
- Time-dependent resuspension factor $K(t)$.
- Breathing rate distribution correlated with activity levels.
- Time-dependent shot-specific dose conversion factors (*DCF*s).
- Bias factors for inhalation *DCF*s.
- Deposition fractions for particle size classes deposited in the thoracic airways of the respiratory tract.
- Deposition fractions for particle size classes deposited in ET_2 tract and cleared to digestive tract.
- Activity fractions for inhalation of descending fallout for three particle size classes; activity fractions vary for Shots FIR/KOA, REDWOOD, and OAK.
- Ingestion rate and soil bulk density for incidental ingestion of soil and dust.

The types of distributions, means, and confidence intervals for each of these distributions are shown in Table B-4 of Appendix B. The values used in the deterministic analysis that generated the doses for the film badge period of April 12 to July 7, 1958 are also summarized in Table B-4 of Appendix B.

5.2.4.3 Results and Discussion

Fifty-year committed equivalent dose (CED) distributions for three organs, thyroid, lung, and lower large intestine (LLI) wall, were derived using the refined uncertainty model for a sample size of 10,000 (i.e., 10,000 Monte Carlo histories). Examples of these results are shown in Appendix B, where the relative frequency distribution and the probability plot of estimated doses to the LLI wall from alpha radiation are shown in Figure B-5 and Figure B-6, respectively, and from beta plus gamma radiation in Figure B-7 and Figure B-8, respectively. The CED distributions are lognormally-distributed, as indicated by their Gaussian (bell) shapes when plotted on a logarithmic axis. These figures for LLI wall are formally similar to those obtained for the other two trial organs.

The results of the internal dose deterministic analysis and the probabilistic analysis are shown in Table 23. These results indicate that the probabilistic analysis yields lower central doses than the doses calculated using deterministic models based on methodologies discussed in Section 3 with nominal or mean values of various parameters as shown in Table B-4 of Appendix B. This result is primarily due to the partitioning of the descending inhalation dose based on estimates of the fraction deposited in the respiratory tract and inhaled versus the fraction deposited in the ET tract and ingested. It is also concluded that the probabilistic 95^{th} percentile doses are lower than the upper-bound deterministic internal doses, indicating that the upper bound factor of 10 used in the deterministic analysis results in a conservative estimate of the upper-bound internal dose for this

Table 23. Internal Dose Summary for Army Units Stationed at Enewetak Island during Operation HARDTACK I

Organ	Mean Dose (rem)		Upper Bound Dose (rem)		
	Probabilistic[a]	Deterministic (NTPR)	Probabilistic (95th Percentile)	Deterministic (NTPR Upper Bound)	Ratio (Deterministic/ Probabilistic)
Alpha Dose					
Thyroid	0.000040 (8.5)	0.00036	0.0014	0.0036	2.6
Lung	0.00054 (8.6)	0.0049	0.019	0.049	2.6
LLI wall	0.000042 (8.3)	0.00036	0.0014	0.0036	2.5
Beta plus Gamma Dose					
Thyroid	0.24 (4.7)	0.57	3.0	5.5	1.8
Lung	0.030 (6.5)	0.31	0.67	3.1	4.6
LLI wall	0.17 (4.7)	0.40	2.1	3.9	1.8

[a] Geometric means (and geometric standard deviations) from the probabilistic analysis are shown

specific set of exposures. Illustrations of the lognormal nature of the internal dose distributions are shown in Figure B-5 and Figure B-7 of Appendix B for the dose to the LLI wall from alpha particles and the dose from beta plus gamma radiation, respectively.

5.3 Case Study #3: Operation PLUMBBOB (1957), 4th Marine Corps Provisional Atomic Exercise Brigade (MCPAEB) Maneuver at Shot HOOD

5.3.1 Case Description and Cohort Participation Scenario

The 4th Marine Corps Provisional Atomic Exercise Brigade (MCPAEB), commonly called the "Brigade" conducted an exercise at the NTS during Operation PLUMBBOB in 1957. The Brigade was organized as a standard air-ground task force totaling approximately 2,000 personnel. One of the units comprising the Brigade is the subject of this case study: Company E of the 2nd Battalion, 5th Marine Regiment, 1st Marine Division.

All of the Brigade troops arrived at Camp Desert Rock (CDR) by June 20, 1957, where they began preparing for a maneuver that was to be held in conjunction with Shot DIABLO. A full rehearsal in the NTS forward area was conducted on June 20 and 21. On the morning of

June 28, with the entire Brigade in place, DIABLO misfired and all Brigade personnel returned to CDR. The maneuver was reassigned to Shot HOOD, and on the morning of July 5, with the Brigade in its trenches 5,360 yards southwest of ground zero (GZ), Shot HOOD was detonated. About 15 minutes later Company E, preceded and flanked by radiation safety personnel, began its march from the trenches in the direction of the HOOD GZ. Having approached to within 1,100 to 1,400 yards of the HOOD GZ, at which time they reached the Rad-Safe limit of 5 R hr^{-1} in that shot's neutron-activated radiation field, the company reversed its direction of march enroute back to the trenches. By 0700 the company had returned to the trench area, then marched to a nearby helicopter landing zone where it enplaned and was transported to a location about 7,000 yards to the west of the trenches. From there, the company participated in a mock assault on a nearby objective. By 1430 they had marched to a nearby road from where they were transported by motor vehicle convoy back to CDR. Company E did not tour the HOOD display area on HOOD shot day. Most Brigade personnel had departed from CDR by July 6, 1957. (Frank et al., 1981; USMC, 1957)

5.3.2 Available Dosimetry

Brigade personnel were issued individual film badges for the duration of their stay at CDR. Film badge dosimetry records for the 2nd Battalion, 5th Marines is available only for senior personnel, and very few low-ranking enlisted men are represented in the dosimetry records. A total of 12 film badge readings are available for Company E personnel for the period prior to and including Shot HOOD. The 12 readings, in mrem, are: 1200, 980, 760, 560, 560, 520, 520, 520, 500, 500, 500 and 480. Although the three highest readings are thought to be outliers, there is not sufficient documentation to definitively conclude that the high readings are not representative of the actual film badge dose received by the majority of Company E personnel. One explanation for the higher readings might be the additional activities known to have been conducted by some of the senior personnel for whom the readings are available. Based on the 12 readings, the mean film badge reading for Company E is 633 mrem and the 95th percentile is 1079 mrem. No environmental bias is associated with PLUMBBOB film badges, so no bias adjustments are necessary. (Frank et al., 1981; NRC, 1989).

5.3.3 External Dose

External gamma dose reconstruction for Company E personnel during Operation PLUMBBOB was accomplished by incorporating uncertainty distributions for various parameters into the model discussed in Section 3. This model incorporates the radiation environments and variables discussed in Appendix C, and the fallout intensity decay model as discussed in Section 3.

5.3.3.1 Exposure Pathways

Company E personnel were potentially exposed to residual radiation at CDR and in forward test areas of the NTS. The sources of potential external radiation exposure for Company E personnel during Operation PLUMBBOB are listed below, grouped by each primary activity in which Company E engaged (Frank et al., 1981):

- During the rehearsal and the misfire, residual radiation from Shot BOLTZMANN and Shot WILSON fallout in the DIABLO test area.
- During the maneuver, residual radiation from Shot BOLTZMANN and Shot WILSON fallout in the HOOD test area.
- During the maneuver, residual radiation from neutron-induced soil radioactivity in the HOOD test area.
- While at CDR, residual radiation from Shot WILSON fallout.

5.3.3.2 Assumptions and Parameter Uncertainty

Probability distributions for the following model parameters were used in the probabilistic analysis for external gamma dose calculations, and are discussed in Section 4 and Appendix C:

- Protection factors for tent-type structures.
- Distributions of fallout intensity at locations at CDR where a veteran most likely spent time, i.e., during time spent outdoors, and location within a tent for the time spent indoors.
- Measurement error associated with intensity measurements and data collection and reporting.
- Interpolation and extrapolation errors associated with creating and using iso-intensity contour maps.
- Uncertainty in shot-specific radiological decay functions.

In addition, probability distributions were used for CDR arrival and departure times, the amount of time spent outdoors at CDR, and several maneuver parameters. The types of distributions, central values and confidence intervals for each of these distributions are shown in Table C-4 of Appendix C. The values used in the deterministic analysis are also summarized in Table C-4.

5.3.3.3 Results and Discussion

The results of the deterministic and probabilistic external gamma dose analyses are shown in Table 24. The pathway that contributes most significantly to the external dose is the external exposure to neutron-induced radionuclides in the soil traversed during the maneuver. This source contributes approximately 96 percent of both the deterministic (NTPR) and mean (probabilistic analysis) doses. The amount of time Company E spent at the radiological safety limit is likely the dominant source of the external dose. Although the deterministic dose is typically considered to be a high-sided dose, it is slightly lower than both the mean film badge dose and the mean dose of the probability distribution. This reflects the use of film badge records that are thought to reflect activities that are not typical for Company E, as well as the use of large upper bound parameter values for certain parameters such as interpolated intensities and linger time at the Rad-Safe limit.

A comparison of the upper-bound doses shows that the deterministic (NTPR) upper bound dose is about 70 percent higher than the 95^{th} percentile dose from the probabilistic analysis. This indicates that the upper bound factor of 3 used in the deterministic external dose analysis results in an adequate estimate of the upper bound external gamma dose for Company E personnel at PLUMBBOB.

Table 24. Summary of External Dose for Company E Personnel of the 4th MCPAEB during Operation PLUMBBOB

Mean Dose (rem)			Upper Bound Dose (rem)			
Film Badge	**Probabilistic(*)**	**Deterministic (NTPR)**	**Film Badge**	**Probabilistic (95th Percentile)**	**Deterministic (NTPR)**	**Ratio (Deterministic/ Probabilistic)**
0.63	0.62 (0.23)	0.58	1.1	1.0	1.8	1.7

(*) The arithmetic mean (and standard deviation) is shown. The geometric mean external dose is 0.57 rem.

5.3.4 Internal Dose

Internal dose reconstruction for Company E personnel at the NTS during Operation PLUMBBOB was accomplished by incorporating probability distributions for input parameters of the models discussed in Section 3. These models incorporate the radiation environments and input parameters discussed in Appendix C.

5.3.4.1 Exposure Pathways

The sources of potential internal radiation exposure for Company E personnel during Operation PLUMBBOB are listed below, grouped by each primary activity in which Company E engaged (Frank et al., 1981):

- During the rehearsal and the misfire, inhalation of resuspended fallout from shots BOLTZMANN and WILSON fallout in the DIABLO test area.
- During the maneuver, inhalation of resuspended fallout from shots BOLTZMANN and WILSON in the HOOD test area.
- During the maneuver, inhalation of highly-resuspended fallout from shots BOLTZMANN and WILSON in the HOOD test area.
- During the maneuver, inhalation of suspended neutron-induced soil contaminants in the HOOD test area.
- While at CDR, inhalation of resuspended fallout from Shot WILSON.
- While at CDR and during all activities in the forward test area, incidental ingestion of contaminated soil and dust.

5.3.4.2 Assumptions and Parameter Uncertainty

Probability distributions for the following model parameters were used in the probabilistic analysis for internal dose calculations, and are discussed in Section 4 and Appendix C:

- Time-dependent resuspension factors for routine activities.

- Resuspension factors for detonation-related and helicopter downwash resuspension.
- Breathing rate distribution correlated with activity levels.
- Time-dependent shot-specific inhalation and ingestion *DCF*s.
- Bias factors for inhalation *DCF*s.
- Soil ingestion rate and soil bulk density.

In addition, probability distributions were used for CDR arrival and departure times, the amount of time spent outdoors at CDR, and several maneuver parameters. The types of distributions, confidence intervals, and central estimates for each of these distributions are shown in Table C-6 of Appendix C. The values used in the deterministic analysis are also summarized in Table C-6.

5.3.4.3 Results and Discussion

Distributions of fifty-year committed equivalent doses (CED) for three organs, thyroid, lung, and lower large intestine (LLI) wall, were derived using the uncertainty model for a sample size of 10,000 (i.e., 10,000 Monte Carlo histories). Examples of these results are shown in Appendix C, where the relative frequency distribution and the probability plot of estimated doses to the LLI wall from alpha radiation are shown in Figure C-4 and Figure C-5, respectively, and from beta plus gamma radiation in Figure C-6 and Figure C-7, respectively.

The results of the deterministic and probabilistic internal dose analyses are shown in Table 25. These results show that each deterministic organ dose is higher than the geometric mean dose from the corresponding probabilistic organ dose distribution. This result is expected, and it reflects the use of high-sided deterministic parameter values, including resuspension factors that result in upper bound internal doses from inhalation of detonation-induced resuspended fallout. Inhalation of detonation-induced resuspended fallout accounts for roughly 90 percent of the alpha organ doses, and between 70 and 90 percent of the total deterministic beta plus gamma organ doses. The deterministic doses due to detonation-induced resuspension are based on resuspension factors that were estimated to result in upper bound inhalation doses from this pathway, so they are not multiplied by 10 in the determination of upper bound deterministic doses. Therefore, the upper-bound deterministic doses are not simple 10× multiples of the deterministic doses.

For this case study, all deterministic upper bound organ doses are lower than the corresponding 95th percentile organ doses. The upper bound ratios in the last column of Table 25 show that the deterministic upper bound alpha organ doses are roughly 60 to 70 percent of the corresponding 95th percentile organ doses, and the deterministic upper bound beta plus gamma organ doses are between approximately 40 and 85 percent of the corresponding 95th percentile organ doses. This outcome was initially attributed to the effects of correlations between very large lognormally distributed parameter uncertainties resulting in large 95th percentiles. However, evaluations accomplished to date that have examined the effects of removing many of the inherent correlations have shown this not to be the cause.

Of the pathways that contribute to internal organ doses, inhalation of resuspended fallout is the primary cause of the observed deterministic upper bound to 95th percentile ratios. This finding is not unique to this NTS case, as an examination of the pathway doses for other case studies included in this report also shows that most of the 95th percentile resuspended fallout doses for

Table 25. Summary of Internal Dose for Company E of the 4th MCPAEB at the NTS during Operation PLUMBBOB

Organ	Mean Dose (rem)		Upper Bound Dose (rem)		
	Probabilistic*	Deterministic (NTPR)	Probabilistic (95th Percentile)	Deterministic (NTPR)	Ratio (Deterministic/ Probabilistic)
Alpha Dose					
Thyroid	0.0000046 (7.3)	0.000051	0.00013	0.000087	0.68
Lung	0.00013 (7.4)	0.0011	0.0036	0.0022	0.58
LLI Wall	0.0000050 (6.9)	0.000051	0.00013	0.000087	0.66
Beta plus Gamma Dose					
Thyroid	0.0042 (5.0)	0.0096	0.062	0.028	0.43
Lung	0.0016 (6.3)	0.016	0.034	0.030	0.87
LLI Wall	0.0016 (5.0)	0.0045	0.025	0.010	0.42

* Geometric means (and geometric standard deviations) from the probabilistic analysis are shown

the three example organs are greater than the deterministic upper bound resuspended fallout doses. Looking more closely at the PLUMBBOB case study, inhalation of resuspended WILSON fallout during the rehearsal and maneuver appears to be the primary cause of the observed ratios of deterministic upper bound organ doses to corresponding 95th percentile organ doses. Additional evaluations of the calculations that lead to such ratios must be undertaken to further explain the outcome.

Factors that will have to be specifically examined include the use of different time-dependent resuspension factors, the detonation-induced resuspension factors, the inclusion of upper-bound pathways (e.g., detonation-induced resuspension) in the deterministic dose calculations, and the very large uncertainties associated with several consequential variables. The time-dependent resuspension factor used in the probabilistic analysis may be a complication when assessing inhalation of fallout that has decayed more than about 200 hours (such as BOLTZMANN fallout in this case), after which the resuspension factor starts to drop appreciably. The large differences (2 or 3 orders of magnitude) between deterministic and probabilistic resuspension factors for detonation-induced resuspension also must be examined further. In addition, the inclusion of upper-bound pathways (most importantly the inhalation of detonation-induced resuspension) in the deterministic dose calculations presents a complication, because for these pathways a single dose is treated as both the deterministic dose and the upper-bound dose. Finally, large uncertainties associated with resuspension factors, inhalation dose conversion factors and the

intensities obtained from iso-intensity contour plots must be examined in more detail. These uncertainty distributions are large (geometric standard deviations between 2 and 5.2), and additional evaluations must be undertaken to verify that they are reasonable.

5.4 Case Study #4: Operation REDWING (1956), USS ESTES (AGC 12)

5.4.1 Case Description and Cohort Participation Scenario

USS ESTES was an amphibious force flagship that served during REDWING as the Flagship Element (Task Element 7.3.0.1) of the Flagship Unit (Task Group 7.3). The ship arrived in the PPG on March 31, 1956, and departed from Enewetak for Bikini on May 3, two days before the first shot of the series. It returned to Enewetak twice: once for Shot SEMINOLE on June 6 and again during the last four days of June when no shots were detonated. USS ESTES was, therefore, present at Enewetak for only one of the eleven shots fired at that atoll. The ship participated in all of the six Bikini shots, providing communications, air control, and facilities for Program 2 (Nuclear Radiation) and radiation safety activities. For each shot at Bikini, the ship was out of the lagoon and on station at sea, departing the lagoon prior to each detonation and not returning until several hours after the detonations. At all other times at Bikini, the ship was moored to buoy Nan-9 at the Eneu Island anchorage. USS ESTES departed from the PPG on July 25, 1956, proceeded to Pearl Harbor, Hawaii, and then to San Diego, California. It arrived at San Diego on August 7, 1956. (Bruce-Henderson et al., 1982).

5.4.2 Available Dosimetry

The entire crew was issued film badges for the duration of the ship's participation in the operation. Two series of badges were issued; the first was from April 25 to June 25 and the second from June 25 to July 25. As was the case with the 7126th Army Unit REDWING study group, most film badges issued to USS ESTES personnel for periods of 4 weeks or more at Operation REDWING were damaged by the high heat and humidity in the test area (Bruce-Henderson et al., 1982; NRC, 1989), and are therefore not suitable for comparison with Monte Carlo dose distributions.

5.4.3 External Dose

External gamma dose reconstruction for the crew of USS ESTES during Operation REDWING was accomplished by incorporating uncertainty distributions for various parameters into the model discussed in Section 3. This model incorporates the fallout-induced radiation environments discussed in detail in Appendix D, and the fallout intensity decay model and effects of shielding as discussed in Section 3.

5.4.3.1 Exposure Pathways

Sources of potential external radiation exposure for the crew of USS ESTES during Operation REDWING include residual gamma radiation from fallout due to Shots ZUNI, FLATHEAD,

NAVAJO, and TEWA, external ship contamination, and shine from lagoon waters. See Appendix D for additional details.

5.4.3.2 Assumptions and Parameter Uncertainty

The following specific uncertainty distributions, discussed in Section 4, were used in the uncertainty analysis for external gamma dose calculations:

- Amount of time spent topside each day.
- Ship shielding factors while present at worksites and billet areas below deck.
- Distributions of fallout intensity at locations on the ship where a veteran most likely spent time, i.e., during time spent topside, worksite location, and billet location.
- Measurement error associated with intensity measurements on the ship.
- Error associated with ship contamination and shine data.
- Uncertainty in shot-specific radiological decay functions.

The types of distributions, means, and confidence intervals for each of these distributions are shown in Table D-6 of Appendix D. The values used in the deterministic analysis that generated the deterministic doses reported for the operational period of May 28 to August 6, 1956, are also summarized in Table D-6.

5.4.3.3 Results and Discussion

The results of the external gamma dose deterministic analysis and the probabilistic analysis are shown in Table 26. These results indicate that the probabilistic analysis yields a slightly higher mean dose than the deterministic analysis, but that the probabilistic 95th percentile dose is lower than the upper-bound deterministic dose.

Table 26. Summary of External Dose for the Crew of USS ESTES during Operation REDWING

Mean Dose (rem)		Upper Bound Dose (rem)		
Probabilistic*	**Deterministic (NTPR)**	**Probabilistic (95th Percentile)**	**Deterministic (NTPR)**	**Ratio (Deterministic/ Probabilistic)**
0.50 (0.28)	0.43	1.0	1.2	1.1

* The arithmetic mean (and standard deviation) is shown. The geometric mean external dose is 0.44 rem.

5.4.4 Internal Dose

Internal dose reconstruction for the crew of USS ESTES during Operation REDWING was accomplished by incorporating uncertainty distributions for various parameters into the models discussed in Section 3. These models incorporate the fallout-induced radiation environments discussed in detail in Appendix D, and the fallout intensity decay model and various other parameters discussed in Sections 3 and 4.

5.4.4.1 Exposure Pathways

Internal dose pathways included in the probabilistic analysis are inhalation of descending fallout and inhalation of resuspended fallout based on the models discussed in Section 3.

5.4.4.2 Assumptions and Parameter Uncertainty

The following specific uncertainty distributions, discussed in Section 4, were used in the uncertainty analysis for internal dose calculations:

- Amount of time spent topside each day.
- Resuspension factor *K* (assumed to be constant with time).
- Breathing rate distribution correlated with activity levels.
- Time-dependent shot-specific dose conversion factors (*DCF*s).
- Bias factors for inhalation *DCF*s.
- Deposition fractions for particle size classes deposited in the thoracic airways of the respiratory tract.
- Deposition fractions for particle size classes deposited in ET_2 and cleared to digestive tract.
- Activity fractions for inhalation of descending fallout for three particle size classes; activity fractions vary for Shots ZUNI, FLATHEAD, NAVAJO, and TEWA.

The types of distributions, means, and confidence intervals for each of these distributions are shown in Table D-8 of Appendix D.

5.4.4.3 Results and Discussion

Distributions of fifty-year committed equivalent doses (CED) to three organs, thyroid, lung, and lower large intestine (LLI) wall, were derived using the refined uncertainty model for a sample size of 10,000 (i.e., 10,000 Monte Carlo histories). Examples of these results are shown in Appendix D, where the relative frequency distribution and the probability plot of estimated doses to the LLI wall from alpha radiation are shown in Figure D-3 and Figure D-4, respectively, and from beta plus gamma radiation in Figure D-5 and Figure D-6, respectively. The CED distributions are lognormally-distributed, as indicated by their Gaussian (bell) shapes when plotted on a logarithmic axis.

The results of the internal dose deterministic analysis and the probabilistic analysis are shown in Table 27. These results indicate that the probabilistic analysis yields lower central doses than the doses calculated using deterministic models based on methodologies discussed in Section 3 with

nominal or mean values of various parameters shown in Table D-8 of Appendix D. This result is primarily due to the partitioning of the descending inhalation dose based on estimates of the fraction deposited in the respiratory tract and inhaled versus the fraction deposited in the ET region and ingested. These results indicate that the probabilistic 95th percentile doses are lower than the upper-bound deterministic internal doses, implying that the upper bound factor of 10 used in the deterministic analysis results in a conservative estimate of the upper-bound internal dose for this set of specific exposures. Note that the probabilistic 95th percentile LLI wall beta plus gamma dose is approximately equal to the deterministic upper bound dose.

Table 27. Summary of Internal Dose for the USS ESTES Crew during Operation REDWING

Organ	Mean Dose (rem)		Upper Bound Dose (rem)		
	Probabilistic[a]	Deterministic (NTPR)	Probabilistic (95th Percentile)	Deterministic (NTPR Upper Bound)	Ratio (Deterministic/ Probabilistic)
Alpha Dose					
Thyroid	0.0000072 (7.8)	0.000032	0.00021	0.00032	1.5
Lung	0.000088 (7.8)	0.00040	0.0026	0.0040	1.5
LLI wall	0.0000076 (7.6)	0.000033	0.00022	0.00033	1.5
Beta plus Gamma Dose					
Thyroid	0.56 (4.6)	0.70	6.6	7.0	1.1
Lung	0.088 (6.0)	0.58	1.8	5.8	3.2
LLI wall	0.36 (4.6)	0.44	4.2	4.4	1.0

[a] Geometric means (and geometric standard deviations) from the probabilistic analysis are shown

5.5 Case Study #5: Operation HARDTACK I (1958), USS BOXER (CVS 21)

5.5.1 Case Description and Cohort Participation Scenario

USS BOXER was an antisubmarine aircraft carrier that served during HARDTACK I as command ship for Commander Joint Task Force 7, flagship for the Commander Task Group (CTG) 7.3 (Navy), headquarters for CTG 7.1 (Scientific) and CTG 7.4 (Air Force), and Air Operations Center for Air Force personnel. The ship also hosted Marine Helicopter Transport Squadron (Light) 361. USS BOXER transported many of the nuclear devices from CONUS to EPG. The ship arrived at Enewetak Atoll on March 3, 1958, with a crew of approximately 1100 personnel. It made numerous transits between Enewetak and Bikini atolls during May and June in support of the test series, finally departing EPG for Pearl Harbor on June 30. The ship

subsequently was present at Johnston Island in late July and August to support the two HARDTACK I shots at that location. During the operation, USS BOXER performed a variety of shot-specific tasks; for example, it served as the launch platform for the balloon that carried the YUCCA device aloft, the evacuation unit for island-based personnel for several shots, and the recovery element for rocket nosecones and other instrumented devices employed at several shots. (Gladeck et al., 1982)

Extensive preparation and planning for radiological safety were performed aboard USS BOXER. The ship was equipped with a washdown system to remove fallout, and was staffed with 18 radiological monitoring teams and two decontamination squads. These teams were used extensively on shot days for fallout watch and decontamination, as needed. Radiological surveys were made hourly during USS BOXER's stay in EPG (Gladeck et al., 1982). Unfortunately, little of this monitoring data has been located to date.

5.5.2 Available Dosimetry

The entire crew was issued film badges prior to the start of testing. The issue date for officers and senior non-commissioned officers was April 11; most enlisted personnel received their badges on April 14. For the majority of crewmembers, the available dosimetry record provides total operational doses but does not include complete information linking the readings to badge numbers and to turn-in dates. Therefore, an additional uncertainty was applied to film badge turn-in dates.

The average of the available film badge readings is 0.735 rem. Removing the 20 percent environmental bias discussed in the NRC film badge dosimetry report (NRC, 1989) results in an unbiased average film badge dose of 0.735/1.2 = 0.612 rem.

5.5.3 External Dose

External gamma dose reconstruction for the crew of USS BOXER during Operation HARDTACK I was accomplished by incorporating uncertainty distributions for various parameters into the model discussed in Section 3. This model incorporates the fallout-induced radiation environments discussed in detail in Appendix E, and the fallout intensity decay model and effects of shielding as discussed in Section 3.

5.5.3.1 Exposure Pathways

Sources of potential external radiation exposure for the crew of USS BOXER during Operation HARDTACK I include residual gamma radiation from fallout due to Shots FIR/KOA, REDWOOD, and OAK (Gladeck et al., 1982).

5.5.3.2 Assumptions and Parameter Uncertainty

The following specific uncertainty distributions were used in the uncertainty analysis for external gamma dose calculations:

- Amount of time spent topside each day.

- Ship shielding factors while present at worksites and billet areas below deck.
- Distribution of fallout intensities at locations on the ship where a veteran most likely spent time, i.e., during time spent topside, worksite location, and billet location.
- Error associated with intensity measurements on the ship.
- Uncertainty in fallout proportion from combined debris clouds for Shots FIR and KOA.
- Uncertainty in shot-specific radiological decay functions.
- Film badge turn-in date.

The types of distributions, means, and confidence intervals for each of these distributions are shown in Table E-1 of Appendix E. The values used in the deterministic analysis that generated the deterministic doses reported for the period starting with the first shot, May 12, 1958, through the turn-in of film badges are also summarized in Table E-1 of Appendix E.

5.5.3.3 Results and Discussion

The results of the external gamma dose deterministic analysis and the probabilistic analysis are shown in Table 28. These results indicate that the probabilistic analysis yields similar mean doses as the deterministic analysis, and that the probabilistic 95th percentile dose is lower than the upper-bound deterministic dose. The mean doses derived deterministically and probabilistically are also in reasonable agreement with the unbiased mean film badge dose. Of the 980 available USS BOXER film badge readings, only one (0.1 percent) exceeds the 95th percentile upper bound of the probabilistic distribution.

Table 28. Summary of External Dose for the Crew of USS BOXER during Operation HARDTACK I

Mean Dose (rem)			Upper Bound Dose (rem)			
Film Badge	**Probabilistic***	**Deterministic (NTPR)**	**Film Badge**	**Probabilistic (95th Percentile)**	**Deterministic (NTPR)**	**Ratio (Deterministic/ Probabilistic)**
0.61	0.53 (0.36)	0.52	0.97	1.2	1.6	1.3

* The arithmetic mean (and standard deviation) is shown. The geometric mean external dose is 0.42 rem.

5.5.4 Internal Dose

Internal dose reconstruction for the crew of USS BOXER during Operation HARDTACK I was accomplished by incorporating uncertainty distributions for various parameters into the models discussed in Section 3. These models incorporate the fallout-induced radiation environments discussed in detail in Appendix E, and the fallout intensity decay model and various other parameters discussed in Sections 3 and 4.

5.5.4.1 Exposure Pathways

Internal dose pathways included in the probabilistic analysis are inhalation of descending fallout and inhalation of resuspended fallout based on the models discussed in Section 3.

5.5.4.2 Assumptions and Parameter Uncertainty

The following specific uncertainty distributions, discussed in Section 4, were used in the uncertainty analysis for internal dose calculations:

- Amount of time spent topside each day.
- Constant resuspension factor *K*.
- Breathing rate distribution correlated with activity levels.
- Time-dependent shot-specific dose conversion factors (*DCF*s).
- Bias factors for inhalation *DCF*s.
- Deposition fractions for particle size classes deposited in the thoracic airways of the respiratory tract.
- Deposition fractions for particle size classes deposited in ET_2 and cleared to digestive tract.
- Activity fractions for inhalation of descending fallout for three particle size classes; activity fractions vary for Shots FIR/KOA, REDWOOD, and OAK.

The types of distributions, means, and confidence intervals for each of these distributions are shown in Table E-3 of Appendix E.

5.5.4.3 Results and Discussion

Fifty-year committed equivalent dose (CED) distributions to three organs, thyroid, lung, and lower large intestine (LLI) wall, were derived using the refined uncertainty model for a sample size of 10,000 (i.e., 10,000 Monte Carlo histories). Examples of these results are shown in Appendix E, where the relative frequency distribution and the probability plot of estimated doses to the LLI wall from alpha radiation are shown in Figure E-3 and Figure E-4, respectively, and from beta plus gamma radiation in Figure E-5 and Figure E-6, respectively. The CED distributions are lognormally-distributed, as indicated by their Gaussian (bell) shapes when plotted on a logarithmic axis.

The results of the internal dose deterministic analysis and the probabilistic analysis are shown in Table 29. These results indicate that the probabilistic analysis yields lower central doses than the doses calculated using deterministic models based on methodologies discussed in Section 3 with nominal or mean values of various parameters as shown in Table E-3 of Appendix E. This result is primarily due to the partitioning of the descending inhalation dose based on estimates of the fraction deposited in the respiratory tract and inhaled versus the fraction deposited in the ET tract and ingested. These results also indicate that the probabilistic 95^{th} percentile doses are lower than the upper-bound deterministic internal doses, implying that the upper bound factor of 10 used in the deterministic analysis results in a conservative estimate of the upper-bound internal dose for this set of specific exposures.

Table 29. Summary of Internal Dose for the Crew of USS BOXER during Operation HARDTACK I

Organ	Mean Dose (rem)		Upper Bound Dose (rem)		
	Probabilistic[a]	Deterministic (NTPR)	Probabilistic (95th Percentile)	Deterministic (NTPR Upper Bound)	Ratio (Deterministic/ Probabilistic)
Alpha Dose					
Thyroid	0.000019 (7.9)	0.00026	0.00061	0.0026	4.2
Lung	0.00025 (8.0)	0.0035	0.0081	0.035	4.2
LLI wall	0.000020 (7.6)	0.00026	0.00063	0.0026	4.0
Beta plus Gamma Dose					
Thyroid	0.32 (4.5)	0.76	3.8	7.6	2.0
Lung	0.032 (5.9)	0.38	0.60	3.8	6.2
LLI wall	0.21 (4.5)	0.49	2.5	4.9	2.0

[a] Geometric means (and geometric standard deviations) from the probabilistic analysis are shown

5.6 Case Study #6: Operation CASTLE (1954), Army Personnel, Enewetak Island

5.6.1 Case Description and Cohort Participation Scenario

This case study applies to Army personnel stationed at Enewetak Island during Operation CASTLE for the period March 1 to May 31, 1954. More than 1,500 Army personnel were at Operation CASTLE during the testing period. Most Army personnel in Joint Task Force (JTF) 7, the civilian-military organization formed to conduct the operation, were assigned to TG 7.2. Most of these were assigned to the 7126th Army Unit that provided ground security, transportation and logistics support. These personnel were primarily stationed at Enewetak Island (Martin and Rowland, 1982). By the nature of their duties and residence, it is likely that most of the personnel remained on the island continuously, or nearly so, throughout the operation and therefore had continuous exposure to deposited fallout.

Because calculated film badge external gamma doses were reported for the operational period of March 1 to May 31, 1954 (Thomas et al., 1984), a comparison is made between these doses and reconstructed external gamma doses calculated using methodologies and uncertainty distributions, described in Sections 3 and 4, over the same time period for the four fallout episodes that occurred at Enewetak Island during Operation CASTLE. In addition to external gamma doses, similar techniques, discussed in Section 3, were used to generate internal dose

distributions for the lung, lower large intestine, and thyroid. Appendix F contains the details of this analysis.

5.6.2 Available Dosimetry

Film badge dosimetry during Operation CASTLE included mission badges issued to individuals when they were expected to enter areas of radioactive contamination other than those encountered during routine activities, and cohort badges that were issued to one individual in a group of individuals who performed similar duties in similar locations (Servis, 1981). However, sufficient dosimetry data are not available for land-based personnel to allow meaningful comparisons between actual film badge data and reconstructed external gamma doses (Thomas et al., 1984). Therefore, reconstructed doses due to fallout exposure during Operation CASTLE cannot be compared to concurrent film badge data.

5.6.3 External Dose

External gamma dose reconstruction for personnel stationed on Enewetak Island during Operation CASTLE was accomplished by incorporating uncertainty distributions for various parameters into the model discussed in Section 3. This model incorporates the fallout-induced radiation environments discussed in detail in Appendix F, and the fallout intensity decay model and effects of shielding as discussed in Section 3.

5.6.3.1 Exposure Pathways

The only sources of potential external radiation exposure for personnel stationed at Enewetak Atoll during Operation CASTLE were residual gamma radiation from fallout due to Shots BRAVO, ROMEO, and NECTAR (Thomas et al., 1984).

5.6.3.2 Assumptions and Parameter Uncertainty

The following specific uncertainty distributions, discussed in Section 4, were used in the uncertainty analysis for external gamma dose calculations:

- Amount of time spent outdoors each day.
- Fraction of time spent indoors that was spent in a tent-type structure or in a building.
- Protection factors for tents and buildings.
- Distributions of fallout intensity at locations on the island where a veteran most likely spent time, i.e., during time spent outdoors, location of the tent for the time spent indoors in a tent, and location of a building for the time spent indoors in a building.
- Error associated with intensity measurements on the island.
- Uncertainty in shot-specific radiological decay functions.

The types of distributions, means, and confidence intervals for each of these distributions are shown in Table F-2 of Appendix F. The values used in the deterministic analysis that generated

the deterministic doses reported for the operational period of March 1 to May 31, 1954, (Thomas et al., 1984) are also summarized in Table F-2 of Appendix F.

5.6.3.3 Results and Discussion

The results of the external gamma dose deterministic analysis and the probabilistic analysis are shown in Table 30. These results indicate that the mean dose of the probabilistic analysis is approximately equal to the deterministic dose. It is also concluded that the probabilistic 95th percentile dose is lower than the upper-bound deterministic external gamma dose, indicating that the upper bound factor of 3 used in the deterministic analysis results in a conservative estimate of the upper bound external gamma dose.

Table 30. Summary of External Dose for Personnel Stationed at Enewetak Island during Operation CASTLE

Mean Dose (rem)		Upper Bound Dose (rem)		
Probabilistic*	**Deterministic (NTPR)**	**Probabilistic (95th Percentile)**	**Deterministic (NTPR)**	**Ratio (Deterministic/ Probabilistic)**
1.3 (0.54)	1.2	2.3	3.5	1.5

* The arithmetic mean (and standard deviation) is shown. The geometric mean external dose is 1.2 rem.

5.6.4 Internal Dose

Internal dose reconstruction for personnel stationed on Enewetak Island during Operation CASTLE was accomplished by incorporating uncertainty distributions for various parameters into the models discussed in Section 3 and 4. These models incorporate the fallout-induced radiation environments discussed in detail in Appendix F, and the fallout intensity decay model and various other parameters discussed in Sections 3 and 4.

5.6.4.1 Exposure Pathways

Internal dose pathways included in the uncertainty analysis are inhalation of descending fallout, inhalation of resuspended fallout, and incidental ingestion of soil and dust based on the models discussed in Section 3 and Section 4.

5.6.4.2 Assumptions and Parameter Uncertainty

The following specific uncertainty distributions, discussed in Section 4, were used in the uncertainty analysis for internal dose calculations:

- Amount of time spent outdoors each day.
- Time-dependent resuspension factor $K(t)$.

- Breathing rate distribution correlated with activity levels.
- Time-dependent shot-specific dose conversion factors (*DCF*s).
- Bias factors for inhalation *DCF*s.
- Deposition fractions for particle size classes deposited in respiratory tract.
- Deposition fractions for particle size classes deposited in ET_2 and cleared to digestive tract.
- Activity fractions for inhalation of descending fallout for three particle size classes; activity fractions vary for Shots BRAVO, ROMEO, and NECTAR.
- Ingestion rate and soil bulk density for incidental ingestion of soil and dust.

The types of distributions, means, and confidence intervals for each of these distributions are shown in Table F-4 of Appendix F. The values used in the deterministic analysis that generated the deterministic doses for the operational period of March 1 to May 31, 1954, are also summarized in Table F-4 of Appendix F.

5.6.4.3 Results and Discussion

Distributions of fifty-year committed equivalent doses (CED) to three organs, thyroid, lung, and lower large intestine (LLI) wall, were derived using the refined uncertainty model for a sample size of 10,000 (i.e., 10,000 Monte Carlo histories). Examples of these results are shown in Appendix F, where the relative frequency distribution and the probability plot of estimated doses to the LLI wall from alpha radiation are shown in Figure F-3 and Figure F-4, respectively, and from beta plus gamma radiation in Figure E-5 and Figure F-6, respectively. The CED distributions are lognormally-distributed, as indicated by their Gaussian (bell) shapes of their histograms when plotted on a logarithmic axis.

The results of the internal dose deterministic analysis and the probabilistic analysis are shown in Table 31. These results indicate that the probabilistic analysis yields lower central doses than the doses calculated using deterministic models based on methodologies discussed in Section 3 with nominal or mean values of various parameters as shown in Table F-4 of Appendix F. This result is primarily due to the partitioning of the descending inhalation dose based on estimates of the fraction deposited in the respiratory tract and inhaled versus the fraction deposited in the ET tract and ingested. These results also indicate that the probabilistic 95^{th} percentile doses are lower than the upper-bound deterministic internal doses, implying that the upper bound factor of 10 used in the deterministic analysis results in a conservative estimate of the upper-bound internal dose for this set of specific exposures.

Table 31. Summary of Internal Dose for Personnel Stationed at Enewetak Island during Operation CASTLE

Organ	Mean Dose (rem)		Upper Bound Dose (rem)		
	Probabilistic[a]	Deterministic (NTPR)	Probabilistic (95th Percentile)	Deterministic (NTPR)	Ratio (Deterministic/ Probabilistic)
Alpha Dose					
Thyroid	0.000039 (8.5)	0.00036	0.0014	0.0036	2.6
Lung	0.00048 (8.6)	0.0044	0.017	0.044	2.6
LLI wall	0.000041 (8.3)	0.00036	0.0014	0.0036	2.5
Beta plus Gamma Dose					
Thyroid	0.20 (4.7)	0.59	2.5	5.7	2.2
Lung	0.066 (6.2)	0.80	1.4	8.0	5.6
LLI wall	0.18 (4.6)	0.54	2.3	5.3	2.2

[a] Geometric means (and geometric standard deviations) from the probabilistic analysis are shown

5.7 Summary of Results and Comparison of Upper Bound Doses

Application of the mathematical models implemented with Mathcad calculation tools to case studies of five military units assigned to nuclear test operations in the PPG and one unit assigned to nuclear test operations at the NTS illustrate the feasibility of performing probabilistic uncertainty analyses for those six cases. A comparison of the upper bound doses determined using Monte Carlo analyses with the upper bound doses estimated using current NTPR deterministic techniques provides a basis for assessing whether the deterministic upper bounds are reasonable.

The ratios of deterministic (NTPR) upper bound doses to the 95th percentile probabilistic doses for the six case studies investigated in this report—called upper bound dose ratios— are compiled in Table 32. The upper bound dose ratios for external doses exceed 1.0 in all cases considered, indicating that the upper bounds of the deterministic external doses are greater than the 95th percentiles of the corresponding probabilistically-calculated doses. The upper bound dose ratios for internal doses equal or exceed 1.0 for case studies involving exposures in the PPG, whereas Case Study #3 of a unit exposed at NTS produced upper bound dose ratios that are consistently less than 1.0.

Table 32. Ratios of Deterministic Upper Bounds to 95th Percentile Probabilistic Doses

Case Study	Study Group	Upper Bound Dose Ratio External	Upper Bound Dose Ratio Internal α	Upper Bound Dose Ratio Internal β+γ		
			All Organs	Thyroid	Lung	LLI wall
1	RW/Enewetak	1.6	1.4	1.5	3.7	1.3
2	HTI/Enewetak	1.5–1.6	2.5–2.6	1.8	4.6	1.8
3	PB	1.7	0.58–0.68	0.43	0.87	0.42
4	RW/USS ESTES	1.1	1.5	1.1	3.2	1.0
5	HTI/USS BOXER	1.3	4.0–4.2	2.0	6.2	2.0
6	CASTLE/Enewetak	1.5	2.5–2.6	2.2	5.6	2.2

Consider trends in upper bound ratios of external doses. The consistency of the ratios for the four land-based cases stands out: all have values of 1.5–1.7. The reason for this consistency is that the models used in these assessments are quite similar. The two ship-based cases have somewhat smaller ratios: 1.1 and 1.3. The difference between these two values can be attributed to the fact that the vessels had different configurations. The USS ESTES was an amphibious force flagship approximately elliptical in topside shape, complex and extensive superstructure, and three habitable decks below topside. The USS BOXER was an aircraft/helicopter carrier with a much larger, approximately rectangular weather deck, relatively little superstructure, and four habitable decks below topside. The ratios for the ship-based cases are smaller than those for land-based primarily because of the manner in which the variation in fallout intensity was modeled. For land-based, this variation is assigned a lognormal distribution with a geometric standard deviation of 1.5. For the ship-based cases, the variability in fallout intensity was modeled as described in Section 4.2.1. The latter distributions are broader, having geometric standard deviations of approximately 2. These broader distributions push the 95th percentiles to larger values and, consequently, suppress the ratios.

Understanding the variations observed in the upper bound internal dose ratios is more challenging. The PPG cases are addressed first, then the NTS case.

The implementation of a probabilistic formulation of internal dose reconstruction involved the integration of new algorithms into a deterministic framework that had been used in past NTPR assessments. The new algorithms, discussed in Section 4, resulted from more thorough modeling of the physics and biokinetics relevant to the various internal dose pathways, and thus represent improvements in the dose reconstruction methodology available to the NTPR Program. The upper bound internal dose ratios derived with this more complex model are dependent on a variety of input parameters, sometimes in relatively subtle ways. These dependencies can be illustrated by varying one input parameter at a time and observing the resulting variations in the upper bound ratios.

Consider, for example, the upper bound ratios for exposures that occurred aboard USS BOXER during HARDTACK I. It is seen in Table 32 that the ratios for alpha radiation are approximately 4, and those for beta-gamma radiation are 2.0 for thyroid and LLI wall and 6.2 for

lung. Internal doses aboard BOXER were accrued primarily from exposures to intermingled fallout from Shots FIR and KOA. It was assumed in deriving the cited values that all fallout came from FIR, so that the time from detonation to peak intensity was about 58 hours. If one assumes that the fallout actually came from KOA, which was detonated about one day after FIR, the ratios for alpha radiation drop to about 3 and those for thyroid, lung, and LLI wall from beta and gamma radiation become 1.2, 5.9, and 1.1, respectively. If, on the other hand, the time of peak deposition had occurred 1 day later (i.e., around 82 hours after the detonation), the upper bound ratios increase to 4.5 for alpha, and to 2.3 (thyroid and LLI wall) and 10 (lung) for beta-gamma radiation. This demonstrates that the timing of the deposition has a significant effect on the upper bound ratios.

Another trend evident in this example and seen more generally in Table 32 is that the upper bound beta-gamma dose ratios for the lung are substantially larger than those for the thyroid and LLI wall. This can be explained as follows. Dose to the lung depends critically on the respirability of the descending fallout particles—unlike the thyroid and LLI wall, the lung receives little dose from the non-respirable fraction that is inhaled and subsequently ingested (see Table 18 in Section 4). Loss of this potential dose component reduces the lung dose from the inhalation of descending fallout and, consequently, its 95th percentile upper bound. The deterministic dose is not affected by this feature because the fallout particles are assumed to have been totally respirable in that formulation. This causes the ratio of deterministic to probabilistic upper bounds to increase with respect to those of the thyroid and LLI wall, as observed.

In contrast to the PPG results, the upper bound internal dose ratios evaluated for the NTS in Case Study #3 are all less than 1.0, indicating that the probabilistic 95th percentile dose is larger than the deterministic upper bound dose. A possible explanation for this disparity between PPG and NTS cases is that that both PPG and NTS case studies include internal dose contributions from inhalation of resuspended fallout, while only the PPG cases include contributions from the inhalation of descending fallout. The components of dose related to the inhalation of resuspended fallout have two large contributors to uncertainty: the DCFs and the resuspension factors. Both of these parameters are modeled as lognormal distributions with large GSDs, so they significantly drive up the probabilistic upper bound doses. As a result, the 95th percentile-to-geometric mean dose ratio for intake of resuspended fallout typically is in the range of 40–50. For the inhalation of descending fallout, *DCF*s are major contributors to uncertainty, with lesser contributions from the collective uncertainties in the activity fractions, deposition fractions, and settling velocities. The 95th percentile-to-geometric mean dose ratios for these components are 10 and typically 2 for beta-gamma dose to the thyroid and LLI wall, which combine logarithmically in quadrature to give a combined ratio of about 12; the combined ratio for lung is about 22. Thus, the resuspension/inhalation internal dose pathway involves a significantly larger uncertainty than does the descending/inhalation pathway. This larger uncertainty tends to increase the 95th percentile dose and decrease the upper bound dose ratios. This results in upper bound internal organ dose ratios of less than 1.0 for Case Study #3, for which inhalation of resuspended fallout dominates the internal doses. For the PPG case studies, the presence of a sizeable dose component from inhalation of descending fallout with its smaller uncertainty moderates the extent of the 95th percentile doses, thereby resulting in upper bound dose ratios that are equal to or greater than 1.0.

6 SENSITIVITY ANALYSIS FOR THE DOSE MODELS OF CASTLE ENEWETAK CASE STUDY

Sensitivity analyses were performed for the external and internal dose models applied to the Army personnel at Enewetak Atoll at Operation CASTLE (1954). These analyses were carried out to confirm prior inference as to the input parameters to which the models are most sensitive, and to develop an approach on how to implement and use sensitivity analyses in NTPR dose reconstructions. In this section, the approach and the results are presented and discussed for both the external and internal dose models. It is not the intent of this analysis to develop generalized conclusions to be applied across many units with a broad range of exposure scenarios.

6.1 Technical Approach

Sensitivity analyses are performed to study how the output of a model is affected by variations or uncertainties in input parameters, both qualitatively or quantitatively (Saltelli et al., 2008). Case study doses were calculated using the Monte Carlo simulation model developed for the Army personnel unit that was stationed at Enewetak Atoll at Operation CASTLE and described in detail in Appendix F.

In the sensitivity analyses conducted in this study, input parameters were varied one at a time keeping all other parameters at their respective nominal value in separate runs of the Monte Carlo simulation. An additional run was performed where all the input parameters were allowed to vary to obtain the distribution of the full probabilistic model. For each parameter varied, the output dose distribution was compared to the distribution that resulted from varying all the parameters at once. One thousand Monte Carlo simulations were performed to generate each distribution. A smaller number of simulations (100 trials) was also tried and results were similar to those presented here as far as the relative sensitivities are concerned. Generally, a smaller number of simulations produces a slightly narrower range in the output distribution. This is acceptable for this type of analysis.

Measures of the sensitivity of the model to its input parameters and how they are evaluated can be defined in many ways (Hoffman and Gardner, 1983; Kirchner, 2008; Saltelli et al., 2008). For this study, a sensitivity score (*SS*) that compares ranges of variations in output dose distributions can be determined as follows:

$$SS_i = \frac{(95_i{}^{th} - 5_i{}^{th})}{(95_{all}{}^{th} - 5_{all}{}^{th})} \tag{6-1}$$

where the 5th and 95th represent the 5th and 95th percentiles of the output dose distribution. The subscript "*i*" indicates that only the i^{th} parameter is randomly varied and the subscript "all" indicates that all the parameters are varied simultaneously as in a full Monte Carlo model simulation. Use of the 5th and 95th percentiles cuts off values in the tails of model output distributions that potentially could incorrectly influence the estimated score. As defined above, *SS* varies theoretically on a scale of 0 to 1. A score close to 0 indicates a low sensitivity of the model to the corresponding parameter. The closer SS_i approaches 1, the more sensitive the dose model is to the i^{th} parameter.

For lognormally distributed variables, such as internal doses, a sensitivity score equivalent to that in Equation 6-1 can be defined by:

$$SS_i = \frac{95_i^{th} / 5_i^{th}}{95_{all}^{th} / 5_{all}^{th}} \tag{6-2}$$

or in log scale, an equivalent expression is given by SS_{log}, such as:

$$SS_{log_i} = \frac{\log(95_i^{th}) - \log(5_i^{th})}{\log(95_{all}^{th}) - \log(5_{all}^{th})} \tag{6-3}$$

Other types of sensitivity scores and measures can be devised. A few examples are as follows:

$$S_i = 1 - 5_i^{th} / 95_i^{th} \tag{6-4}$$

$$S_i = 95_i^{th} / 5_i^{th} \tag{6-5}$$

$$S_i = 95_i^{th} / (central\ estimate)_i \tag{6-6}$$

$$S_i = 95_i^{th} - 5_i^{th} \tag{6-7}$$

It is important that the analyst have a good understanding of the characteristics of the output and the underlying distributions and true range of variations of each input parameter so as to apply an appropriate sensitivity score. It is therefore essential to decide *a priori* over which range and scale input parameters are varied. Further discussions on sensitivity analyses and screening procedures can be found in Hoffman and Gardner (1983) and Kirchner (2008).

6.2 External Dose Model Sensitivity Analysis

The nine input parameters to the external dose model in the CASTLE Enewetak case study were varied one at a time. All were assumed independent of each other because they present at most a weak correlation. The three normalized intensity variables I_1, I_2, and I_3 reflect the non-uniform distribution of fallout. They were sampled simultaneously from the same distribution and a combined sensitivity score for a "lumped" sensitivity parameter labeled "fallout distribution" was determined. This resulted in calculating a total of seven sensitivity scores. Input parameters with weak correlation from shot-to-shot were selected independently for each fallout event (see Section 4.3).

The results of the external dose sensitivity analysis are listed in Table 33. In addition to *SS*, calculated using Equation 6-1, other sensitivity measures, shown in Equations 6-5 and 6-6, are included for comparison purposes. Figure 39 shows a comparison of the *SS* for each input parameter. These results show that the external dose model is most significantly sensitive to the variability and uncertainty in, by decreasing order of importance, intensity measurement and data errors, fallout distribution and decay constants. Each of these three parameters is a direct

Table 33. Sensitivity Scores for Input Parameters to the External Dose Model

	Input Parameter Varied							
	All	F_{os}	F_t	PF_t	PF_b	**Fallout (FO) Distribution**	**Intensity Measurement**	**Decay**
5th Percentile	0.58	0.98	1.0	1	0.97	0.87	0.59	0.95
Geometric Mean (GM)	1.2	1.1	1.1	1.1	1.1	1.1	1.1	1.2
95th Percentile	2.3	1.2	1.1	1.2	1.2	1.5	1.7	1.5
Ratio 95th/5th	4.0	1.2	1.2	1.2	1.2	1.7	2.9	1.6
Ratio 95th/GM	2.0	1.1	1.1	1.1	1.1	1.3	1.6	1.3
SS(*)	**1.0**	**0.13**	**0.089**	**0.093**	**0.13**	**0.36**	**0.64**	**0.31**

(*) Sensitivity Scores may differ from the exact results of their calculation due to rounding.
F_{os} is fraction of time outside; F_t is time in a tent; PF_t is tent protection factor; PF_b is building protection factor

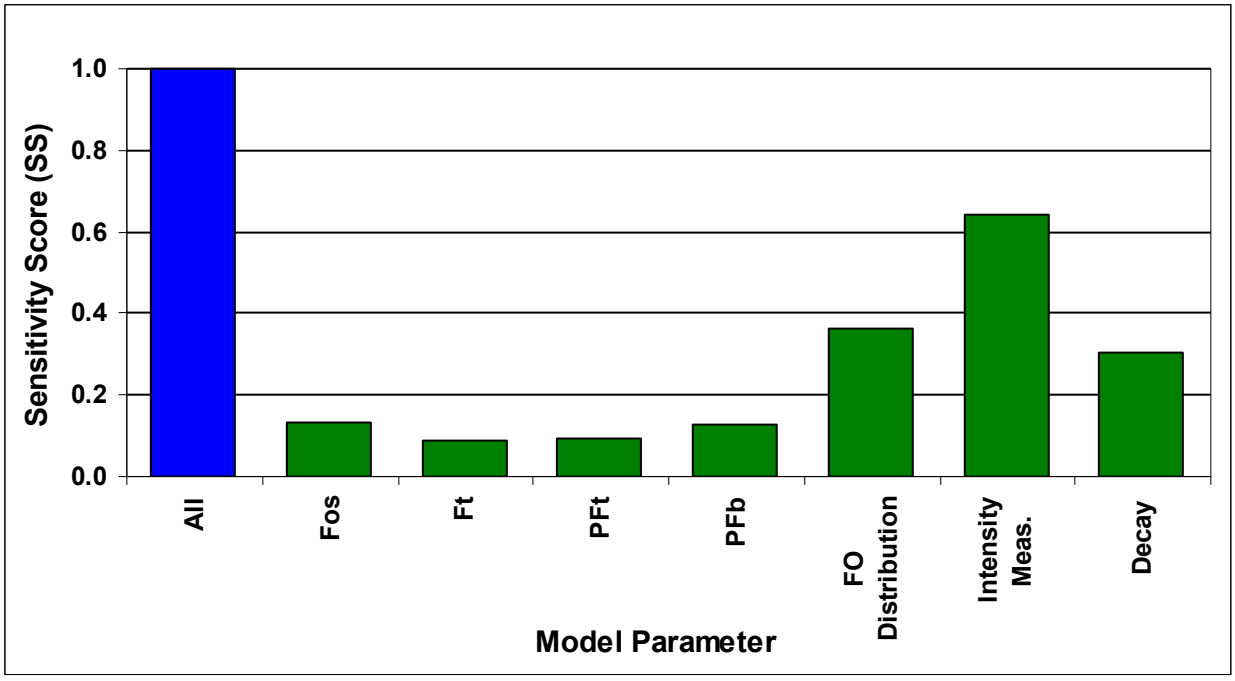

Figure 39. Sensitivity Scores for Input Parameters to Total External Dose Model for the CASTLE Enewetak Case Study

multiplier in the dose model. While the fallout distribution, which reflects the spatial variability of deposited radioactive materials, and decay may have broader intrinsic distributions, the intensity measurement and data uncertainty, which combines intensity measurement and data processing errors, is the only one fully correlated from shot-to-shot. Hence, deviations are larger

as values corresponding to each shot are added, and this source of uncertainty propagates more influence on the resultant dose distribution. The other model input parameters contribute much less to the overall variability of the total external dose. Ranked in decreasing sensitivity score, these are F_{os}, PF_b, PF_t and F_t.

The sensitivity analysis of the external dose model for the CASTLE Enewetak cohort shows that uncertainties of two parameters, F_t and PF_t, each contribute less than 10 percent to the overall variability of the external dose based on the 5^{th} to 95^{th} percentile ranges. It also indicates that the uncertainty attributed to intensity measurement, arising collectively from instrument precision, operator error and data recording and manipulation, constitutes the single largest contributor to the overall distribution of the external dose model. This was due to both the distribution assigned to this source of uncertainty but also to the assumption that this uncertainty was fully correlated from shot-to-shot. It is therefore necessary to perform a more thorough assessment of the values and uncertainty related to intensity data, when such a model is used for dose reconstruction.

6.3 Internal Dose Model Sensitivity Analysis

Model input parameters to the internal dose model in the CASTLE Enewetak case study were each varied one at a time. Each input parameter was randomly sampled from its distribution and was considered independent from the other parameters. However, several input parameters were treated as a group and varied simultaneously while the other parameters and parameter groups were fixed. For groups of parameters that were varied together, one sensitivity score was determined for the group. The groups of input parameters as well as those parameters that were kept single are as follows:

- Intensity measurement data and decay factors (designated INT).
- Inhalation dose conversion factors (DCF Inh).
- Ingestion dose conversion factors (DCF Ing).
- Settling Velocity (V).
- All deposition fractions for respirable and non-respirable fallout particle sizes (RND).
- Activity fraction parameters AF_{100}, $frac_1$, and $frac_2$ (RNA).
- Breathing rate (BR).
- Intensity distribution of fallout near outdoor location normalized to the intensity averaged over the whole island, I_{os}, and then multiplied by F_{os} (OD).
- Resuspension factor (K).
- Incidental ingestion of soil and dust parameters: ingestion rate and soil density ("q and ρ").

The results of the sensitivity analysis of the internal dose to the lung for the CASTLE at Enewetak case study are shown in Table 34 and Table 35. In addition to SS_{log}, calculated using Equation 6-3, other sensitivity measures (depicted by Equations 6-5 and 6-6) are included for comparison purposes. Equation 6-3 was used because internal dose distributions tend to exert highly skewed lognormal behavior, so sensitivity scores were determined for the logarithm of the

Table 34. Sensitivity Scores for Input Parameters to the Internal (α) Dose Model (Lung)

	Model Input Parameter Varied (*)										
	All	**INT**	**DCF Inh**	**DCF Ing**	**V**	**RND**	**RNA**	**BR**	**OD**	**K**	**q and ρ**
5th Percentile	1.7E-05	2.0E-04	3.5E-05	5.4E-04	5.0E-04	5.4E-04	5.3E-04	1.7E-04	2.0E-04	8.0E-05	5.3E-04
Geometric Mean (GM)	4.7E-04	3.9E-04	3.4E-04	5.4E-04	5.1E-04	5.4E-04	6.2E-04	3.7E-04	3.9E-04	4.3E-04	5.3E-04
95th Percentile	1.7E-02	7.2E-04	4.4E-03	5.4E-04	5.5E-04	5.4E-04	7.6E-04	6.2E-04	8.1E-04	3.6E-03	5.3E-04
Ratio 95th/GM	37	1.8	13	1.0	1.1	1.0	1.2	1.7	2.0	8.3	1.0
Ratio 95th/5th	991	3.6	128	1.0	1.1	1.0	1.4	3.6	4.1	45	1.0
SS_{log} (**)	**1.0**	**0.19**	**0.70**	**0.001**	**0.015**	**0.001**	**0.052**	**0.18**	**0.20**	**0.55**	**0.0001**

(*) Input parameters as defined in the bulleted list above.

(**) Sensitivity Scores may differ from the exact results of their calculation due to rounding.

dose distributions. Figure 40 and Figure 41 show a comparison of SS_{log}, which correspond to each input parameter or lumped group of parameter for alpha and for beta-plus-gamma doses, respectively. These results show that, for this exposure scenario and organ, the internal alpha and beta-plus-gamma dose models are most significantly sensitive to the uncertainty in DCF for inhalation and resuspension factor. The models are moderately sensitive to the errors in intensity and decay factors, fallout distribution and breathing rate. Finally, the models for this exposure

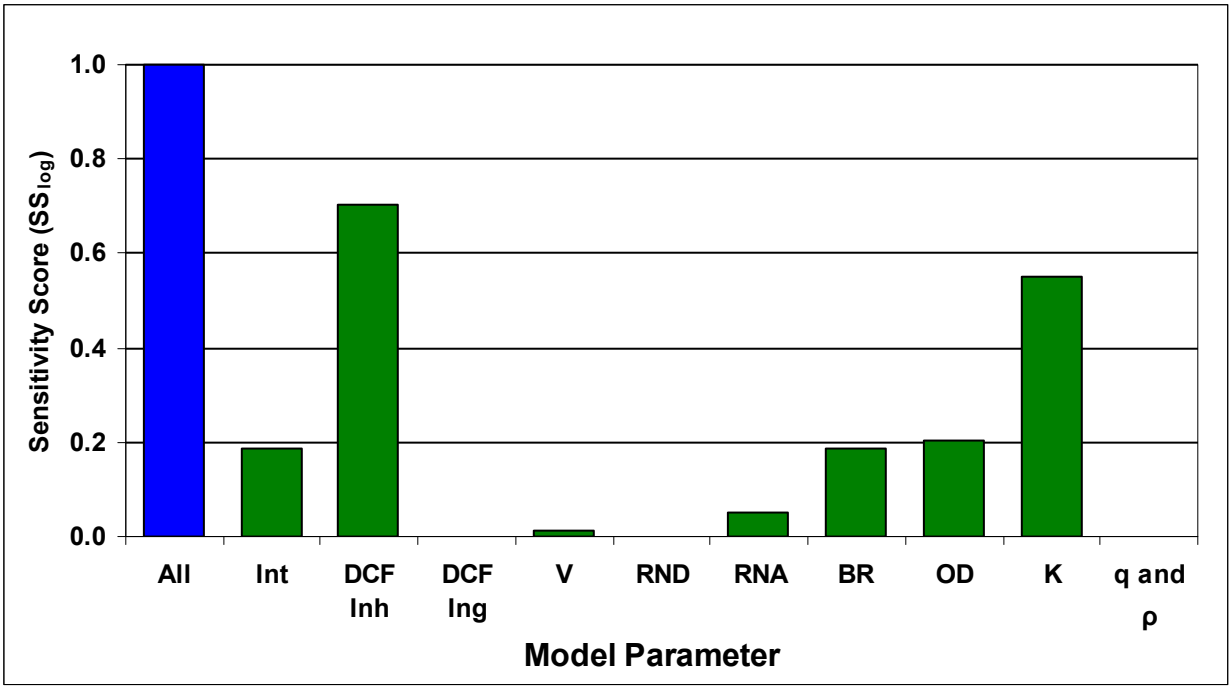

Figure 40. Sensitivity Scores for Input Parameters to Total Internal (α) Dose Model (Lung) for the CASTLE Enewetak Case Study

scenario and organ show no or very little sensitivity to the remaining parameters or groups thereof, i.e., RND, RNA, DCF for ingestion and "q and ρ".

Table 35. Sensitivity Scores for Input Parameters to the Internal (β+γ) Dose Model (Lung)

	Input Parameter Varied (*)										
	All	**INT**	**DCF Inh**	**DCF Ing**	**Vs**	**RND**	**RNA**	**BR**	**OD**	**K**	**q and ρ**
5th Percentile	3.1E-03	2.6E-02	5.8E-03	6.7E-02	5.4E-02	6.7E-02	6.9E-02	2.5E-02	3.4E-02	2.0E-02	6.8E-02
Geometric Mean (GM)	7.1E-02	5.1E-02	4.6E-02	6.8E-02	6.0E-02	6.7E-02	9.5E-02	5.2E-02	5.6E-02	6.5E-02	6.8E-02
95th Percentile	1.4E+00	8.5E-02	3.5E-01	7.1E-02	7.1E-02	6.7E-02	1.4E-01	8.7E-02	9.8E-02	4.1E-01	6.8E-02
Ratio 95th/GM	19	1.7	7.6	1.0	1.2	1.0	1.4	1.7	1.7	6.3	1.0
Ratio 95th/5th	444	3.3	60	1.1	1.3	1.0	2.0	3.5	2.9	20	1.0
SS_{log} (**)	**1.0**	**0.20**	**0.67**	**0.0084**	**0.045**	**0.0017**	**0.11**	**0.21**	**0.17**	**0.49**	**0.0002**

(*) Input parameters as defined in the bulleted list above.
(*) Sensitivity Scores may differ from the exact results of their calculation due to rounding.

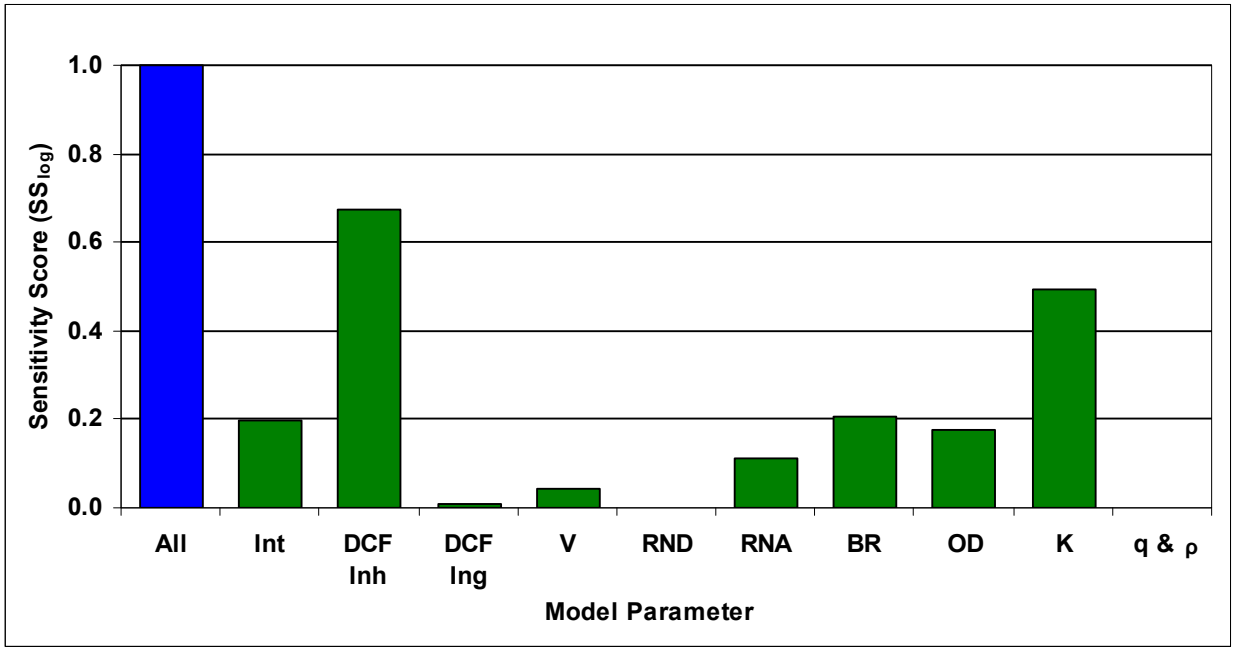

Figure 41. Sensitivity Scores for Input Parameters to Total Internal (β + γ) Dose Model (Lung) for the CASTLE Enewetak Case Study

The sensitivity analysis of the internal alpha and beta-plus-gamma lung dose models for the CASTLE Enewetak cohort shows that the uncertainty and variability RND, DCF Ing and "q and ρ", contribute less than 1 percent each to the overall variability of internal doses based on the 5^{th} to 95^{th} percentile range of logarithmic dose. The uncertainty in the internal alpha and beta-plus-gamma dose models is each dominated by the dose conversion factors for inhalation (DCF Inh) and the resuspension factor. In the intermediate to low range and in descending order, the breathing rate, intensity distribution variability and fraction of time spent outdoors, uncertainty due to intensity measurement and processing, the activity fraction adjustment factors, and settling velocity have a lesser but sizeable influence on internal doses. It is emphasized that these observations relate only to lung dose to participants at Enewetak during Operation CASTLE. The results of sensitivity studies for other organs and other exposure scenarios may vary significantly.

When models such as these are implemented for dose reconstruction, a thorough assessment of the values and uncertainties related to parameters to which the model is most sensitive should be conducted. Conversely, less attention should be paid to the parameters for which the models exhibit little or no sensitivity.

7 CONCLUSIONS AND RECOMMENDATIONS

The main goal of this study was to investigate and demonstrate a methodology and the enabling computational tools to perform probabilistic radiation dose assessments for NTPR atomic veterans. This goal was achieved through the use of Monte Carlo simulation techniques and available data and information. Probabilistic models for both external and internal dose calculations that account for uncertainty and variability of input parameters were developed, tested, and applied in six case studies. Physics-based models, analysis of available operational and test data, and the keen judgment of analysts experienced in NTPR dose reconstruction, health physics, and related specialties were employed to develop realistic central values and distributions of model input parameters. Experience in coding the various dose components' formulations and reconstruction techniques using Mathcad was essential.

The six case studies applied probabilistic dose assessment models to five PPG cohorts and one NTS unit. Conventional NTPR deterministic doses were also estimated and the upper bounds were compared with the probabilistic 95th percentile doses. The PPG case studies comprised three scenarios for land-based personnel that were stationed at Enewetak Island during Operations CASTLE, REDWING, and HARDTACK I. The two other scenarios were for ship-based units, one that participated at Operation REDWING aboard the amphibious force flagship USS ESTES and the second at Operation HARDTACK I aboard the aircraft carrier USS BOXER. The NTS unit participated in a rehearsal and a maneuver at Shot HOOD during Operation PLUMBBOB.

A pilot study developed the initial scope of the effort and quantified the uncertainty of most dose model parameters. Additional consultations with experts and a more refined assessment of available studies and literature provided further insight in parameters with more complex uncertainties and biases in existing models. This included improved estimates of the central values and uncertainties for dose conversion factors, time-dependent resuspension factors, resuspension factors in regions of high resuspension near detonation sites, and gamma source modification factors accounting for shielding afforded by ship superstructure, to name a few.

Extensive research of the relationship of fallout deposition times to particle size distributions constituted one of the most difficult aspects of exposure characterization due to the limited availability of applicable data. Fallout deposition models to address fallout activity distributions based on particle settling velocities and activity fractions were developed and benchmarked with the limited available data to provide reasonable estimates of the activity fractions in respirable and non-respirable classes. Although it is believed that the methodology developed is acceptable for the purpose of this study, additional investigations are warranted to further elucidate other important factors that affect airborne concentrations of radioactivity, such as fractionation.

A comparison between reconstructed model doses and film badge readings was carried out for units where reliable dosimetry data were available. These units are the Army personnel at Enewetak during REDWING and HARDTACK I, the crew of the USS BOXER during HARDTACK I, and the Marine unit at NTS during PLUMBBOB. For these four groups, reconstructed probabilistic external doses matched well with the film badge doses. The 95th percentile of the probabilistic dose distribution exceeded the 95th percentile of the film badge dose distribution.

Results show that in all cases, deterministic (NTPR) upper bound external gamma doses were higher than the corresponding probabilistic 95th percentile doses. Deterministic upper bounds were 50 to 60 percent higher than the probabilistic 95th percentile doses for the land-based PPG and NTS cases. For ship-based groups, the deterministic upper bound external doses were 10 and 30 percent higher. The case studies are consistent with each other in that upper bound external doses calculated using the NTPR deterministic "high-sided" approach and an upper bound factor of 3 are higher that the 95th percentile confidence limit determined by a comprehensive probabilistic analysis using Monte Carlo simulations. The consistency of these results shall be verified in other scenarios of participation for application in future NTPR dose assessments.

For internally-deposited radioactive materials, the NTPR deterministic method resulted in internal upper bound doses, determined by multiplying the doses by a factor of 10, higher than the probabilistic 95th percentile doses, except in the case of the Marine unit at PLUMBBOB discussed below. For all the PPG cases, the deterministic upper bound doses from alpha radiation to three sample organs (thyroid, lung, and lower large intestine wall) were 1.4 to 4.2 times higher than the probabilistic 95th percentile doses. The highest ratios of 4 to 4.2 were those for the crew of the USS BOXER at HARDTACK I. For beta-plus-gamma radiation, the deterministic upper bound doses ranged from about 1 to 6 times the probabilistic 95th percentile doses, with the ratio of 1.0 observed for the dose to the LLI wall of personnel aboard the USS ESTES during Operation REDWING. Although it is clear that for all the PPG case studies, the deterministic model has captured at least the 95th percentile confidence limit, a broad conclusion cannot be made for all types of scenarios. Having said that, the case studies included in this investigation varied in type (land and two very different types of ships), number and time of occurrence of fallout events, radiation intensities and fallout deposition, time veterans spent at the PPG, etc. Therefore, implementation of the probabilistic methodologies can proceed but with the expectation that further refinements should take place and any adjustments will require revision of the standard methods as applicable.

In the PLUMBBOB case study, the NTPR deterministic upper bound internal doses were lower than the 95th percentile doses calculated using the probabilistic model. The deterministic upper bound alpha doses to the three selected organs are about 60 to 70 percent of the corresponding 95th percentile doses estimated by the probabilistic analysis. For beta-plus-gamma radiation, the deterministic upper bound internal doses are 42 to 87 percent of the corresponding probabilistic 95th percentile doses. It is clear that in this case, either the deterministic model is not high-sided enough to capture at least the 95th percentile of the dose distribution, or the probabilistic model overestimates the uncertainty and variability of key influential input parameters. For the probabilistic model, the multiplicative effect of several input parameter distributions with 95th percentile factors of 10 or more produces, in the case studied, 95th percentile doses that are 15 to 30 times their corresponding geometric means. These parameters include dose conversion factors, resuspension factors and radiation intensities when extrapolated from iso-intensity maps. Although the geometric means are 2 to 11 times lower than the deterministic doses, the 95th percentiles are higher than the deterministic upper bounds by factors of 1.1 to 2.4.

It is evident that a broad-based conclusion about the comparison of deterministic and probabilistic upper bounds cannot be made based on the study of the PLUMBBOB Marine unit given the specific scenario of exposure and activities. Nevertheless, the probabilistic analysis methodology and capability for estimating uncertainty for NTS participation has been

demonstrated and can be applied to other units and individual cases. As for PPG cases, further refinements are recommended with emphasis on additional analysis of individual dose components that contribute to the total internal dose and their corresponding input parameters and distributions. In addition, investigation of the impacts of revised distributions of resuspension factors, uncertainty factors for dose coefficients for alpha particles, and estimated uncertainties for other internal dose parameters in the recently published update to Kocher et al. (2006)[7] may contribute to further understanding of these results. The results and findings summarized in the preceding paragraphs were based on the best available information on parameter distributions as of the time the models for the case studies were last ran.

A sensitivity analysis was performed to identify the possibility of screening out sources of uncertainty with small or limited impact on dose. A simple method that varied model parameters one-at-a-time was applied for both external and internal doses using the Army personnel at Enewetak during CASTLE as an example. Each parameter or group of parameters in the dose models was varied individually according to its probability distribution while all other parameters or groups of parameters were held fixed. In this way, the variation of that single parameter or group of parameters was studied for its individual influence on the model output.

The findings of the sensitivity analysis show that, in the case of external dose to participants who served at Enewetak during Operation CASTLE, the most significant source of uncertainty is that related to intensity measurements and intensity data recording and processing, with the variability resulting from the non-uniform distribution of fallout and uncertainty in fallout decay rates showing lower, but significant influence. The least influential parameters for this scenario are the tent and building protection factors and fraction of time a person spent outdoors or inside a tent versus a building. For internal lung dose, the dominant source of uncertainty is that associated with the inhalation dose conversion factors, followed closely by the uncertainty in resuspension factors. In the medium range of influence were the uncertainties related to the breathing rate and the radiation environment, which included intensity measurement and related data collection and processing, and the non-uniform distribution of fallout. The least influential parameters were the ingestion dose conversion factors, deposition fraction, and activity fraction. The uncertainty on parameters specific to the incidental ingestion of soil (rate of ingestion and soil density) had no effect on internal dose. It is useful to note, however, that these model sensitivities are specific to the sample organ and scenario used to illustrate how to use sensitivity analyses in dose reconstruction. Successful application of this methodology to a broader range of organs and exposure scenarios will provide a basis for future refinements of existing dose models.

Therefore, it is concluded from this study that methods for applying probabilistic uncertainty analyses in NTPR radiation dose reconstructions are feasible. In particular, these methods, to the level of modeling and parameterization described herein, have been shown to perform successfully when applied to the estimation of radiation doses received by participants in six cases of exposure during atmospheric nuclear testing. In addition, the results of the case studies support conclusions that the deterministic upper bound factors of "3" and "10" proscribed in DTRA policy provide reasonable upper bounds, except for the internal doses in the PLUMBBOB

[7] Kocher, D. C., Trabalka, J.R., and Apostoaei, A.J., 2009. Derivation of Effective Resuspension Factors in Scenarios for Inhalation Exposure Involving Resuspension of Previously Deposited Fallout by Nuclear Detonations at Nevada Test Site. DTRA-TR-09-15, *SENES, Oak Ridge, Inc.*, Oak Ridge, TN and Defense Threat Reduction Agency, Fort Belvior, VA.

scenario of exposure. For this and similar scenarios where the dose component from inhalation of resuspended materials dominates the overall internal dose, an uncertainty factor higher than "10" is possible, as for the PLUMBBOB case study. Such scenarios of exposure need to be assessed using a more detailed uncertainty analysis, such as the one described in this report.

The results discussed above and in Section 5 are valid for the six case studies only and cannot be generalized to all exposure scenarios. Only the methodologies developed and presented in this report can be applied and expanded to other scenarios of exposure. The analyses conducted in this study provide reasonable estimates of dose and associated uncertainties for the types of exposure scenarios investigated and support implementation of the probabilistic approach to radiation dose assessments in the NTPR Program. The following recommendations are offered to achieve implementation of the approach:

- Conduct testing of probabilistic methods applied to other exposure scenarios, test series, and participant units to develop experience with preparing reasonable distributions of parameters to support implementation of these methods.
- Incorporate probabilistic approaches developed in this report to NTPR RDA procedures and methodologies.
- Implement the probabilistic analyses described herein when performing future radiation dose reconstructions and adapt model parameter distributions when case-specific scenarios are well documented.

8 REFERENCES

Anspaugh, L.R., Simon, S.L., Gordeev, K.I., Likhtarev, I.A., Maxwell, R.M., and Shinkarev, S.M., 2002. Movement of Radionuclides in Terrestrial Ecosystems by Physical Processes. Health Physics 82:669–679 (2002).

Barrett, M., Goetz, J., Klemm, J., McRaney, W., and Phillips, J., 1986. Low Level Internal Dose Screen – CONUS Tests. DNA-TR-85-317 (Defense Nuclear Agency, Washington, D.C.).

Bolch, Wesley. E., Farfán, E.B., Huh, C., Huston, T.E., and Bolch, W. Emmett, 2001. Influence of Parameter Uncertainties within the ICRP 66 Respiratory Tract Model: Particle Deposition. Health Physics 81(4):378 –394 (2001).

Bruce-Henderson, S., Gladeck, F.R., Hallowell, J.H., Martin, E.J., McMullan, F.W., Miller, R.H., Rogers, W.E., Rowland, R.H., Shelton, C.F., Sturman, P., Berkhouse, L.H., Davis, S., DeSantis, H., Dean, P., Doyle, M.K., and Patterson, D.S. , 1982. Operation REDWING: 1956, United States Atmospheric Nuclear Weapons Tests, Nuclear Test Personnel Review. DNA 6037F (Defense Nuclear Agency, Washington, D.C.).

Bulmer, M.G., 1979. *Principles of Statistics*. Dover, New York.

Chehata, M., 2009. Guidelines for Estimating Uncertainty from Measured Intensity Data and Iso-Intensity Maps. NTPR-TM-09-13 (Science Applications International Corporation. McLean, VA.)

Chehata, M., Jasinski, D., Monteith, M.C., and Samuels, W.B., 2007. Mapping Three-Dimensional Water Quality Data in the Chesapeake Bay Using Geostatistics. Journal of the American Water Resources Association (JAWRA), Vol. 43, No. 3, pp. 813–828, June 2007.

Chehata, M., and Stiver, J., 2009. Evaluation of Internal Doses from the Incidental Ingestion of Contaminated Soil and Dust for NTPR Participants. NTPR-TM-09-03 (Science Applications International Corporation, McLean, VA).

Chilès, J.P., and Delfiner, P., 1999. Geostatistics, Modeling Spatial Uncertainty. Wiley Series in *Probability and Statistics*, John Wiley and Sons, New York.

Danon, Y., 2008. DIGITIZE-PRO, Version 4.1. http://www.rpi.edu/~danony/software.htm (Accessed February 23, 2010) or http://www.nuceng.com/Digitizepro.htm (Accessed February 23, 2010), Rensselaer Polytechnic Institute, Troy, NY.

Doane, D.P. and Seward, L.E., 2009. *Applied Statistics in Business and Economics*, 2nd edition. McGraw Hill Irwin, Burr Ridge, IL.

DoD/DVA (Department of Defense/Department of Veterans Affairs), 2004. Radiation Dose Reconstruction Program of the Department of Defense (DoD) Report to Congress. June 3, 2004.

DoD (Department of Defense), 2009. Guidance for the Determination and Reporting of Nuclear Radiation Dose for DoD Participants in the Atmospheric Nuclear Test Program (1945–1962). Title 32 Code of Federal Regulations Part 218, Government Printing Office. Current version is March 24, 2009.

Donley, H.E., 2009. The Drag Force on a Sphere, a module available at http://www.ma.iup.edu/projects/CalcDEMma/drag/drag.html (Accessed February 23, 2010). Mathematics Department, Indiana University of Pennsylvania, Indiana, PA.

DTRA (Defense Threat Reduction Agency), 2003. Letter from C. Benavides (Contracting Officer) to Mr. Steve Powell (Titan Corporation), re: DTRA01-01-C-0007, July 16, 2003.

DTRA (Defense Threat Reduction Agency), 2007a. Policy and Guidance Manual – Nuclear Test Personnel Review Program. Revision 7 (Defense Threat Reduction Agency, Fort Belvoir, VA), November 26, 2007.

DTRA (Defense Threat Reduction Agency), 2007b. Director's Letter to Chairman. VBDR, December 10, 2007.

DVA (U.S. Department of Veterans Affairs), 2002. Title 38, Code of Federal Regulations, Part 3, Section 309, Disease Subject to Presumptive Service Connection.

Eckerman, K.F., Leggett, R.W., Nelson, C.B., Puskin, J.S., and Richardson, A.C.B., 1999. Cancer Risk Coefficients for Environmental Exposure to Radionuclides. Federal Guidance Report No. 13, EPA 402-R-99-001, U.S. Environmental Protection Agency, Washington, DC.

Finn, S.P., Simmons, G.L., and Spencer, L.V., 1979. Calculation of Fission Product Gamma Ray and Beta Spectra at Selected Times after Fast Fission of U^{238} and U^{235} and Thermal Fission of U^{235}. SAI Report SAI-78-782-LJ/F, prepared by Science Applications, Inc., for National Bureau of Standards.

Frank, G., Goetz, J., Klemm, J., Thomas, C., Weitz, R., 1981. Analysis of Radiation Exposure, 4^{th} Marine Corps Provisional Atomic Exercise Brigade, Exercise Desert Rock VII, Operation PLUMBBOB. DNA 5774F (Defense Nuclear Agency, Washington, D.C.).

Gladeck, F.R., Gould, K.G., Hallowell, J.H., Martin, E.J., McMullan, F.W., Miller, R.A., Osborn, M.J., Shelton, C.F., Berkhouse, L., and Calhoun, F.S., 1982. Operation HARDTACK I (1958). DNA 6038F (Defense Nuclear Agency, Washington, D.C.).

Glasstone, S., and Dolan, P.J., 1977. *The Effects of Nuclear Weapons*, U.S. Department of Defense and U.S. Department of Energy (3rd Edition).

Goetz, J.L., Kaul, D., Klemm, J., and McGahan, J.T., 1979. Analysis of Radiation Exposure for Task Force Warrior – Shot SMOKY – Exercise Desert Rock VII–VIII Operation PLUMBBOB. DNA 4747F (Defense Nuclear Agency, Washington, D.C.).

Goetz, J., Kaul, D., Klemm, J., McGahan, J., and Weitz, R., 1980. Analysis of Radiation Exposure for Troop Observers, Exercise Desert Rock VI, Operation TEAPOT. DNA 5354F, July 15, 1980.

Goetz, J., Klemm, J., Phillips, J., and Thomas, C., 1987. Analysis of Radiation Exposure—Service Personnel on Rongerik Atoll, Operation CASTLE—Shot BRAVO. DNA-TR-86-120 (Defense Nuclear Agency, Washington, D.C.).

Hahn, G.J and Shapiro, S.S., 1967. *Statistical Models in Engineering*. John Wiley, New York.

Halbleib, J.A., Kensek, R.P., Mehlhorn, T.A., Valdez, G.D., Seltzer, S.M., and Berger, M.J., 1992. ITS Version 3.0: The Integrated TIGER Series of Coupled Electron/Photon Monte Carlo Transport Codes. SAND 91-1634 (Sandia National Laboratories, Albuquerque, NM).

Harrison, J.D., Leggett, R.W., Noßke, D., Paquet, F., Phipps, A.W., Taylor, D.M. and Metivier, H., 2001. Reliability of the ICRP's Dose Coefficients for Members of the Public, II. Uncertainties in the Absorption of Ingested Radionuclides and the Effect on Dose Estimates. Radiation Protection Dosimetry, 95:295–308 (2001), Oxford University Press.

Hawthorne, H.A. (ed.), 1979. Compilation of Local Fallout Data from Test Detonations 1945–1962 Extracted from DASA 1251, Volume I—Continental U.S. Tests. DNA 1251-1-EX (Defense Nuclear Agency, Washington, D.C.).

Hicks, H. G., 1984. Results of Calculations of External Gamma Radiation Exposure Rates from Local Fallout and the Related Radionuclide Compositions of Selected U.S. Pacific Events. UCRL-53505 (Lawrence Livermore National Laboratory, Livermore, CA).

Hillel, D., 1980. *Fundamentals of Soil Physics*. Acad. Press, N.Y. 413 p.

Hoffman, F.O. and Gardner, R.H., 1983. Evaluation of Uncertainties in Radiological Assessment Models. Chapter 11 in *Radiological Assessment, A Textbook on Environmental Dose Analysis*, Till, J.E. and Meyer, H.R., Eds., NUREG/CR-3332; ORNL-5968 (Oak Ridge National Laboratory, Oak Ridge, Tennessee).

Holmes & Narver, 1956. Completion Report, Operation REDWING, Pacific Proving Ground,1954–1956. Holmes & Narver for U. S. Atomic Energy Commission.

HydeSoft Computing, 2008. DPLOT, Graph Software for Scientists and Engineers. http://www.dplot.com/ (Accessed February 23, 2010), HydeSoft Computing, LLC, Vicksburg, MS.

ICRP (International Commission on Radiological Protection), 1977. Recommendations of the International Commission on Radiological Protection. ICRP Publication 26, Annals of the ICRP 1(3), Pergamon Press, Oxford, England.

ICRP (International Commission on Radiological Protection), 1979. Limits for Intakes by Workers, A Report of Committee 2 of the International Commission on Radiological Protection. ICRP Publication 30, Annals of the ICRP 2(3/4), Pergamon Press, Elmsford, NY.

ICRP (International Commission on Radiological Protection), 1994. Human Respiratory Tract Model for Radiological Protection. ICRP Publication 66, Pergamon Press, Elmsford, NY.

ICRP (International Commission on Radiological Protection), 1996. Age-Dependent Doses to the Members of the Public from Intake of Radionuclides Part 5, Compilation of Ingestion and Inhalation Coefficients. ICRP Publication 72, Ann. ICRP 26/1, Pergamon Press, Elmsford, NY.

ICRP (International Commission on Radiological Protection), 2002. The ICRP Database of Dose Coefficients: Workers and Members of the Public. Compact Disc Version 2.01, ICRP, Stockholm, Sweden.

Jacobson, M.Z., 1998. *Fundamentals of Atmospheric Modeling*. Cambridge University Press, New York, NY.

Kellogg, W.W., Rapp, R.R., and Greenfield, S.M., 1957. Close-in Fallout. Journal of Meteorology, 14(1):1–8 (February, 1957).

Kirchner, T.B., 2008. Estimating and Applying Uncertainty in Assessment Models, in *Radiological Assessment and Environmental Analysis*, Till, J. E. and Grogan, H. A., Editors, Oxford University Press, Oxford, New York.

Kocher, D.C., Trabalka, J.R., Apostoaei, A.I., 2006. Evaluation of Inhalation Doses in Scenarios Involving Resuspension by Nuclear Detonations at Nevada Test Site (Revision 2). December, 2006. (SENES Oak Ridge, Inc., Center for Risk Analysis, Oak Ridge, TN).

Lorence, L.J., Morel, J.E., and Valdez, G.D, 1989. Users Guide to CEPXS/ONEDANT: A One-Dimensional Coupled Electron-Photon Discrete Ordinates Code Package, Version 1.0. SAND 89-1661 (Sandia National Laboratories, Albuquerque, NM).

Martin, E.J. and Rowland, R.H., 1982. CASTLE Series: 1954, United States Atmospheric Nuclear Weapons Tests, Nuclear Test Personnel Review. DNA 6035F (Defense Nuclear Agency, Washington, D. C.).

McKay, M. D. Beckman, R. J. and Conover, W. J., 1979. A Comparison of Three Methods for Selecting Values of Input Variables in the Analysis of Output from a Computer Code. Technometrics, Vol. 21(2), pp. 239–245, May, 1979.

McKenzie-Carter, M., 2009. Bias Adjustments for Use with FIIDOS Inhalation Dose Conversion Factors. NTPR-TM-09-08 (Science Applications International Corporation. McLean, VA).

McKenzie-Carter, M. and Stiver, J. 2009. Deposition Fraction Modifications for Inhalation of Descending Fallout. NTPR-TM-09-09 (Science Applications International Corporation. McLean, VA).

Molumphy, G.G., and Bigger, M.M., 1957. Proof Testing of Atomic Weapons Ship Countermeasures. WT-927 (U.S. Naval Radiological Defense Laboratory).

Morgan, M.G. and Henrion , M., 1990. *Uncertainty: A Guide to Dealing with Uncertainty in Quantitative Risk and Policy Analysis*. Cambridge University Press, New York.

NCRP (National Council on Radiological Protection and Measurements), 1996. A Guide for Uncertainty Analysis in Dose and Risk Assessments Related to Environmental Contamination. NCRP Commentary No. 14 (National Council on Radiation Protection and Measurements, Bethesda, Maryland).

NCRP (National Council on Radiological Protection and Measurements), 1997. Deposition, Retention and Dosimetry of Inhaled Radioactive Substances, NCRP Report No. 125 (National Council on Radiation Protection and Measurements, Bethesda, Maryland).

NCRP (National Council on Radiological Protection and Measurements), 2007. Uncertainties in the Measurement and Dosimetry of External Radiation. NCRP Report No. 158 (National Council on Radiation Protection and Measurements, Bethesda, Maryland).

NIST (National Institute of Standards and Technology), 2009. *NIST/SEMATECH e-Handbook of Statistical Methods*. http://www.itl.nist.gov/div898/handbook/ (Accessed February 23, 2010), (National Institute of Standards and Technology, Gaithersburg, Maryland).

NRC (National Research Council),1989. Film Badge Dosimetry in Atmospheric Nuclear Tests. (National Research Council, Washington, D.C.).

NRC (National Research Council), 2003. A Review of the Dose Reconstruction Program of the Defense Threat Reduction Agency. (National Research Council, Washington, D.C.).

PDAS (Public Domain Aeronautical Software), 2009. Available at http://www.pdas.com/m1.htm (Accessed February 23, 2010), Public Domain Aeronautical Software, Santa Cruz, CA.

Phalen, R.F., Oldham, M.J., Beaucage, C.B., Crocker, T.T., and Mortensen, J.D., 1985. Post-Natal Enlargement of Human Tracheobronchial Airways and Implications for Particle Deposition. The Anatomical Record, 212(4), 368–380 (1985).

Raabe, O.G., 1972. Instruments and Methods for Characterizing Radioactive Aerosols. IEEE Transactions on Nuclear Science, Vol. NS19, No. 1 (February, 1972).

Raine, D.A. III, Egbert, S.D., Stiver, J.H., and Case, D.R., 2007. FIIDOS—A Computer Code for the Computation of Fallout Inhalation and Ingestion Dose to Organs, Computer User's Guide (Revision 4). DTRA-TR-07-11 (Science Applications International Corporation, McLean, VA and Defense Threat Reduction Agency, Fort Belvoir, VA).

Rapp, R.R., 1959. Summary Report of RAND Work on the AFSWP Fallout Project. AFSWP 1134 (The RAND Corporation, Santa Monica, CA).

Rinnert, H.R., 1957. Project 2.71: Ship Shielding Studies, Operation REDWING. WT-1321 (U.S. Naval Radiological Defense Laboratory, San Francisco, CA).

Saltelli, A., Ratto, M., Andres, T., Campolongo, F., Cariboni, J., Gatelli, D. Saisana, M., and Tarantola, S., 2008. *Global Sensitivity Analysis, The Primer*. John Wiley & Sons.

Scoville, H., 1954. Radiological Survey of Downwind Atolls Contaminated by BRAVO. TU-13-54-375 (memorandum from Technical Director, AFSWP, to Headquarters Task Unit 13).

Servis, J.D., 1981. Operation CASTLE Radiological Safety. WT-942 (EX) (Defense Nuclear Agency, Washington D.C.).

Soule, R.R. and Shirasawa, T.H., 1981. Operation REDWING, Project 2.61, Rocket Determination of Activity Distribution Within the Stabilized Cloud. WT-1315 (EX) (Defense Nuclear Agency, Washington, D.C.).

Spellman, F.R., and Whiting, N.E., 2004. *Environmental Engineer's Mathematical Handbook*. CRC Press, Boca Raton, FL.

Stearns, F., 1968. A Method for Estimating the Quantitative Reliability of Isoline Maps. Annals of the Association of American Geographers, Vol. 58, No. 3, pp. 590–600, September 1968.

Stevens, P.N., and Trubey, D.K., 1972. Weapons Radiation Shielding Handbook – Chapter 3: Methods for Calculating Neutron and Gamma-Ray Attenuation. DNA-1892-3 (Defense Nuclear Agency, Washington, D.C.).

Thomas, C., Goetz, J., Klemm, J., and Weitz, R., 1984. Analysis of Radiation Exposure for Naval Personnel at Operation CASTLE. DNA-TR-84-6 (Defense Nuclear Agency, Washington, D.C.).

Till, J.E. and Meyer, H.E., 1983. *Radiological Assessment, A Textbook on Environmental Dose Analysis.* NUREG/CR-3332, ORNL-5968, September, 1983 (U.S. Nuclear Regulatory Commission, Washington, D.C.).

Tomoeda, S., Kreger, W.E., Hastings, M.B., and Miller, W.G., 1959. Gamma Ray Penetration into the Compartments of a Light Aircraft Carrier. USNRDL-TR-343 (U.S. Naval Radiological Defense Laboratory, San Francisco, CA).

Triffet, T. and LaRiviere, P.D., 1982. Operation REDWING, Project 2.63, Characterization of Fallout. WT-1317 (EX) (Defense Nuclear Agency, Washington, D.C.).

USACHPPM (U.S. Army Center for Health Promotion and Preventive Medicine), 2003. Reference Document (RD) 230, Exposure Guidelines for Deployed Military, a Companion Document to Technical Guide (TG) 230, Chemical Exposure Guidelines for Deployed Military Personnel, Version 1.3 (updated May 2003). RD-230.

USD (Undersecretary of Defense), 2004. Advisory Board on Veterans Dose Reconstruction Charter. Memorandum, November 17, 2004.

USEPA (U.S. Environmental Protection Agency), 1996. Soil Screening Guidance: Technical Background Document. EPA/540/R-95/128 (U.S. Environmental Protection Agency, Washington, D.C.).

USEPA (U.S. Environmental Protection Agency), 1997. Exposure Factors Handbook. EPA/600/P-95/002Fa, Fb, Fc. (U.S. Environmental Protection Agency, Washington, D.C.).

USEPA (U.S. Environmental Protection Agency), 2001. Risk Assessment Guidance for Superfund (RAGS) Volume III – Part A: Process for Conducting Probabilistic Risk Assessment. EPA 540-R-02-002, OSWER 9285.7-45, PB2002 963302, December 2001.

USEPA (U.S. Environmental Protection Agency), 2002. Supplemental Guidance for Developing Soil Screening Levels for Superfund Sites. OSWER 9355.4-24 (U.S. Environmental Protection Agency, Washington, D.C.).

USMC (United States Marine Corps), 1957. "USMC Final Report of Exercise Desert Rock VII," circa 1957.

VBDR (Veteran's Advisory Board on Dose Reconstruction), 2007. Letter from Chairman of VBDR to Director of DTRA. October 16, 2007.

Vose, D., 2008. *Risk Analysis: A Quantitative Guide*. John Wiley, Chichester, England

Waldorf, W.F., 1959. A Correlation Between Theory and Experiment in Ship Shielding Studies. USNRDL-TR-373 (U.S. Naval Radiological Defense Laboratory, San Francisco, CA).

Weitz, R.L., 2009a. Internal Dose from Inhalation of Descending Fallout. NTPR-TM-09-07 (Science Applications International Corporation, McLean, VA).

Weitz, R.L., 2009b. Model of Topside Intensity Distributions from Fallout on Ship Weather Deck. NTPR-TM-09-05 (Science Applications International Corporation, McLean, VA).

Weitz, R.L., 2009c. Modeling of Protection Factors for Land-Based Structures. NTPR-TM-09-10 (Science Applications International Corporation, McLean, VA).

Weitz, R.L., 2009d. Modeling of Shielding Factors for Ships. NTPR_TM-09-11 (Science Applications International Corporation, McLean, VA).

Weitz, R.L., 2009e. Formulation of the Gamma Source Modification Factor (GSMF) for Ship-based Applications. NTPR-TM-09-04 (Science Applications International Corporation, McLean, VA).

Weitz, R.L., 2009f. Characterization of Descending Fallout. NTPR-TM-09-06 (Science Applications International Corporation, McLean, VA).

APPENDIX A Monte Carlo Analysis of Dose to Army Units Stationed on Enewetak Island During Operation REDWING

Carol Mason

APPENDIX A Monte Carlo Analysis of Dose to Army Units Stationed on Enewetak Island During Operation REDWING

Introduction

Distributions of external and internal doses were generated by Monte Carlo techniques for personnel of the Headquarters (HQ) Detachment of the 7126th Army Unit (AU) stationed on Enewetak Island of Enewetak Atoll during Operation REDWING (1956). Doses are reported for the period extending from the film badge issue date of July 11, 1956, until the film badge return date of August 3, 1956.

Background

Operation REDWING was a series of 17 atmospheric nuclear tests, conducted from May 5 to July 22, 1956, at the Pacific Proving Ground (PPG) in the Marshall Islands. The PPG consisted of the land areas of Enewetak and Bikini Atolls, their lagoons, and the waters within 2.6 nautical miles (3 statute miles) of their seaward sides. (Bruce-Henderson, 1982)

The HQ Detachment of the 7126th AU, consisting of 39 officers and 348 enlisted personnel, was stationed on Enewetak Island during Operation REDWING. The 7126th AU provided most of the personnel for Task Group (TG) 7.2. It was the permanent garrison force at Enewetak Island between Operations CASTLE and REDWING. Except for its military police detachment and several mail clerks on Eneu and Parry Islands, the 7126th AU was stationed on Enewetak Island. To accommodate the buildup to Operations REDWING's operational phase, the 7126th AU was reorganized into the following four detachments: Headquarters, Service, Transportation, and Military Police. TG 7.2 was, in effect, a housekeeping unit, providing garrison and support elements for the joint task force in the PPG.

Assigned personnel arrived at Enewetak Island prior to the first nuclear detonation of the series. By the nature of their duties, it is likely that most of these personnel remained on the island continuously, or nearly so, throughout the operation.

Exposure Scenario

Enewetak, Parry, and Japtan Islands were the residence islands of Enewetak Atoll, where most land-based personnel were stationed. Fallout from four Operation REDWING detonations contributed to the radiation environment at the residence islands. Table A-1 identifies these shots and the corresponding peak fallout intensities in units of mR hr^{-1} at the indicated elapsed times after the detonations in hours (H+hours). Additional early-time intensity data for Enewetak Island are provided after the table. (Jacks, 1957)

The early-time intensity function for Enewetak Island following Shot ZUNI is defined by the time-intensity pairs shown in Table A-2.

Table A-1. Peak Radiation Intensities on Enewetak Island during Operation REDWING

Shot	Shot Date (1956) (Time)	Peak Intensity (mR hr^{-1})
ZUNI	May 28 (0556)	0.25 at H+11 hours
MOHAWK	Jul 3 (0606)	12 at H+3 hours
APACHE	Jul 9 (0606)	0.84 at H+20.9 hours
TEWA	Jul 21 (0546)	120 at H+26 hours

Table A-2. Early Time Intensity Function on Enewetak Island following Shot ZUNI

Time After Detonation (hr)	Intensity (mR hr^{-1})
8.5	0.01
11	0.25
18	0.13

The early-time intensity data for Shot MOHAWK contains 25 time-intensity data pairs and is not included here. The intensity for MOHAWK fallout on Enewetak Island peaked at 12 mR hr^{-1} 3 hours after the detonation and then reached a second, lower peak of about 4 mR hr^{-1} at 9 hours after the detonation.

The early-time intensity function for Enewetak Island following Shot APACHE is defined by the time-intensity pairs shown in Table A-3.

Table A-3. Early Time Intensity Function on Enewetak Island following Shot APACHE

Time After Detonation (hr)	Intensity (mR hr^{-1})
16.9	< 0.01
17.4	0.01
17.65	0.69
17.9	0.74
20.9	0.84
21.9	0.74
25.9	0.60

Shot TEWA resulted in most of the dose accrued by personnel at the residence islands in late July 1956. Fallout radiation intensities from TEWA were measured at two locations on Parry Island: HQ JTF 7 and the Radsafe Building. Those measurements form the basis for the Shot TEWA early-time intensity model for the residence islands. Decontamination at HQ JTF 7 began on July 26 (H+114 hours) and was completed on July 31 (H+258 hours). On August 10, the entire island was monitored and most readings were 0.003 rep·hr^{-1} (beta plus gamma) or less. Using the Radsafe Building data decayed to August 10 yields an intensity of about 1.5 mR hr^{-1}, which is consistent with the survey results, assuming a ratio of (beta plus gamma)/gamma of 1.5 to 2. The modeled early time intensity data for the residence islands are presented in Table A-4.

Table A-4. Early Time Intensity Function on Enewetak Island following Shot TEWA

Time After Detonation (*T* in hr)	Intensity (*EarlyI* in mR hr^{-1})
1	0.129
5	0.145
9	0.638
11	4.913
12	21.338
14	53.875
15	84.000
18	100.351
19	94.063
21	108.438
25	115.500
26	112.125
29	87.375
33	71.938
47	39.277
57	33.205
67	28.854
77	23.572
96	17.964
114	15.254

There was no documented decontamination effort on Enewetak Island soon after Shot TEWA, suggesting that the intensity levels were lower. As a conservative estimate, the intensities at Enewetak Island are taken to be the average of measurements from HQ JTF 7 and the Radsafe building at Parry Island to July 26 (prior to decontamination at Parry Island). The last early-time intensity data point for Enewetak Island is 15.25 mR hr^{-1} at 114 hours after detonation.

Extrapolation beyond the time of the last time-intensity point for each shot is accomplished by assuming $t^{-1.2}$ decay for deterministic calculations and by utilizing the shot-specific FIIDOS decay functions for probabilistic calculations as discussed in Section 3.2.

External Dose: Approach

Film Badge Data

Complete records of film badge results are available for the HQ Detachment. Most personnel in the unit were issued three consecutive permanent film badge dosimeters during their stay in the test area, which covered a total period extending from mid-April to early August 1956. However, most film badges issued for periods of 4 weeks or more at Operation REDWING were damaged by the high heat and humidity in the test area (NRC, 1989), which resulted in overstated readings. Thus, most of the badges for the unit were not suitable as a benchmark for comparison with reconstructed doses. It was, therefore, necessary to identify a set of badges worn for a shorter period and for which previous analysis had demonstrated the integrity of the readings. Based on previous experience in identifying damaged dosimeter films and a review of the Operation REDWING dosimetry database, a group of film badge doses for this unit was analyzed for a period extending from July 11 to August 3, 1956. As a result, a set of 323 badges was selected. Bias was removed from the film badge readings based on guidance on film badge dosimetry (NRC, 1989). Both the distribution of film badge readings and the cumulative distribution function (CDF) (Figure A-1) demonstrate that the unbiased film badge readings for the HQ Detachment follow a Gaussian distribution, which suggests relative internal cohesion in the unit with regard to radiation exposure conditions. The average unbiased film badge reading for the distribution is 2.9 rem, with a standard deviation of 0.61 rem.

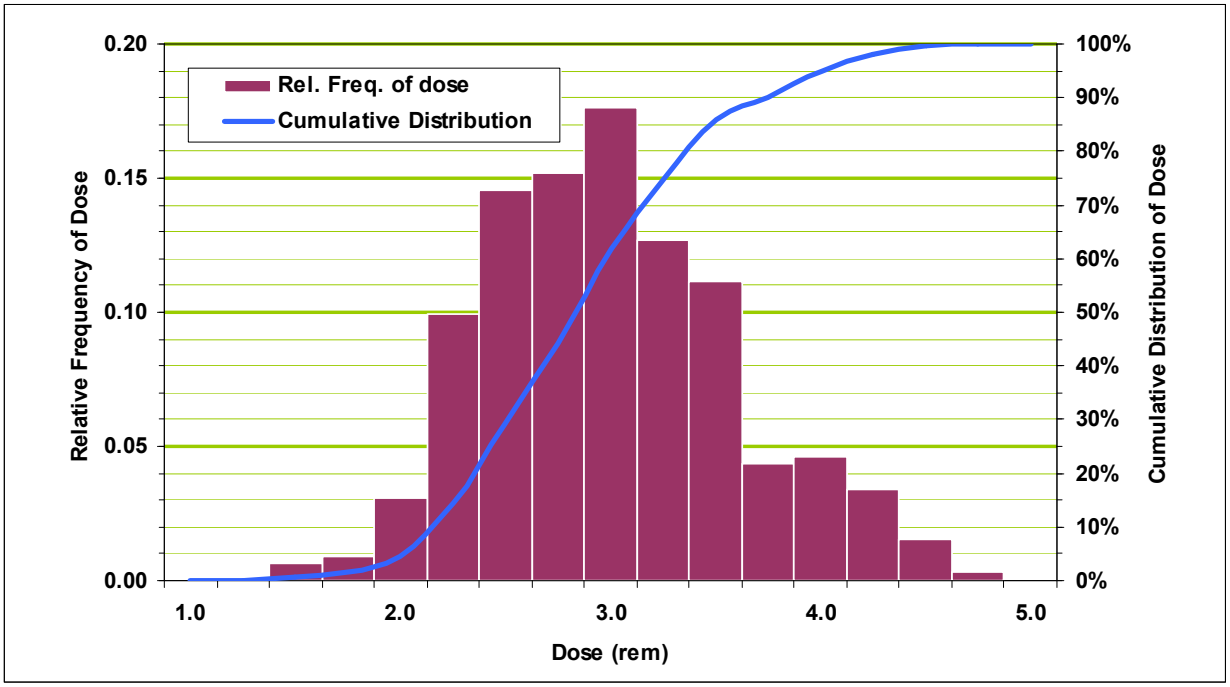

Figure A-1. Distribution of Unbiased Film Badge Results for HQ Detachment Personnel

Monte Carlo-Based Dose Reconstruction

Probabilistic external gamma dose reconstruction for personnel stationed on Enewetak Island during Operation REDWING was accomplished by incorporating uncertainty distributions for various parameters into the model discussed in Section 3. The specific parameters used in both the deterministic and uncertainty analyses of external dose are shown in Table A-5.

Table A-5. Input Parameter Specification for External Gamma Dose Reconstruction, Case Study #1

Parameter	Definition	Distribution for Probabilistic Analysis (*)	Nominal Value for Central Estimation	Deterministic(**)
EXTERNAL DOSE MULTIPLIER (EDM) FOR LAND-BASED PERSONNEL				
F_{os}	Fraction of time spent outside	Triangular min = 2/24 peak = 8/24 max = 16/24	0.34 (or 8/24)	0.6 (or 14.4/24)
F_t	Fraction of inside time spent in tent	Triangular min = 0 peak = 0.5 max = 1	0.5	0
PF_t	Protection factor for tent	Numerical model (see Section 4.2.2) $\mu = 1.4$ UB95 = 1.9	1.4 (median of distribution)	1.5
PF_b	Protection factor for building	Numerical model (see Section 4.2.2) $\mu = 2.1$ UB95 = 3.9	2.0 (median of distribution)	2.0
I_i	Intensity of fallout near outdoor location (i=1), tent location (i=2), and building location (i=3) frequented by veteran, normalized to the intensity averaged over entire island	Lognormal GM = 1.0 GSD = 1.5	1.0	1.0
INTENSITY MEASUREMENTS FOR LAND-BASED PERSONNEL				
I_m	Measured intensities	Normal $\mu = I_m$, $\sigma = 0.3 \cdot I_m$ (to account for measurement error)	1.0	1.0
a	Exponent of multiplicative error factor $(t/t_0)^{\pm a}$ applied to FIIDOS-generated intensity functions	Normal $\mu = 0$ $\sigma = 0.15$	0	0

Parameter	Definition	Distribution for Probabilistic Analysis (*)	Nominal Value for Central Estimation	Deterministic(**)

(*) μ = arithmetic mean; σ = standard deviation; GM = geometric mean; GSD = geometric standard deviation;
UB95 = upper bound at the 95th percentile.
(**) High-sided per guidance in NTPR Policy and Guidance Manual (DTRA, 2007).

External Dose Results

The Monte Carlo dose distribution derived for a sample size of 10,000 for the film badge period of July 11 to August 3, 1956 is displayed in Figure A-2 and compared with the distribution of unbiased film badge results. The probability plot is shown in Figure A-3. The statistics of this distribution are compared with those of a deterministic calculation in Table A-6.

Table A-6. Summary of Estimated External Dose for Army Units stationed at Enewetak Island during Operation REDWING

Mean Dose (rem)			Upper Bound Dose (rem)			
Film Badge	Probabilistic(*)	Deterministic (NTPR)	Film Badge (95th Percentile)	Probabilistic (95th Percentile)	Deterministic (NTPR)	Ratio (Deterministic/ Probabilistic)
2.9	3.5 (1.5)	3.4	4.0	6.2	10	1.6

(*) The arithmetic mean (and standard deviation) are shown. The geometric mean external dose is 3.2 rem.

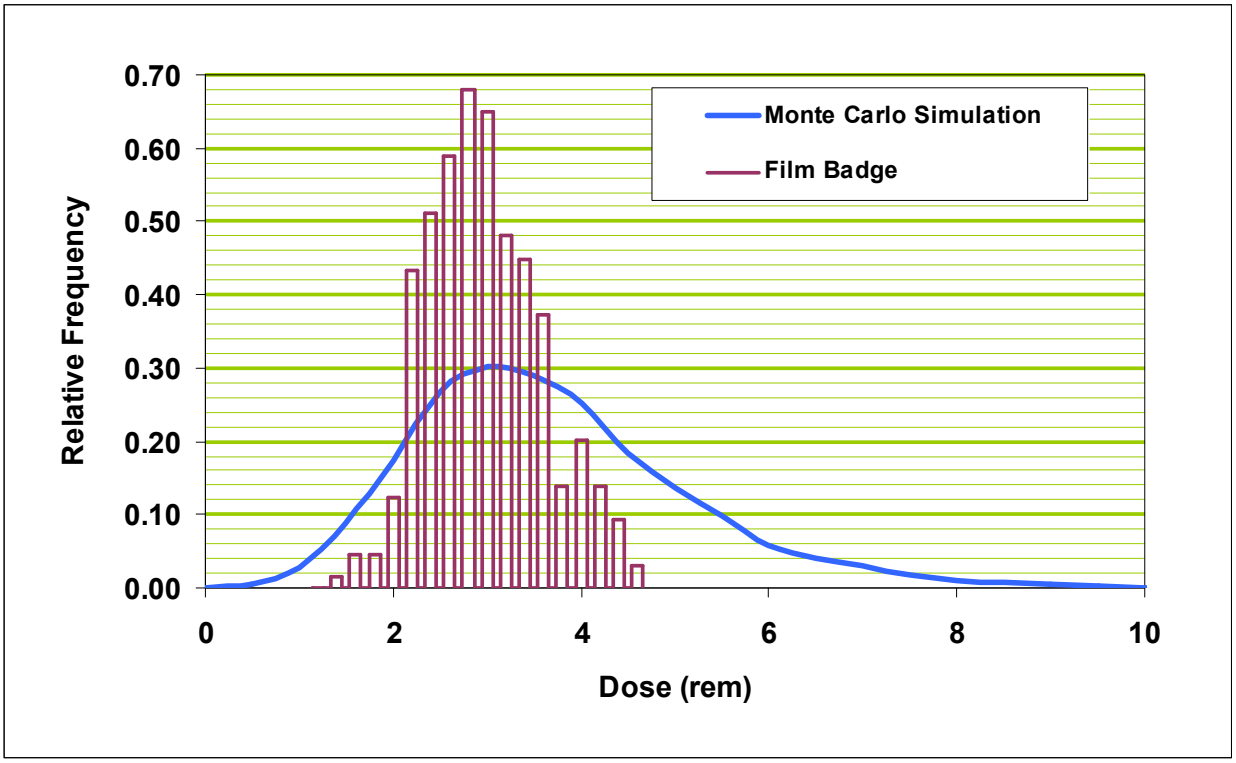

Figure A-2. Comparison of Distribution of Estimated External Gamma Doses from Monte Carlo Analysis with Distribution of Unbiased Film Badge Results for the 7126th Army Unit Stationed at Enewetak Island during Operation REDWING

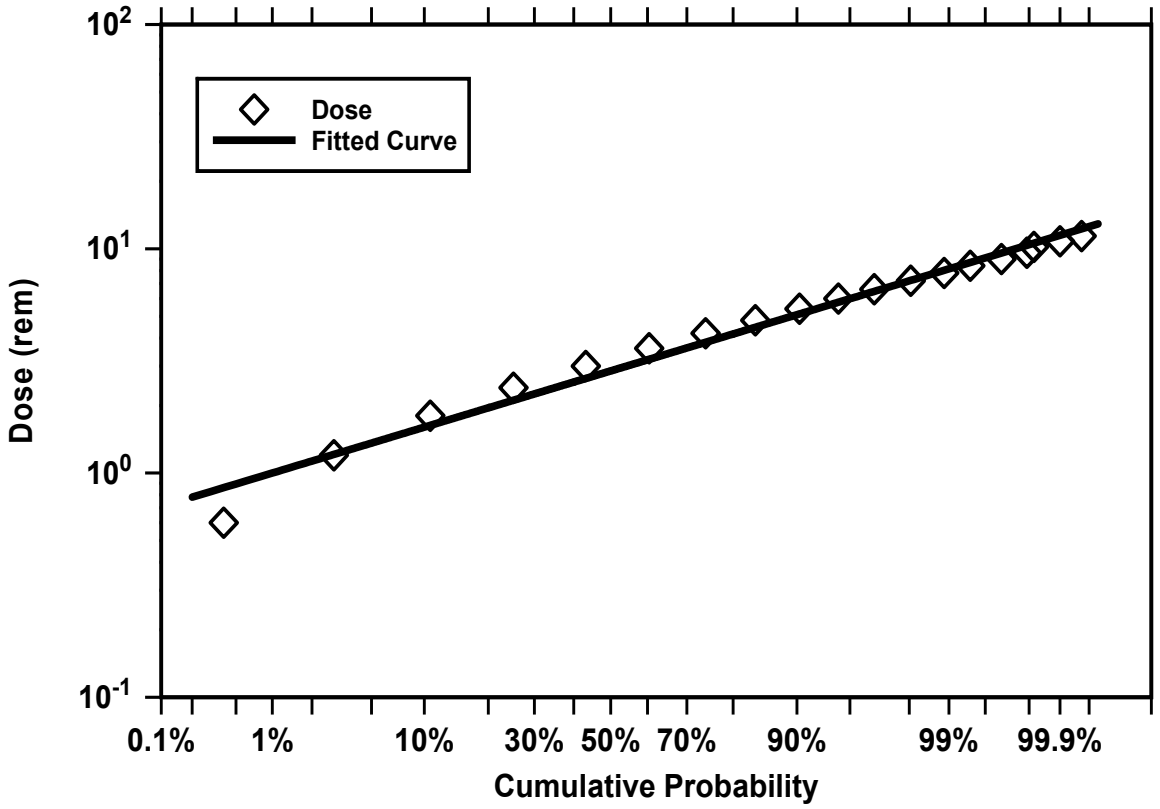

Figure A-3. Probability Plot of Estimated External Gamma Doses for 7126th Army Unit Stationed at Enewetak Island during Operation REDWING

Internal Dose: Approach

Internal dose reconstruction for Army units stationed on Enewetak Island during Operation REDWING was accomplished by incorporating uncertainty distributions for the fallout-induced radiation environments discussed above and for various other parameters as discussed in Sections 3 and 4. The specific parameters used in both the deterministic and probabilistic analyses are shown in Table A-7.

Table A-7. Input Parameter Specification for Internal Dose Reconstruction, Case Study #1

Parameter	Definition	Distribution for Probabilistic Analysis	Nominal Value for Central Estimation	Deterministic(*)
INTERNAL DOSE (GENERAL)				
DCFInhα *DCFIngα*	Inhalation and ingestion dose conversion factors for fallout α emitters	*DCF*s calculated with FIIDOS multiplied by Lognormal with GM=1.0, GSD=5.19	*DCF*s calculated with FIIDOS (see Section 4.2.8)	DCFs calculated with FIIDOS (see Section 4.2.8)
DCFInhβγ *DCFIngβγ*	Inhalation and ingestion dose conversion factors for fallout β+γ radiation	*DCF*s calculated with FIIDOS multiplied by Lognormal with GM=1.0, GSD=4.05	*DCF*s calculated with FIIDOS (see Section 4.2.8)	DCFs calculated with FIIDOS (see Section 4.2.8)
Biasα	Bias factors to adjust high-sided inhalation *DCF* values	Assigned Constant α: 1.3 for each organ	α: 1.3 for each organ	1.0
Biasβγ		βγ: 1.2 for thyroid & LLI, 1.35 for lung	βγ: 1.2 for thyroid & LLI, 1.35 for lung	1.0
BR	Breathing rate	Triangular distribution derived from USEPA (1997) data (see Section 4.2.7): min = 0.33 $m^3\ hr^{-1}$ peak = 1.53 $m^3\ hr^{-1}$ max = 2.79 $m^3\ hr^{-1}$	Mean of Distribution ~1.5 $m^3\ hr^{-1}$	1.2 $m^3\ hr^{-1}$
DESCENDING INHALATION DOSE (†)				
RND_{Res1}	Deposition fractions for particle sizes deposited in Regions BB, bb and AI	1.0 (assumed constant)	1.0 (assumed constant)	n/a
RND_{Res2}		Lognormal: GM, GSD 0.0056, 1.744	Geometric Mean 0.0056	
RND_{Res3}		Lognormal: GM, GSD 0.001, 1.65	0.001	
$RND_{Nonres1}$	Deposition fractions for particle sizes deposited in Region ET_2 and cleared to digestive tract	0.0 (assumed constant)	0.0 (assumed constant)	n/a
$RND_{Nonres2}$		Lognormal: GM, GSD 0.363, 1.106	Geometric Mean 0.363	
$RND_{Nonres3}$		Lognormal: GM, GSD 0.285, 1.185	0.285	
V_1	Particle settling velocities	Logtriangular min, peak, max (cm s^{-1}) 0.22/2, 0.22, 27.8	0.22 cm s^{-1}	10^6(cm)/T(sec)
V_2		0.83/2, 0.83, 27.8	0.83 cm s^{-1}	
V_3		13.0/2, 13.0, 27.8	13.0 cm s^{-1}	

Parameter	Definition	Distribution for Probabilistic Analysis	Nominal Value for Central Estimation	Deterministic(*)
AF_{100}	Surface activity fraction <100 μm particles	Triangular (min, mode ,max) ZUNI (0.094, 0.280, 0.565) MOHAWK (0.013, 0.070, 0.140) APACHE (0.939, 0.973, 1.000) TEWA (0.403, 0.572, 0.732)	Peak of Distributions ZUNI 0.280 MOHAWK 0.070 APACHE 0.973 TEWA 0.572	1.0
$frac_1$ $frac_2$	Surface fraction of Class 1-2 from 1-100 μm particles	Triangular Min, peak, max 0, 0.00136, 0.01 0, 0.025, 0.1	Peak of Distribution 0.00136 0.025	n/a
RESUSPENDED INHALATION DOSE				
$K(t)$	Time-dependent resuspension factor	Lognormal multiplier of Anspaugh equation GM=1, GSD=4.05	Anspaugh equation	Till and Meyer, 1983
INCIDENTAL INGESTION DOSE				
q_{ing}	Soil ingestion rate	Triangular min, peak, max ($mg\ d^{-1}$) 10, 100, 500	Peak of Distribution 100 $mg\ day^{-1}$	500 $mg\ day^{-1}$
ρ_{soil}	Soil bulk density	Triangular $g\ cm^{-3}$ Min, peak, max 1.3, 1.45, 1.6	Peak of Distribution 1.45 $g\ cm^{-3}$	1.3 $g\ cm^{-3}$

(*) High-sided per guidance in NTPR Policy and Guidance Manual (DTRA, 2007).
(†) AMAD particle size classes: 1 = 1–10 μm, 2 = 10–20 μm, 3 = 20–100 μm.

Internal Dose Results

Fifty-year committed equivalent dose (CED) distributions to three organs, thyroid, lung, and lower large intestine (LLI), were derived using the probabilistic model for a sample size of 10,000. The geometric mean and 95th percentile CEDs of the various distributions are given in Table A-8, along with analogous doses derived deterministically. The ratio of the deterministic upper bound CED to the probabilistic 95th percentile CED is provided in the rightmost column. Examples of these distributions are shown in Figure A-4 through Figure A-7, where the relative frequency distribution and probability plot of CED to the LLI wall from alpha radiation and from beta plus gamma radiation, respectively, are plotted.

Table A-8. Summary of Estimated Internal Doses for 7126th Army Unit Stationed at Enewetak Island during Operation REDWING

Organ	Mean Dose (rem)		Upper Bound Dose (rem)		
	Probabilistic(*)	Deterministic (NTPR)	Probabilistic (95th Percentile)	Deterministic (NTPR)	Ratio (Deterministic/ Probabilistic)
Alpha Dose					
Thyroid	0.000024 (8.6)	0.00011	0.00083	0.0011	1.4
Lung	0.00029 (8.7)	0.0014	0.010	0.014	1.4
LLI Wall	0.000024 (8.5)	0.00011	0.00085	0.0011	1.4
Beta plus Gamma Dose					
Thyroid	0.72 (4.8)	1.5	9.8	14	1.5
Lung	0.16 (6.7)	1.4	3.8	14	3.7
LLI Wall	0.54 (4.8)	1.0	7.3	9.6	1.3

(*) Geometric mean and (geometric standard deviation) are shown for the probabilistic analysis results.

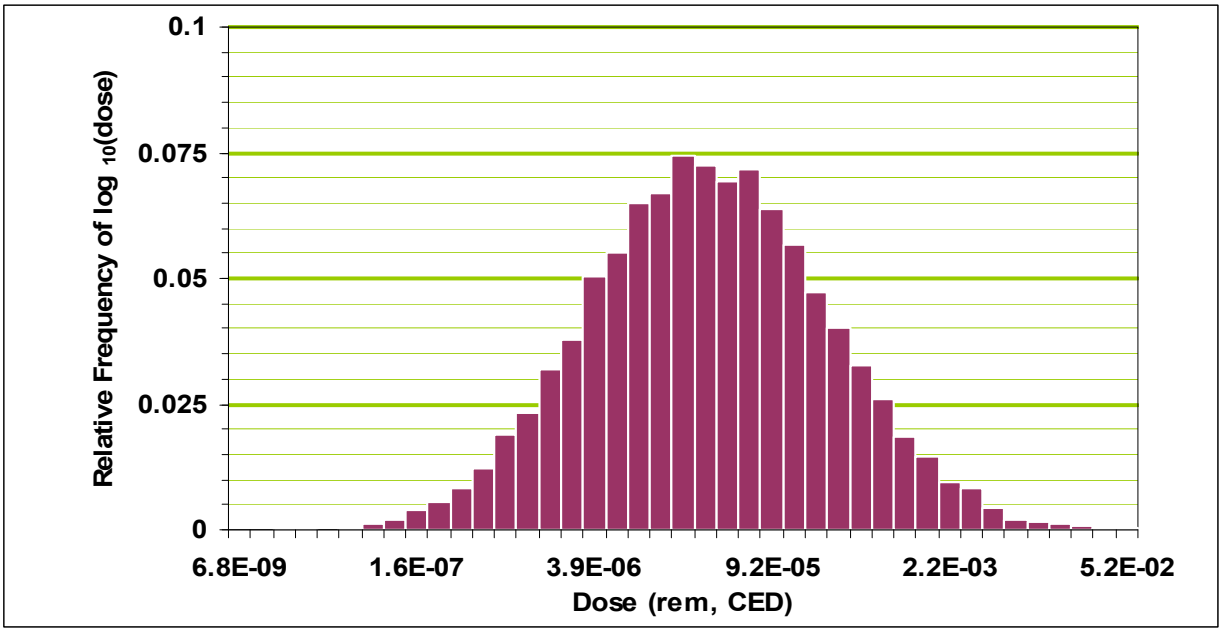

Figure A-4. Distribution of Estimated LLI Wall Dose from Alpha Radiation for 7126th Army Unit Stationed at Enewetak Island during Operation REDWING

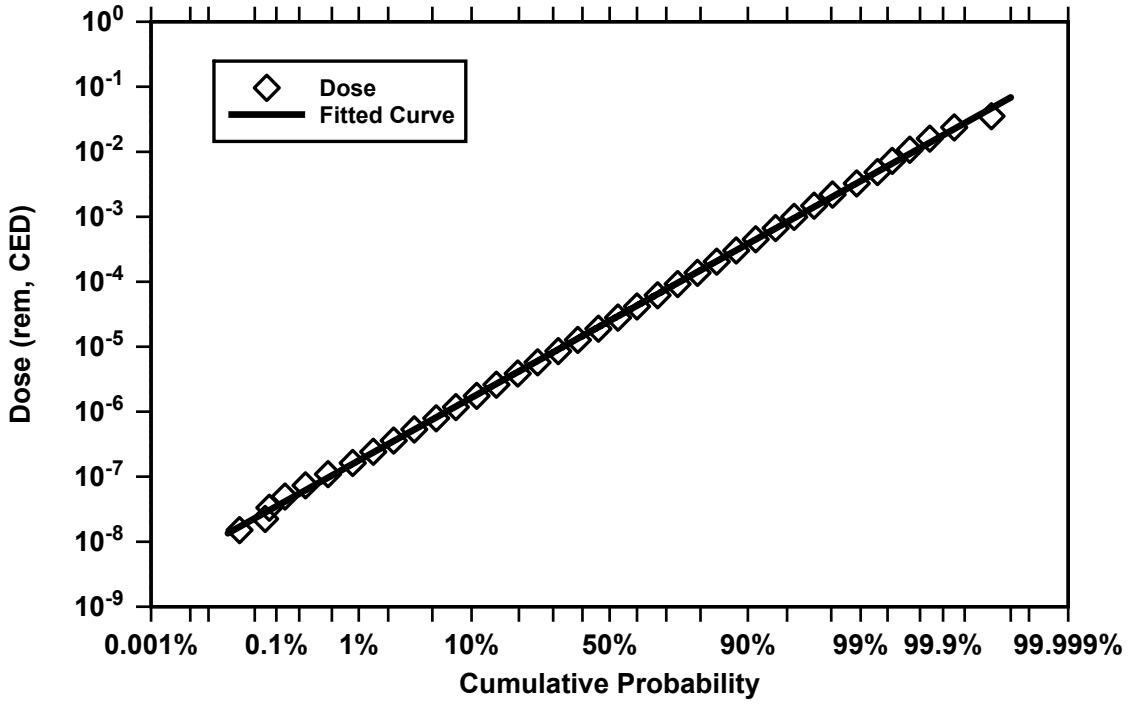

Figure A-5. Probability Plot of Estimated LLI Wall Dose from Alpha Radiation for 7126th Army Unit Stationed at Enewetak Island during Operation REDWING

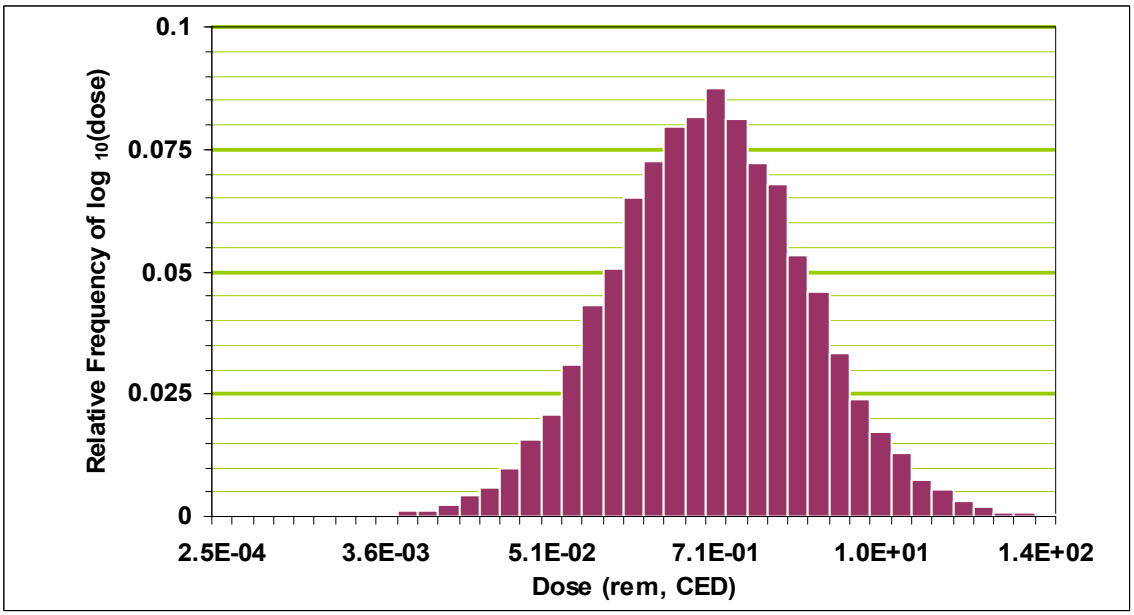

Figure A-6. Distribution of Estimated LLI Wall Dose from Beta plus Gamma Radiation for 7126th Army Unit Stationed at Enewetak Atoll during Operation REDWING

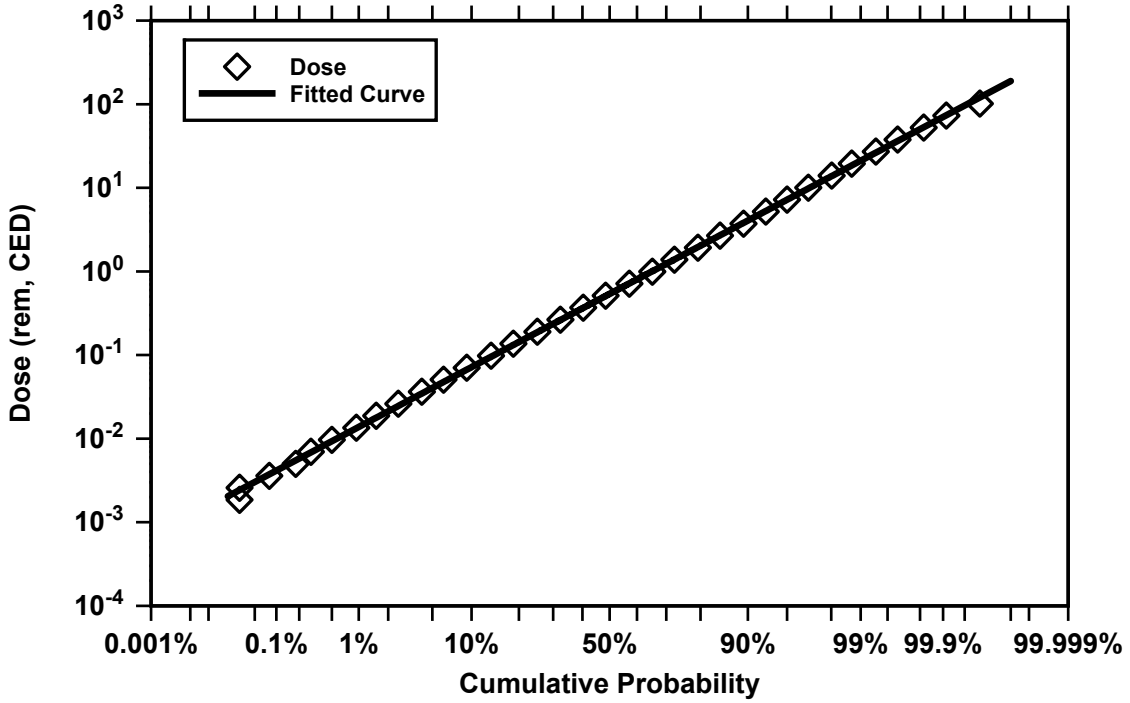

Figure A-7. Probability Plot of Estimated LLI Wall Doses from Beta plus Gamma Radiation for 7126th Army Unit Stationed at Enewetak Atoll during Operation REDWING

References

Bruce-Henderson, S., Gladeck, F.R., Hallowell, J.H., Martin, E.J., McMullan, F.W., Miller, R.H., Rogers, W.E., Rowland, R.H., Shelton, C.F., Sturman, P., Berkhouse, L.H., Davis, S., DeSantis, H., Dean, P., Doyle, M.K., and Patterson, D.S. , 1982. Operation REDWING: 1956, United States Atmospheric Nuclear Weapons Tests, Nuclear Test Personnel Review. DNA 6037F (Defense Nuclear Agency, Washington, D.C.).

DTRA, 2007. Policy and Guidance Manual – Nuclear Test Personnel Review Program. Revision 7 (Defense Threat Reduction Agency, Fort Belvoir, VA).

Jacks, G. L., 1957. Operation REDWING Radiological Safety. WT-1366 (extracted version prepared for DNA in 1983; Defense Nuclear Agency, Washington D.C.).

NRC (National Research Council), 1989. Film Badge Dosimetry in Atmospheric Nuclear Tests. (National Research Council, Washington, D.C.).

Till, J.E. and Meyer, H.R. (eds), 1983. "Radiological Assessment – A Textbook on Environmental Dose Analysis," NUREG/CR-3332, (United States Nuclear Regulatory Commission), September 1983.

USEPA, 1997. Exposure Factors Handbook. EPA/600/P-95/002Fa-c (Office of Research and Development, U.S. Environmental Protection Agency, Washington, D.C.).

APPENDIX B Monte Carlo Analysis of Dose to Army Units Stationed on Enewetak Island During Operation HARDTACK I

Ron Weitz

APPENDIX B Monte Carlo Analysis of Dose to Army Units Stationed on Enewetak Island During Operation HARDTACK I

Introduction

Distributions of external and internal reconstructed doses were generated by Monte Carlo techniques for two Army units, the Administrative Detachment and the Operations Detachment, stationed on Enewetak Island during Operation HARDTACK I (1958). Doses are reported for periods of time corresponding to available film badge readings. The deterministic and probabilistic external dose results are also compared to the mean and upper bound values of available film badge readings for the units.

Background

Operation HARDTACK I was a series of 35 atmospheric nuclear weapon tests conducted in the Pacific Ocean from April 28 to August 18, 1958. All but three of these shots occurred at the Enewetak Proving Ground (EPG), which consisted of the land areas of Enewetak and Bikini Atolls, their lagoons, and the waters within 2.6 nautical miles (nmi) (3 statute miles) of their seaward sides. (Gladeck et al., 1982)

Permanent base camps were established on three islands to support the operations at Enewetak Atoll. The largest of the three, Enewetak Island (or Site Fred), was manned continuously during the operation with a maximum population of approximately 3200 people. Among the units assigned to Enewetak Island were two Army detachments, the Army Administrative Detachment and the Army Operations Detachment. The compositions and duties of these detachments are as follows (Gladeck et al., 1982):

- Administrative Detachment (AD): Personnel of this detachment supported the Chaplain, the Provost Marshal, and the Finance, Information, and Postal Sections. Its scheduled strength was 50 officers and 482 enlisted men during the operational period.
- Operations Detachment (OD): Duties of this detachment were administrative and logistic support for assigned personnel, including laundry, medical, dental, commissary, engineering, depot, gear loft, truck motor pool, and maintenance support. Its scheduled strength was 25 officers and 379 enlisted men.

The personnel assigned to these units arrived at Enewetak Island prior to the first nuclear detonation of the series. By the nature of their duties, it is likely that most of these personnel remained on the island continuously, or nearly so, throughout the operation.

Exposure Scenario

All HARDTACK I detonations took place at least 10 nmi from Enewetak Island. In consideration of these distances and shot yields, none of the island-based participants was exposed to measurable levels of initial gamma and neutron radiation. (Gladeck et al., 1982; Glasstone and Dolan, 1977; Goetz et al., 1985) They were, however, exposed to residual gamma radiation from fallout on the islands.

Prior to the first HARDTACK I fallout deposition on May 14, 1958, the only source of residual radiation exposure on the residence islands of Enewetak Atoll was fallout from Shot TEWA, fired at Bikini on July 21, 1956, as part of Operation REDWING. During the HARDTACK I operational period, the intensity of the TEWA fallout at Enewetak Atoll was on the order of 0.01 milli-Roentgen per hour (mR hr^{-1}) (Thomas, 1991). Because its intensity was so small, this source was not included in the present assessment.

The first and most significant episode of HARDTACK I fallout on Enewetak Island occurred during May 14–15, 1958, and apparently contained contributions from both the FIR and KOA shots. Subsequent minor incidences of fallout were recorded on these islands on June 28 (from Shot REDWOOD), June 29 (Shot OAK), July 12 (Shot POPLAR), and July 18 (Shot PISONIA). However, because the film badges for the Army units considered in this study are evaluated through July 7, radiation environments from Shots POPLAR and PISONIA are not included herein. A Rad-Safe Center, established on Parry Island (Site Elmer) prior to the operation, provided primary radiological survey support; a similar facility did not exist on Enewetak Island (Minkkinen et al., 1959). Therefore, the following quantitative descriptions of these fallout events are based on intensity measurements made on Parry Island. The adaptation of these data for modeling the intensity on Enewetak is discussed subsequently.

FIR-KOA Fallout (May 14–15)

The following significant events of the FIR-KOA fallout episode are taken from Minkkinen et al. (1959):

- 0550 hours, May 12 – Shot FIR was detonated at Bikini Atoll
- 0630 hours, May 13 – Shot KOA was detonated at Enewetak Atoll
- 0300 hours, May 14 – Background radiation intensity on Parry Island started to rise
- 1600 hours, May 14 – Peak intensity of 25 mR hr^{-1} reported on Parry Island
- 0730 hours, May 15 – Intensity of 10–15 mR hr^{-1} reported on Parry Island

Due to meteorological conditions, it was difficult at the time to determine whether the observed fallout came from Shot FIR or Shot KOA. In contemporary reports the fallout was variously attributed individually to Shot FIR and to Shot KOA; in retrospect it appears likely that the clouds from the two shots intermingled somewhat to produce the observed fallout (Gladeck et al., 1982). The most substantial piece of available evidence in determining the origin of the fallout is a decay curve (Minkkinen et al., 1959) that was derived from measurements made on a fallout sample collected on Parry Island during May 15–17. Using the computer code FIIDOS (Raine et al., 2007) with shot-specific radionuclide inventories, the beta activities for both Shot FIR and Shot KOA were calculated and compared with the measured beta activity from the fallout sample. It was found that neither of the decay rates of the individual shots agrees well with the measured rate, but that a mixture of 40 percent Shot FIR and 60 percent Shot KOA (based on the fraction of total fission events attributed to each shot) provides a very good fit to the data.

Shot REDWOOD Fallout (June 28)

Shot REDWOOD was detonated on Bikini Atoll at 0530 hours, June 28. Rainout at Enewetak Atoll started at 1600 hours on that day and continued for approximately 3 hours, during which the background intensity on Parry Island rose to 0.7 mR hr^{-1} (Minkkinen et al., 1959). The time of this peak intensity reading was not reported.

Shot OAK Fallout (June 29)

Shot OAK was detonated at 0730 hours, June 29, at Enewetak Atoll. At 1945 hours on that date, it began to rain on Parry Island and the background intensity began to rise slowly, reaching a peak intensity of 2.5 mR hr^{-1} at 2130 hours before subsiding. Although this fallout episode has been reported as occurring at Eneu Island, Bikini Atoll (Minkkinen et al., 1959), there is substantial evidence (Weitz, 2006) that it actually took place on Parry Island.

A deterministic model was developed on the basis of the radiation intensity data described above (Weitz, 1995), which subsequently evolved into the stochastic model utilized for this case study. The adequacy of this intensity model is supported by a comparison of model results with an extensive set of intensity measurements taken on Parry Island by the Public Health Service (PHS, 1958). The daily averages of these measurements are displayed in Figure B-1 along with the curve of daily-averaged intensities generated with the model. It is seen that the agreement is generally good. The one notable discrepancy is the absence in the measurements of an intensity peak corresponding to the Shot PISONIA deposition on July 18. Because that intensity excursion lasted only about 2 hours and the PHS readings were not continuous but taken periodically throughout the day, it is likely that they simply missed this brief event. The fact that the calculated values progressively overestimate the intensity with increasing time between/after shots most likely results from the omission of weathering effects in the intensity model.

The detailed information on the HARDTACK I fallout events (Minkkinen et al., 1959) for Parry Island is not available for Enewetak Island. However, PHS (1958) provides daily averages of intensity readings on Enewetak Island from May 19 through July 31, 1958, as shown in Figure B-2. These data indicate that the intensities on Enewetak Island were somewhat less than those on Parry Island. The model described above for Parry Island is adapted for application to Enewetak Island exposures as follows. It is assumed that the fallout deposition on Enewetak Island from the Bikini-based Shot REDWOOD was the same as that on Parry Island. For the combined FIR-KOA event and the Enewetak-based Shot OAK, the time profiles are retained but the intensity readings are scaled to achieve best fit to the PHS data. Thus, the FIR/KOA intensities are reduced to 75 percent of the values for Parry Island, while the OAK intensities are reduced to 30 percent of the Parry Island values. These reductions are not unreasonable, since Enewetak Island was farther from the relevant local detonation sites than was Parry Island. The resulting model output is compared with the PHS data in Figure B-1. As noted with respect to Figure B-2, the overestimation of intensity between and after shots most likely results from weathering effects which are not included in the intensity model.

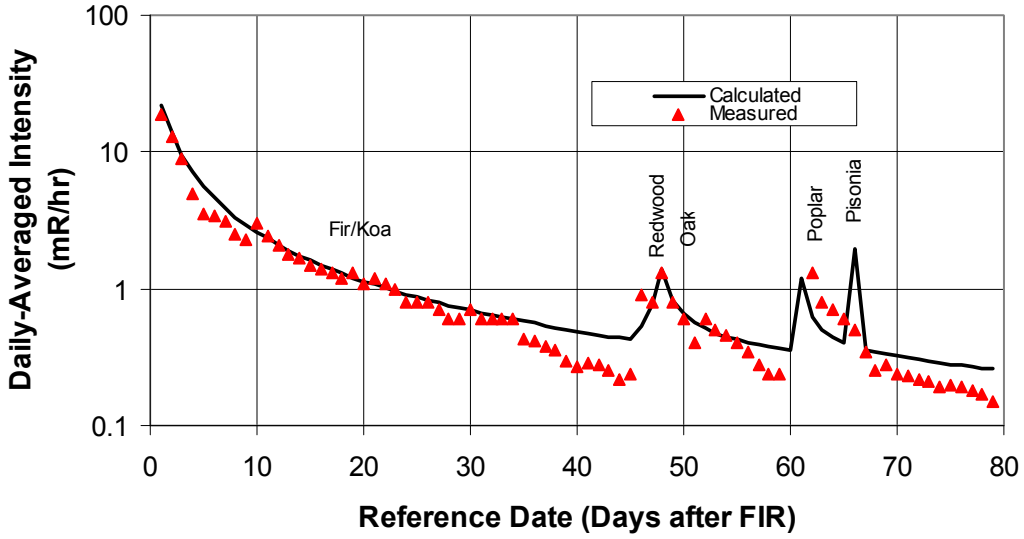

Figure B-1. Comparison of Parry Island Intensity Model with PHS Measurements

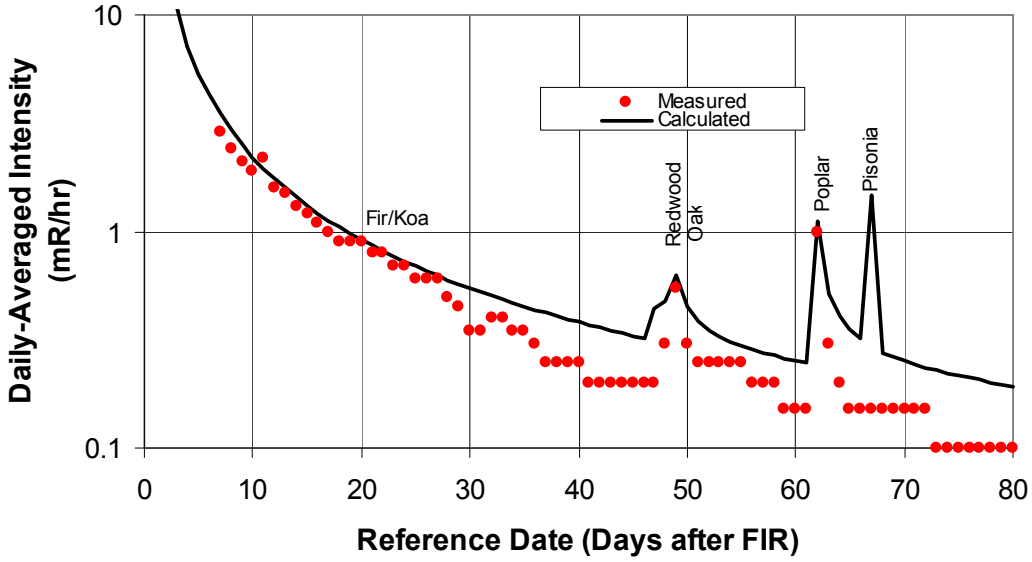

Figure B-2. Comparison of Enewetak Island Intensity Model with PHS Measurements

External Dose: Approach

Film Badge Data

About 18,000 test participants received film badge dosimetry during HARDTACK I to measure exposure to external gamma radiation, and approximately 62,000 individual film badges were issued and processed. Most participants had such dosimetry throughout their period of service at EPG. The film packets used at HARDTACK I were designed to measure exposures up to 800 roentgen (R) with a minimum detectable exposure of approximately 0.04 R. A study of the HARDTACK I film badge design and the calibration, issue, exchange, and processing procedures utilized during the operation concluded that the dosimetry, while generally reliable, over-reported exposures by about 20 percent due to environmental effects in the hot, humid Pacific test area. (NRC, 1989)

Complete files of film badge data were obtained for the two Army detachments. The databases were then processed to (1) correct for apparent inconsistencies in the recorded return dates of some badges and (2) distill the records to a subset that most likely represent valid readings of those personnel continuously resident on Enewetak Island throughout the operation. In the first step, the return dates of badges were revised, when necessary, to correspond to the issue dates of subsequently issued badges. (This was done under the assumption that the return of a badge and the issue of the next occurred concurrently.) The second step involved screening all badge entries and eliminating from further consideration those records that fall into one or more of the following categories:

- Badges without return dates recorded in the database (indicative of lost or damaged badges);
- Badges with anomalous zero readings (i.e., those issued for periods when island residents are known to have been exposed to residual radiation);
- Complete sets of badges for those personnel with unusual or confusing badge sequences (taken as an indicator of an unusual duty assignment);
- Badges that required excessive adjustments in return date (typically greater than 10 days) to accomplish (1) above;
- Badges with identification numbers lower than those used for the initial general issue (lower than #27442 for the Administrative Detachment and lower than #31042 for the Operations Detachment; badges falling into this group were apparently issued to personnel with more specialized assignments than the general population);
- Badges for personnel known to have been assigned to duty on Japtan Island (all such personnel were previously identified).

The badges remaining in the database after this screening process were then sorted by issue and/or return date and the exposure statistics compiled. The statistics thus derived for badges issued on or about April 12, 1958, before the first fallout event of the series (May 14), are summarized in Table B-1 for turn-in date groupings that have sample sizes of ten or more, identified as “subunits.”

Table B-1. Film Badge Data for HARDTACK I Army Subunits

Parent Unit(*)	FB Turn-in Date (1958)	Subunit Size	Average FB Dose (mrem)	Unbiased Average FB Dose (mrem)	Unbiased FB Standard Deviation (mrem)	Relative Error (%)
AD	May 31	41	642	535	88	17
OD	May 31	24	687	573	122	21
OD	Jun 4	45	1074	895	154	17
AD	Jun 5	16	907	756	173	23
OD	Jun 5	36	1072	893	193	22
AD	Jun 7	28	1303	1086	150	14
AD	Jun 10	33	1174	978	135	14
OD	Jun 10	69	1269	1058	195	18
OD	Jun 11	43	1653	1378	307	22
OD	Jun 12	93	864	720	163	23
OD	Jun 13	16	1573	1311	288	22
AD	Jun 17	18	1328	1107	133	12
AD	Jun 27	121	1202	1002	189	19
AD	Jun 28	108	1303	1086	166	15
AD	Jun 29	22	1201	1001	189	19
AD	Jul 7	22	1207	1006	238	24

(*) AD: Administrative Detachment OD: Operations Detachment

Monte Carlo-Based Dose Reconstruction

External gamma dose reconstruction for Army units stationed on Enewetak Island during Operation HARDTACK I was accomplished by incorporating uncertainty distributions for various parameters into the model discussed in Section 3. Time-dependent radiological decay for the uncertainty analysis was modeled using shot-specific decay functions derived with the FIIDOS code (Raine et al., 2007). The specific parameters used in both the deterministic and uncertainty analyses of external dose are shown in Table B-2.

Table B-2. Input Parameter Specification for External Gamma Dose Reconstruction, Case Study #2

Parameter	Definition	Distribution for Probabilistic Analysis (*)	Nominal Value for Central Estimation	Deterministic(**)
SHOT MIXTURE FRACTION				
Fallout Composition	Fallout proportion from each shot (applies to FIR/KOA only)	Triangular min=0 peak=0.4 max=1 for FIR fraction	Intensity data based on 0.4/0.6 mixture of FIIDOS-derived FIR/KOA intensity functions	Intensity data based on time-dependent decay exponents for FIR/KOA mixture
EXTERNAL DOSE MULTIPLIER (EDM) FOR LAND-BASED PERSONNEL				
F_{os}	Fraction of time spent outside	Triangular min = 2/24 peak = 8/24 max = 16/24	0.34 (or 8/24)	0.6 (or 14.4/24)
F_t	Fraction of inside time spent in tent	Triangular min = 0 peak = 0.5 max = 1	0.5	0
PF_t	Protection factor for tent	Numerical model (see Section 4.2.2) $\mu = 1.4$ UB95 = 1.9	1.4 (median of distribution)	1.5
PF_b	Protection factor for building	Numerical model (see Section 4.2.2) $\mu = 2.1$ UB95 = 3.9	2.0 (median of distribution)	2.0
I_i	Intensity of fallout near outdoor location (i=1), tent location (i=2), and building location (i=3) frequented by veteran, normalized to the intensity averaged over entire island	Lognormal GM = 1.0 GSD = 1.5	1.0	1.0
INTENSITY MEASUREMENTS FOR LAND-BASED PERSONNEL				
I_m	Measured intensities	Normal $\mu = I_m$, $\sigma = 0.3 \cdot I_m$ (to account for measurement error)	1.0	1.0
a	Exponent of multiplicative error factor $(t/t_0)^{\pm a}$ applied to FIIDOS-generated intensity functions	Normal $\mu = 0$ $\sigma = 0.15$	0	0

(*) μ = arithmetic mean; σ = standard deviation; GM = geometric mean; GSD = geometric standard deviation; UB95 = upper bound at the 95th percentile.
(**) High-sided per guidance in NTPR Policy and Guidance Manual (DTRA, 2007).

External Dose Results

Dose distributions were derived for a sample size of 10,000 for the film badge turn-in dates identified in Table B-1. The sample dose distribution shown in Figure B-3 is for personnel who returned their badges on June 12. The relative frequency (probability density function) is shown in Figure B-3 and the Probability Plot is shown in Figure B-4. The distributions for the other badge turn-in dates have very similar lognormal shapes.

The Monte Carlo-derived (arithmetic) mean and 95th percentile doses for each subunit are listed in Table B-3. Also provided for comparison are similar statistics based on the distribution of film badge doses, NTPR deterministic doses, and NTPR upper bound doses calculated using the 3× upper bound convention. The last column displays the ratio of the deterministic upper bound dose to the probabilistic 95th percentile dose. It is seen that both the probabilistic and deterministic approaches compute mean doses that are generally consistent with the average film badge doses of the various subunits. The deterministic upper bound doses exceed the probabilistic 95th percentile doses by a nearly constant factor of 1.5; the latter doses exceed the 95th percentile film badge doses for all subunits except one.

From a total of 735 film badges issued to all subunits, only 2 (or 0.3%) exceed the 95th percentile doses of the respective subunits. Both of these high readings come from the Operations Detachment subunit that turned their badges in on June 11.

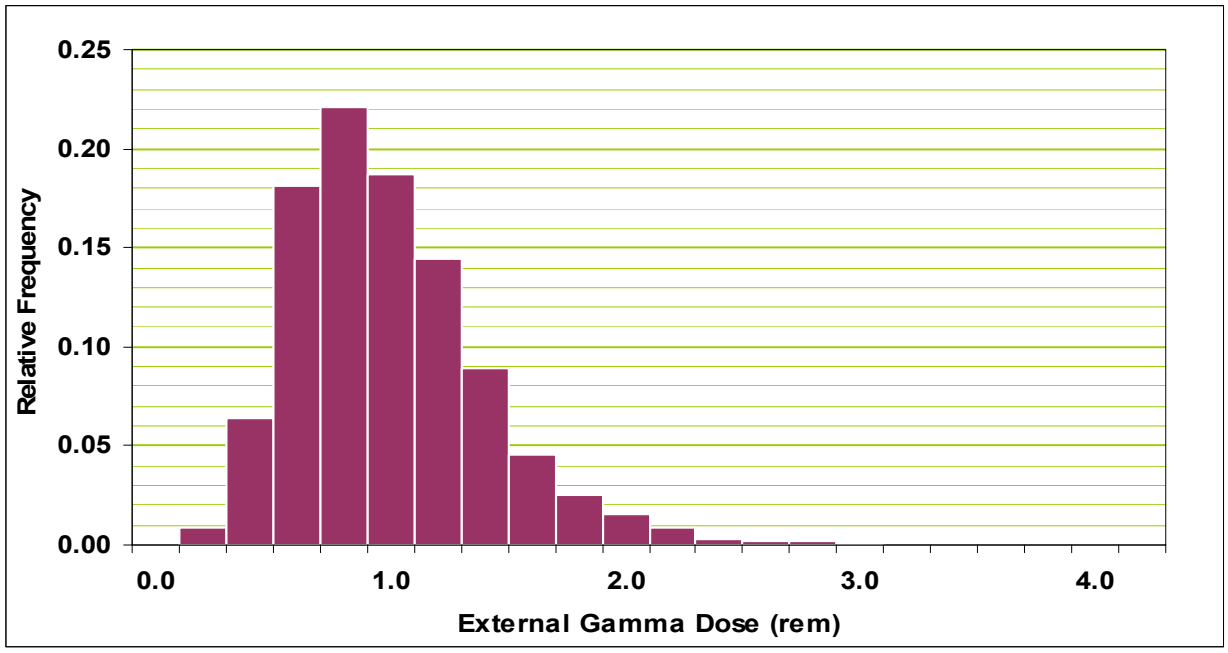

Figure B-3. Distribution of Estimated External Gamma Doses for Army Personnel at Enewetak Island during Operation HARDTACK I (Turn-in Date: June 12)

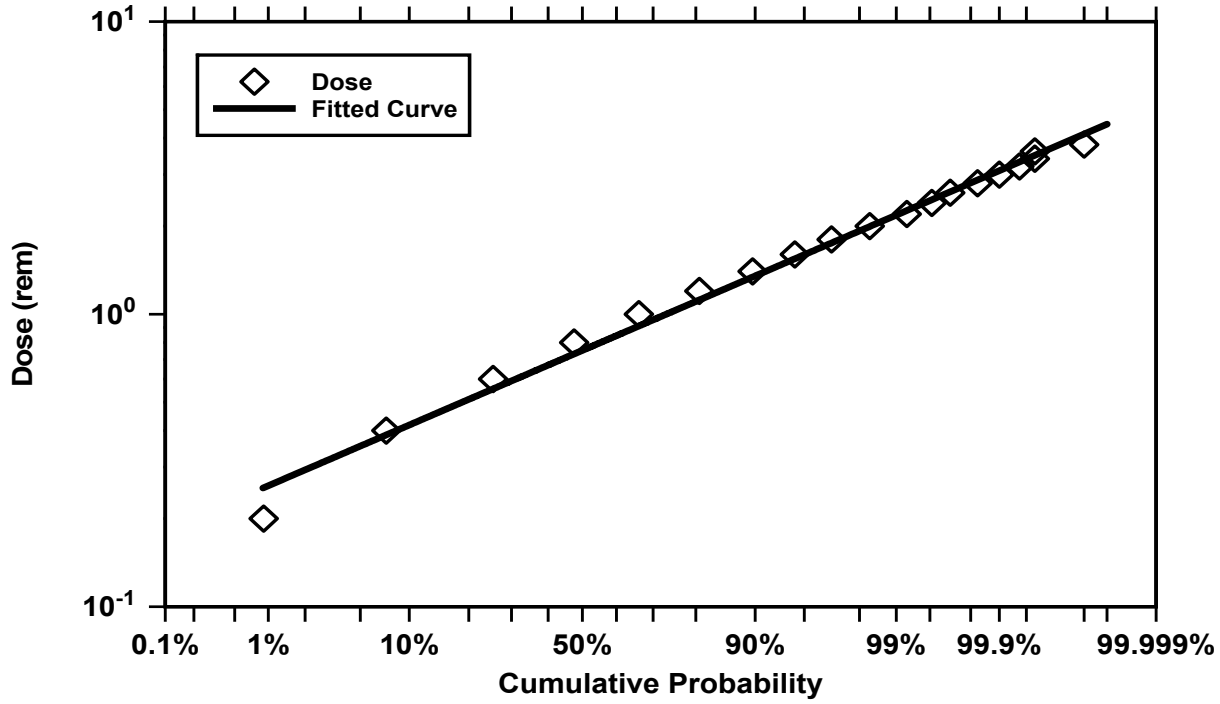

Figure B-4. Probability Plot Estimated External Gamma Doses for Army Personnel at Enewetak Island during Operation HARDTACK I (Turn-in Date: June 12)

Table B-3. Summary of External Doses for Army Subunits Stationed at Enewetak Island during HARDTACK I

Parent Unit	FB Turn-in Date (1958)	Dose (rem)			Upper Bound (NTPR) or 95th Percentile Doses (rem)			
		Mean FB	Mean MC	NTPR Det.	FB	MC	NTPR UB	Ratio NTPR UB/ MC
AD	May 31	0.54	0.889	0.85	0.74	1.65	2.6	1.6
OD	May 31	0.57	0.889	0.85	0.76	1.65	2.6	1.6
OD	Jun 4	0.89	0.939	0.90	1.15	1.75	2.7	1.5
AD	Jun 5	0.76	0.950	0.91	1.04	1.77	2.7	1.5
OD	Jun 5	0.89	0.950	0.91	1.26	1.77	2.7	1.5
AD	Jun 7	1.09	0.970	0.93	1.38	1.82	2.8	1.5
AD	Jun 10	0.98	0.997	0.95	1.18	1.87	2.9	1.5
OD	Jun 10	1.06	0.997	0.95	1.38	1.87	2.9	1.5
OD	Jun 11	1.39	1.01	0.96	1.85	1.88	2.9	1.5
OD	Jun 12	0.72	1.01	0.97	0.97	1.90	2.9	1.5
OD	Jun 13	1.31	1.02	0.98	1.84	1.91	2.9	1.5
AD	Jun 17	1.11	1.05	1.00	1.28	1.97	3.0	1.5
AD	Jun 27	1.00	1.10	1.05	1.28	2.09	3.1	1.5
AD	Jun 28	1.09	1.12	1.05	1.40	2.10	3.2	1.5
AD	Jun 29	1.00	1.12	1.06	1.25	2.11	3.2	1.5
AD	Jul 7	1.01	1.17	1.10	1.49	2.20	3.3	1.5

FB: film badge dose
MC: dose from the probabilistic model (Monte Carlo simulation)
Det.: dose from the deterministic model (NTPR)

Internal Dose: Approach

Internal dose reconstruction for Army units stationed on Enewetak Island during Operation HARDTACK I was accomplished by incorporating uncertainty distributions for various parameters into the models discussed in Section 3. These models incorporate the fallout-induced radiation environments discussed above, the fallout intensity decay model discussed in Section 3, and various other parameters discussed in Sections 3 and 4. The specific parameters used in both the deterministic and probabilistic analyses are shown in Table B-4.

Table B-4. Input Parameter Specification for Internal Dose Reconstruction, Case Study #2

Parameter	Definition	Distribution for Probabilistic Analysis	Nominal Value for Central Estimation	Deterministic(*)
INTERNAL DOSE (GENERAL)				
DCFInhα *DCFIngα*	Inhalation and ingestion dose conversion factors for fallout α emitters	*DCF*s calculated with FIIDOS multiplied by Lognormal with GM=1.0, GSD=5.19	*DCF*s calculated with FIIDOS (see Section 4.2.8)	DCFs calculated with FIIDOS (see Section 4.2.8)
DCFInhβγ *DCFIngβγ*	Inhalation and ingestion dose conversion factors for fallout β+γ radiation	*DCF*s calculated with FIIDOS multiplied by Lognormal with GM=1.0, GSD=4.05	*DCF*s calculated with FIIDOS (see Section 4.2.8)	DCFs calculated with FIIDOS (see Section 4.2.8)
Biasα	Bias factors to adjust high-sided inhalation DCF values	Assigned Constant α: 1.3 for each organ	α: 1.3 for each organ	1.0
Biasβγ		βγ: 1.2 for thyroid & LLI, 1.35 for lung	βγ: 1.2 for thyroid & LLI, 1.35 for lung	1.0
BR	Breathing rate	Triangular distribution derived from USEPA (1997) data (see Section 4.2.7): min = 0.33 $m^3\ hr^{-1}$ peak = 1.53 $m^3\ hr^{-1}$ max = 2.79 $m^3\ hr^{-1}$	Mean of Distribution ~1.5 $m^3\ hr^{-1}$	1.2 $m^3\ hr^{-1}$
DESCENDING INHALATION DOSE (†)				
RND_{Res1}	Deposition fractions for particle sizes deposited in Regions BB, bb, and AI	1.0 (assumed constant)	1.0 (assumed constant)	n/a
RND_{Res2}		Lognormal: GM, GSD 0.0056, 1.744	Geometric Mean 0.0056	
RND_{Res3}		Lognormal: GM, GSD 0.001, 1.65	0.001	
$RND_{Nonres1}$	Deposition fractions for particle sizes deposited in Region ET_2 and cleared to digestive tract	0.0 (assumed constant)	0.0 (assumed constant)	n/a
$RND_{Nonres2}$		Lognormal: GM, GSD 0.363, 1.106	Geometric Mean 0.363	
$RND_{Nonres3}$		Lognormal: GM, GSD 0.285, 1.185	0.285	
V_1	Particle settling velocities	Logtriangular min, peak, max (cm s^{-1}) 0.22/2, 0.22, 27.8	0.22 cm s^{-1}	10^6(cm)/T(sec)
V_2		0.83/2, 0.83, 27.8	0.83 cm s^{-1}	
V_3		13.0/2, 13.0, 27.8	13.0 cm s^{-1}	

Parameter	Definition	Distribution for Probabilistic Analysis	Nominal Value for Central Estimation	Deterministic(*)
AF_{100}	Surface activity fraction <100 μm particles	Triangular (min,peak,max) FIR/KOA (1.000, 1.000, 1.000) REDWOOD (0.609, 0.787, 0.971) OAK (0.469, 0.732, 0.975)	Peak of Distributions FIR/KOA 1.000 REDWOOD 0.787 OAK 0.732	1.0
$frac_1$	Surface fraction of Class 1–2 from 1–100 μm particles	Triangular Min, peak, max 0, 0.00136, 0.01	Peak of Distribution 0.00136	n/a
$frac_2$		0, 0.025, 0.1	0.025	
RESUSPENDED INHALATION DOSE				
$K(t)$	Time-dependent resuspension factor	Lognormal multiplier of Anspaugh equation GM=1, GSD=4.05	Anspaugh equation	Till and Meyer, 1983
INCIDENTAL INGESTION DOSE				
q_{ing}	Soil ingestion rate	Triangular min, peak, max ($mg\ d^{-1}$) 10, 100, 500	Peak of Distribution 100 $mg\ day^{-1}$	500 $mg\ day^{-1}$
ρ_{soil}	Soil bulk density	Triangular $g\ cm^{-3}$ Min, peak, max 1.3, 1.45, 1.6	Peak of Distribution 1.45 $g\ cm^{-3}$	1.3 $g\ cm^{-3}$

(*) High-sided per guidance in NTPR Policy and Guidance Manual (DTRA, 2007).
(†) AMAD particle size classes: 1 = 1–10 μm, 2 = 10–20 μm, 3 = 20–100 μm.

Internal Dose Results

Distributions of fifty-year committed equivalent doses (CED) for three organs, thyroid, lung, and lower large intestine (LLI) wall, were derived using the refined uncertainty model for a sample size of 10,000. Examples of these results are shown in Figure B-5 through Figure B-8, where the relative frequencies and probability plots of CED to the LLI wall from alpha radiation and from beta plus gamma radiation, respectively, are shown. The CED distributions are lognormal, as indicated by their Gaussian (bell) shapes when plotted on a logarithmic axis and the straight-line nature of their probability plots.

The geometric mean and 95th percentile CEDs of the various distributions are given in Table B-5, along with corresponding doses derived deterministically. The ratio of the deterministic upper bound CED to the probabilistic 95th percentile CED, provided in the rightmost column, ranges from 1.8 to 4.6 for the organs reported.

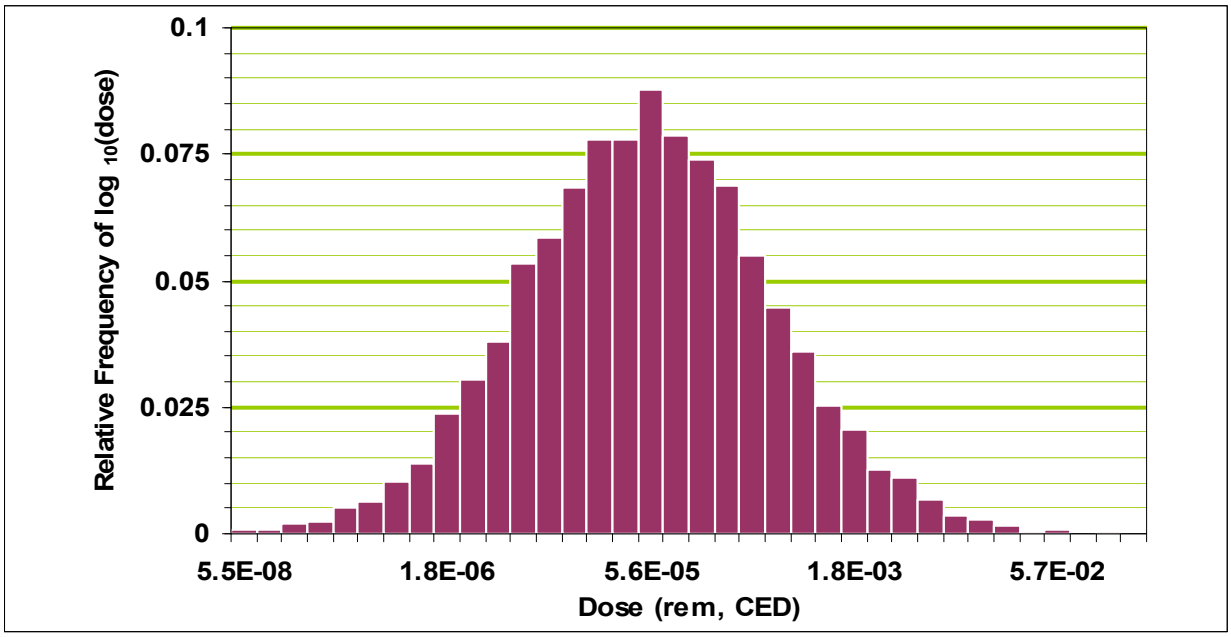

Figure B-5. Distribution of Estimated LLI Wall Doses from Alpha Radiation for Army Personnel at Enewetak Island during Operation HARDTACK I

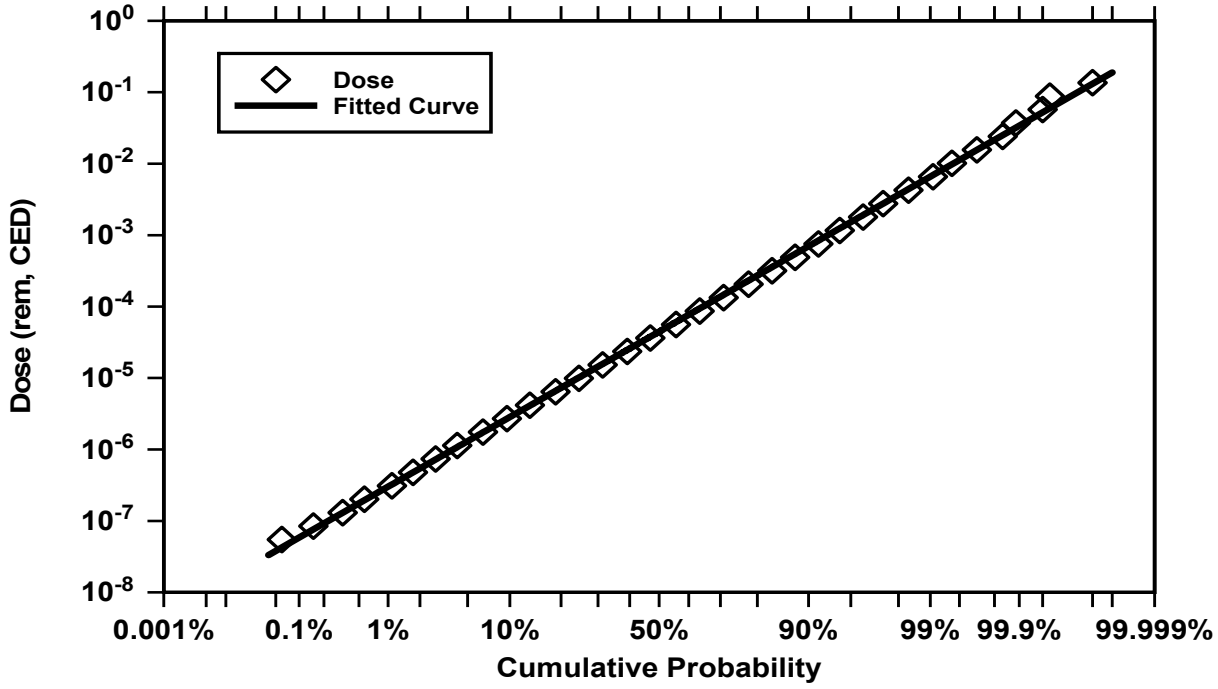

Figure B-6. Probability Plot of Estimated LLI Wall Doses from Alpha Radiation for Army Personnel at Enewetak Island during Operation HARDTACK I

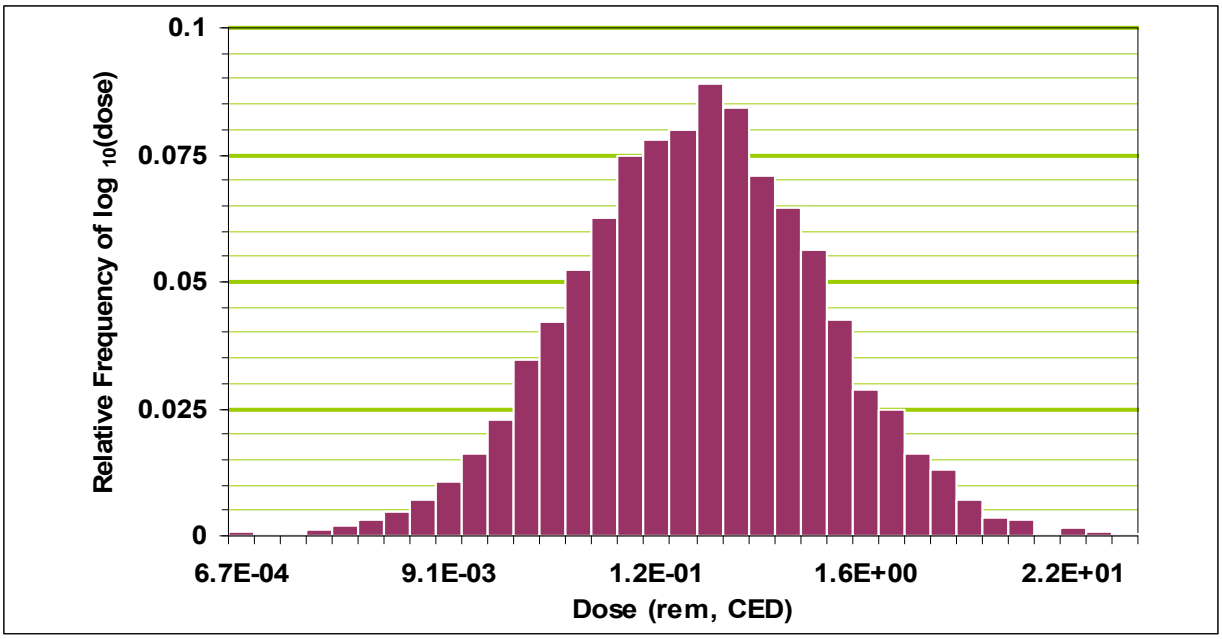

Figure B-7. Distribution of Estimated LLI Wall Doses from Beta plus Gamma Radiation for Army Personnel at Enewetak Island during Operation HARDTACK I

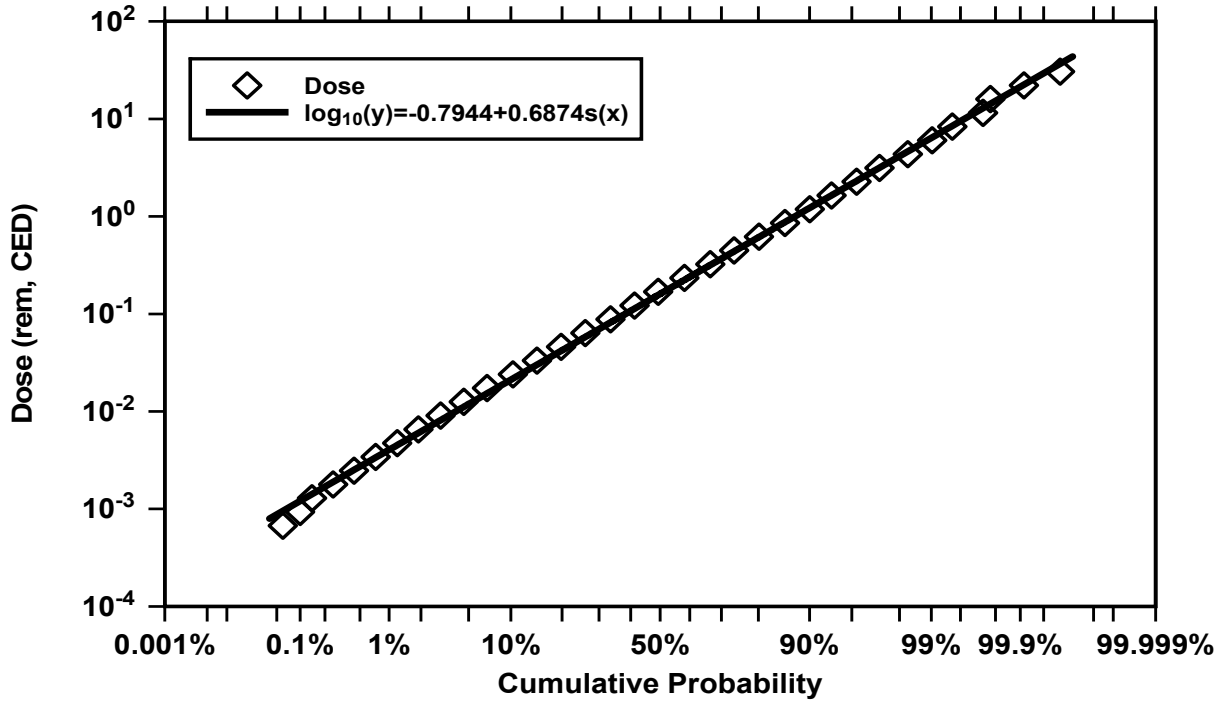

Figure B-8. Probability Plot of Estimated LLI Wall Doses from Beta plus Gamma Radiation for Army Personnel at Enewetak Island during Operation HARDTACK I

Table B-5. Summary of Internal Dose for Army Personnel at Enewetak Island during Operation HARDTACK I

Organ	Mean Dose (rem)		Upper Bound Dose (rem)		
	Probabilistic*	Deterministic (NTPR)	Probabilistic (95th Percentile)	Deterministic (NTPR Upper Bound)	Ratio (Deterministic ÷ Probabilistic)
Alpha Dose					
Thyroid	0.000040 (8.5)	0.00036	0.0014	0.0036	2.6
Lung	0.00054 (8.6)	0.0049	0.019	0.049	2.6
LLI wall	0.000042 (8.3)	0.00036	0.0014	0.0036	2.5
Beta plus Gamma Dose					
Thyroid	0.24 (4.7)	0.57	3.0	5.5	1.8
Lung	0.030 (6.5)	0.31	0.67	3.1	4.6
LLI wall	0.17 (4.7)	0.40	2.1	3.9	1.8

* Geometric mean and (geometric standard deviation) are shown for probabilistic analysis results.

References

DTRA (Defense Threat Reduction Agency), 2007. Policy and Guidance Manual – Nuclear Test Personnel Review Program. Revision 7, (Defense Threat Reduction Agency, Fort Belvoir, VA), November 26, 2007.

Gladeck, F.R., Gould, K.G., Hallowell, J.H., Martin, E.J., McMullan, F.W., Miller, R.A., Osborn, M.J., Shelton, C.F., Berkhouse, L., and Calhoun, F.S., 1982. Operation HARDTACK I (1958). DNA 6038F (Defense Nuclear Agency, Washington, D.C.).

Glasstone, S., and Dolan, P. J., 1977. *Effects of Nuclear Weapons*, 3rd Edition (U.S. Department of Defense and U.S. Department of Energy).

Goetz, J., Klemm, J., Thomas, C., and Weitz, R., 1985. Neutron Exposure for DoD Nuclear Test Personnel. DNA-TR-84-405 (Defense Nuclear Agency, Washington, D.C.).

Minkkinen, C., Schlacks, H. P., Goeke, R. H., and Weaver, C. L., 1959. Task Group 7.5 Radiological Safety Support, Operation HARDTACK, Phase I. OTO-58-3 (Holmes & Narver, Inc., Los Angeles, CA).

NRC (National Research Council), 1989. Film Badge Dosimetry in Atmospheric Nuclear Tests. (National Research Council, Washington, D.C.).

PHS (US Public Health Service), 1958. Report of Public Health Service Off-Site Radiological Monitoring Data, Operation Hardtack, Phase I. Report # 410975 (Public Health Service, Washington, D.C.).

Raine, D. A. III, Egbert, S. D., Stiver, J. H., and Case, D. R., 2007. FIIDOS—A Computer Code for the Computation of Fallout Inhalation and Ingestion Dose to Organs, Computer User's Guide (Revision 4). DTRA-TR-07-11 (Science Applications International Corporation, McLean, VA and Defense Threat Reduction Agency, Fort Belvoir, VA).

Thomas, C., 1991. REDWING Fallout Intensity Model. Internal memorandum (Science Applications International Corporation, McLean, VA).

Weitz, R. L., 1995. Dose Estimates for Residence Islands during Operation HARDTACK I. Memorandum to Defense Nuclear Agency (Science Applications International Corporation, McLean, VA).

Weitz, R. L., 2006. Analysis of 29 June 1958 Fallout Event at Operation HARDTACK I. Internal memorandum (Science Applications International Corporation, McLean, VA).

APPENDIX C Monte Carlo Analysis of Dose for Company E of the 4th Marine Corps Provisional Atomic Exercise Brigade (MCPAEB) Maneuver at Shot HOOD During Operation PLUMBBOB (1957)

Michael A. McKenzie-Carter

APPENDIX C Monte Carlo Analysis of Dose for Company E of the 4th Marine Corps Provisional Atomic Exercise Brigade (MCPAEB) Maneuver at Shot HOOD During Operation PLUMBBOB (1957)

Introduction

External and internal dose distributions were generated using probabilistic analysis techniques for a Nevada Test Site (NTS) participant unit case study and are documented in this Appendix. The unit participated in a maneuver during Shot HOOD of Operation PLUMBBOB in 1957. The probabilistic and deterministic (NTPR) dose model parameters are described and results of the upper bound doses are compared for both external and internal reconstructed doses for members of the participating unit. The deterministic and probabilistic external dose results are also compared to the mean and upper bound values of available film badge readings for the unit.

Background

During Operation PLUMBBOB, 24 nuclear shots were fired and 6 safety experiments were conducted at the NTS from May 28 to October 7, 1957 (Harris et al., 1981; DNA, 1996). Table C-1 presents information on the nuclear shots that are relevant to this case study.

Table C-1. Data On Selected Operation PLUMBBOB Shots

Shot	1957 Date	Time	Type	Yield (kT)*	HOB† (ft)
BOLTZMANN	May 28	0455	Tower	12	500
WILSON	June 18	0455	Balloon	10	500
HOOD	July 5	0440	Balloon	74	1,500

* kiloton
† height of burst

The 4th Marine Corps Provisional Atomic Exercise Brigade (MCPAEB), or the "Brigade," conducted an exercise during Operation PLUMBBOB. The exercise took place over a period of slightly more than 2 weeks, during which the Brigade trained, rehearsed, experienced a misfire, and eventually observed and conducted maneuvers at Shot HOOD on July 5, 1957. The Brigade was organized as a standard air-ground task force totaling approximately 2,000 personnel. One unit of the Brigade is the subject of the special study described in this Appendix: Company E of the 2nd Battalion, 5th Marine Regiment, 1st Marine Division. (Frank et al., 1981)

The 2nd Battalion, 5th Marine Regiment constituted the infantry battalion assault force for the exercise, and was composed of 5 companies, each of which conducted somewhat different activities during portions of their participation. All of the Brigade troops arrived at Camp Desert Rock (CDR) by June 20, 1957, where they began preparing for a maneuver that was to be held in conjunction with Shot DIABLO, which was planned for June 27, 1957. A full rehearsal in the NTS forward area was conducted on June 20 and 21. On June 26, the Brigade was notified that DIABLO had been postponed until June 28. At 0430 on June 28, with the entire Brigade in

place, DIABLO misfired and all Brigade personnel returned to CDR. Instead of waiting for DIABLO, which had been rescheduled for July 12, the Brigade was assigned to conduct its maneuver on July 3, 1957, in conjunction with Shot HOOD. On July 2, based on a weather forecast, Shot HOOD was postponed until July 5. By 2230 on July 4, the Brigade had departed from CDR enroute to the forward area to maneuver in conjunction with HOOD. (Frank et al., 1981; USMC, 1957)

At 0440 on July 5, 1957, with the Brigade in its trenches 5,360 yards (3 miles) southwest of ground zero (GZ), Shot HOOD was detonated (Figure C-1). About 15 minutes later Company E, preceded and flanked by radiation safety personnel, began its march from the trenches in the direction of the HOOD GZ. Having approached to within 1,100 to 1,400 yards of the HOOD GZ, at which time they reached the Rad-Safe limit of 5 R/hr in that shot's neutron-activated radiation field, the company reversed its direction of march enroute back to the trenches. By 0700 the company had returned to the trench area, then marched to a nearby helicopter landing zone where it enplaned and was transported to a location about 7,000 yards (4.4 miles) to the west of the trenches. From there, the Company participated in a mock assault on a nearby objective. By 1430 they had marched to a nearby road from where they were transported by motor vehicle convoy back to CDR. Company E did not tour the HOOD display area on HOOD shot day. Most Brigade personnel had departed from CDR by July 6, 1957. (Frank et al., 1981; USMC, 1957)

Film Badge Data

A total of 12 film badge readings are available for Company E personnel for the period prior to and including Shot HOOD: 1200, 980, 760, 560, 560, 520, 520, 520, 500, 500, 500 and 480 (Frank et al., 1981). The mean of these 12 readings is 633 mrem.

Sources of External Exposure

Company E personnel were exposed to residual radiation during Operation PLUMBBOB while they were housed and trained at CDR, and also while participating in activities in the forward area of the NTS. The most significant source of external radiation exposure for members of Company E was neutron-activated radionuclides in the ground resulting from the detonation of HOOD, which the Marines traversed during the company's march toward the HOOD GZ. To model the intensity gradient from this source, an intensity array was developed that described the intensities encountered during traversal of the radiation field. The primary source of intensity data was the H+1 iso-intensity lines plotted for the HOOD test area, as depicted in Figure C-1 (Figure 4-3 of Frank et al., 1981). For use in subsequent time-dependent equations, these intensities were converted to H+0 intensities, using Equation C-1.

$$Int_0 = \frac{Int_{1hr}}{0.668 \cdot \left(e^{-\lambda_{Na24} \cdot 1hr}\right) + 0.274 \cdot \left(e^{-\lambda_{Mn56} \cdot 1hr}\right) + 0.058 \cdot \left(e^{-\lambda_{K42} \cdot 1hr}\right)} \qquad \text{(C-1)}$$

where:

Int_0 = H+0 intensity (R hr^{-1})

Int_{1hr} = H+1 intensity (R hr^{-1})

λ_{Na24} = decay constant for Na-24 (0.0462 hr^{-1})

λ_{Mn56} = decay constant for Mn-56 (0.269 hr^{-1})

λ_{K42} = decay constant for K-42 (0.0559 hr^{-1})

The values 0.668, 0.274, and 0.058 are the initial fractional contributions to intensity of Na-24, Mn-56, and K-42, respectively. Although accurate values for initial fractional contributions depend on site-specific conditions, the use of these average values does not significantly affect the calculations.

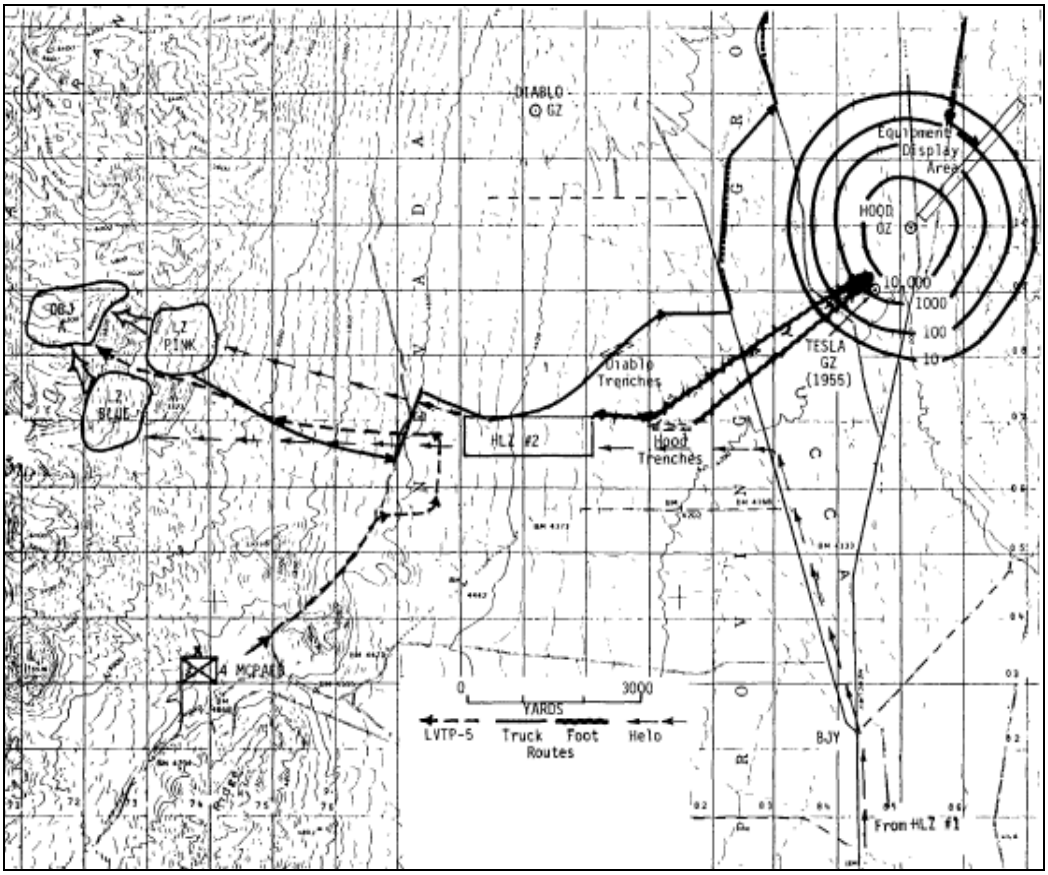

Figure C-1. Shot HOOD Residual Radiation (mrem hr^{-1} at H+1) and MCPAEB Movements (Frank et al., 1981)

Using a start time (ST) and march rate (Rate) from Frank et al. (1981), the distances to each iso-intensity line and the times of arrival at each iso-contour line were calculated. From these times and the H+0 intensities, an array was created defining the intensities encountered at the location of each iso-intensity line at the time of traversal, using equation C-2.

$$Int_{en\,i} = Int_{0_i} \cdot \left[0.668 \cdot \left(e^{-\lambda_{Na\,24} \cdot t_i}\right) + 0.274 \cdot \left(e^{-\lambda_{Mn\,56} \cdot t_i}\right) + 0.058 \cdot \left(e^{-\lambda_{K\,42} \cdot t_i}\right)\right] \quad \text{(C-2)}$$

where, in addition to previously-defined variables:

Int_{eni} = intensity encountered at each iso-intensity line (R hr^{-1})

t_i = time each iso-intensity line was encountered during approach toward the HOOD GZ and return toward the trenches (hr)

Equation C-1 was also used to calculate the H+0 intensity at the location the Rad-Safe limit was reached, using the calculated time this point was reached. A logarithmic fitting function was then used with the array calculated with Equation C-2 to create a time-dependent function for the intensities encountered by Company E. The H+1 intensities, corresponding H+0 intensities, nominal H+ times each iso-contour line was traversed, and encountered intensities are listed in Table C-2.

Fallout from shots BOLTZMANN and WILSON were also sources of external exposure. During the rehearsal, DIABLO misfire, and maneuver at HOOD, the Brigade personnel likely operated in NTS forward areas where fallout from these shots had deposited. The test areas for shots DIABLO and HOOD were relatively close (the DIABLO trenches used for the rehearsal and misfire were located about 1,500 yards from the HOOD trenches), and therefore the activities conducted during the rehearsal and misfire took place very near the area eventually used during Shot HOOD. Fallout from Shot WILSON had also descended at CDR on June 18, prior to the arrival of most Brigade personnel. (Frank et al., 1981; Maag et al., 1983)

Fallout intensities that are relevant to each primary activity of Company E in forward test areas and at CDR are characterized in Table C-3. Radiological decay for the deterministic calculations was modeled as $t^{-1.2}$. For the probabilistic model, radiological decay was determined from shot-specific fallout decay functions using the FIIDOS software (Raine et al., 2007).

Table C-2. Deterministic Intensities (R hr^{-1}) and Times (hr) Associated with Traversal of Shot HOOD Test Area by Company E

Location	H+1 Intensity† at Location	H+0 Intensities at Location	H+ Time Location Was Reached	Intensities Encountered at Location
Depart trenches	0.00	0.000	0.25	0.000
0.01 R hr^{-1} Iso-intensity line (Approach)	0.01	0.011	0.85	0.010
0.1 R hr^{-1} Iso-intensity line (Approach)	0.10	0.111	0.92	0.101
1 R hr^{-1} Iso- intensity line (Approach)	1.00	1.11	1.00	1.00
Rad-Safe Limit (Arrival)	5.03	5.58	1.06	5‡
Rad-Safe Limit (Departure)	5.03	5.58	1.13	4.97
1 R hr^{-1} Iso- intensity line (Return)	1.00	1.11	1.19	0.982
0.1 R hr^{-1} Iso- intensity line (Return)	0.10	0.111	1.27	0.097
0.01 R hr^{-1} Iso- intensity line (Return)	0.01	0.011	1.34	0.010
Arrive trenches	0.00	0.000	1.94	0.000

† H+1 intensity at each iso-intensity line was obtained from an iso-intensity plot.
‡ This intensity is the measured Rad-Safe limit.

Table C-3. Fallout Intensities for Company E in Forward Test Areas and at CDR

Activity/Source of Fallout	Intensity*	Reference
Rehearsal and Misfire (near the DIABLO trenches)		
BOLTZMANN	0.001 R hr^{-1*} at H+1 (deterministic) 0.0004 R hr^{-1*} at H+1 (probabilistic)	Figure 168, Hawthorne (1979) Figure 168, Hawthorne (1979)
WILSON	0.01 R hr^{-1} at H+12	Figure 4-2, Frank et al. (1981)
HOOD Maneuver (near the HOOD trenches)		
BOLTZMANN	0.01 R hr^{-1} at H+1 (near HOOD trenches) 2 R hr^{-1} at H+1 (1000-2000 yd from HOOD GZ)	Figure 168, Hawthorne (1979) Figure 168, Hawthorne (1979)
WILSON	0.045 R hr^{-1} at H+12	Figure 4-2, Frank et al. (1981)
Camp Desert Rock		
WILSON	0.0004 R hr^{-1} at H+12.9	Placak et al. (1957)

* Except where indicated, listed intensities were used for both the deterministic and probabilistic models

Values for other parameters used in both the deterministic and probabilistic external analyses are shown in Table C-4. Intensities encountered during the maneuver for the probabilistic analysis were calculated using Equation C-2, with arrival times derived probabilistically according to variable definitions in Table C-4. Modeled correlations associated with these parameters in the probabilistic analysis are identified and discussed in Appendix G.

Reconstructed External Doses

A probabilistic dose reconstruction for Company E personnel was accomplished by incorporating distributions of uncertainty and variability for model input parameters discussed in Section 3 and 4 of this report. The distribution of results for 10,000 probabilistic simulations of the dose calculations is shown in Figure C-2, and is supplemented with a probability plot in Figure C-3. Key statistics from the distribution are compared with those of the deterministic (NTPR) model in Table C-5. These results show that the deterministic dose and the geometric mean dose from the probabilistic analysis are identical, and are the same as the external dose previously reported in an analysis done for NTPR (Frank et al., 1981). Both are comparable to but less than the arithmetic mean of the probabilistic analysis and the mean film badge reading of available film badge readings for Company E. The neutron-activated radionuclides in the soil resulting from the detonation of Shot HOOD resulted in approximately 96% of the external gamma dose to personnel of Company E. Fallout from previous shots at various locations resulted in the remaining external dose. The doses in Table C-5 also show that the 95th percentile dose from the probabilistic analysis is lower than the upper bound deterministic dose, indicating that the generic upper bound uncertainty factor of 3 used in the deterministic model results in a conservative estimate of the upper bound dose for Company E cohort at Shot HOOD, Operation PLUMBBOB. The deterministic upper bound dose is 70 percent higher that the 95th percentile probabilistic dose.

Table C-4. Input Parameters for External Gamma Dose Reconstruction,Case Study #3

Parameter	Definition	Distribution for Probabilistic Analysis	Nominal Value for Central Estimation	Deterministic*
DATES AND TIMES				
$Date_{Arrived}$	CDR start date[time]	Triangular min=19 Jun[0800] peak=19 Jun[1600] max=20 Jun[1600]	19 Jun[1600]	19 Jun[0800]
$Date_{Departed}$	CDR end date[time]	Triangular min=5 Jul[1800] peak=6 Jul[0800] max=6 Jul[2400]	6 Jul[0800]	6 Jul[2400]
EXTERNAL DOSE				
F_{os}	Fraction of time spent outside at CDR	Triangular min=5/24 peak=12/24 max=18/24	0.5 (or 12/24)	0.6 (or 14.4/24)
PF_t	Protection factor for a tent	Numerical model (see Section 4.2.2)	1.4 (median of distribution)	1.5
I_i	Intensity distribution of fallout while outdoors (i=1) and indoors (i=2) normalized to average CDR intensity	Lognormal (GM=1.0; GSD=1.5) (used with F_{os} and PF_t)	1.0	1.0
INTENSITIES				
I_m	Measured intensities (CDR and Rad-safe limit)	Normal (mean=I_m; SD=0.304 · I_m)	see Table C-2 and Table C-3	see Table C-2 and Table C-3
Contour intensities	Intensities obtained from iso-intensity plots (all forward test area intensities)	Interpolated values: Lognormal (GM=1.0; GSD=1.95) Extrapolated values: Lognormal (GM=1.0; GSD=4.05)	see Table C-2 and Table C-3	see Table C-2 and Table C-3
a	Exponent of multiplicative error factor $(t/t_0)^{\pm a}$ applied to FIIDOS-generated fallout intensity functions	Normal (mean=0; SD=0.15)	0	0
MANUEVER PARAMETERS				
ST	Start time of maneuver	Normal (mean=15; SD=1.83)	H+15 min	H+15 min
$Rate$	Walk rate during maneuver	Triangular (min=50, peak=70, max=100)	70 yd min^{-1}	88 yd min^{-1}
LT	Linger time at Rad-Safe limit location	Triangular (min=1,peak=2, max=10)	2 min	4.1 min

* High-sided per guidance in NTPR Policy and Guidance Manual (DTRA, 2007).

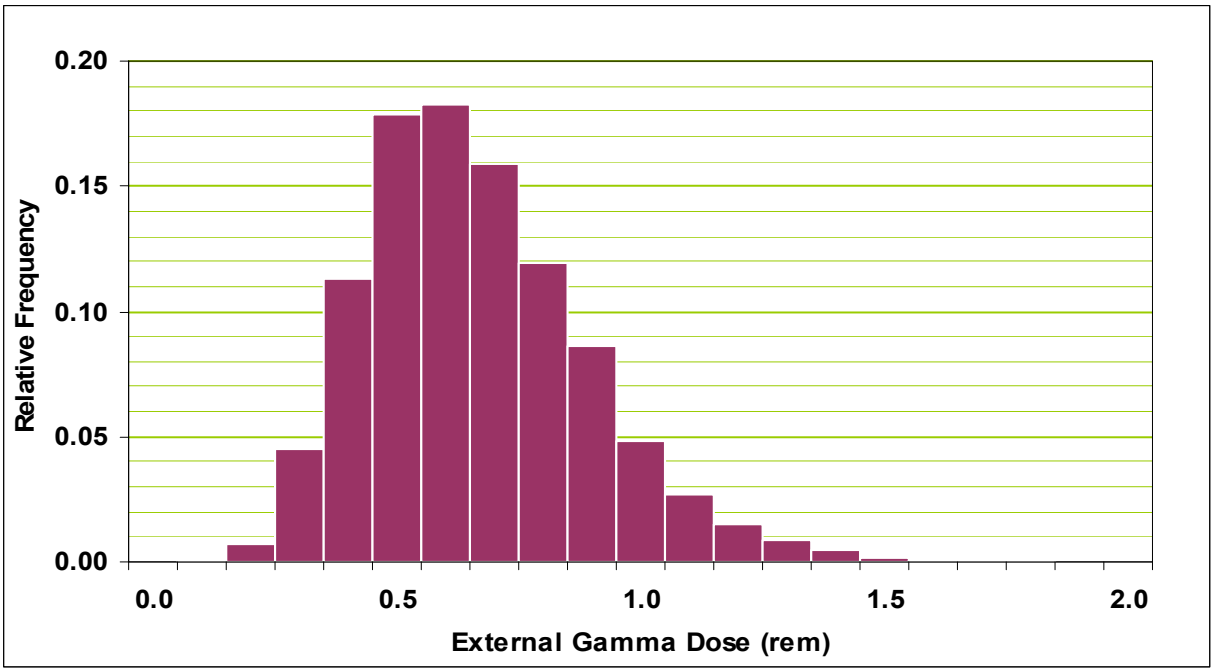

Figure C-2. Distribution of Estimated External Gamma Dose for Company E Personnel at the NTS during Operation PLUMBBOB

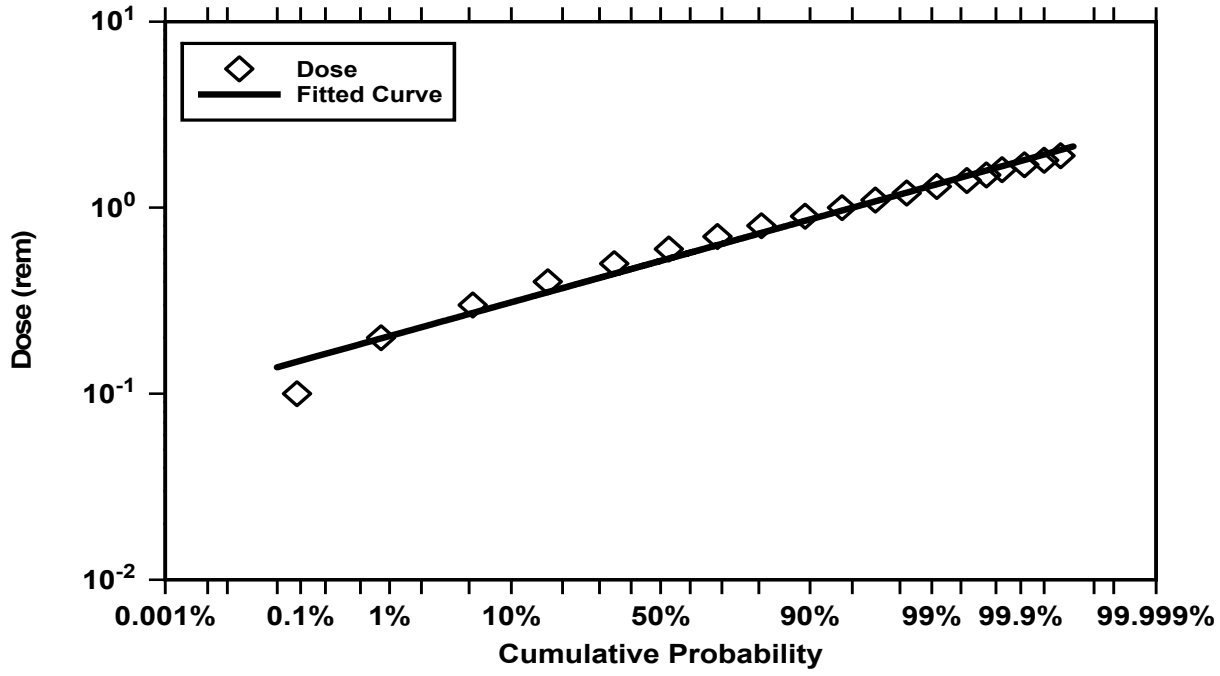

Figure C-3. Probability Plot of Estimated External Gamma Dose for Company E Personnel at the NTS during Operation PLUMBBOB

Table C-5. Summary of Estimated External Dose for Company E Personnel of the 4th MCPAEB during Operation PLUMBBOB

Mean Doses (rem)			Upper Bound Doses (rem)			
Film Badge	**Probabilistic***	**Deterministic (NTPR)**	**Film Badge**	**Probabilistic (95th Percentile)**	**Deterministic (NTPR)**	**Ratio (Deterministic ÷ Probabilistic)**
0.63†	0.62 (0.23)	0.58	1.0‡	1.1	1.8	1.7

* The arithmetic mean and standard deviation (SD) are shown. The geometric mean external dose is 0.57 rem.
† Arithmetic mean of 12 available film badge readings.
‡ 95th percentile value of the 12 available film badges.

Internal Reconstructed Doses

A probabilistic internal dose reconstruction for Company E personnel who participated during Operation PLUMBBOB was accomplished by incorporating uncertainty distributions for various input parameters into the models discussed in Section 3 and 4. These models incorporate the fallout-induced radiation environments, time-dependent intensities discussed above, and various other parameters discussed in Sections 3 and 4. The specific parameters used in both the deterministic and uncertainty analyses are shown in Table C-6. Modeled correlations associated with these parameters in the probabilistic analysis are identified and discussed in Appendix G.

Table C-6. Input Parameter Specification for Internal Dose Reconstruction, Case Study #3

Parameter	Definition	Distribution for Probabilistic Analysis	Nominal Value for Central Estimation	Deterministic*
DATES AND TIMES				
$Date_{Arrived}$	CDR start date[time]	Triangular (see Table C-4)	19Jun[1600]	19Jun[0800]
$Date_{Departed}$	CDR end date[time]	Triangular (see Table C-4)	6Jul[0800]	6Jul[2400]
INTERNAL DOSE (GENERAL)				
DCFInhα *DCFIngα*	Inhalation and ingestion dose conversion factors for fallout α emitters	*DCF*s calculated with FIIDOS multiplied by lognormal multiplier (GM=1; GSD=5.19)	Unbiased FIIDOS DCFs (see Section 4.2.8)	FIIDOS DCFs (see Section 3.3)
DCFInhβγ *DCFIngβγ*	Inhalation and ingestion dose conversion factors for fallout α emitters	*DCF*s calculated with FIIDOS multiplied by lognormal multiplier (GM=1; GSD=4.05)	Unbiased DCFs calculated with FIIDOS (see Section 4.2.8)	DCFs calculated with FIIDOS (see Section 3.3)
Biasα *Biasβγ*	Bias factors to adjust high-sided inhalation DCF values	Assigned Constant α: 1.3 for each organ βγ: 1.2 for thyroid & LLI wall, 1.35 for lung	α: 1.3 for each organ βγ: 1.2 for thyroid & LLI wall, 1.35 for lung	1.0
BR	Breathing rate	Triangular distribution: min=0.33 $m^3 \cdot hr^{-1}$ peak=1.53 $m^3 \cdot hr^{-1}$ max=2.79 $m^3 \cdot hr^{-1}$ (see Section 4.2.7)	mean of distribution (app. 1.5 $m^3 \cdot hr^{-1}$)	1.2 m^3 hr^{-1}
RESUSPENDED INHALATION DOSE				
$K(t)$	Time-dependent resuspension factor	Lognormal multiplier (GM=1; GSD=4.05)	See Sections 3.3 and 4.2	See Sections 3.3 and 4.2.6
K_{pc}, K_{bw}	Resuspension factors for fallout in thermal pulse or blast wave regions due to detonation effects	Lognormal (see Section 4.2.6)	Respirable: $K_{pc} = 1\times10^{-6}$ $K_{bw} = 1\times10^{-7}$ NonRespirable: $K_{pc} = 8\times10^{-6}$ $K_{bw} = 8\times10^{-7}$	Respirable & Nonrespirable: $K_{pc} = 1\times10^{-3}$ $K_{bw} = 1\times10^{-4}$
F_{os}	Fraction of time spent outside at CDR	Triangular min=5/24 peak=12/24 max=18/24	0.5 (or 12/24)	0.6 (or 14.4/24)
I_i	Intensity distribution of fallout while outdoors (i=1) and indoors (i=2) normalized to average CDR intensity	Lognormal (GM=1.0; GSD=1.5) (used with F_{os})	1.0	1.0
INCIDENTAL INGESTION DOSE				
q_{ing}	Soil ingestion rate	Triangular min=10 mg day^{-1} peak=100 mg day^{-1} Max=500 mg day^{-1}	100 mg day^{-1}	500mg day^{-1}

Parameter	Definition	Distribution for Probabilistic Analysis	Nominal Value for Central Estimation	Deterministic*
ρ_{soil}	Soil bulk density	Triangular min=1.3 g cm^{-3} peak=1.45 g cm^{-3} max=1.6 g cm^{-3}	1.45 g cm^{-3}	1.3 g cm^{-3}

* High-sided per guidance in NTPR Policy and Guidance Manual (DTRA, 2007).

Internal Dose Results

Distributions of the fifty-year committed equivalent dose (CED) resulting from 10,000 probabilistic simulations were calculated according to the details described above. CED distributions were calculated for three representative organs: thyroid, lung, and lower large intestine (LLI) wall. Examples of relative frequencies and probability distributions of dose to the LLI wall from alpha radiation are shown in Figure C-4 and Figure C-5, respectively. The same properties for the doses to LLI wall from beta-plus-gamma radiation are displayed in Figure C-6 and Figure C-7, respectively. These figures for LLI wall are similar to those obtained for the other two organs included in the analysis.

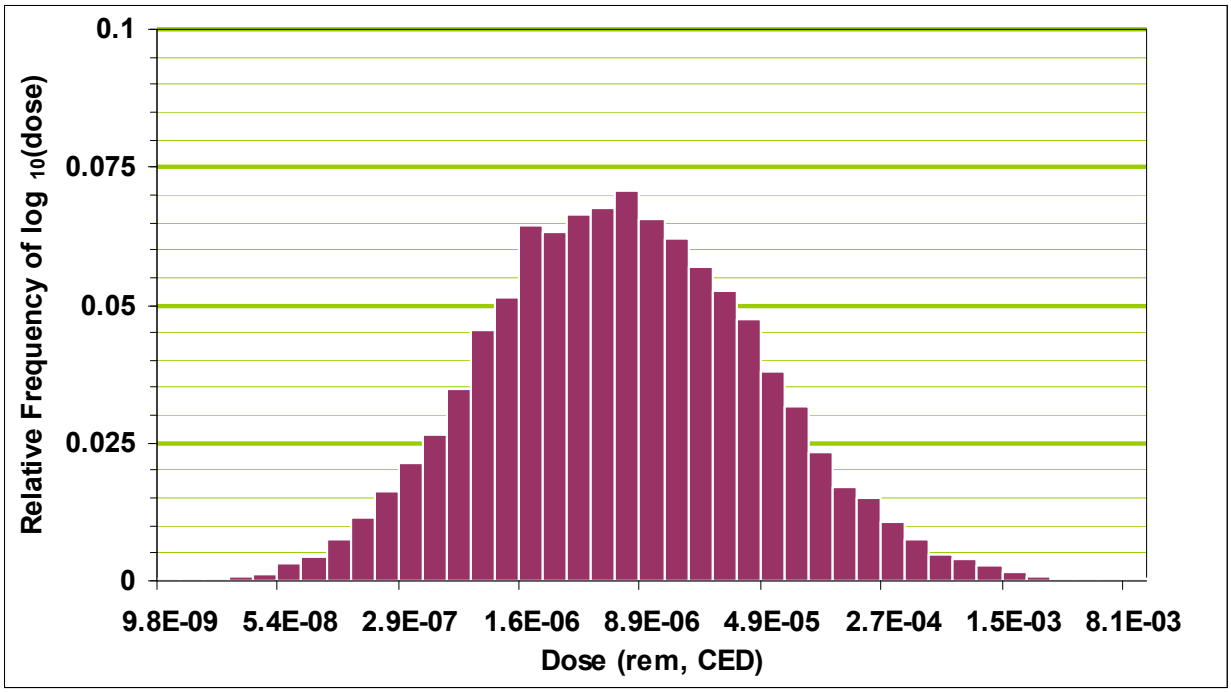

Figure C-4. Distribution of Estimated Dose for LLI Wall from Alpha Radiation for Company E Personnel during Operation PLUMBBOB

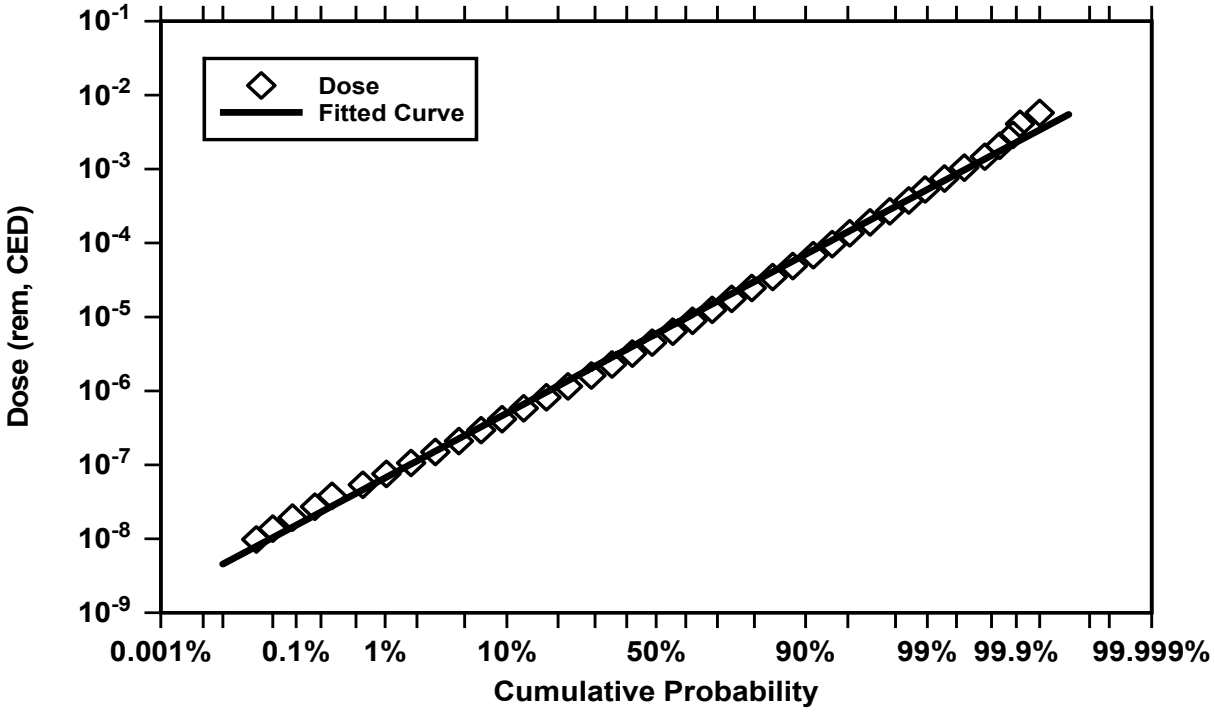

Figure C-5. Probability Plot of Distribution of Estimated LLI Wall Dose from Alpha Radiation for Company E Personnel during Operation PLUMBBOB

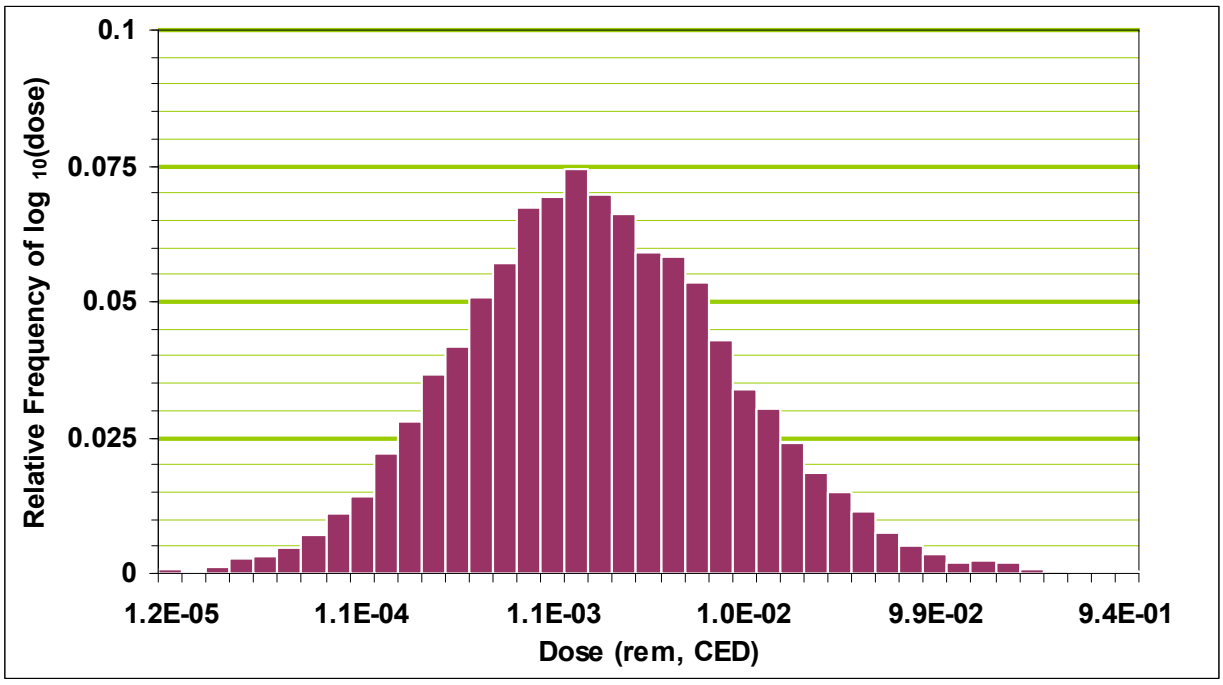

Figure C-6. Distribution of Estimated LLI Wall Dose from Beta plus Gamma Radiation for Company E Personnel during Operation PLUMBBOB

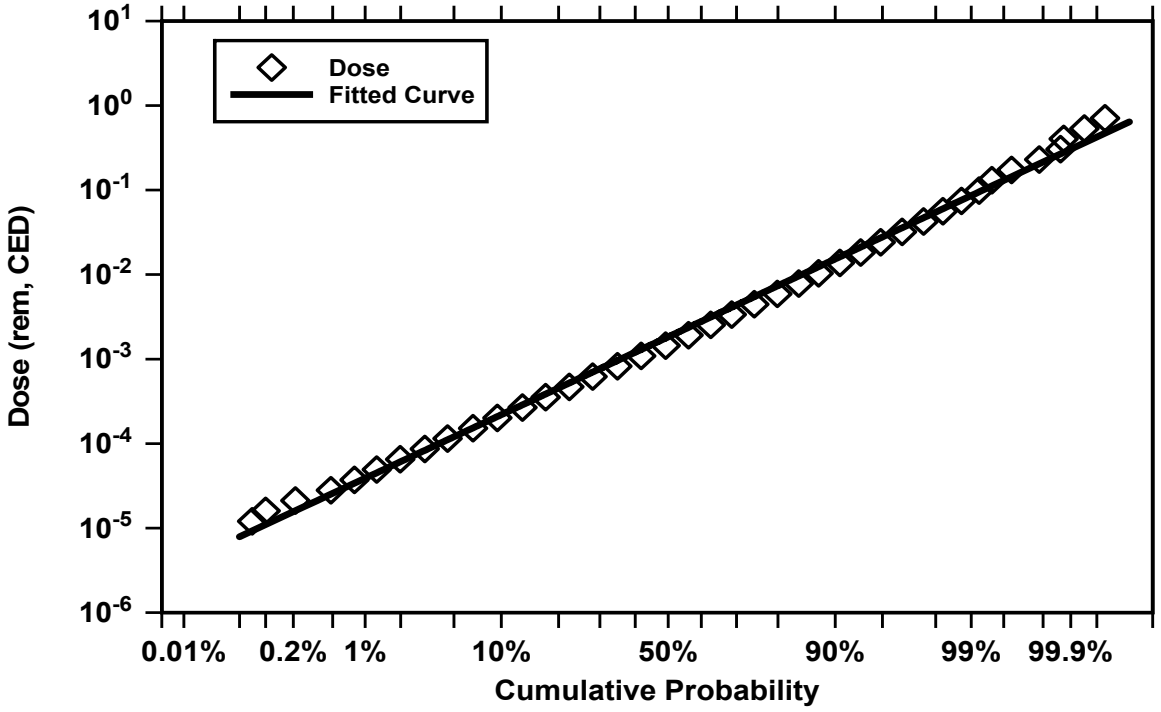

Figure C-7. Probability Plot of Estimated LLI Wall Dose from Beta plus Gamma Radiation for Company E Personnel during Operation PLUMBBOB

Key statistics from the internal dose distributions are compared with those of the deterministic model in Table C-7. Note that geometric means are given as central estimates of the probabilistic analysis, because they are judged to be more representative central estimates of approximately lognormal distributions whose range is several orders of magnitude. Although not displayed, arithmetic mean alpha and beta plus gamma organ doses are approximately 8× larger and 4×–5× larger than the geometric mean alpha and beta plus gamma doses listed in Table C-7, respectively. These results show that each deterministic organ dose is higher than the geometric mean of the corresponding probabilistic organ dose distribution, by factors of between about 9× to 11× for alpha doses, and between 2× and 10× for beta plus gamma doses. This result

Table C-7. Summary of Estimated Internal Dose for Company E Personnel during Operation PLUMBBOB

Organ	Mean Dose (rem)		Upper Bound Dose (rem)		
	Probabilistic*	Deterministic (NTPR)	Probabilistic (95th Percentile)	Deterministic (NTPR)	Ratio (Deterministic ÷ Probabilistic)
Alpha Dose					
Thyroid	0.0000046 (7.3)	0.000051	0.00013	0.000087	0.68
Lung	0.00013 (7.4)	0.0011	0.0036	0.0022	0.58
LLI Wall	0.0000050 (6.9)	0.000051	0.00013	0.000087	0.66
Beta plus Gamma Dose					
Thyroid	0.0042 (5.0)	0.0096	0.063	0.028	0.43
Lung	0.0016 (6.3)	0.016	0.034	0.030	0.87
LLI Wall	0.0016 (5.0)	0.0045	0.025	0.010	0.42

* Geometric means and geometric standard deviations (GSD) are shown.

reflects the contributions to the total deterministic organ doses of the very high-sided internal doses from inhalation of highly-resuspended fallout, which accounts for roughly 90 percent of the alpha organ doses, and between 70–90 percent of the beta plus gamma organ doses. The ratios of upper bound organ doses show the opposite result of the deterministic dose comparison, i.e., all deterministic upper bound organ doses are lower than the corresponding 95th percentile organ doses. The ratios of upper bound doses in Table C-7 show that the deterministic upper bound alpha organ doses are roughly 60–70 percent of the corresponding 95th percentile organ doses, and the deterministic upper bound beta plus gamma organ doses are between about

40–85 percent of the corresponding 95th percentile organ doses. These general comparisons reflect the effects of the combined large uncertainties associated with resuspension factors, dose conversion factors and intensities, and are expected to be the same for all organs if similar input variable uncertainties are used.

References

DNA (Defense Nuclear Agency), 1996. For the Record – A History of the Nuclear Test Personnel Review Program, 1978–1993. DNA 6041F (Defense Nuclear Agency, Washington, D.C.), March 1, 1996.

DTRA (Defense Threat Reduction Agency), 2007. Policy and Guidance Manual – Nuclear Test Personnel Review Program. Revision 7. (Defense Threat Reduction Agency, Fort Belvoir, VA), November 26, 2007.

Frank, G., Goetz, J., Klemm, J., Thomas, C., Weitz, R. 1981. Analysis of Radiation Exposure, 4th Marine Corps Provisional Atomic Exercise Brigade, Exercise Desert Rock VII, Operation PLUMBBOB. DNA 5774F (Defense Nuclear Agency, Washington, D.C.), June 15, 1981.

Harris, P. S., Obermiller, S., Lowery, C., Ozeroff, W. J., Nelson, A., Weary, S.E. 1981. PLUMBBOB Series, 1957. DNA 6005F (Defense Nuclear Agency, , Washington, D.C.), September 15, 1981.

Hawthorne, H.A. (ed.), 1979. Compilation of Local Fallout Data from Test Detonations 1945–1962, Extracted from DASA 1251. Volume I-Continental U.S. Tests, DNA 1251-1-EX, May 1, 1979 (General Electric Company-TEMPO, Santa Barbara, CA).

Maag, C., Wilkinson, M., Striegel, J., Collins, B. 1983. Shot HOOD, A Test of the PLUMBBOB Series, DNA 6002F (Defense Nuclear Agency, Washington, D.C.), May 13, 1983.

Placak, O. R., Carter, M.W., Gilmore, R.A., Goeke, R.H., Weaver, C.L. 1957. Operation PLUMBBOB, Off-Site Radiological Safety Report, Nevada Test Site, OTO-57-3 (Reynolds Electrical & Engineering Co., Inc., Las Vegas, NV), 1957.

Raine, D.A. III, Egbert, S.D., Stiver, J.H., and Case, D.R., 2007. FIIDOS—A Computer Code for the Computation of Fallout Inhalation and Ingestion Dose to Organs, Computer User's Guide (Revision 4). DTRA-TR-07-11 (Science Applications International Corporation, McLean, VA and Defense Threat Reduction Agency, Fort Belvoir, VA).

USMC (United States Marine Corps), 1957. USMC Final Report of Exercise Desert Rock VII, circa 1957.

APPENDIX D Monte Carlo Analysis of Dose to Personnel Aboard USS ESTES During Operation REDWING

Ron Weitz

APPENDIX D Monte Carlo Dose Probabilistic Analysis of Dose to Personnel Aboard USS ESTES During Operation REDWING

Introduction

Distributions of external and internal doses were generated by Monte Carlo techniques for personnel who served aboard USS ESTES (AGC 12) during Operation REDWING (1956). Doses are reported for the period extending from the arrival of USS ESTES in the Pacific Proving Grounds (PPG) on March 31, 1956, until the end of Operation REDWING on August 6, 1956.

Background

Operation REDWING was a series of 17 atmospheric nuclear tests, conducted from May 5 to July 22, 1956, at the Pacific Proving Ground (PPG) in the Marshall Islands. The PPG consisted of the land areas of Enewetak and Bikini Atolls, their lagoons, and the waters within 2.6 nautical miles (3 statute miles) of their seaward sides (Bruce-Henderson et al., 1982).

USS ESTES was an amphibious force flagship that served during REDWING as the Flagship Element (Task Element 7.3.0.1) of the Flagship Unit (Task Group 7.3). The ship arrived in the PPG on March 31, 1956, and departed from Enewetak for Bikini on May 3, two days before the first shot of the series. It returned to Enewetak twice: once for Shot SEMINOLE on June 6 and again during the last four days of June when no shots were detonated. USS ESTES was, therefore, present at Enewetak for only one of the eleven shots fired at that atoll. The ship participated in all of the six Bikini shots, providing communications, air control, and facilities for Program 2 (Nuclear Radiation) and radiation safety activities. It sortied at Bikini just before, during, and following each shot. At all other times at Bikini, the ship was moored to buoy Nan-9 at the Eneu Island anchorage. USS ESTES departed from the PPG on July 25, 1956, proceeded to Pearl Harbor, Hawaii, and then to San Diego, California. It arrived at San Diego on August 7, 1956 (Bruce-Henderson et al., 1982).

Exposure Scenario

Residual Radiation from Topside Fallout Contamination

Shipboard radiological data for USS ESTES during Operation REDWING is minimal. The absence of such data likely results from the ship having received relatively little fallout following any of the REDWING detonations. In the absence of ship-specific data, it is assumed that, while at anchor in Bikini Lagoon (or operating in close proximity to that atoll) during periods of documented fallout on nearby ships and islands, USS ESTES was similarly affected. Topside intensities are inferred from recorded intensity data on Eneu Island (ZUNI and TEWA) and USNS FRED C. AINSWORTH (Shots FLATHEAD and NAVAJO), as listed in Table D-1. Peak intensities are reported in units of mR hr^{-1} at the indicated elapsed time from the detonation (H+hours). (Bruce-Henderson et al.,1982; Jacks, 1957)

Table D-1. Peak Radiation Intensities on USS ESTES during Operation REDWING

Shot	Shot Date (1956) (Time)	Peak Intensity (mR hr^{-1})
ZUNI *	May 28 (0556)	11.6 at H+37.4 hours
FLATHEAD**	Jun 12 (0626)	1.12 at H+43.6 hours
NAVAJO**	Jul 11 (0556)	1.49 at H+22 hours
TEWA *	Jul 21 (0546)	3.68 at H+18.3 hours
* Inferred from Eneu Island data ** Inferred from USNS FRED C. AINSWORTH data		

The early time-intensity pairs for fallout on USS ESTES from Shot ZUNI, as inferred from measurements taken on Eneu Island, are provided in Table D-2. Allowance has been made for the effectiveness of washdown as documented in the ship's deck logs (USS ESTES, 1956).

Table D-2. Early Time-Intensity Data for USS ESTES After Shot ZUNI

Time After Detonation (hr)	Intensity (mR hr^{-1})
27	0.1
28	2.0
30	6.0
32	8.0
34	11
37.4	11.6
37.6	5.8
40	6.63
42	6.26

The radiological environment on USS ESTES following FLATHEAD fallout is presumed to have been the same as on USNS FRED C. AINSWORTH, as specified in Table D-3.

The radiological environment on USS ESTES following NAVAJO fallout is presumed to have been the same as on USNS FRED C. AINSWORTH is shown in Table D-4.

Table D-3. Early Time-Intensity Data on USS ESTES After Shot FLATHEAD

Time After Detonation (hr)	Intensity (mR hr^{-1})
17.6	0.01
29.6	0.08
33.6	0.33
41.6	0.89
43.6	1.12
65.6	0.69

Table D-4. Early Time-Intensity Data on USS ESTES After Shot NAVAJO

Time After Detonation (hr)	Intensity (mR hr^{-1})
10	0.01
14	0.02
18	0.49
22	1.49
26	1.19
30	0.96
34	0.69
38	0.60

The TEWA fallout intensity profile on USS ESTES is presumed to have been the same as on Eneu Island, as indicated in Table D-5.

Table D-5. Early Time-Intensity Data on USS ESTES After Shot TEWA

Time After Detonation (hr)	Intensity (mR hr^{-1})
15	0.1
18.25	3.68

Extrapolation beyond the time of the last time-intensity point for each shot is accomplished by assuming $t^{-1.2}$ decay for deterministic calculations and by utilizing the shot-specific FIIDOS decay functions for probabilistic calculations as discussed in Section 3.2.

Residual Radiation from Ship Operation in Contaminated Water

USS ESTES also accumulated radioactive materials on its underwater hull and in salt water piping and evaporators when the ship operated in contaminated lagoon water at Bikini and Enewetak Atolls, a phenomenon termed "ship contamination." Although partially attenuated by the hull and piping structures, the gamma radiation emitted by these contaminants was a source of exposure to crewmembers in below-deck spaces. In addition, crewmen who were topside when the ship operated in contaminated water were exposed to gamma radiation emitted directly from the contaminants in the water (often called "shine"). Daily external gamma dose increments from shine and ship contamination have been computed for personnel assigned to USS ESTES (Stiver, 2000). (For perspective, the dose reconstructions discussed below indicate that approximately 10 percent of the dose to a representative USS ESTES crewman came from exposure to ship contamination, and about 1 percent resulted from exposure to water shine.)

External Dose: Approach

Film Badge Data

The entire crew was issued film badges for the duration of the ship's participation in the operation. Two series of badges were issued, the first covering the period April 25 to June 25 and the second from June 25 to July 25. As was the case with the 7126th Army Unit REDWING study group discussed in Appendix A, most film badges issued to USS ESTES personnel for periods of 4 weeks or more at Operation REDWING were damaged by the high heat and humidity in the test area (Bruce-Henderson et al., 1982; NRC, 1989). Therefore film badge dosimetry is not available for comparison with the probabilistic dose distributions of USS ESTES.

Monte Carlo-Based Dose Reconstruction

Probabilistic external gamma dose reconstruction for the crew of USS ESTES during Operation REDWING was accomplished by incorporating uncertainty distributions for various parameters into the model discussed in Section 3. The specific parameters used in both the deterministic and uncertainty analyses of external dose are shown in Table D-6.

External Dose Results

The Monte Carlo dose distribution derived for a sample size of 10,000 is displayed in Figure D-1. The probability plot is shown in Figure D-2. The statistics of this distribution are compared with those of a deterministic calculation in Table D-7.

Table D-6. Input Parameter Specification for External Gamma Dose Reconstruction, Case Study # 4

Parameter	Definition	Distribution for Uncertainty Analysis*	Nominal Value for Central Estimation	Deterministic Analysis**
EXTERNAL DOSE MULTIPLIER (EDM) FOR SHIP-BASED PERSONNEL				
F_{ts}	Fraction of time spent topside	Triangular min=4/24 peak=9.6/24 max=18/24	0.4 (or 9.6/24)	0.4 (or 9.6/24)
SF_w	Shielding factor at below-deck worksite (assumed equally likely on 1st or 2nd decks below topside)	Elliptical ship model (see Section 4.2.3) GM = 0.079	0.079	0.1
SF_b	Shielding factor at below-deck billet location (assumed on 3rd deck below topside)	Elliptical ship model (see Section 4.2.3) GM = 0.016	0.016	0.1
I_i	Intensity of fallout near topside location (i=1), topside location above below-deck worksite (i=2), and topside location above below-deck billet area (i=3) frequented by veteran, normalized to the intensity averaged over the entire topside deck	Post-decon model for elliptical ships (see Section 4.2.1) $\mu = 1.0$ $\sigma = 0.70$	0.88 (median of distribution)	1.0
INTENSITY MEASUREMENTS FOR SHIP-BASED PERSONNEL				
I_m	Measured topside intensities	Normal $\mu = I_m$, $\sigma = 0.3 \cdot I_m$ (to account for measurement error)	1.0	1.0
a	Exponent of multiplicative error factor $(t/t_0)^{\pm a}$ applied to FIIDOS-generated intensity functions	Normal $\mu = 0$ $\sigma = 0.15$	0	0
I_{sc}	Ship contamination intensity	Lognormal multiplier GM=1 UB95=3.2	1.0	1.0
I_{ws}	Water shine intensity	Lognormal multiplier GM=1 UB95=2.4	1.0	1.0

* μ = arithmetic mean; σ = standard deviation; GM = geometric mean; GSD = geometric standard deviation; UB95 = upper bound at the 95th percentile.
** High-sided per guidance in NTPR Policy and Guidance Manual (DTRA, 2007).

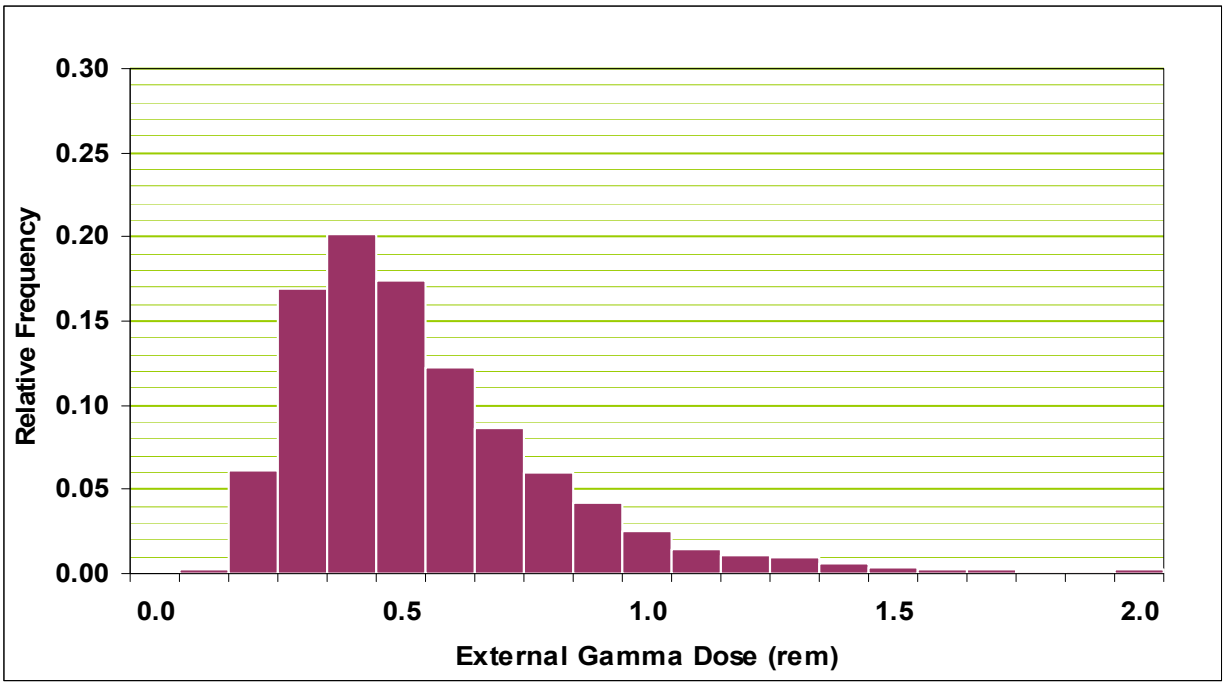

Figure D-1. Distribution of Estimated External Gamma Doses from Monte Carlo Analysis for Crew of USS ESTES during Operation REDWING

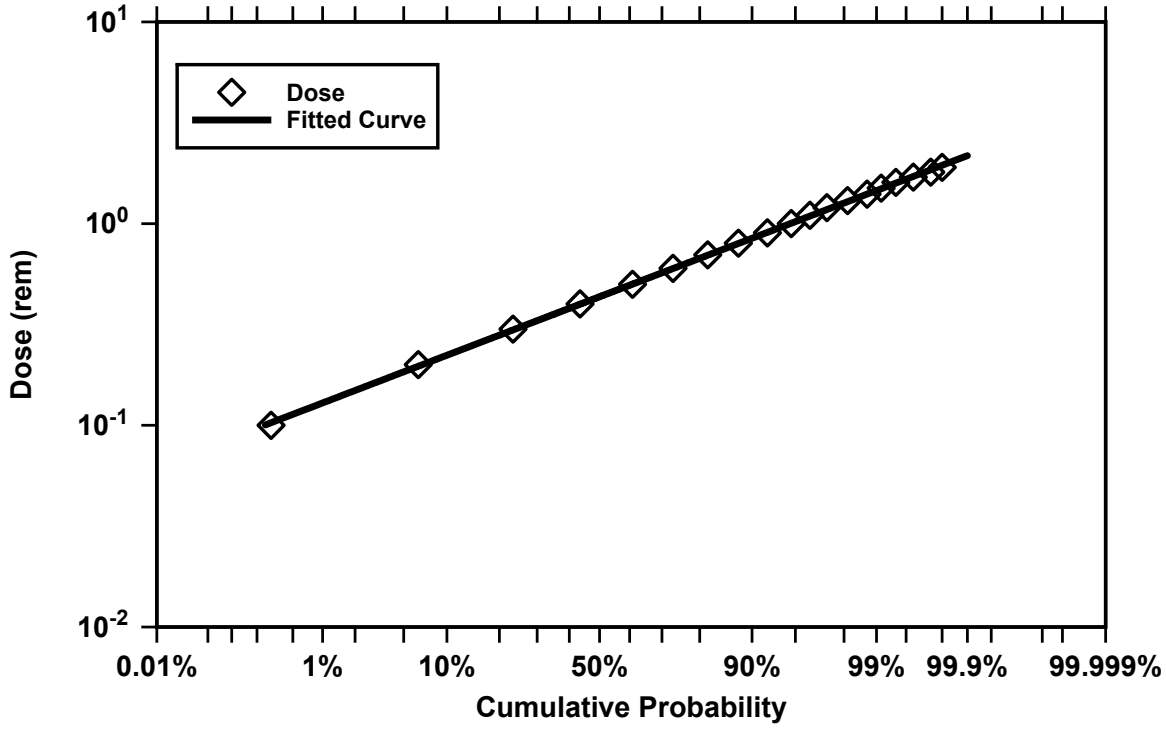

Figure D-2. Probability Plot of Estimated External Gamma Doses from Monte Carlo Analyses for Crew of USS ESTES during Operation REDWING

Table D-7. Summary of Estimated External Dose for Crew of USS ESTES during Operation REDWING

Mean Doses (rem)		Upper Bound Doses (rem)		
Probabilistic(*)	**Deterministic (NTPR)**	**Probabilistic (95th Percentile)**	**Deterministic (NTPR)**	**Ratio (Deterministic/ Probabilistic)**
0.50 (0.28)	0.43	1.0	1.2	1.1

(*) The arithmetic mean (and standard deviation) are shown. The geometric mean external dose is 0.44 rem.

Internal Dose: Approach

Internal dose reconstruction for the crew of USS ESTES during Operation REDWING was accomplished by incorporating uncertainty distributions for the fallout-induced radiation environments discussed above and for various other parameters as discussed in Sections 3 and 4. The specific parameters used in both the deterministic and probabilistic analyses are shown in Table D-8.

Table D-8. Input Parameter Specification for Internal Dose Reconstruction, Case Study #4

Parameter	Definition	Distribution for Probabilistic Analysis	Nominal Value for Central Estimation	Deterministic(*)
INTERNAL DOSE (GENERAL)				
DCFInhα *DCFIngα*	Inhalation and ingestion dose conversion factors for fallout α emitters	*DCF*s calculated with FIIDOS multiplied by Lognormal with GM=1.0, GSD=5.19	*DCF*s calculated with FIIDOS (see Section 4.2.8)	DCFs calculated with FIIDOS (see Section 4.2.8)
DCFInhβγ *DCFIngβγ*	Inhalation and ingestion dose conversion factors for fallout β+γ radiation	*DCF*s calculated with FIIDOS multiplied by Lognormal with GM=1.0, GSD=4.05	*DCF*s calculated with FIIDOS (see Section 4.2.8)	DCFs calculated with FIIDOS (see Section 4.2.8)
Biasα	Bias factors to adjust high-sided inhalation DCF values	Assigned Constant α: 1.3 for each organ	α: 1.3 for each organ	1.0
Biasβγ		βγ: 1.2 for thyroid & LLI, 1.35 for lung	βγ: 1.2 for thyroid & LLI, 1.35 for lung	1.0
BR	Breathing rate	Triangular distribution derived from USEPA (1997) data (see Section 4.2.7): min = 0.33 $m^3\ hr^{-1}$ peak = 1.53 $m^3\ hr^{-1}$ max = 2.79 $m^3\ hr^{-1}$	Mean of Distribution ~1.5 $m^3\ hr^{-1}$	1.2 $m^3\ hr^{-1}$

Parameter	Definition	Distribution for Probabilistic Analysis	Nominal Value for Central Estimation	Deterministic(*)
DESCENDING INHALATION DOSE (†)				
RND_{Res1}	Deposition fractions for particle sizes deposited in Regions BB, bb, and AI	1.0 (assumed constant)	1.0 (assumed constant)	n/a
RND_{Res2}		Lognormal: GM, GSD 0.0056, 1.744	Geometric Mean 0.0056	
RND_{Res3}		Lognormal: GM, GSD 0.001, 1.65	0.001	
$RND_{Nonres1}$	Deposition fractions for particle sizes deposited in Region ET_2 and cleared to digestive tract	0.0 (assumed constant)	0.0 (assumed constant)	n/a
$RND_{Nonres2}$		Lognormal: GM, GSD 0.363, 1.106	Geometric Mean 0.363	
$RND_{Nonres3}$		Lognormal: GM, GSD 0.285, 1.185	0.285	
V_1	Particle settling velocities	Logtriangular min, peak, max (cm s^{-1}) 0.22/2, 0.22, 27.8	0.22 cm s^{-1}	10^6(cm)/T(sec)
V_2		0.83/2, 0.83, 27.8	0.83 cm s^{-1}	
V_3		13.0/2, 13.0, 27.8	13.0 cm s^{-1}	
AF_{100}	Surface activity fraction <100 μm particles	Triangular (min,peak,max) ZUNI (0.999,1.000, 1.000) FLATHEAD (1.000,1.000,1.000) NAVAJO (0.707, 0.869, 0.988) TEWA (0.396, 0.587, 0.801)	Peak of Distributions ZUNI 1.000 FLATHEAD 1.000 NAVAJO 0.869 TEWA 0.587	1.0
$frac_1$	Surface fraction of Class 1–2 from 1–100 μm particles	Triangular Min, peak, max 0, 0.00136, 0.01	Peak of Distribution 0.00136	n/a
$frac_2$		0, 0.025, 0.1	0.025	
RESUSPENDED INHALATION DOSE				
$K(t)$	Time-dependent resuspension factor	Lognormal multiplier GM=1, GSD=4.05	10^{-5} m^{-1} for first 4 days post-deposition, 0 thereafter	10^{-5} m^{-1} for first 4 days post-deposition, 0 thereafter

(*) High-sided per guidance in NTPR Policy and Guidance Manual (DTRA, 2007).
(†) AMAD particle size classes: 1 = 1–10 μm, 2 = 10–20 μm, 3 = 20–100 μm.

Internal Dose Results

Fifty-year committed equivalent dose (CED) distributions to three organs, thyroid, lung, and lower large intestine (LLI) wall, were derived using the probabilistic model for a sample size of

10,000. The geometric mean and 95th percentile CEDs of the various distributions are given in, Table D-9 along with analogous doses derived deterministically. The ratio of the deterministic upper bound CED to the probabilistic 95th percentile CED is provided in the rightmost column. Examples of these distributions are shown in Figure D-3 through Figure D-6, which show the relative frequency distributions and probability plots of CED to the LLI wall from alpha radiation and from beta plus gamma radiation, respectively.

Table D-9. Summary of Estimated Internal Doses for Crew of USS ESTES during Operation REDWING

Organ	Mean Dose (rem)		Upper Bound Dose (rem)		
	Probabilistic(*)	Deterministic (NTPR)	Probabilistic (95th Percentile)	Deterministic (NTPR Upper Bound)	Ratio (Deterministic/ Probabilistic)
Alpha Dose					
Thyroid	0.0000072 (7.8)	0.000032	0.00021	0.00032	1.5
Lung	0.000088 (7.8)	0.00040	0.0026	0.0040	1.5
LLI	0.0000076 (7.6)	0.000033	0.00022	0.00033	1.5
Beta plus Gamma Dose					
Thyroid	0.56 (4.6)	0.70	6.6	7.0	1.1
Lung	0.088 (6.0)	0.58	1.8	5.8	3.2
LLI	0.36 (4.6)	0.44	4.2	4.4	1.0

(*) Geometric mean and (geometric standard deviation) are shown for the probabilistic analysis results.

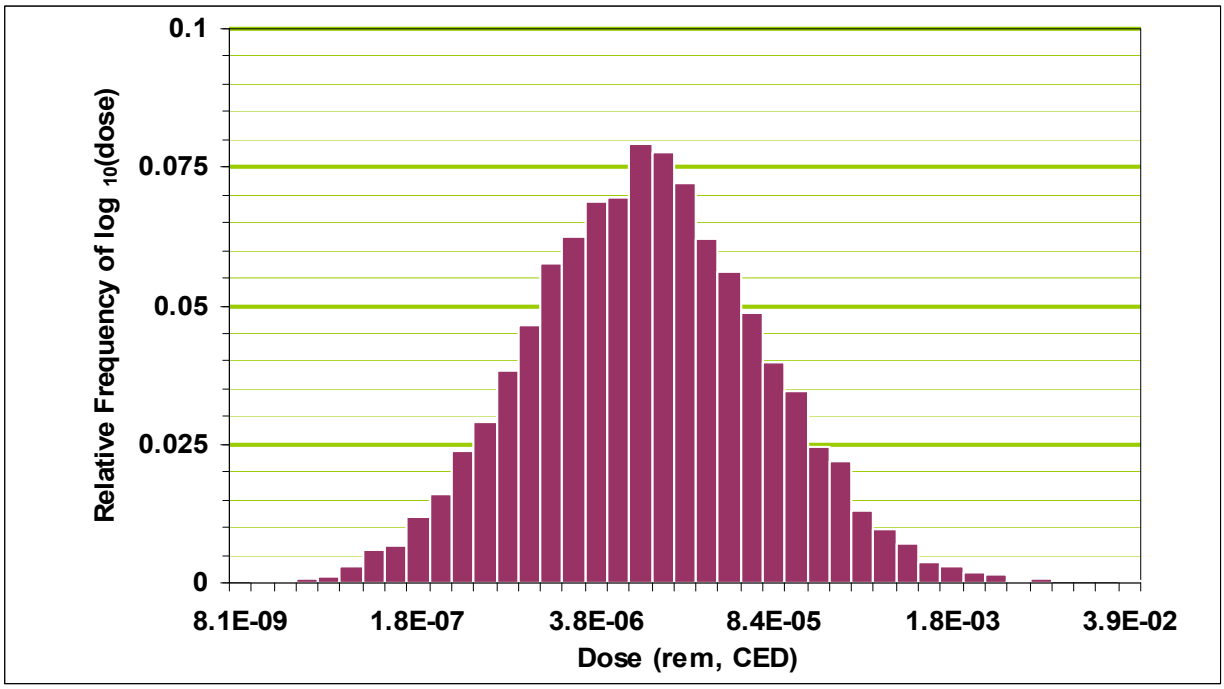

Figure D-3. Distribution of Estimated LLI Wall Dose from Alpha Radiation for Crew of USS ESTES during Operation REDWING

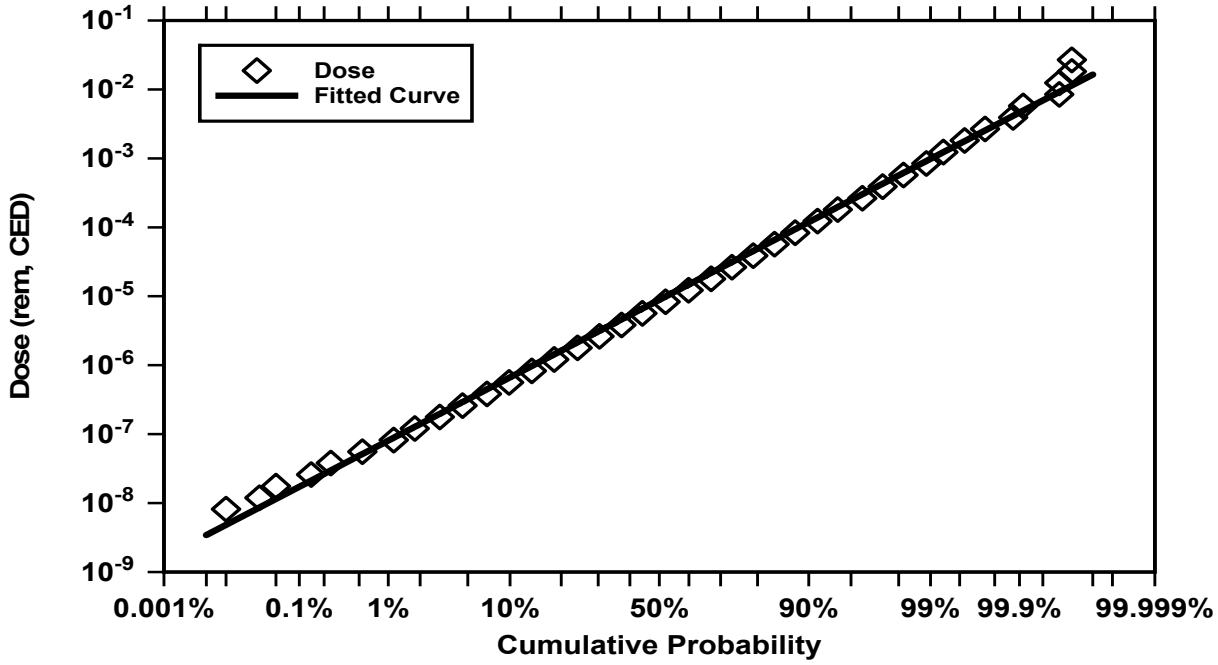

Figure D-4. Probability Plot of Estimated LLI Wall Dose from Alpha Radiation for Crew of USS ESTES during Operation REDWING

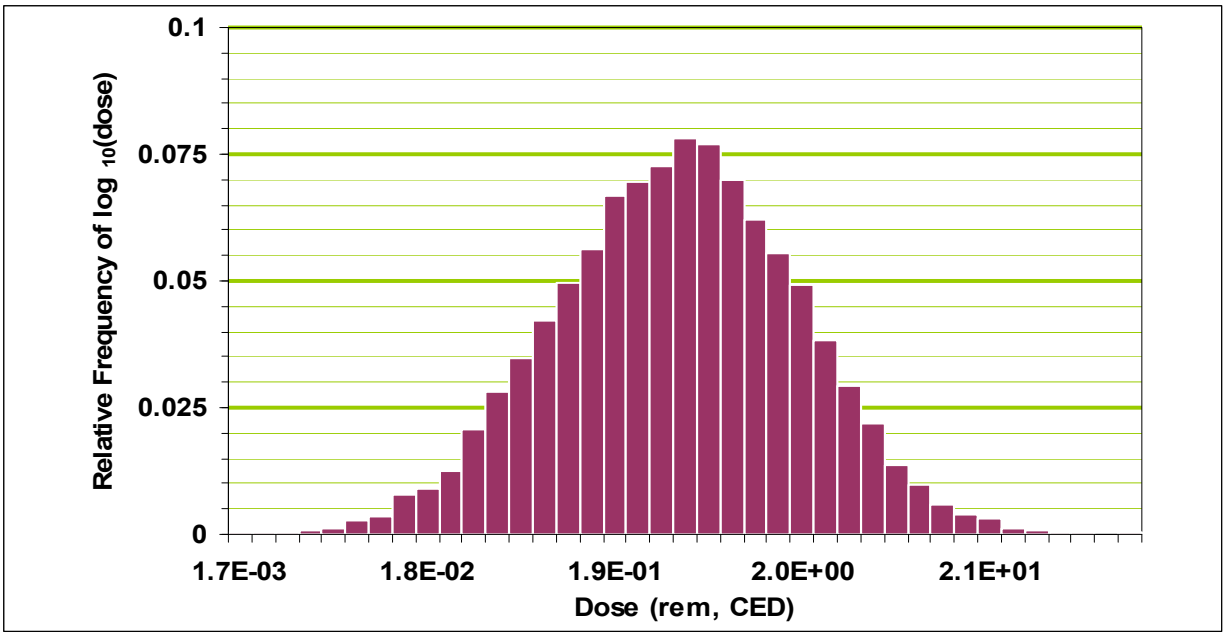

Figure D-5. Distribution of Estimated LLI Wall Dose from Beta plus Gamma Radiation for Crew of USS ESTES during Operation REDWING

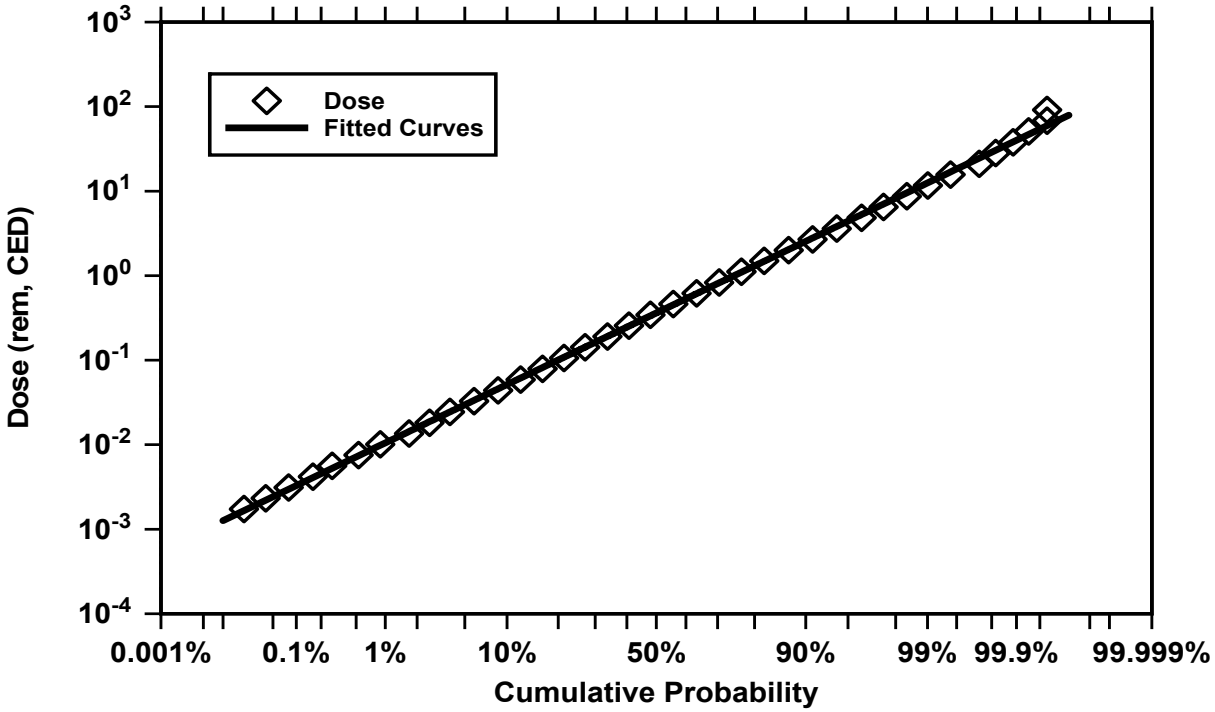

Figure D-6. Probability Plot of Estimated LLI Wall Dose from Beta plus Gamma Radiation for Crew of USS ESTES during Operation REDWING

References

Bruce-Henderson, S., Gladeck, F.R., Hallowell, J.H., Martin, E.J., McMullan, F.W., Miller, R.H., Rogers, W.E., Rowland, R.H., Shelton, C.F., Sturman, P., Berkhouse, L.H., Davis, S., DeSantis, H., Dean, P., Doyle, M.K., and Patterson, D.S., 1982. Operation REDWING: 1956, United States Atmospheric Nuclear Weapons Tests, Nuclear Test Personnel Review. DNA 6037F (Defense Nuclear Agency, Washington, D.C.).

DTRA (Defense Threat Reduction Agency), 2007. Policy and Guidance Manual – Nuclear Test Personnel Review Program. Revision 7 (Defense Threat Reduction Agency, Fort Belvoir, VA), November 26, 2007.

Jacks, G. L., 1957. Operation REDWING Radiological Safety. WT-1366 (extracted version prepared for DNA in 1983; Defense Nuclear Agency, Washington D.C.).

NRC (National Research Council), 1989. Film Badge Dosimetry in Atmospheric Nuclear Tests. (National Academy Press, Washington, D.C.).

Stiver, J.H., 2000, "REDWING fallout intensity model, codified in Excel spreadsheet" Dose Tables-Island based-1.xls," (Science Applications International Corporation), 2000.

USEPA, 1997. Exposure Factors Handbook. EPA/600/P-95/002Fa, Fb, Fc (Office of Research and Development, U.S. Environmental Protection Agency, Washington, D.C.).

USS ESTES (AGC 12), Deck log excerpts, March–July 1956.

APPENDIX E Monte Carlo Analysis of Dose to Personnel Aboard USS BOXER During Operation HARDTACK I

Ron Weitz

APPENDIX E Monte Carlo Analysis of Dose to Personnel Aboard USS BOXER During Operation HARDTACK I

Introduction

Distributions of external and internal doses were generated by Monte Carlo techniques for personnel who served aboard USS BOXER (CVS 21) during Operation HARDTACK I (1958). Doses are reported for the period extending from May 12, 1958, until the turn-in of film badges (date unknown, treated as an uncertainty).

Background

Operation HARDTACK I was a series of 35 atmospheric nuclear weapon tests conducted in the Pacific Ocean from April 28 to August 18, 1958. All but three of these shots occurred at the Enewetak Proving Ground (EPG), which consisted of the land areas of Enewetak and Bikini Atolls, their lagoons, and the waters within 2.6 nautical miles (nmi) (3 statute miles) of their seaward sides. Enewetak Atoll is located about 2400 nmi southwest of Hawaii; Bikini Atoll is approximately 190 nmi east of Enewetak Atoll. (Gladeck et al., 1982)

USS BOXER was an antisubmarine aircraft carrier that served during HARDTACK I as command ship for Commander Joint Task Force 7, flagship for the Commander Task Group (CTG) 7.3 (Navy), headquarters for CTG 7.1 (Scientific) and CTG 7.4 (Air Force), and Air Operations Center for Air Force personnel. The ship also hosted Marine Helicopter Transport Squadron (Light) 361. USS BOXER transported many of the nuclear devices from CONUS to EPG. The ship arrived at Enewetak Atoll on March 3, 1958, with a crew of approximately 1100 personnel. It made numerous transits between Enewetak and Bikini atolls during May and June in support of the test series, finally departing EPG for Pearl Harbor, Hawaii, on June 30. The ship subsequently was present at Johnston Island in late July and August to support the two HARDTACK I shots at that location. During the operation, USS BOXER performed a variety of shot-specific tasks; for example, it served as the launch platform for the balloon that carried the Shot YUCCA device aloft, the evacuation unit for island-based personnel for several shots, and the recovery element for rocket nosecones and other instrumented devices employed at several shots. (Gladeck et al., 1982, and ship's deck log)

Extensive preparation and planning for radiological safety were performed aboard USS BOXER. The ship was equipped with a washdown system to remove fallout, and was staffed with 18 radiological monitoring teams and two decontamination squads. These teams were used extensively on shot days for fallout watch and decontamination, as needed. Radiological surveys were made hourly during USS BOXER's stay in EPG (Gladeck et al., 1982). Unfortunately, little of this monitoring data has been located to date.

Exposure Scenario

There was only one recorded incidence of fallout on USS BOXER, as reported in USS BOXER CO (1958):

> *Only one instance of contamination by fallout occurred. This was on 14 May 1958 at 0630 M while at anchor in Eniwetok Atoll after the KOA shot. Intensities topside rose to an average of 8 MR/HR (Gamma) with high levels of 20/30 MR/HR. Washdown system was not activated immediately due to flight operations, however.....all monitoring stations [were] manned. After approximately 1 hour of washdown operation intensity had dropped to 4 MR/HR and subsequently decayed to background.....*

It is likely that mixed FIR-KOA fallout began to descend on USS BOXER at approximately 0300 hours that morning and continued until 1600 hours that afternoon, as indicated by measurements taken with a continuous monitor on nearby Parry Island (Appendix B). The ship's deck log for that day states that the washdown system was activated four times on the morning of May 14: during the periods 0736 to 0805, 0920 to 1010, 1047 to 1056, and 1130 to 1144. The effectiveness of the washdown system is uncertain in view of a second, ostensibly contradictory statement in USS BOXER CO (1958) implying that the system only succeeded in leveling off the rise in radiation intensity on the flight deck during operation, and that it was 30 percent efficient in other areas. In any case, it is apparent from the measurements on Parry Island that the fallout continued to descend in the area after USS BOXER's washdown system was secured for the final time at 1144.

Although USS BOXER CO (1958) identified the mid-May episode as the only fallout event to impact USS BOXER, that report is dated June 18, 1958, midway through the operation. It is likely that two unreported incidences of fallout occurred in the two days prior to the ship's departure from EPG on June 30:

- USS BOXER was operating in the vicinity of Enewetak Atoll when light fallout was measured on Parry Island during rainfall on the afternoon of June 28, following the detonation of Shot REDWOOD at Bikini Atoll that morning (see Appendix B). The deck log states that USS BOXER departed Enewetak Atoll late that afternoon and steamed to the southeast, in the general direction of increasing REDWOOD fallout (based on the fallout pattern shown in Figure 40 of Gladeck et al., 1982). The deck log weather observation sheet for that day indicates that the ship could have spent up to 6 hours that evening in rain showers.
- On the evening of June 29, while USS BOXER was anchored in Enewetak Lagoon, fallout from Shot OAK descended during rain showers in the vicinity of Enewetak Atoll.

External Dose: Approach

Film Badge Data

The entire crew was issued film badges prior to the start of testing. The issue date for officers and senior non-commissioned officers was April 11; most enlisted personnel received their badges on April 14. For the majority of crewmembers (979 personnel, comprising 89 percent of the crew), the available dosimetry record (referred to as the "fourth quarter report") provides total operational doses but does not include complete information linking the readings to badge

numbers and to turn-in dates. Because of its impact on dose reconstruction, the question of badge turn-in date was examined carefully. According to rad-safe policy, film badges were to be turned in upon recall by the Task Group Rad-Safe organization, upon exit from a contaminated area, or upon departure from EPG. In keeping with this policy, the badges worn by the USS BOXER crew should have been returned on or just prior to June 30, when the ship departed Enewetak for Pearl Harbor. However, based on an analysis of all available USS BOXER dosimetry records, ship logs and personnel diaries, and interviews with members of the ship's crew, it is concluded that the embarked crew turned their badges in while the ship was underway for Pearl Harbor from June 30 to July 6; the turn-in date is treated as an uncertainty in the probabilistic assessment. Consequently, these badges were probably processed at Pearl Harbor in early July and not at the film badge stations established at Enewetak and Bikini Atolls for that purpose. This may explain the lack of completed film badge records of the type available for most ships and units supporting HARDTACK I.

It appears that the remaining 11 percent of the crew, for whom more detailed film badge information is recorded, either transferred off USS BOXER prior to its departure from EPG or was involved in special activities requiring their absence from the ship during operations at EPG. This has been confirmed for individuals reassigned from USS BOXER during the May–June period, and for a contingent of USS BOXER-based Marines who were on temporary duty off the ship during the badging period. These personnel probably turned their badges in prior to their departure from EPG, so that these badges were processed and recorded at the test site.

The average of these film badge readings is 0.735 rem. Removing the 20 percent environmental bias discussed in the NRC film badge dosimetry report (NRC, 1989) results in an unbiased average film badge dose of 0.735/1.2 = 0.612 rem.

Monte Carlo-Based Dose Reconstruction

Probabilistic external gamma dose reconstruction for the crew of USS BOXER during Operation HARDTACK I was accomplished by incorporating uncertainty distributions for various parameters into the model discussed in Section 3. The specific parameters used in both the deterministic and uncertainty analyses of external dose are shown in Table E-1.

External Dose Results

The Monte Carlo dose distribution derived for a sample size of 10,000 is displayed in Figure E-1. The probability plot is shown in Figure E-2. The statistics of this distribution are compared with those of a deterministic calculation and of the film badge distribution in Table E-2.

Table E-1. Input Parameter Specification for External Gamma Dose Reconstruction, Case Study #5

Parameter	Definition	Distribution for Uncertainty Analysis*	Nominal Value for Central Estimation	Deterministic Analysis**
FILM BADGE DATA				
$Date_{Fbend}$	Date of film badge turn-in	Daily probabilities for period Jun 30 to Jul 6, 1958: 0.2, 0.3, 0.1, 0.1, 0.1, 0.1, 0.1.	July 2, 1958	July 2, 1958
SHOT MIXTURE FRACTION				
Fallout Composition	Fallout proportion from each shot (applies to FIR/KOA only)	Triangular min = 0 peak = 0.4 max = 1 for FIR fraction	Intensity based on 0.4/0.6 mixture of FIIDOS-derived FIR/KOA decay functions	Intensity data based on time-dependent decay exponents for FIR/KOA mixture
EXTERNAL DOSE MULTIPLIER (EDM) FOR SHIP-BASED PERSONNEL				
F_{ts}	Fraction of time spent topside	Triangular min=4/24 peak=9.6/24 max=18/24	0.4 (or 9.6/24)	0.4 (or 9.6/24)
SF_w	Shielding factor at below-deck worksite (assumed equally likely on 1st or 2nd decks below flight deck)	Rectangular ship model (see Section 4.2.3) GM = 0.11	0.11	0.1
SF_b	Shielding factor at below-deck billet location (assumed equally likely on 3rd or 4th decks below flight deck)	Rectangular ship model (see Section 4.2.3) GM = 0.021	0.021	0.1
I_i	Intensity of fallout near topside location (i=1), topside location above below-deck worksite (i=2), and topside location above below-deck billet area (i=3) frequented by veteran, normalized to the intensity averaged over the entire topside deck	Post-decon model for rectangular ships (see Section 4.2.1) $\mu = 1.0$ $\sigma = 0.63$	0.92 (median of distribution)	1.0
INTENSITY MEASUREMENTS FOR SHIP-BASED PERSONNEL				
I_m	Measured topside intensities	Normal $\mu = I_m$, $\sigma = 0.3 \cdot I_m$ (to account for measurement error)	1.0	1.0
a	Exponent of multiplicative error factor $(t/t_0)^{\pm a}$ applied to FIIDOS-generated intensity functions	Normal $\mu = 0$ $\sigma = 0.15$	0	0

* μ = arithmetic mean; σ = standard deviation; GM = geometric mean; GSD = geometric standard deviation; UB95 = upper bound at the 95th percentile.
** High-sided per guidance in NTPR Policy and Guidance Manual (DTRA, 2007).

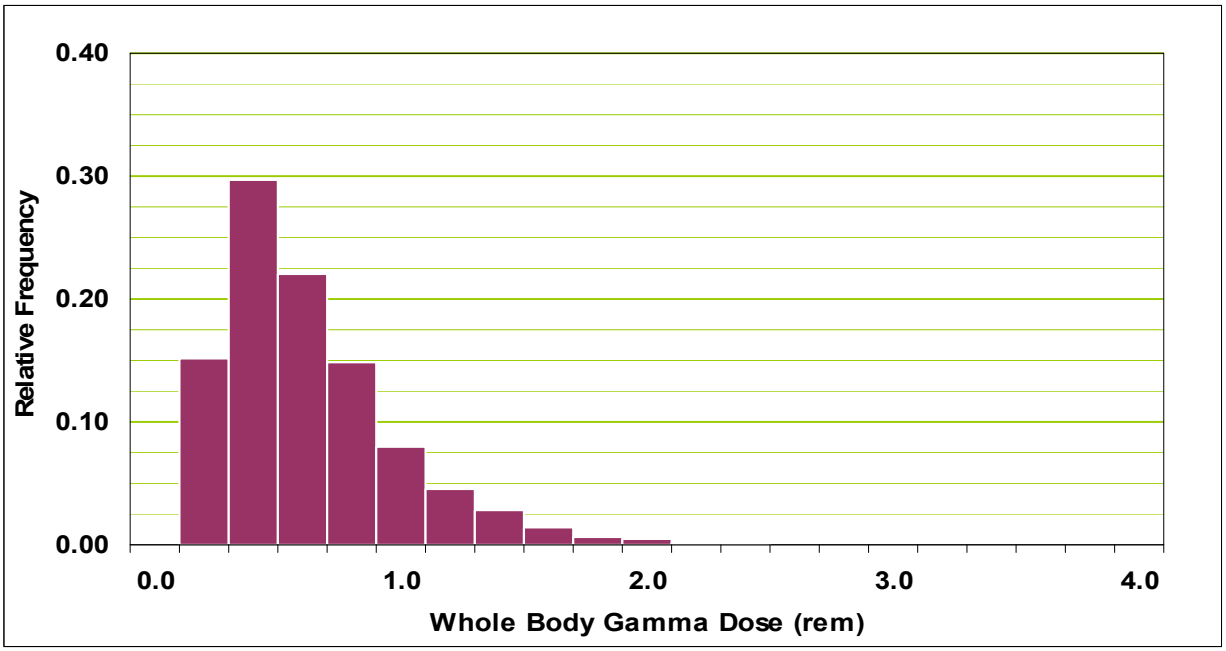

Figure E-1. Distribution of Estimated External Gamma Doses for Crew of USS BOXER during Operation HARDTACK I

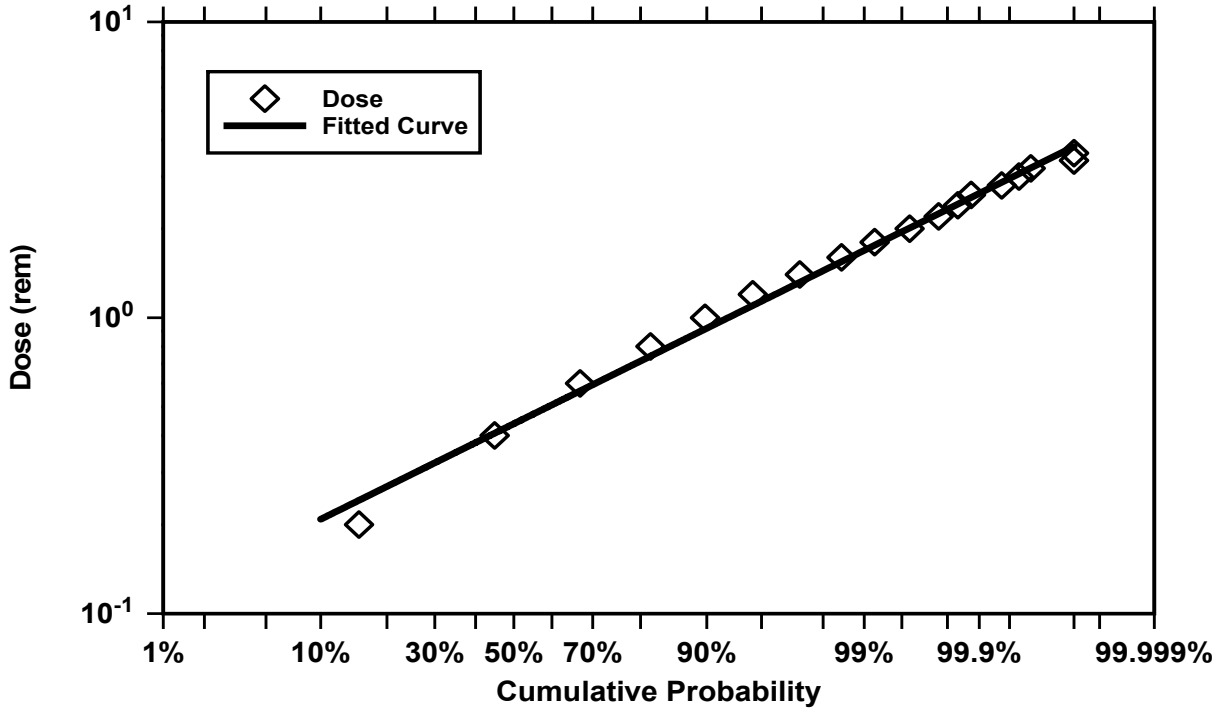

Figure E-2. Probability Plot of Estimated External Gamma Doses for Crew of USS BOXER during Operation HARDTACK I

Table E-2. Summary of Estimated External Dose for Crew of USS BOXER during Operation HARDTACK I

Mean Dose (rem)			Upper Bound Dose (rem)			
Film Badge	**Probabilistic(*)**	**Deterministic (NTPR)**	**Film Badge**	**Probabilistic (95th Percentile)**	**Deterministic (NTPR)**	**Ratio (Deterministic/ Probabilistic)**
0.61	0.53 (0.36)	0.52	0.97	1.2	1.6	1.3

(*) The arithmetic mean (and standard deviation) are shown. The geometric mean external dose is 0.42 rem.

Internal Dose: Approach

Internal dose reconstruction for the crew of USS BOXER during Operation HARDTACK I was accomplished by incorporating uncertainty distributions for the fallout-induced radiation environments discussed above and for various other parameters discussed in Sections 3 and 4. The specific parameters used in both the deterministic and probabilistic analyses are shown in Table E-3.

Table E-3. Input Parameter Specifications for Internal Dose Reconstruction,Case Study #5

Parameter	Definition	Distribution for Probabilistic Analysis	Nominal Value for Central Estimation	Deterministic(*)
INTERNAL DOSE (GENERAL)				
DCFInhα *DCFIngα*	Inhalation and ingestion dose conversion factors for fallout α emitters	*DCF*s calculated with FIIDOS multiplied by Lognormal with GM=1.0, GSD=5.19	*DCF*s calculated with FIIDOS (see Section 4.2.8)	DCFs calculated with FIIDOS (see Section 4.2.8)
DCFInhβγ *DCFIngβγ*	Inhalation and ingestion dose conversion factors for fallout β+γ radiation	*DCF*s calculated with FIIDOS multiplied by Lognormal with GM=1.0, GSD=4.05	*DCF*s calculated with FIIDOS (see Section 4.2.8)	DCFs calculated with FIIDOS (see Section 4.2.8)
Biasα	Bias factors to adjust high-sided inhalation DCF values	Assigned Constant α: 1.3 for each organ	α: 1.3 for each organ	1.0
Biasβγ		βγ: 1.2 for thyroid & LLI, 1.35 for lung	βγ: 1.2 for thyroid & LLI, 1.35 for lung	1.0
BR	Breathing rate	Triangular distribution derived from USEPA (1997) data (see Section 4.2.7): min = 0.33 $m^3\ hr^{-1}$ peak = 1.53 $m^3\ hr^{-1}$ max = 2.79 $m^3\ hr^{-1}$	Mean of Distribution ~1.5 $m^3\ hr^{-1}$	1.2 $m^3\ hr^{-1}$

Parameter	Definition	Distribution for Probabilistic Analysis	Nominal Value for Central Estimation	Deterministic(*)
DESCENDING INHALATION DOSE (†)				
RND_{Res1}	Deposition fractions for particle sizes deposited in Regions BB, bb, and AI	1.0 (assumed constant)	1.0 (assumed constant)	n/a
RND_{Res2}		Lognormal: GM, GSD 0.0056, 1.744	Geometric Mean 0.0056	
RND_{Res3}		Lognormal: GM, GSD 0.001, 1.65	0.001	
$RND_{Nonres1}$	Deposition fractions for particle sizes deposited in Region ET_2 and cleared to digestive tract	0.0 (assumed constant)	0.0 (assumed constant)	n/a
$RND_{Nonres2}$		Lognormal: GM, GSD 0.363, 1.106	Geometric Mean 0.363	
$RND_{Nonres3}$		Lognormal: GM, GSD 0.285, 1.185	0.285	
V_1	Particle settling velocities	Logtriangular min, peak, max ($cm\ s^{-1}$) 0.22/2, 0.22, 27.8	0.22 $cm\ s^{-1}$	10^6(cm)/T(sec)
V_2		0.83/2, 0.83, 27.8	0.83 $cm\ s^{-1}$	
V_3		13.0/2, 13.0, 27.8	13.0 $cm\ s^{-1}$	
AF_{100}	Surface activity fraction <100 μm particles	Triangular (min,peak,max) FIR/KOA (1.000, 1.000, 1.000) REDWOOD (0.624,0.816, 0.986) OAK (0.469, 0.732, 0.975)	Peak of Distributions FIR/KOA 1.000 REDWOOD 0.816 OAK 0.732	1.0
$frac_1$	Surface fraction of Class 1–2 from 1–100 μm particles	Triangular Min, peak, max 0, 0.00136, 0.01	Peak of Distribution 0.00136	n/a
$frac_2$		0, 0.025, 0.1	0.025	
RESUSPENDED INHALATION DOSE				
$K(t)$	Time-dependent resuspension factor	Lognormal multiplier GM=1, GSD=4.05	$10^{-5}\ m^{-1}$ for first 4 days post-deposition, 0 thereafter	$10^{-5}\ m^{-1}$ for first 4 days post-deposition, 0 thereafter

(*) High-sided per guidance in NTPR Policy and Guidance Manual (DTRA, 2007).
(†) AMAD particle size classes: 1 = 1–10 μm, 2 = 10–20 μm, 3 = 20–100 μm.

Internal Dose Results

Fifty-year committed equivalent dose (CED) distributions to three organs, thyroid, lung, and lower large intestine (LLI) wall were derived using the probabilistic model for a sample size of 10,000. The geometric mean and 95th percentile CEDs of the various distributions are given in Table E-4, along with analogous doses derived deterministically. The ratio of the deterministic upper bound CED to the probabilistic 95th percentile CED is provided in the rightmost column. Examples of these distributions are shown in Figure E-3 through Figure E-6, where the relative frequency distribution and probability plot of CED to the LLI wall from alpha radiation and from beta plus gamma radiation, respectively, are plotted.

Table E-4. Summary of Estimated Internal Doses for Crew of USS BOXER during Operation HARDTACK I

Organ	Mean Doses (rem)		Upper Bound Doses (rem)		
	Probabilistic(*)	Deterministic (NTPR)	Probabilistic (95th Percentile)	Deterministic (NTPR Upper Bound)	Ratio (Deterministic/ Probabilistic)
Alpha Doses					
Thyroid	0.000019 (7.9)	0.00026	0.00061	0.0026	4.2
Lung	0.00025 (8.0)	0.0035	0.0081	0.035	4.2
LLI	0.000020 (7.6)	0.00026	0.00063	0.0026	4.0
Beta plus Gamma Doses					
Thyroid	0.32 (4.5)	0.76	3.8	7.6	2.0
Lung	0.032 (5.9)	0.38	0.60	3.8	6.2
LLI	0.21 (4.5)	0.49	2.5	4.9	2.0

(*) Geometric mean and (geometric standard deviation) are shown for the probabilistic analysis results.

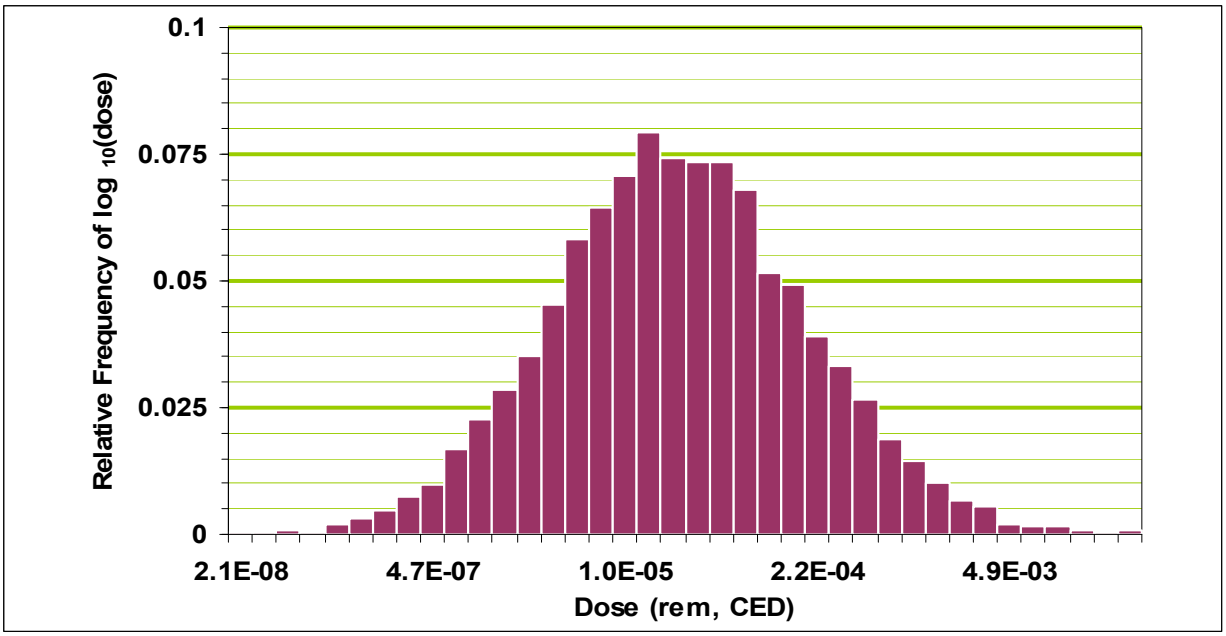

Figure E-3. Distribution of Estimated LLI Wall Dose from Alpha Radiation for Crew of USS BOXER during Operation HARDTACK I

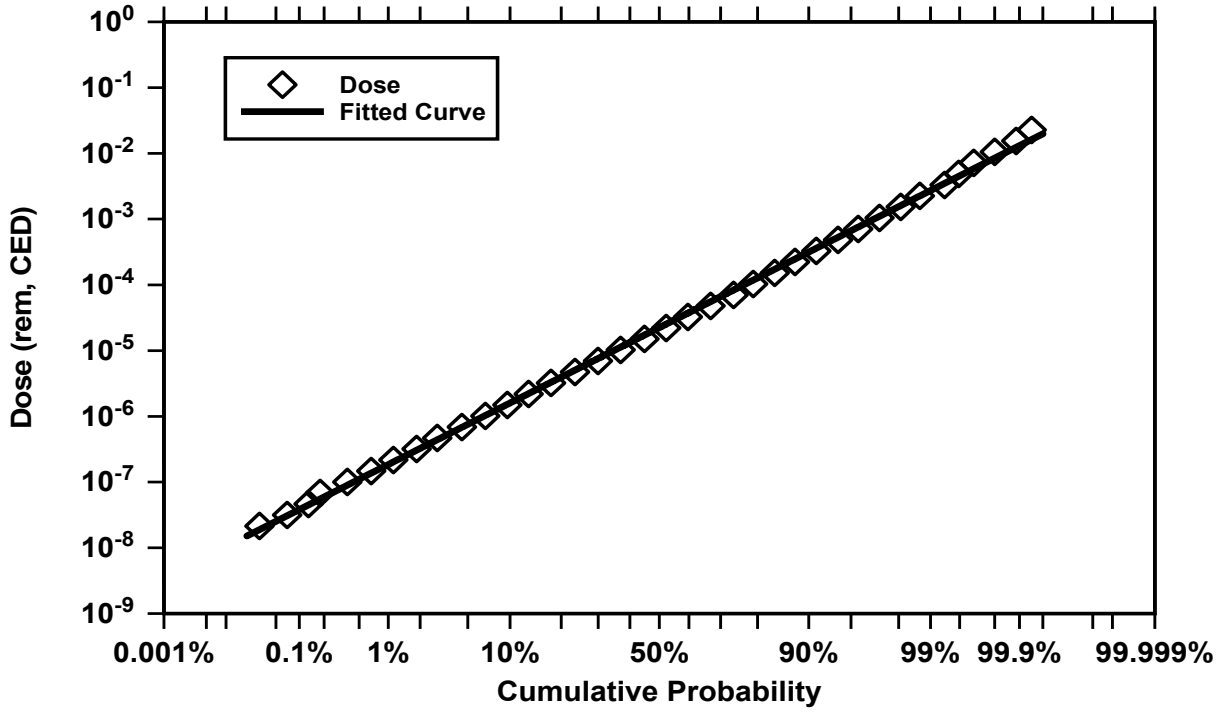

Figure E-4. Probability Plot of Estimated LLI Wall Dose from Alpha Radiation for Crew of USS BOXER during Operation HARDTACK I

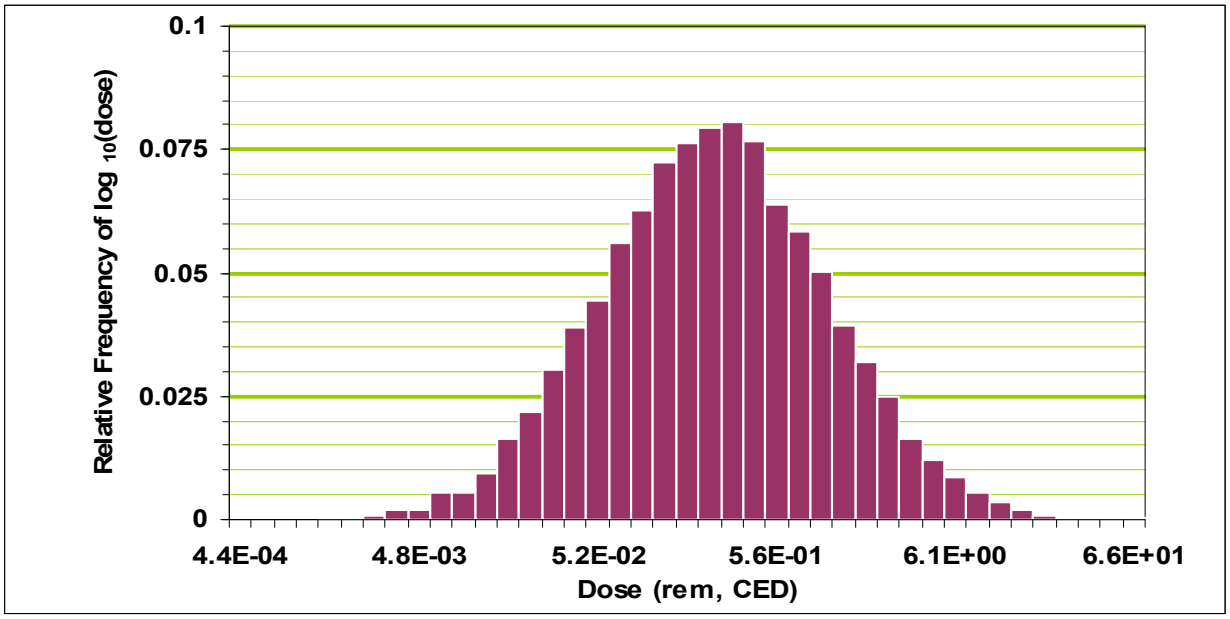

Figure E-5. Distribution of Estimated LLI Wall Dose from Beta plus Gamma Radiation for Crew of USS BOXER during Operation HARDTACK I

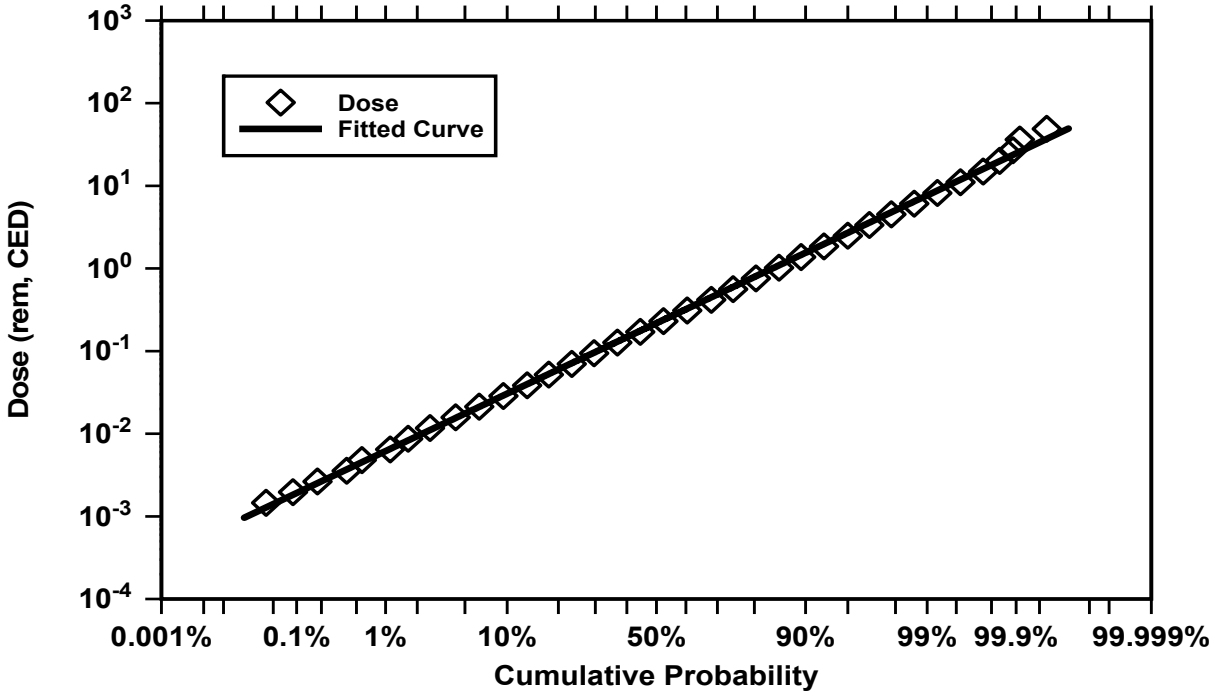

Figure E-6. Probability Plot of Estimated LLI Wall Dose from Beta plus Gamma Radiation for Crew of USS BOXER during Operation HARDTACK I

References

DTRA (Defense Threat Reduction Agency), 2007. Policy and Guidance Manual – Nuclear Test Personnel Review Program. Revision 7 (Defense Threat Reduction Agency, Fort Belvoir, VA), November 26, 2007.

Gladeck, F.R., Gould, K.G., Hallowell, J.H., Martin, E.J., McMullan, F.W., Miller, R.A., Osborn, M.J., Shelton, C.F., Berkhouse, L., and Calhoun, F.S., 1982. Operation HARDTACK I (1958). DNA 6038F (Defense Nuclear Agency, Washington, D.C.).

NRC (National Research Council), 1989. Film Badge Dosimetry in Atmospheric Nuclear Tests. (National Academy Press, Washington, D.C.)

USEPA, 1997. Exposure Factors Handbook. EPA/600/P-95/002Fa, Fb, Fc (Office of Research and Development, U.S. Environmental Protection Agency, Washington, D.C.).

APPENDIX F Monte Carlo Analysis of Dose for Personnel Stationed on Enewetak Island During Operation CASTLE

Carol Mason

APPENDIX F Monte Carlo Analysis of Dose for Personnel Stationed on Enewetak Island During Operation CASTLE

Introduction

Distributions of external and internal doses were generated by Monte Carlo techniques for personnel stationed at Enewetak Island, Enewetak Atoll, during Operation CASTLE (1954). Doses are reported for the entire operational period from March 1, 1954, through May 31, 1954.

Background

Operation CASTLE, the fifth nuclear test series at the Pacific Proving Ground (PPG), consisted of the six nuclear weapon tests identified in Table F-1. The operation was conducted by a joint military and civilian organization, designated Joint Task Force (JTF) 7, for the Atomic Energy Commission (AEC) from March 1 through May 14, 1954. The PPG consisted principally of Enewetak and Bikini Atolls in the northwestern Marshall Islands in the central Pacific Ocean. Enewetak Atoll, located about 2400 nautical miles (nmi) southwest of Hawaii and approximately 190 nmi west of Bikini Atoll, served as a base of operations and the location of the last shot in the series (NECTAR). The other five tests were conducted at Bikini Atoll. (DNA, 1996; Martin and Rowland, 1982)

Table F-1. Operation CASTLE Detonations

Shot	Date (1954) and Time	Location
BRAVO	Mar 1 at 0645	Bikini
ROMEO	Mar 27 at 0630	Bikini
KOON	Apr 7 at 0629	Bikini
UNION	Apr 26 at 0605	Bikini
YANKEE	May 5 at 0610	Bikini
NECTAR	May 14 at 0620	Enewetak

This case study applies to personnel in the 7126th Army Unit (AU) stationed at Enewetak Island during the period March 1 to May 31, 1954. The 7126th AU provided ground security, transportation and logistics support (Martin and Rowland, 1982). By the nature of their duties and residence, it is likely that most of the personnel remained on the island continuously, or nearly so, throughout the operation and therefore had continuous exposure to deposited fallout.

Exposure Scenario

Extensive radiation intensity readings obtained at Bikini Atoll following Shot BRAVO indicated decay rates that varied considerably from the standard $t^{-1.2}$ rule, where t denotes time after

detonation. Average values for the decay exponent (λ) for various time intervals were derived from measurements made with several gamma ionization time-intensity meters on Bikini Atoll (Thomas et al., 1984). These time-dependent decay rates are used in reconstructing the radiation environments on the residence islands of Enewetak and Parry Islands.

Of the six CASTLE shots, only Shots BRAVO, ROMEO, and NECTAR caused measurable fallout on the residence islands of Enewetak Atoll. Generally, such fallout was secondary (onset was well after the time of detonation) and relatively minor in nature. The time-intensity data for measurements collected during each fallout event are fitted by an interpolating function to produce the early-time intensity function denoted as $I_{early}(t)$ over the interval $T_o \leq t < T_{end}$, where T_o and T_{end} are the beginning and end of fallout deposition for the specific shot. The type of interpolating function is selected to obtain the best fit of the data pairs. The equations describing the free-field gamma radiation intensity (I in R hr^{-1}) as functions of time t (in hours) on Enewetak Island are defined for several periods of time using either the specific decay constants derived from the measurements or the standard 1.2 decay constant, as appropriate. These equations were used to obtain the deterministic results reported below.

Shot BRAVO

The equations describing the free-field gamma radiation intensity of the fallout from Shot BRAVO descending on Enewetak Island are as follows:

$$I(t) = 0 \qquad \text{if } t < 9.5$$

$$I(t) = I_{early}(t) \qquad \text{if } 9.5 \leq t < 16$$

$$I(t) = 0.010\,(16/t)^{0.82} \qquad \text{if } 16 \leq t < 65.25$$

$$I(t) = 0.010\,(16/65.25)^{0.82}\,(65.25/t)^{1.5} \qquad \text{if } 65.25 \leq t < 473.25$$

$$I(t) = 0.010\,(16/65.25)^{0.82}\,(65.25/473.25)^{1.5}\,(473.25/t)^{1.2} \qquad \text{if } 473.25 \leq t < 4380$$

Shot ROMEO

Fallout from Shot ROMEO occurred in two waves, referred to as ROMEO1 and ROMEO2. The equations describing the free-field gamma radiation intensity of the fallout from Shot ROMEO descending on Enewetak Island are as follows:

For ROMEO1 fallout:

$$I(t) = 0 \qquad \text{if } t < 10.5$$

$$I(t) = I_{early}(t) \qquad \text{if } 10.5 \leq t < 14.5$$

$$I(t) = 0.003\,(14.5/t)^{0.82} \qquad \text{if } 14.5 \leq t < 39.5$$

For ROMEO2 fallout:

$$I(t) = 0 \qquad \text{if } t < 39.5$$
$$I(t) = I_{early}(t) \qquad \text{if } 39.5 \le t < 77.5$$
$$I(t) = 0.009\,(77.5/t)^{1.5} \qquad \text{if } 77.5 \le t < 473.25$$
$$I(t) = 0.009\,(77.5/473.25)^{1.5}\,(473.25/t)^{1.2} \qquad \text{if } 473.25 \le t < 4380$$

Shot NECTAR

The equations describing the free-field gamma radiation intensity of the fallout from Shot NECTAR descending on Enewetak Island are as follows:

$$I(t) = 0 \qquad \text{if } t < 12$$
$$I(t) = I_{early}(t) \qquad \text{if } 12 \le t < 14.7$$
$$I(t) = 0.002\,(14.7/t)^{0.82} \qquad \text{if } 14.7 \le t < 65.7$$
$$I(t) = 0.002\,(14.7/65.7)^{0.82}\,(65.7/t)^{1.5} \qquad \text{if } 65.7 \le t < 473.7$$
$$I(t) = 0.002\,(14.7/65.7)^{0.82}\,(65.7/473.7)^{1.5}\,(473.7/t)^{1.2} \qquad \text{if } 473.7 \le t < 4380$$

External Dose: Approach

Film Badge Data

Film badge dosimetry during Operation CASTLE included two types (Servis, 1981). Mission badges were issued to individuals when it was anticipated that they had the potential to enter areas of radioactive contamination other than those encountered during routine activities. Cohort badges were issued to one individual in a group of individuals who collectively performed similar duties in similar locations. Even so, sufficient dosimetry data are not available for land-based personnel to allow meaningful comparisons between actual film badge data and reconstructed external gamma doses (Thomas et al., 1984). Therefore, reconstructed doses due to fallout exposure during Operation CASTLE cannot be compared to concurrent film badge data.

Monte Carlo-Based Dose Reconstruction

Probabilistic external gamma dose reconstruction for personnel the 7126th AU stationed on Enewetak Island during Operation CASTLE was accomplished by incorporating uncertainty distributions for various parameters into the model discussed in Section 3. The specific parameters used in both the deterministic and uncertainty analyses are shown in Table F-2.

Table F-2. Input Parameter Specification for External Gamma Dose Reconstruction, Case Study #6

Parameter	Definition	Distribution for Probabilistic Analysis (*)	Nominal Value for Central Estimation	Deterministic(**)
EXTERNAL DOSE MULTIPLIER (EDM) FOR LAND-BASED PERSONNEL				
F_{os}	Fraction of time spent outside	Triangular min = 2/24 peak = 8/24 max = 16/24	0.34 (or 8/24)	0.6 (or 14.4/24)
F_t	Fraction of inside time spent in tent	Triangular min = 0 peak = 0.5 max = 1	0.5	0
PF_t	Protection factor for tent	Numerical model (see Section 4.2.2) $\mu = 1.4$ UB95 = 1.9	1.4 (median of distribution)	1.5
PF_b	Protection factor for building	Numerical model (see Section 4.2.2) $\mu = 2.1$ UB95 = 3.9	2.0 (median of distribution)	2.0
I_i	Intensity of fallout near outdoor location (i=1), tent location (i=2), and building location (i=3) frequented by veteran, normalized to the intensity averaged over entire island	Lognormal GM = 1.0 GSD = 1.5	1.0	1.0
INTENSITY MEASUREMENTS FOR LAND-BASED PERSONNEL				
I_m	Measured intensities	Normal $\mu = I_m$, $\sigma = 0.3 \cdot I_m$ (to account for measurement error)	1.0	1.0
a	Exponent of multiplicative error factor $(t/t_0)^{\pm a}$ applied to FIIDOS-generated intensity functions	Normal $\mu = 0$ $\sigma = 0.15$	0	0

(*) μ = arithmetic mean; σ = standard deviation; GM = geometric mean; GSD = geometric standard deviation; UB95 = upper bound at the 95th percentile.
(**) High-sided per guidance in NTPR Policy and Guidance Manual (DTRA, 2007).

External Dose Results

The Monte Carlo dose distribution derived for a sample size of 10,000 is displayed in Figure F-1. The cumulative probability distribution is shown in Figure F-2. The statistics of this distribution are compared with those of a deterministic calculation in Table F-3.

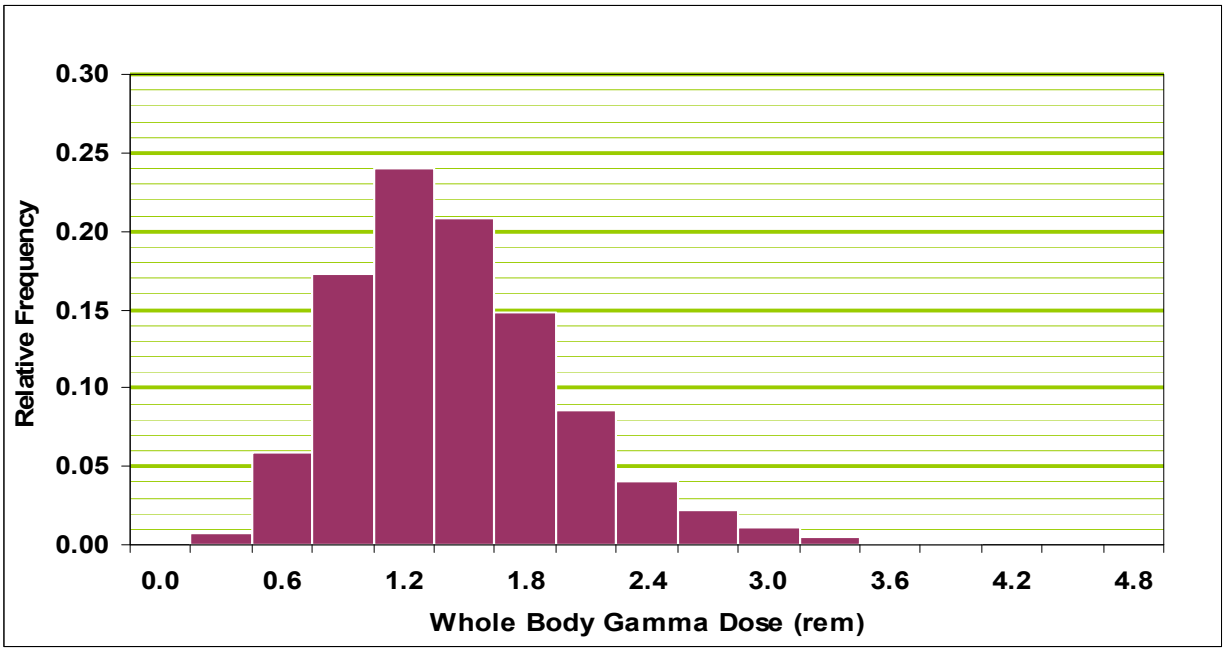

Figure F-1. Distribution of Estimated External Gamma Dose from Uncertainty Analysis for Personnel Stationed at Enewetak Island during Operation CASTLE

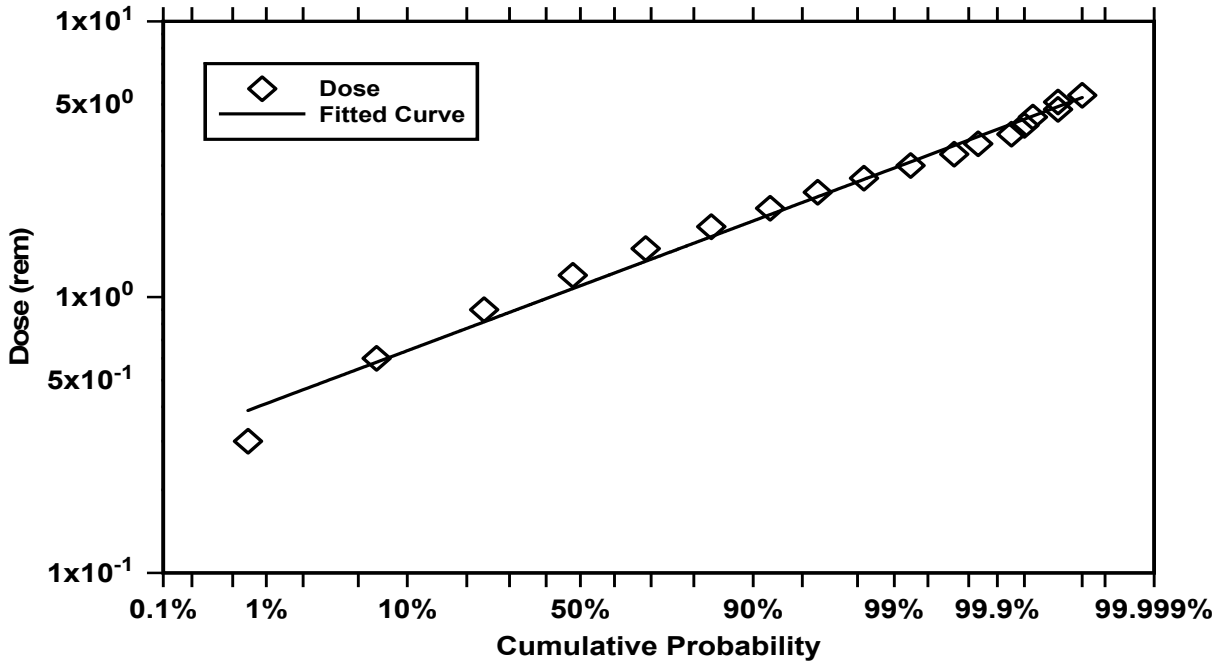

Figure F-2. Probability Plot of Estimated External Gamma Dose from Uncertainty Analysis for Personnel Stationed at Enewetak Island during Operation CASTLE

Table F-3. Summary of External Dose for Personnel Stationed at Enewetak Island during Operation CASTLE

Mean Dose (rem)		Upper Bound Dose (rem)		
Probabilistic(*)	**Deterministic (NTPR)**	**Probabilistic (95th Percentile)**	**Deterministic (NTPR)**	**Ratio (Deterministic ÷ Probabilistic)**
1.3 (0.54)	1.2	2.3	3.5	1.5

(*) The arithmetic mean and (standard deviation) are shown. The geometric mean external dose is 1.2 rem.

Internal Dose: Approach

Internal dose reconstruction for personnel stationed on Enewetak Island during Operation CASTLE was accomplished by incorporating uncertainty distributions for various parameters into the models discussed in Section 3. These models incorporate the fallout-induced radiation environments discussed above, the fallout intensity decay model discussed in Section 3, and various other parameters discussed in Sections 3 and 4. The specific parameters used in both the deterministic and uncertainty analyses are shown in Table F-4.

Table F-4. Input Parameter Specification for Internal Dose Reconstruction, Case Study #6

Parameter	Definition	Distribution for Probabilistic Analysis	Nominal Value for Central Estimation	Deterministic(*)
INTERNAL DOSE (GENERAL)				
DCFInhα *DCFIngα*	Inhalation and ingestion dose conversion factors for fallout α emitters	*DCF*s calculated with FIIDOS multiplied by Lognormal with GM=1.0, GSD=5.19	*DCF*s calculated with FIIDOS (see Section 4.2.8)	DCFs calculated with FIIDOS (see Section 4.2.8)
DCFInhβγ *DCFIngβγ*	Inhalation and ingestion dose conversion factors for fallout β+γ radiation	*DCF*s calculated with FIIDOS multiplied by Lognormal with GM=1.0, GSD=4.05	*DCF*s calculated with FIIDOS (see Section 4.2.8)	DCFs calculated with FIIDOS (see Section 4.2.8)
Biasα	Bias factors to adjust high-sided inhalation DCF values	Assigned Constant α: 1.3 for each organ	α: 1.3 for each organ	1.0
Biasβγ		βγ: 1.2 for thyroid & LLI, 1.35 for lung	βγ: 1.2 for thyroid & LLI, 1.35 for lung	1.0
BR	Breathing rate	Triangular distribution derived from USEPA (1997) data (see Section 4.2.7): min = 0.33 $m^3\ hr^{-1}$ peak = 1.53 $m^3\ hr^{-1}$ max = 2.79 $m^3\ hr^{-1}$	Mean of Distribution ~1.5 $m^3\ hr^{-1}$	1.2 $m^3\ hr^{-1}$

Parameter	Definition	Distribution for Probabilistic Analysis	Nominal Value for Central Estimation	Deterministic(*)
DESCENDING INHALATION DOSE (†)				
RND_{Res1}	Deposition fractions for particle sizes deposited in Regions BB, bb and AI	1.0 (assumed constant)	1.0 (assumed constant)	n/a
RND_{Res2}		Lognormal: GM, GSD 0.0056, 1.744	Geometric Mean 0.0056	
RND_{Res3}		Lognormal: GM, GSD 0.001, 1.65	0.001	
$RND_{Nonres1}$	Deposition fractions for particle sizes deposited in Region ET_2 and cleared to digestive tract	0.0 (assumed constant)	0.0 (assumed constant)	n/a
$RND_{Nonres2}$		Lognormal: GM, GSD 0.363, 1.106	Geometric Mean 0.363	
$RND_{Nonres3}$		Lognormal: GM, GSD 0.285, 1.185	0.285	
V_1	Particle settling velocities	Logtriangular min, peak, max (cm s^{-1}) 0.22/2, 0.22, 27.8	0.22 cm s^{-1}	10^6(cm)/T(sec)
V_2		0.83/2, 0.83, 27.8	0.83 cm s^{-1}	
V_3		13.0/2, 13.0, 27.8	13.0 cm s^{-1}	
AF_{100}	Surface activity fraction <100 μm particles	Triangular (min,peak,max) BRAVO (0.071, 0.391, 0.770) ROMEO1 (0.132, 0.462, 0.812) ROMEO2 (1.000, 1.000, 1.000) NECTAR (0.543, 0.781, 0.971)	Peak of Distributions BRAVO 0.391 ROMEO1 0.462 ROMEO2 1.000 NECTAR 0.781	1.0
$frac_1$	Surface fraction of Class 1–2 from 1–100 μm particles	Triangular Min, peak, max 0, 0.00136, 0.01	Peak of Distribution 0.00136	n/a
$frac_2$		0, 0.025, 0.1	0.025	
RESUSPENDED INHALATION DOSE				
$K(t)$	Time-dependent resuspension factor	Lognormal multiplier of Anspaugh equation GM=1, GSD=4.05	Anspaugh equation	Till and Meyer, 1983

Parameter	Definition	Distribution for Probabilistic Analysis	Nominal Value for Central Estimation	Deterministic(*)
INCIDENTAL INGESTION DOSE				
q_{ing}	Soil ingestion rate	Triangular min, peak, max (mg d^{-1}) 10, 100, 500	Peak of Distribution 100 mg day^{-1}	500 mg day^{-1}
ρ_{soil}	Soil bulk density	Triangular g cm^{-3} Min, peak, max 1.3, 1.45, 1.6	Peak of Distribution 1.45 g cm^{-3}	1.3 g cm^{-3}

(*) High-sided per guidance in NTPR Policy and Guidance Manual (DTRA, 2007).
(†) AMAD particle size classes: 1 = 1–10 μm, 2 = 10–20 μm, 3 = 20–100 μm.

Internal Dose Results

Distributions of the fifty-year committed equivalent doses (CED) to three organs, thyroid, lung, and lower large intestine (LLI) wall, were derived using the refined uncertainty model for a sample size of 10,000. Examples of these results are shown in Figure F-3 through Figure F-6, where the relative frequency distributions and probability plots of CED to the LLI wall from alpha radiation and from beta plus gamma radiation, respectively, are plotted. The geometric mean and 95th percentile CEDs of the various distributions are given in Table F-5, along with analogous doses derived deterministically. The ratio of the deterministic upper bound CED to the probabilistic 95th percentile CED is provided in the rightmost column.

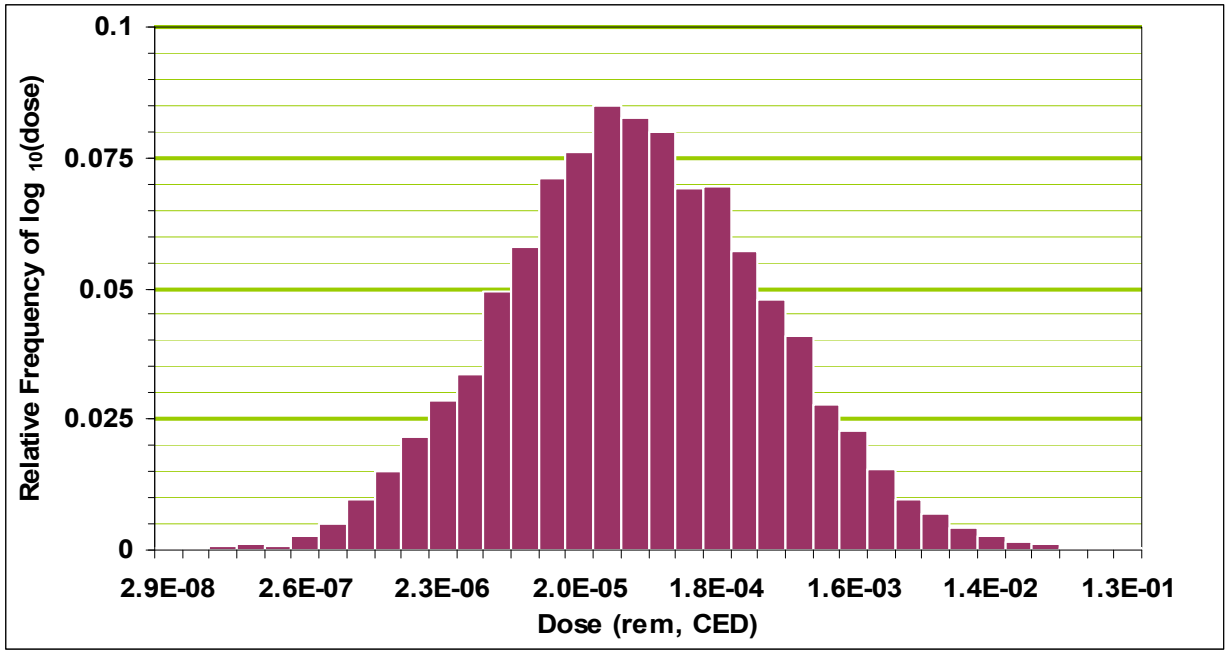

Figure F-3. Distribution of Estimated LLI Wall Doses from Alpha Radiation for Personnel Stationed at Enewetak Island during Operation CASTLE

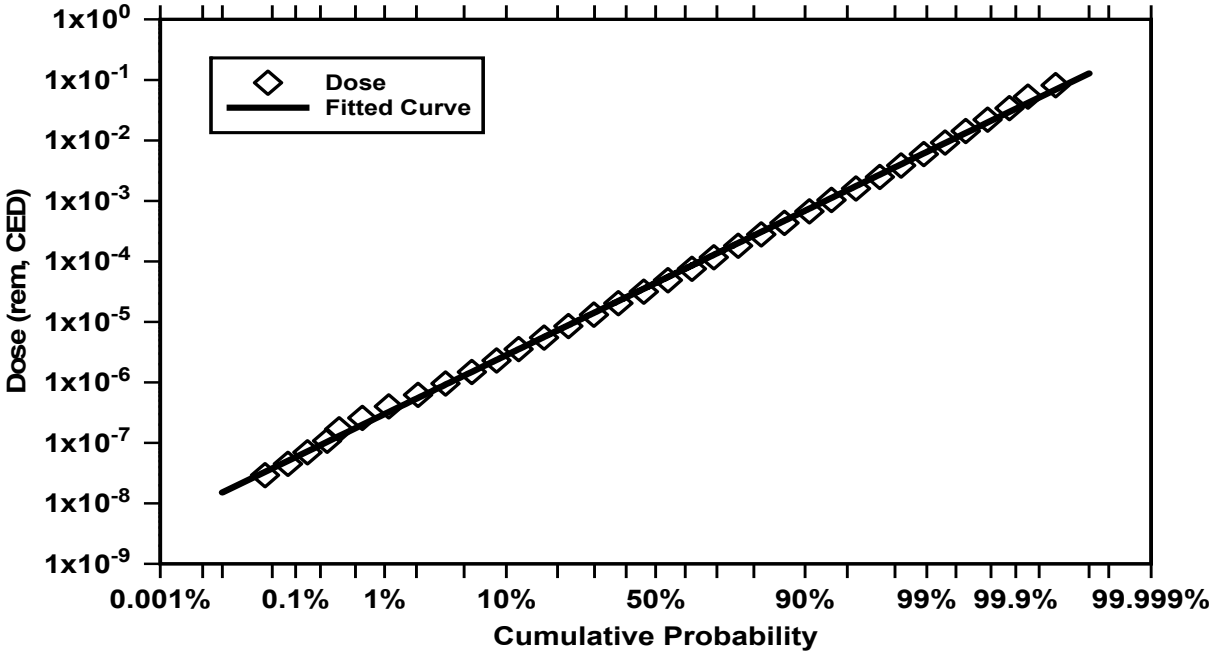

Figure F-4. Probability Plot of Estimated LLI Wall Doses from Alpha Radiation for Personnel Stationed at Enewetak Island during Operation CASTLE

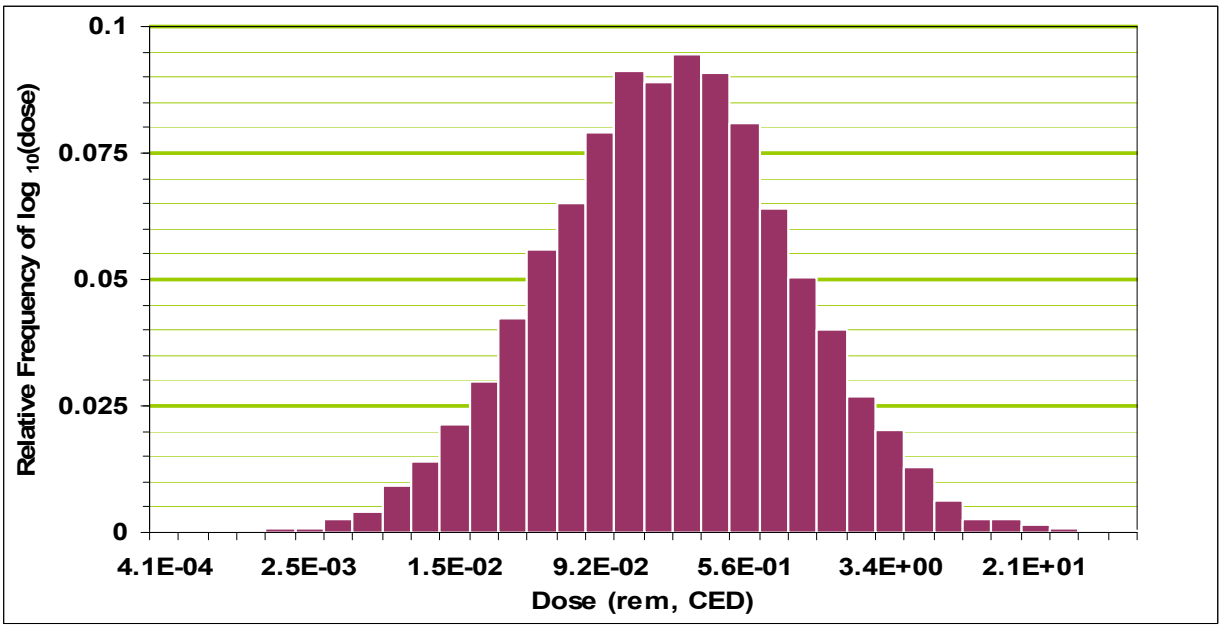

Figure F-5. Distribution of Estimated LLI Wall Doses from Beta plus Gamma Radiation for Personnel Stationed at Enewetak Island during Operation CASTLE

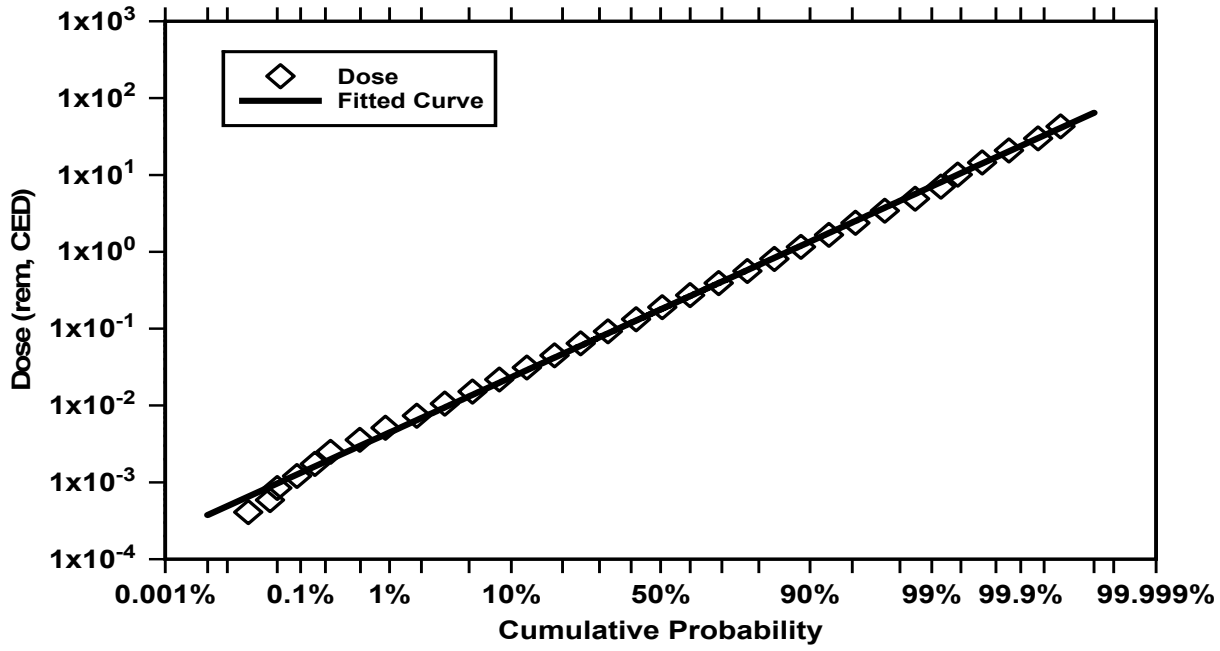

Figure F-6. Probability Plot of LLI Wall Doses from Beta plus Gamma Radiation for Personnel Stationed at Enewetak Island during Operation CASTLE

Table F-5. Internal Dose Summary for Personnel Stationed at Enewetak Island during Operation CASTLE

Organ	Mean Dose (rem)		Upper Bound Dose (rem)		
	Probabilistic	Deterministic (NTPR)	Probabilistic (95th Percentile)	Deterministic (NTPR)	Ratio (Deterministic ÷ Probabilistic)
Alpha Dose					
Thyroid	0.000039 (8.5)	0.00036	0.0014	0.0036	2.6
Lung	0.00048 (8.6)	0.0044	0.017	0.044	2.6
LLI	0.000041 (8.3)	0.00036	0.0014	0.0036	2.5
Beta plus Gamma Dose					
Thyroid	0.20 (4.7)	0.59	2.5	5.6	2.2
Lung	0.066 (6.2)	0.80	1.4	8.0	5.6
LLI	0.18 (4.6)	0.55	2.3	5.2	2.2

* Geometric mean and (geometric standard deviation) are shown for the probabilistic analysis results.

References

DNA (Defense Nuclear Agency), 1996. "For the Record—A History of the Nuclear Test Personnel Review Program, 1978-1993." DNA 6041F (Defense Nuclear Agency, Washington, D.C.), March 1996.

DTRA (Defense Threat Reduction Agency), 2007. Policy and Guidance Manual – Nuclear Test Personnel Review Program. Revision 7 (Defense Threat Reduction Agency, Fort Belvoir, VA), November 26, 2007.

Martin, E. J. and Rowland, R. H., 1982. "CASTLE Series: 1954, United States Atmospheric Nuclear Weapons Tests, Nuclear Test Personnel Review," DNA 6035F (Defense Nuclear Agency, Washington, D.C.), April 1, 1982.

Servis, J. D., 1981. "Operation CASTLE Radiological Safety," WT-942, Defense Nuclear Agency, Extracted Version, (Defense Nuclear Agency, Washington, D.C.), April 1, 1981.

Thomas, C., Goetz, J., Klemm, J., and Weitz, R., 1984. "Analysis of Radiation Exposure for Naval Personnel at Operation CASTLE," DNA-TR-84-6 (Defense Nuclear Agency, Washington, D.C.), February 28, 1984.

Till, J.E. and Meyer, H.R. (eds), 1983. "Radiological Assessment – A Textbook on Environmental Dose Analysis," NUREG/CR-3332 (United States Nuclear Regulatory Commission), September 1983.

APPENDIX G Model Variables Dependencies and Correlations

Stephen D. Egbert, Ph.D.

APPENDIX G Model Variables Dependencies and Correlations

Table G-1 lists the input parameters which were used in the Monte Carlo modeling calculations for external and internal dose. As discussed in Section 4.3, 49 input parameters were allowed to vary within their assigned uncertainty distributions, and five parameters explicitly listed did not vary. The table describes each input parameter and explains why each would change or stay the same during a single history of the case study. Although all dose input parameters have a partial degree of correlation with themselves at other times, they were categorized into either 1) full correlation, or 2) no or weak correlation, which is mathematically treated as zero correlation.

Table G-1. Case Study Model Variables – Dependencies and Correlations

Parameter	Definition	Correlation*	Basis
DATES and TIMES			
Shot Dates	Shot dates and times from appropriate references	No distribution No correlation	Shot dates and times are well documented. Any differences from these times are likely to have causes independent from shot-to-shot.
Fallout Event Times	Fallout event and intensity measurement times	No distribution No correlation	Intensity measurement dates and times are well documented. Any differences from these times are likely to have causes independent from shot-to-shot or fallout event -to- fallout event.
$Date_{Arrived}$ (skew-tri^{+})	Start date for study group analysis	Distribution for PLUMBBOB-HOOD only No correlation	Usually arrival dates and times are well documented. PLUMBBOB-HOOD study group was the only case where the arrival uncertainty extended over a significant period. This group did not have any other arrival events affecting dose. However, if other arrival events would have taken place, any differences from the nominal times are likely to have independent causes.
$Date_{Departed}$ (skew-tri^{+})	End date for study group analysis	Distribution for PLUMBBOB-HOOD only No correlation	Usually departure dates and times are well documented. PLUMBBOB-HOOD study group was the only case where the arrival uncertainty extended over a significant period. This group did not have any other departure events affecting dose. However, if other departure events would have taken place, any differences from the nominal times are likely to have independent causes.

Table G-1. Case Study Model Variables – Dependencies and Correlations

Parameter	Definition	Correlation*	Basis
FILM BADGE DATA			
$Date_{FBstart}$	Start date and time for film badge(s)	No distribution No correlation	Usually start date for a film badge is well documented. There was no study group where the start-date uncertainty extended over a significant period. However, if other film badges with uncertain dates would have been worn, any differences in their start date have independent causes.
$Date_{FBend}$	End date and time for film badge(s)	Distribution for HARDTACK I BOXER only Multiple end dates for HARDTACK I Enewetak No correlation	Usually end date for a film badge is well documented. HARDTACK I-BOXER study group was the only case where the end-date uncertainty extended over a significant period. However, if other film badges with uncertain dates would have been worn, any differences in their end date have independent causes.
SHOT MIXTURE FRACTION			
Composite Shots (skew-tri^{+})	Fallout proportion from combined debris clouds	Distribution for HARDTACK I FIR/KOA Enewetak and BOXER only No correlation of mixture fraction for combined shots' fallout to any other shots	FIR and KOA fallout were the only debris clouds which arrived and deposited fallout simultaneously. However, if other debris clouds had combined, the fraction is not correlated.

Table G-1. Case Study Model Variables – Dependencies and Correlations

Parameter	Definition	Correlation*	Basis
EXTERNAL DOSE MULTIPLIER (EDM) FOR LAND-BASED PERSONNEL			
F_{os} (skew-tri^{+})	Fraction of time spent outside	Fully correlated with all shots	Personnel participated in essentially the same activities from day-to-day and from shot-to-shot. Therefore, the fraction of time spent at the usual outside location, $Frac_{os}$, is likely the same for him throughout the operation.
F_t (skew-tri^{+})	Fraction of time spent in a tent while not outside	Fully correlated with all shots	Personnel participated in essentially the same activities from day-to-day and from shot-to-shot. Therefore, the fraction of time spent in a tent while not outside, FIS_{tent}, is likely the same for him throughout the operation.
PF_t (numeric)	Protection factor for tent	Fully correlated with all shots	Personnel participated in essentially the same activities from day-to-day and from shot-to-shot. Thus, location in the tent where he worked, slept or rested is the same day-to-day and from shot-to-shot. Therefore, the protection factor for the tent, PF_t, is likely the same for him throughout the operation.
PF_b (numeric)	Protection factor for building	Fully correlated with all shots	Personnel participated in essentially the same activities from day-to-day and from shot-to-shot. Thus, location in the building where he worked, slept or rested is the same day-to-day and from shot-to-shot. Therefore, the protection factor for the building, PF_b, is likely the same for him throughout the operation.
I_{os} × (lognormal) Also for OD calc	Intensity distribution of fallout near outside location normalized to the intensity averaged over the whole island	Weak correlation between separate fallout depositions	Fallout deposition from each debris cloud had a different pattern over the island, because of variations in wind direction, surface adhesion, etc. Thus, the intensity at the outside location is likely to have varied independently from the average island for each deposition event.
I_t × (lognormal)	Intensity distribution of fallout near tent location normalized to the intensity averaged over the whole island	Weak correlation between separate fallout depositions	Fallout deposition from each debris cloud had a different pattern over the island, because of variations in wind direction, surface adhesion, etc. Thus, the intensity at the tent location is likely to have varied independently from the average island for each deposition event.

Table G-1. Case Study Model Variables – Dependencies and Correlations

Parameter	Definition	Correlation*	Basis
I_b × (lognormal)	Intensity distribution of fallout near building location normalized to the intensity averaged over the whole island	Weak correlation between separate fallout depositions	Fallout deposition from each debris cloud had a different pattern over the island, because of variations in wind direction, surface adhesion, etc. Thus, the intensity at the building location is likely to have varied independently from the average island for each deposition event.
EXTERNAL DOSE MULTIPLIER (EDM) FOR SHIP-BASED PERSONNEL			
F_{ts} (skew-tri^{+})	Fraction of time spent topside	Fully correlated with all shots	Personnel participated in essentially the same activities from day-to-day and from shot-to-shot. Therefore, the fraction of time spent at his usual topside location, $Frac_{ts}$, is likely the same for him throughout the operation.
SF_w (numeric)	Shielding factor at worksite	Fully correlated with all shots	Personnel participated in essentially the same activities from day-to-day and from shot-to-shot. Thus, location in the ship where he worked was the same day-to-day and from shot-to-shot. Therefore, the shielding factor for his worksite, SF_w, is likely the same for him throughout the operation.
SF_b (numeric)	Shielding factor at billet location	Fully correlated with all shots	Personnel participated in essentially the same activities from day-to-day and from shot-to-shot. Thus, location in the ship where he billeted was the same day-to-day and from shot-to-shot. Therefore, the shielding factor for his billet location, SF_b, is likely the same for him throughout the operation.
I_{ts} (numeric) Also for TS	Intensity distribution of fallout topside, which affects topside activity area, normalized to the intensity averaged over the whole topside deck	Weak correlation between separate fallout depositions	Fallout deposition from each debris cloud had a different pattern over the ship, because of variations in wind direction, surface adhesion, etc. Thus, the intensity at the topside location is likely to have varied independently from the expected topside intensity for each deposition event.
I_w (numeric)	Intensity distribution of fallout topside, which affects workplace area, normalized to the intensity averaged over the whole topside deck	Weak correlation between separate fallout depositions	Fallout deposition from each debris cloud had a different pattern over the ship, because of variations in wind direction, surface adhesion, etc. Thus, the intensity at the topside location above the worksite is likely to have varied independently from the expected topside intensity for each deposition event.

Table G-1. Case Study Model Variables – Dependencies and Correlations

Parameter	Definition	Correlation*	Basis
I_b (numeric)	Intensity distribution of fallout topside, which affects billet area, normalized to the intensity averaged over the whole topside deck	Weak correlation between separate fallout depositions	Fallout deposition from each debris cloud had a different pattern over the ship, because of variations in wind direction, surface adhesion, etc. Thus, the intensity at the topside location above the billet area is likely to have varied independently from the expected topside intensity for each deposition event.
INTENSITY MEASUREMENTS FOR LAND-BASED PERSONNEL			
I_m × (normal)	Measurement error applied to initial and peak intensity data for each shot	Fully correlated with all shots	Intensity measurements were made by the same personnel using the same or similar instruments for all shots. Therefore, measurement error is likely the same from day-to-day and from shot-to-shot throughout the operation.
a × $((t/t_m)^{normal})$	Decay-rate error applied to FIIDOS-generated decay model	Weak correlation between shots	The deviation from the FIIDOS-generated decay model appeared to be generally independent according to the three examples shown in Section 4.2.4.2 It is reasonable that because the sources for deviation (i.e. fractionation, weathering, etc) vary for each shot, that the decay model error factor is likely independent for each shot.
MANUEVERS (NTS ONLY)			
Contour Intensity × (lognormal)	Error in intensity obtained from interpolation or extrapolation from iso-intensity contour maps	Fully correlated with all shots and contours	Intensity contours derived from intensity measurements were made by the same personnel using the same methods for all shots and contour levels. Therefore, contour interpolation error is likely the same from day-to-day, from shot-to-shot and from contour-to-contour throughout the operation. Furthermore, contour extrapolation error is both larger and fully correlated to the interpolation error.
ST × (normal)	Start time of unit maneuver	Distribution for PLUMBBOB-HOOD Maneuver only No correlation between maneuvers	The PLUMBBOB-HOOD maneuver was the only one where the dose significantly depended on the start time of the maneuver. If other maneuvers had contributed to the total dose, the start times would likely be uncorrelated to each other. This is because the error is due to rounding to the nearest 5 minutes.

Table G-1. Case Study Model Variables – Dependencies and Correlations

Parameter	Definition	Correlation*	Basis
Rate (skew-tri^{+})	Walk rate during unit maneuver	Distribution for PLUMBBOB-HOOD Maneuver only No correlation between maneuvers	The PLUMBBOB-HOOD maneuver was the only one where the dose significantly depended on the walk rate of the maneuver. If other maneuvers had contributed to the total dose, the walk rates would likely be uncorrelated to each other. This is because the error is due to the walking conditions during the maneuver.
LT (skew-tri^{+})	Linger time at closest approach to the <5 R/hr location during unit maneuver	Distribution for PLUMBBOB-HOOD Maneuver only No correlation between maneuvers	The PLUMBBOB-HOOD maneuver was the only one where the dose significantly depended on the linger time of the maneuver. If other maneuvers had contributed to the total dose, the linger time would likely be uncorrelated to each other. This is because the error is due to the different objectives of maneuvers.
INTENSITY MEASUREMENTS FOR SHIP-BASED PERSONNEL			
I_m × (normal)	Measurement error applied to initial and peak intensity data for each shot	Weak correlation between shots	Intensity measurements for ships were made by different personnel using the different instruments based on the islands or neighboring ships, which recorded each shot's deposition. Therefore, the ship measurement error is likely to differ from shot-to-shot.
a × $((t/t_m)^{normal})$	Decay-rate error applied to FIIDOS-generated decay model	Weak correlation between shots	The deviation from the FIIDOS-generated decay model appeared to be generally independent according to the three examples shown in Section 4.2.4.2. It is reasonable that because the sources for deviation (i.e. fractionation, weathering, etc) vary for each shot, that the decay-constant error factor is likely independent for each shot.

Table G-1. Case Study Model Variables – Dependencies and Correlations

Parameter	Definition	Correlation*	Basis
Contamination Intensity I_{sc} × (lognormal)	Measurement error applied to ship contamination data	Fully correlated with all shots	The model for calculating ship contamination dose is based on a limited number of experimental observations and from using a ship (or an average of ships) that differs from the particular ship used for this study. Also, personnel participated in essentially the same activities on the ship from shot-to-shot. The error is likely to be biased in the same amount and direction when applied to all shots for the particular ship. Therefore, the measurement error applied to ship contamination is likely the same for him throughout the operation.
Shine Intensity I_{ws} × (lognormal)	Measurement error applied to shine intensity data	Fully correlated with all shots	The model for calculating ship shine dose is based on a limited number of experimental observations and from using a ship (or an average of ships) that differs from the particular ship used for this study. Also, personnel participated in essentially the same activities on the ship from shot-to-shot. The error is likely to be biased in the same amount and direction when applied to all shots for the particular ship. Thus, for one ship, this error is the same shot-to-shot. Therefore, the measurement error applied to shine intensity is likely the same for him throughout the operation.
INTERNAL DOSE (GENERAL)			
$DCFinh_{\alpha}$ $DCFing_{\alpha}$ ×(lognormal)	Inhalation and ingestion dose conversion factors for α fallout radiation	Fully correlated for inhalation and ingestion with all shots	Deposition times are from several hours to several days, and significant resuspension doses are accrued on the following days. Any very short-lived isotopes are gone. Most of the internal dose comes primarily from the same α isotopes, thus there is likely to be significant correlation. The error is likely the same from day-to-day and shot-to-shot.
$DCFinh_{\beta\gamma}$ $DCFing_{\beta\gamma}$ ×(lognormal)	Inhalation and ingestion dose conversion factors for β+γ fallout radiation	Fully correlated for inhalation and ingestion with all shots	Deposition times are from several hours to several days, and significant resuspension doses are accrued on the following days. The very short-lived isotopes are gone. Most of the internal dose comes primarily from the same few βγ isotopes, thus there is likely to be some correlation. The error is likely the same from day-to-day and shot-to-shot.
$Bias\alpha$ $Bias\beta\gamma$	Bias factors to adjust high-sided inhalation DCF values	No distribution for each organ	Different values for different organs and α, βγ *DCF*s – no uncertainty.

Table G-1. Case Study Model Variables – Dependencies and Correlations

Parameter	Definition	Correlation*	Basis
BR_{frac}	Fraction of time at rest, or in light, moderate, or heavy activity	No distribution	Personnel participated in essentially the same activities for any day and any shot.
BR_{dist} (skew-tri^{+})	Breathing rate distribution	Fully correlated with all shots and activities	Health and metabolic rates remained the same for the veteran through out the operation. Therefore, a veteran's breathing rates are likely to have the same deviation from the average breathing rate for any activity, any day and any shot.
BR	Breathing rate from combined BR_{frac} and BR_{dist}	See BR_{dist}	See BR_{dist}
DESCENDING INHALATION DOSE			
RND_{Res2} × (lognormal)	Deposition fraction for 10–20 µm particles (Class 2) in Regions BB, bb, and AI	Fully correlated with all shots	Error is due to ICRP lung model parameters and their interpretation and manipulation – same resulting distribution used for all shots.
RND_{Res3} × (lognormal)	Deposition fraction for 20–100 µm particles (Class 3) in Regions BB, bb, and AI	Fully correlated with all shots	Error is due to ICRP lung model parameters and their interpretation and manipulation – same resulting distribution used for all shots.
$RND_{NonRes2}$ × (lognormal)	Deposition fraction for 10–20 µm particles (Class 2) in Region ET_2	Fully correlated with all shots	Error is due to ICRP lung model parameters and their interpretation and manipulation – same resulting distribution used for all shots.
$RND_{NonRes3}$ × (lognormal)	Deposition fraction for 20–100 µm particles (Class 3) in Region ET_2	Fully correlated with all shots	Error is due to ICRP lung model parameters and their interpretation and manipulation – same resulting distribution used for all shots.

Table G-1. Case Study Model Variables – Dependencies and Correlations

Parameter	Definition	Correlation*	Basis
AF_{100} × (triangle)	Fraction of all activity carried to surface on particles with aerodynamic diameter <100 μm	Weak correlation between shots	Variation is from distribution obtained from three initial distribution models, three activity/size correlation models and two temporal deposition models Cloud height measurements were made by the same personnel using the same or similar methods for all shots in operation – Also debris height distribution ought to be from one model for all shots suggesting correlation possible Activity/size typically applied at similar conditions, downwind distance and time suggesting correlation possible Temporal models from very early fallout at one shot, REDWING-TEWA. then applied to all other shots suggesting correlation possible In spite of possible shot-to-shot correlations due to these components, variations in weather make overall AF choice from models independent from shot-to-shot
$frac_1$ × (triangle)	Fraction of AF carried by Class 1 particles	Weak correlation between shots	Variations in weather cause deposition to be independent from shot-to-shot
$frac_2$ × (triangle)	Fraction of AF carried by Class 2 particles	Weak correlation between shots	Variations in weather cause deposition to be independent from shot-to-shot
V_1 × (log-triangle)	Particle settling velocities for 1–10 μm particles (Class 1)	Weak correlation between shots	Variations in weather cause settling velocity for Class 1 particles to be independent from shot-to-shot
V_2 × (log-triangle)	Particle settling velocities for 10–20 μm particles (Class 2)	Weak correlation between shots	Variations in weather cause settling velocity for Class 2 particles to be independent from shot-to-shot
V_3 × (log-triangle)	Particle settling velocities for 20–100 μm particles (Class 3)	Weak correlation between shots	Variations in weather cause settling velocity for Class 3 particles to be independent from shot-to-shot

Table G-1. Case Study Model Variables – Dependencies and Correlations

Parameter	Definition	Correlation*	Basis
RESUSPENDED INHALATION DOSE (LAND-BASED PERSONNEL)			
$K(t)$ × (lognormal)	Time-dependent resuspension factor	Fully correlated with all shots	Mechanical disturbances, wind and weather conditions remain essentially the same from day-to-day and from shot-to-shot. Personnel participated in essentially the same activities from shot-to-shot. Therefore, the resuspension factor, K, is likely the same for him throughout the operation.
K_{pc}, K_{bw} × (lognormal)	Resuspension factors for highly-resuspended fallout at NTS (thermal pulse and blast-wave regions)	Fully correlated with all shots	Mechanisms of resuspension and environment are essentially the same from shot-to-shot. Personnel participated in essentially the same activities from shot-to-shot. Therefore, the resuspension factors, K_{pc} and K_{bw}, are likely the same for him throughout the operation.
OD	Intensity distribution of fallout near outside location normalized to the intensity averaged over the whole island	Same as I_{os} above	Because it is the same modification, it is fully correlated to the I_{os} modification above.
RESUSPENDED INHALATION DOSE (SHIP-BASED PERSONNEL)			
K × (lognormal)	Resuspension factor (assumed constant with time)	Fully correlated with all shots	Mechanical disturbances, wind and weather conditions remain essentially the same from day-to-day and from shot-to-shot for 4 days on a ship. Personnel participated in essentially the same activities topside from shot-to-shot. Therefore, the resuspension factor, K, is likely the same for him throughout the operation.
TS	Intensity distribution of fallout topside, which affects topside activity area, normalized to the intensity averaged over the whole topside deck	Same as I_{ts} above	Because it is the same modification, it is fully correlated to the I_{ts} modification above.

Table G-1. Case Study Model Variables – Dependencies and Correlations

Parameter	Definition	Correlation*	Basis
$<GSMF>$ (numeric)	Topside-averaged gamma source modification factor	Fully correlated with all shots	$<GSMF>$ depends on uncertainties related to the dimensions of the ship and topside obstructions (e.g., superstructure). Therefore, the average gamma source modification factor, $<GSMF>$, is likely the same for him throughout the operation.
INCIDENTAL INGESTION DOSE (LAND-BASED PERSONNEL ONLY)			
q_{ing} (skew-tri^{+})	Soil ingestion rate	Fully correlated with all shots	Personnel activities remain essentially the same from day-to-day and from shot-to-shot. Therefore, the soil ingestion rate, q, is likely the same for him throughout the operation.
ρ_{soil} (tri)	Soil bulk density	Fully correlated with all shots	Personnel activities and soil density in those locations remain essentially the same from day-to-day and from shot-to-shot. Therefore, the soil bulk density, ρ, is likely the same for him throughout the operation.

***** For fallout dose calculations associated with different shots, this column indicates how the parameter uncertainty is correlated and whether it is modeled exactly the same for each shot (Full), or modeled as independent for each shot (Weak or No Correlation).

Except for two pairs (I_{os} and OD) and (I_{ts} and TS), all parameters that are on different rows are at most weakly correlated to each other. They are considered independent and modeled without correlation.

$^{+}$ skew-tri means skewed triangular distribution.

Distribution List

DTRA-TR-09-13

Additional copies are available at:

http://www.dtra.mil/rd/programs/nuclear_personnel/pubs.cfm

DEPARTMENT OF DEFENSE

Defense Technical Information Center
8725 John J. Kingman Road, Suite 0944
Fort Belvoir, VA 22060-6201
ATTN: DTIC/OCA

Defense Threat Reduction Agency
8725 John J. Kingman Road, RD-NTSN
Fort Belvoir, VA 22060-6201

Defense Threat Reduction Information Analysis Center
8725 John J. Kingman Road, OP-CSUI
Fort Belvoir, VA 22060-6201

DEPARTMENT OF VETERANS AFFAIRS

Department of Veterans Affairs
Chief, Public Health & Environmental Hazards
VA Central Office (13)
810 Vermont Ave., NW
Washington, DC 20420

DEPARTMENT OF HEALTH AND HUMAN SERVICES

National Institute of Occupational Safety and Health
Director, Compensation Analysis and Support
Robert A. Taft Laboratories
4676 Columbia Parkway
Cincinnati, OH 45226-1998

DEPARTMENT OF LABOR

U. S. Department of Labor, DEEOIC
200 Constitution Avenue NW, Room C-3321
Washington, DC 20210

FEDERAL AGENCY ADVISORY BOARDS

Advisory Board on Radiation and Worker Health
4676 Columbia Parkway, MS: C-46
Cincinnati, OH 45226

Veterans' Advisory Board on Dose Reconstruction
801 North Quincy Street, Suite 600
Arlington, VA 22203

Veterans' Advisory Committee on Environmental Hazards
Department of Veterans Affairs
Compensation & Pension Service (211)
810 Vermont Avenue, NW
Washington, DC 20420

DEPARTMENT OF DEFENSE CONTRACTORS

L3 Communications
11410 Isaac Newton Square North, Suite 103
Reston, VA 20190-5005

Oak Ridge Associated Universities
9950 W. 80Th Ave.
Arvada, CO 80005
ATTN: Ms. Nancy Daugherty CHP

SAIC
8301 Greensboro Drive, M/S E-5-5
McLean, VA 22102

SENES Oak Ridge, Inc.
102 Donner Drive
Oak Ridge, TN 37830
ATTN: Dr. David Kocher